第55回 フラーレン・ナノチューブ・グラフェン 総合シンポジウム講演要旨集

平成30年9月11日～13日

FNTG
Research Society

第 55 回
フラーレン・ナノチューブ・グラフェン総合シンポジウム
The 55th Fullerenes–Nanotubes–Graphene General Symposium

TOHOKU UNIVERSITY

Faculty of Science
Graduate School of Science
TOHOKU UNIVERSITY

講演要旨集
Abstracts

2018 年 9 月 11 日（火） ～ 13 日（木）
東北大学理学研究科　青葉サイエンスホール
Aoba Science Hall, Graduate School of Science, Tohoku University

主催　フラーレン・ナノチューブ・グラフェン学会
The Fullerenes, Nanotubes and Graphene Research Society

共催・後援

日本化学会	The Chemical Society of Japan
東北大学理学研究科	Graduate School of Science, Tohoku University

協賛

日本物理学会	The Physical Society of Japan
応用物理学会	The Japan Society of Applied Physics
高分子学会	The Society of Polymer Science, Japan
電気化学会	The Electrochemical Society of Japan

Princeton Instruments

高感度

高ダイナミックレンジ

高繰り返し

高感度近赤外線２次元InGaAsカメラ

NIRvana™:640

- 低暗電流ノイズ（電子冷却：-80℃、液体窒素：-190℃）
- 110fps（ビデオレート以上）
- 標準GigEインターフェースで50mまで延長可
- 空冷ファンと水冷を切替可能

アプリケーション例

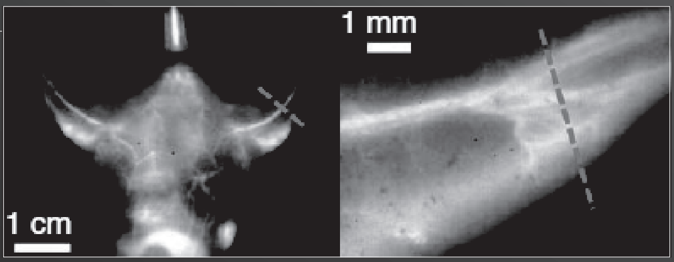

- ・フォトニック結晶PLイメージング及びスペクトル
- ・一重項酸素イメージング及びスペクトル
- ・太陽電池PLイメージング及びスペクトル
- ・天体観測微弱光イメージング
- ・食品断面イメージング
- ・In-Vivoイメージング　など

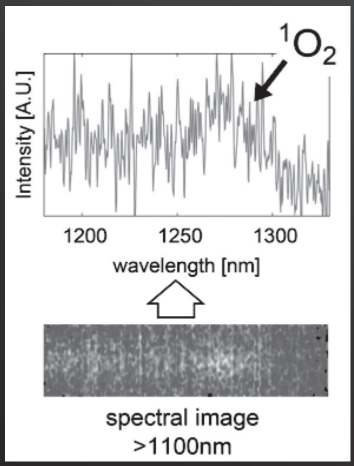

仕様

モデル	NIRvana:640ST	NIRvana:640	NIRvana:640LN
センサー	640 x 512 x InGaAs		
素子サイズ	20μm x 20μm		
波長範囲	0.9 ～ 1.7 μm		
冷却温度	-60℃	-80℃	-190℃
ダークチャージ	1500 e-/p/sec	300 e-/p/sec	<8 e-/p/sec
読み出しノイズ	<120 e-rms		15 e-rms
ダイナミックレンジ	16 Bit (>15Bit@1 素子)		
フレームレート	110 fps@10MHz		2.77 fps@250KHz
インターフェース	Gig E		
ソフトウェア	LightField, SITK-LabVIEW, WinX32		

www.pi-j.jp

NIPPON ROPER

株式会社 日本ローパー　ＰＩ事業部
〒135-0033 東京都江東区深川2-8-19 サクライビル3F
電話 03-5639-2741　FAX 03-5639-2775

Abstract of
The 55th Fullerenes-Nanotubes-Graphene General Symposium

Sponsored by : The Fullerenes, Nanotubes and Graphene Research Society

Co-Sponsored by : The Chemical Society of Japan
: Graduate School of Science, Tohoku University

Supported by : The Physical Society of Japan
The Japan Society of Applied Physics
The Society of Polymer Science, Japan
The Electrochemical Society of Japan

Date : September 11th (Tue.) –13th (Thu.), 2018

Place : Aoba Science Hall, Science Complex C(H-04),
Graduate School of Science, Tohoku University
6-3 Aoba, Aramaki, Aoba-ku, Sendai 980-8578, Japan

Presentation Time : Special Lecture (25 min presentation + 5min discussion)
Award Nominee Lecture (10 min presentation + 10 min discussion)
General Lecture (10 min presentation + 5min discussion)
Poster Preview (1 min presentation without discussion)

第55回フラーレン･ナノチューブ･グラフェン総合シンポジウム
講演要旨集

主催 ： フラーレン･ナノチューブ･グラフェン学会

共催･後援 ： 日本化学会
： 東北大学理学研究科

協賛 ： 日本物理学会、応用物理学会、高分子学会、電気化学会

日時 ： 平成30年9月11日(火)～9月13日(木)

場所 ： 東北大学 理学研究科 合同C棟（H-04）青葉サイエンスホール
〒980-8578　仙台市青葉区荒巻字青葉6-3

発表時間 ： 特別講演（発表　25分 + 質疑応答　5分）
受賞対象者講演（発表　10分 + 質疑応答　10分）
一般講演（発表　10分 + 質疑応答　5分）
ポスタープレビュー（発表 1分・質疑応答　なし）

展示団体御芳名 （五十音順、 敬称略）

AIST ナノチューブ実用化研究センター
ｓａｎｔｅｃ（株）
（株）シンキー
（株）セントラル科学貿易
（株）日本レーザー
（株）日本ローパー
（株）名城ナノカーボン

広告掲載団体御芳名 （五十音順、 敬称略）

エクセルソフト（株）
工機ホールディングス（株）
（株）セントラル科学貿易
ソーラボジャパン（株）
日本電子（株）
（株）日本レーザー
（株）日本ローパー
（株）堀場製作所

Contents

目次

プログラム早見表

	9月11日（火）
	受付開始 8:30〜 開会挨拶 8:55〜
9:00	一般講演 2件 9:00-9:30 （バイオ・ナノ環境と安全評価）
9:30	特別講演（湯田坂 雅子） 9:30-10:00
10:00	一般講演 2件 10:00-10:30 （ナノチューブの応用・原子層）
10:30	休憩 10:30-10:45
10:45	特別講演（千賀 亮典） 10:45-11:15
11:15	一般講演 1件 11:15-11:30 （グラフェンの物性）
11:30	ポスタープレビュー （ 1P-1 〜 1P-36 ） 11:30-12:15
12:15	昼食 （幹事会） 12:15-13:30
13:30	ポスターセッション 13:30-14:00 若手奨励賞候補審査優先時間 【多目的室，C棟2Fロビー】 13:30-15:15
15:15	特別講演（野々口 斐之） 15:15-15:45
15:45	一般講演 3件 （ナノチューブの物性・グラフェンの物性・原子層） 15:45-16:30
16:30	休憩 16:30-16:45
16:45	一般講演 4件 （原子層・グラフェンの応用・グラフェンの物性・その他） 16:45-17:45
17:45	展示企業との交流会 【合同B棟エントランス2F】 17:45-19:00
19:00	

	9月12日（水）
	受付開始 8:45〜 講演開始 9:00〜
9:00	大澤賞・飯島賞 受賞対象者講演 4件 9:00-10:25
10:25	休憩 10:25-10:45
10:45	特別講演（田中 丈士） 10:45-11:15
11:15	一般講演 1件 11:15-11:30 （ナノチューブの生成と精製）
11:30	ポスタープレビュー （ 2P-1 〜 2P-36 ） 11:30-12:15
12:15	昼食 12:15-13:30
13:30	ポスターセッション 13:30-14:00 若手奨励賞候補審査優先時間 【多目的室，C棟2Fロビー】 13:30-15:15
15:15	授賞式 15:15-15:30
15:30	総会 15:30-16:00
16:00	特別講演（平原 佳織） 16:00-16:30
16:30	休憩 16:30-16:45
16:45	特別講演（井上 翼） 16:45-17:15
17:15	一般講演 2件 （フラーレン） 17:15-17:45
17:45	移動
18:30	懇親会 【ホテルレオパレス仙台 B1Fイベントホール】 18:30-20:30
20:30	

	9月13日（木）
	受付開始 8:45〜 講演開始 9:00〜
9:00	一般講演 2件 9:00-9:30 （ナノチューブの応用）
9:30	特別講演（大野 雄高） 9:30-10:00
10:00	一般講演 2件 10:00-10:30 （ナノチューブの応用・ナノチューブの物性）
10:30	休憩 10:30-10:45
10:45	特別講演（河野 行雄） 10:45-11:15
11:15	一般講演 1件 11:15-11:30 （ナノチューブの物性）
11:30	ポスタープレビュー （ 3P-1 〜 3P-36 ） 11:30-12:15
12:15	昼食 12:15-13:30
13:30	ポスターセッション 13:30-14:00 若手奨励賞候補審査優先時間 【多目的室，C棟2Fロビー】 13:30-15:15
15:15	特別講演（大淵 真理） 15:15-15:45
15:45	一般講演 5件 （原子層・ナノチューブの生成と精製 ・ グラフェンの応用） 15:45-17:00
17:00	

講演会場 青葉サイエンスホール

特別講演 発表25分・質疑5分
賞対象者講演 発表10分・質疑10分
一般講演 発表10分・質疑5分
ﾎﾟｽﾀｰﾌﾟﾚﾋﾞｭｰ 発表1分・質疑なし

Time table

	September 11 (Tue.)
	Registration begins at 8:30 Opening greeting at 8:55
9:00	General Lectures [2] 9:00–9:30 (Bio・Environmental/Safety characterization of nanomaterials)
9:30	Special Lecture 9:30–10:00 (Masako Yudasaka)
10:00	General Lectures [2]10:00–10:30 (Applications of nanotubes・Atomic Layers)
10:30	Coffee Break 10:30–10:45
10:45	Special Lecture 10:45–11:15 (Ryosuke Senga)
11:15	General Lectures [1]11:15–11:30 (Properties of graphene)
11:30	Poster Preview (1P–1 through 1P–36) 11:30–12:15
12:15	Lunch (Administrative meeting) 12:15–13:30
13:30	Poster Session During 13:30–14:00, please give priority to selection of candidates for Young Scientist Poster Award 【 Event Space 】 【 Lobby on 2F, Building C 】 13:30–15:15
15:15	Special Lecture 15:15–15:45 (Yoshiyuki Nonoguchi)
15:45	General Lectures [3] 15:45–16:30 (Properties of nanotubes・Properties of graphene・Atomic Layers)
16:30	Coffee Break 16:30–16:45
16:45	General Lectures [4] (Atomic Layers・Applications of graphene・Properties of graphene・Other topics) 16:45–17:45
17:45	Exchange meeting with corporate exhibitors 【 Entrance on 2F, Building B 】 17:45–19:00
19:00	

	September 12 (Wed.)
	Registration begins at 8:45 Lectures begin at 9:00
9:00	Lectures of Osawa Award and Iijima Award Nominees 9:00–10:25
10:25	Coffee Break 10:25–10:45
10:45	Special Lecture 10:45–11:15 (Takeshi Tanaka)
11:15	General Lectures [1]11:15–11:30 (Formation and purification of nanotubes)
11:30	Poster Preview (2P–1 through 2P–36) 11:30–12:15
12:15	Lunch 12:15–13:30
13:30	Poster Session During 13:30–14:00, please give priority to selection of candidates for Young Scientist Poster Award 【 Event Space 】 【 Lobby on 2F, Building C 】 13:30–15:15
15:15	Awards Ceremony 15:15–15:30
15:30	General Meeting 15:30–16:00
16:00	Special Lecture 16:00–16:30 (Kaori Hirahara)
16:30	Coffee Break 16:30–16:45
16:45	Special Lecture 16:45–17:15 (Yoku Inoue)
17:15	General Lectures [2] (Fullerenes) 17:15–17:45
17:45	Moving
18:30	Banquet 【 B1F Event Hall, Hotel Leopalace Sendai 】 18:30–20:30
20:30	

	September 13 (Thu.)
	Registration begins at 8:45 Lectures begin at 9:00
9:00	General Lectures [2] 9:00–9:30 (Applications of nanotubes)
9:30	Special Lecture 9:30–10:00 (Yutaka Ohno)
10:00	General Lectures [2]10:00–10:30 (Applications of nanotubes・Properties of nanotubes)
10:30	Coffee Break 10:30–10:45
10:45	Special Lecture 10:45–11:15 (Yukio Kawano)
11:15	General Lectures [1]11:15–11:30 (Properties of nanotubes)
11:30	Poster Preview (3P–1 through 3P–36) 11:30–12:15
12:15	Lunch 12:15–13:30
13:30	Poster Session During 13:30–14:00, please give priority to selection of candidates for Young Scientist Poster Award 【 Event Space 】 【 Lobby on 2F, Building C 】 13:30–15:15
15:15	Special Lecture 15:15–15:45 (Mari Ohfuchi)
15:45	General Lectures [5] (Atomic Layers・Formation and purification of nanotubes・Applications of graphene) 15:45–17:00
17:00	

Place : Aoba Science Hall
Special Lecture : 25 min (Presentation) + 5 min (Discussion)
Award Nominee Lecture : 10 min (Presentation) + 10 min (Discussion)
General Lecture : 10 min (Presentation) + 5 min (Discussion)
Poster Preview : 1 min (Presentation)

座長一覧 (Chairpersons)

9月11日（火）

（敬称略）

セッション	時　　間	座　　長
一般講演	9:00 ~ 9:30	田中 丈士
特別講演（湯田坂 雅子）	9:30 ~ 10:00	
一般講演	10:00 ~ 10:30	
特別講演（千賀 亮典）	10:45 ~ 11:15	片浦 弘道
一般講演	11:15 ~ 11:30	
ポスタープレビュー	11:30~ 12:15	中島 秀朗 西原 大志
特別講演（野々口 斐之）	15:15 ~ 15:45	梅山 有和
一般講演	15:45 ~ 16:30	
一般講演	16:45 ~ 17:45	野田 優

9月12日（水）

セッション	時　　間	座　　長
一般講演（受賞対象者）	9:00 ~ 10:25	斎藤 晋
特別講演（田中 丈士）	10:45 ~11:15	北浦 良
一般講演	11:15 ~11:30	
ポスタープレビュー	11:30 ~ 12:15	田島 奈穂子 IL JEON
特別講演（平原 佳織）	16:00 ~ 16:30	大野 雄高
特別講演（井上 翼）	16:45 ~ 17:15	岡崎 俊也
一般講演	17:15 ~ 17:45	

9月13日（木）

セッション	時　　間	座　　長
一般講演	9:00 ~ 9:30	加藤 俊顕
特別講演（大野 雄高）	9:30 ~ 10:00	
一般講演	10:00 ~ 10:30	
特別講演（河野 行雄）	10:45 ~ 11:15	加藤 雄一郎
一般講演	11:15 ~ 11:30	
ポスタープレビュー	11:30 ~ 12:15	内田 勇気 Feng Yang
特別講演（大淵 真理）	15:15 ~ 15:45	岡田 晋
一般講演	15:45 ~ 17:00	

9月11日（火）

特別講演　発表 25分 ・ 質疑応答 5分
一般講演　発表 10分 ・ 質疑応答 5分
ポスタープレビュー　発表 1分 ・ 質疑応答 なし

一般講演（ 9:00-9:30 ）

バイオ ・ ナノ環境と安全評価

特別講演（ 9:30-10:00 ）

一般講演（ 10:00-10:30 ）

ナノチューブの応用 ・ 原子層

＞＞＞＞＞＞＞ 休憩（ 10:30-10:45 ）＜＜＜＜＜＜＜

特別講演（ 10:45-11:15 ）

一般講演（ 11:15-11:30 ）

グラフェンの物性

ポスタープレビュー（ 11:30-12:15 ）　（☆） 若手奨励賞候補

若手奨励賞候補

9月11日（火）

フラーレンの化学

ナノチューブの物性

9月11日（火）

ナノチューブの応用

ナノチューブの生成と精製

内包ナノチューブ

グラフェン生成

グラフェンの応用

9月11日（火）

グラフェンの物性

原子層

ナノ炭素粒子

バイオ

9月11日（火）

＞＞＞＞＞＞＞ 昼食 （ 12:15-13:30 ）＜＜＜＜＜＜＜

ポスターセッション （ 13:30-15:15 ）

13:30-14:00 若手奨励賞候補審査優先時間

特別講演 （ 15:15-15:45 ）

一般講演 （ 15:45-16:30 ）

ナノチューブの物性 ・ グラフェンの物性 ・ 原子層

＞＞＞＞＞＞＞ 休憩 （ 16:30-16:45 ）＜＜＜＜＜＜＜

一般講演 （ 16:45-17:45 ）

原子層 ・ グラフェンの応用 ・ グラフェンの物性 ・ その他

展示企業との交流会 （ 17:45-19:00 ）

9月12日（水）

特別講演　　発表 25分 ・ 質疑応答 5分
一般講演　　発表 10分 ・ 質疑応答 5分
大澤賞・飯島賞受賞対象者講演　　発表 10分 ・ 質疑応答 10分
ポスタープレビュー　　発表 1分 ・ 質疑応答 なし

一般講演 (9:00-10:25)

大澤賞・飯島賞受賞対象者講演

2-1　Ni-Fe合金を用いた多層h-BNの成長制御とその成長メカニズム　23
＊内田 勇気, 仲村渠 翔, 河原 憲治, 山崎 重人, 光原 昌寿, 吾郷 浩樹

2-2　Visualization of local defects affecting electrical transport properties of large area graphene films via lock-in thermography　24
＊中島 秀朗, 森本 崇宏, 生田 美植, 沖川 侑揮, 山田 貴壽, 河原 憲治, 吾郷 浩樹, 岡崎 俊也

2-3　In Situ Study on Catalysts for Controlled Growth of Carbon Nanotubes　25
＊Feng Yang, Yan Li

2-4　Narrow-band thermal exciton radiation in single-walled carbon nanotubes　26
＊Taishi Nishihara, Akira Takakura, Yuhei Miyauchi, Kenichiro Itami

＞＞＞＞＞＞＞ 休憩 (10:25-10:45)＜＜＜＜＜＜＜

特別講演 (10:45-11:15)

2S-4　単層カーボンナノチューブのゲルカラムクロマトグラフィーによる分離とその応用　4
＊田中 丈士

一般講演 (11:15-11:30)

ナノチューブの生成と精製

2-5　繰り返し分散法によるSWCNTの低欠陥分散　27
＊片浦 弘道, 都築 真由美, 久保田 真理子, 杉田 知子, 王 国偉, 田中 丈士

ポスタープレビュー (11:30-12:15)　　(☆) 若手奨励賞候補

若手奨励賞候補

2P-1　General Method for the Synthesis of Transition-metal Dichalcogenide Nanoribbons Inside Carbon Nanotubes　77
☆　*＊Motoki Aizaki, Ellne Park, Zheng Liu, Kazu Suenaga, Yusuke Nakanishi, Hisanori Shinohara*

2P-2　Morphology-dependent Thermal Transport of Single-walled Carbon Nanotube Films　78
☆　*＊北野 拓也, 河合 壯, 野々口 斐之*

9月12日（水）

フラーレンの化学

ナノチューブの物性

9月12日（水）

ナノチューブの応用

ナノチューブの生成と精製

ナノホーン

グラフェン生成

グラフェンの物性

グラフェンの応用

9月12日（水）

原子層

ナノ炭素粒子

その他

＞＞＞＞＞＞＞ 昼食（12:15-13:30）＜＜＜＜＜＜＜

ポスターセッション（13:30-15:15）

13:30-14:00 若手奨励賞候補審査優先時間

授賞式（15:15-15:30）

総会（15:30-16:00）

9月12日（水）

特別講演（16:00-16:30）

＞＞＞＞＞＞＞ 休憩（16:30-16:45）＜＜＜＜＜＜＜

特別講演（16:45-17:15）

一般講演（17:15-17:45）

フラーレン

移動

懇親会（18:30-20:30）

9月13日（木）

特別講演　　発表 25分 ・ 質疑応答 5分
一般講演　　発表 10分 ・ 質疑応答 5分
ポスタープレビュー　　発表 1分 ・ 質疑応答 なし

一般講演 (9:00-9:30)

ナノチューブの応用

3-1　Progress Review on Single-walled Carbon Nanotube Electrodes in Flexible Photovoltaics　30
＊Il Jeon, Esko I. Kaupinnen, Yutaka Matsuo, Shigeo Maruyama

3-2　Lightweight Copper-matrix/Carbon Nanotube Composites with Electrical Performances Rivalling Copper　31
Rajyashree Sundaram, Guohai Chen, Takeo Yamada, Don Futaba, Kenji Hata, ＊Atsuko Sekiguchi

特別講演 (9:30-10:00)

3S-7　カーボンナノチューブ薄膜を用いた透明で柔軟なエネルギーハーベスター　7
＊大野 雄高

一般講演 (10:00-10:30)

ナノチューブの応用 ・ ナノチューブの物性

3-3　Flexible carbon nanotube ultraviolet sensing and memorizing array　32
Ting-Yu Qu, Yun Sun, Hui-Ming Cheng, ＊Dongming Sun

3-4　Molecular screening effects on exciton-carrier interactions in suspended carbon nanotubes　33
Takushi Uda, Shunsuke Tanaka, ＊Yuichiro K. Kato

＞＞＞＞＞＞＞ 休憩 (10:30-10:45) ＜＜＜＜＜＜＜

特別講演 (10:45-11:15)

3S-8　ナノカーボンテラヘルツ帯イメージャー
～マルチビュー・超回折限界計測と物質・生体非破壊分析～　8
＊河野 行雄

一般講演 (11:15-11:30)

ナノチューブの物性

3-5　単一カーボンナノチューブ量子ドットのテラヘルツ分光　34
＊吉田 健治, 鶴谷 琢磨, 矢島 史彬, 清水 麻希, 本間 芳和, 平川 一彦

ポスタープレビュー (11:30-12:15)　　(☆) 若手奨励賞候補

若手奨励賞候補

3P-1　Dynamic Behavior of a Single *but* Hydrogen-Bonded Water Molecule inside a Hydroxy Open-Cage Fullerene C_{60} Derivative　113
☆　*＊長谷川 翔大, 橋川 祥史, 村田 靖次郎*

9月13日（木）

フラーレンの応用

金属内包フラーレン

9月13日（木）

ナノチューブの物性

ナノチューブの応用

ナノチューブの生成と精製

グラフェン生成

グラフェンの応用

9月13日（木）

グラフェンの物性

原子層

バイオ

その他

＞＞＞＞＞＞＞ 昼食 (12:15-13:30) ＜＜＜＜＜＜＜

9月13日（木）

ポスターセッション（13:30-15:15）

13:30-14:00 若手奨励賞候補審査優先時間

特別講演（15:15-15:45）

一般講演（15:45-17:00）

原子層 ・ ナノチューブの生成と精製 ・ グラフェンの応用

September 11th, Tue.

Special Lecture: 25min (Presentation) + 5min (Discussion)
General Lecture: 10min (Presentation) + 5min (Discussion)
Poster Preview: 1min (Presentation)

General Lecture （ 9:00–9:30 ）

Bio ・ Environmental/Safety characterization of nanomaterials

1-1 Protein oxidation by carbon nanotubes is affected by metals originating from the catalyst 11
* *Atsushi Hirano, Momoyo Wada, Takeshi Tanaka, Hiromichi Kataura*

1-2 Complete Degradation of Carbon Nanomaterials by Using Hypochlorite 12
* *Minfang Zhang, Mei Yang, Hideaki Nakajima, Masako Yudasaka, Sumio Iijima, Toshiya Okazaki*

Special Lecture （ 9:30–10:00 ）

1S-1 Near-Infrared Photoluminescent Carbon Nanotubes for Imaging Brown Adipose Tissue 1
* *Masako Yudasaka*

General Lecture （ 10:00–10:30 ）

Applications of nanotubes ・ Atomic Layers

1-3 Brain Tissue Compatible Neural Probes Made from High Aspect Ratio (60:1) Free-Standing Carbon Nanotube Microelectrode Arrays 13
* *Guohai Chen, Don N. Futaba, Robert C. Davis*

1-4 Formation and Photophysical Properties of Transition Metal Dichalcogenide–Fullerene Nanohybrids on Semiconducting Electrodes 14
* *Tomokazu Umeyama, Jinseok Baek, Hiroshi Imahori*

＞＞＞＞＞＞＞ Coffee Break （ 10:30–10:45 ）＜＜＜＜＜＜＜

Special Lecture （ 10:45–11:15 ）

1S-2 Advanced STEM-EELS characterization of low-dimensional materials 2
* *Ryosuke Senga*

General Lecture （ 11:15–11:30 ）

Properties of graphene

1-5 Observation of Edge States of Graphene by FEM and FIM 15
* *Yahachi Saito, Yuhdai Watanabe, Tohru Hoshino, Hitoshi Nakahara*

Poster Preview （ 11:30–12:15 ） （☆）Candidates for the Young Scientist Poster Award

Candidates for the Young Scientist Poster Award

1P-1 ☆ Electronic and vibrational properties of boron-doped armchair graphene nanoribbons 41
* *Md Shafiqul Islam, Nguyen Tuan Hung, Ahmad Ridwan Tresna Nugraha, Riichiro Saito*

September 11th, Tue.

Chemistry of fullerenes

September 11th, Tue.

Properties of nanotubes

Applications of nanotubes

Formation and purification of nanotubes

September 11th, Tue.

Formation and purification of nanotubes・Endohedral nanotubes

Graphene synthesis

Applications of graphene

Properties of graphene

Atomic Layers

September 11th, Tue.

Carbon nanoparticles

Bio

＞＞＞＞＞＞＞ Lunch Time （ 12:15–13:30 ）＜＜＜＜＜＜＜

Poster Session （ 13:30–15:15 ）

During 13:30–14:00, please give priority to selection of candidates for Young Scientist Poster Award

Special Lecture （ 15:15–15:45 ）

General Lecture （ 15:45–16:30 ）

Properties of nanotubes ・ Properties of graphene ・ Atomic Layers

September 11th, Tue.

>>>>>>> Coffee Break（16:30-16:45）<<<<<<<

General Lecture（16:45-17:45）

Atomic Layers ・ Applications of graphene ・ Properties of graphene ・ Other topics

Exchange meeting with corporate exhibitors（17:45-19:00）

September 12th, Wed.

Special Lecture: 25min (Presentation) + 5min (Discussion)
General Lecture: 10min (Presentation) + 5min (Discussion)
Award Nominee Lecture: 10min (Presentation) + 10min (Discussion)
Poster Preview: 1min (Presentation)

General Lecture (9:00-10:25)

Lectures of Osawa Award and Iijima Award Nominees

2-1 Controlled growth of multilayer h-BN using Ni-Fe alloy and its growth mechanism 23
** Yuki Uchida, Sho Nakandakari, Kenji Kawahara, Shigeto Yamasaki, Masatoshi Mitsuhara, Hiroki Ago*

2-2 Visualization of local defects affecting electrical transport properties of large area graphene films via lock-in thermography 24
** Hideaki Nakajima, Takahiro Morimoto, Yoshiue Ikuta, Yuki Okigawa, Takatoshi Yamada, Kenji Kawahara, Hiroki Ago, Toshiya Okazaki*

2-3 In Situ Study on Catalysts for Controlled Growth of Carbon Nanotubes 25
** Feng Yang, Yan Li*

2-4 Narrow-band thermal exciton radiation in single-walled carbon nanotubes 26
** Taishi Nishihara, Akira Takakura, Yuhei Miyauchi, Kenichiro Itami*

>>>>>>> Coffee Break (10:25-10:45) <<<<<<<

Special Lecture (10:45-11:15)

2S-4 Separation of single-wall carbon nanotubes by gel column chromatography and their applications 4
** Takeshi Tanaka*

General Lecture (11:15-11:30)

Formation and purification of nanotubes

2-5 Low-defective dispersion of SWCNTs by repetitive sonication process 27
** Hiromichi Kataura, Mayumi Tsuzuki, Mariko Kubota, Tomoko Sugita, Guowei Wang, Takeshi Tanaka*

Poster Preview (11:30-12:15) (☆)Candidates for the Young Scientist Poster Award

Candidates for the Young Scientist Poster Award

2P-1 General Method for the Synthesis of Transition-metal Dichalcogenide Nanoribbons Inside Carbon Nanotubes 77
☆ ** Motoki Aizaki, Ellne Park, Zheng Liu, Kazu Suenaga, Yusuke Nakanishi, Hisanori Shinohara*

2P-2 Morphology-dependent Thermal Transport of Single-walled Carbon Nanotube Films 78
☆ ** Takuya Kitano, Tsuyoshi Kawai, Yoshiyuki Nonoguchi*

September 12th, Wed.

Chemistry of fullerenes

Properties of nanotubes

Applications of nanotubes

Formation and purification of nanotubes

Nanohorns

September 12th, Wed.

Graphene synthesis

Properties of graphene

Applications of graphene

Atomic Layers

Carbon nanoparticles

2P-35 Laser Induced Phosphorescence of Polyyne Molecules at 20 K 111
** Tomonari Wakabayashi, Kazunori Ozaki, Hal Suzuki, Yusuke Morisawa, Urszula Szczepaniak*

Other topics

2P-36 Correlation between Pore Size Distribution and Hydrogen Production in Thermal Catalytic Decomposition of Methane using Carbon Catalysts 112
** Dai Miyamoto, Yoshito Umeda, Hiroaki Hamaguchi, Masashi Suzuki, Toru Harigai, Tsuyoshi Tanimoto, Hirofumi Takikawa, Yoshiyuki Suda*

＞＞＞＞＞＞＞ Lunch Time （ 12:15–13:30 ）＜＜＜＜＜＜＜

Poster Session （ 13:30–15:15 ）

During 13:30–14:00, please give priority to selection of candidates for Young Scientist Poster Award

Awards Ceremony （ 15:15–15:30 ）

Genaral Meeting （ 15:30–16:00 ）

Special Lecture （ 16:00–16:30 ）

2S-5 Determination of temperature distribution on a carbon nanotube by transmission electron microscopy 5
** Kaori Hirahara, Michihiro Hashimoto*

＞＞＞＞＞＞＞ Coffee Break （ 16:30–16:45 ）＜＜＜＜＜＜＜

Special Lecture （ 16:45–17:15 ）

2S-6 Growth of spin-capable MWCNT forest and application of aligned CNT assemblies 6
** Yoku Inoue*

General Lecture （ 17:15–17:45 ）

Fullerenes

2-6 Electronic states of A_3C_{60} in the Mott boundary viewed from electrical transport 28
** Katsumi Tanigaki, Yuki Matsuda, Satoshi Heguri*

2-7 Achieving High Efficiency in Solution-Processed Perovskite Solar Cells using C_{60}/C_{70} Mixed Fullerenes 29
** Hao-Sheng Lin, Jeon Il, Shigeo Maruyama, Yutaka Matsuo*

Moving

Banquet （ 18:30–20:30 ）

September 13th, Thu.

Special Lecture: 25min (Presentation) + 5min (Discussion)
General Lecture: 10min (Presentation) + 5min (Discussion)
Poster Preview: 1min (Presentation)

General Lecture (9:00–9:30)

Applications of nanotubes

3–1 Progress Review on Single-walled Carbon Nanotube Electrodes in Flexible Photovoltaics 30
** Il Jeon, Esko I. Kaupinnen, Yutaka Matsuo, Shigeo Maruyama*

3–2 Lightweight Copper-matrix/Carbon Nanotube Composites with Electrical Performances Rivalling Copper 31
*Rajyashree Sundaram, Guohai Chen, Takeo Yamada, Don Futaba, Kenji Hata, * Atsuko Sekiguchi*

Special Lecture (9:30–10:00)

3S–7 Flexible and transparent energy harvesters with carbon nanotube thin films 7
** Yutaka Ohno*

General Lecture (10:00–10:30)

Applications of nanotubes ・ Properties of nanotubes

3–3 Flexible carbon nanotube ultraviolet sensing and memorizing array 32
*Ting-Yu Qu, Yun Sun, Hui-Ming Cheng, * Dongming Sun*

3–4 Molecular screening effects on exciton-carrier interactions in suspended carbon nanotubes 33
*Takushi Uda, Shunsuke Tanaka, * Yuichiro K. Kato*

＞＞＞＞＞＞＞ Coffee Break (10:30–10:45) ＜＜＜＜＜＜＜

Special Lecture (10:45–11:15)

3S–8 Nano-carbon terahertz imagers: Multi-view and super-resolution measurements and their applications to materials and biological non-destructive analysis 8
** Yukio Kawano*

General Lecture (11:15–11:30)

Properties of nanotubes

3–5 Terahertz spectroscopy of individual carbon nanotube quantum dots 34
** Kenji Yoshida, Takuma Tsurugaya, Fumiaki Yajima, Maki Shimizu, Yoshikazu Homma, Kazuhiko Hirakawa*

September 13th, Thu.

Poster Preview（11:30–12:15）（☆)Candidates for the Young Scientist Poster Award

Candidates for the Young Scientist Poster Award

September 13th, Thu.

Applications of fullerenes

Endohedral metallofullerenes

Properties of nanotubes

Applications of nanotubes

Formation and purification of nanotubes

Graphene synthesis

Applications of graphene

Properties of graphene

Atomic Layers

September 13th, Thu.

3P-32 Energetics and electronic structures of MoS_2 nanoribbons 144
** Hisaki Sawahata, Mina Maruyama, Susumu Okada*

3P-33 Fabrication and transport properties of PN diodes based on monolayer MoS_2/WSe_2 vertical heterostructures 145
** Shintaro Yoshimura, Yu Kobayashi, Takahiko Endo, Hong En Lim, Yutaka Maniwa, Yasumitsu Miyata*

3P-34 Resonance characteristics of the cantilevered BN by electrostatic actuation 146
** Daiki Yoshikawa, Kuniharu Takei, Takayuki Arie, Seiji Akita*

Bio

3P-35 Vibrational spectra of methylated forms of the cytosine in the region specific to hydrogen bonding relative to graphene pore interaction 147
** Tatiana Zolotoukhna, Toshihito Nitta*

Other topics

3P-36 First-principles study of magnetism in vanadium selenide thin films 148
** Mohammad Saeed Bahramy, Masaki Nakano, Satoshi Yoshida, Yue Wang, Hideki Matsuoka, Yuki Majima, Yuta Ohigashi, Yuta Kashiwabara, Masato Sakano, Kyoko Ishizaka, Yoshiro Iwasa*

>>>>>>> Lunch Time （12:15–13:30） <<<<<<<

Poster Session （13:30–15:15）

During 13:30–14:00, please give priority to selection of candidates for Young Scientist Poster Award

Special Lecture （15:15–15:45）

3S-9 Ab Initio Study on Chemical and Optical Properties of Single-Wall Carbon Nanotubes Adsorbed by Atoms and Molecules 9
** Mari Ohfuchi*

General Lecture （15:45–17:00）

Atomic Layers・Formation and purification of nanotubes・Applications of graphene

3-6 pH-dependent photoluminescence of monolayer transition-metal dichalcogenides in an aqueous solution 35
** Wenjin Zhang, Kazunari Matsuda, Yuhei Miyauchi*

3-7 Single-walled carbon nanotubes co-axially wrapped with mono- and few-layer boron nitride nanotubes and beyond 36
** Rong Xiang, Taiki Inoue, Yongjia Zheng, Akihito Kumamoto, Yuichi Ikuhara, Ming Liu, Yang Qian, Shohei Chiashi, Esko Kauppinen, Shigeo Maruyama*

September 13th, Thu.

特別講演
Special Lecture

1S – 1 ～ 1S – 3
2S – 4 ～ 2S – 6
3S – 7 ～ 3S – 9

1S-1

Near-Infrared Photoluminescent Carbon Nanotubes for Imaging Brown Adipose Tissue

Masako Yudasaka

Nanomaterials Research Institute, National Institute of Advanced Industrial Science and Technology, Tsukuba, Ibaraki 305-8565, Japan
Graduate School of Science and Technology, Meijo University, Nagoya 468-8502, Japan

Near-infrared (NIR) photoluminescent single-walled carbon nanotubes (CNTs) are effective bio-imaging agents, because the NIR light absorption and scattering in the body are weak, and autofluorescence intensity is low in NIR region. The CNT probes are studied for the vascular imaging in most cases; however, besides the vascular systems, they can also image brown adipose tissues (BATs), heat productive fats, by optimizing the CNT surface coating materials [1]. Moreover, the BAT imaging with CNTs reflects the body condition, namely, BATs of fasted mice were more brightly imaged by CNTs than those of non-fasted mice. Its mechanism is that the fasting induced the collagen bands disorders in the extracellular matrix as confirmed by the histological observation and gene analysis, and the collagen bands disorders resulted in the vascular permeability enhancement, therefore, the increase of extravasation of CNTs in BATs. These phenomena are difficult to be found without using CNTs, and these newly found phenomena may suggest another mechanism for the organisms to survive the starving.

As our study shows, CNTs are more valuable imaging agents than so far believed, especially as a probe for the flow dynamics in sub-tissue levels. Comparing with dye imaging agents, CNTs can stay in parenchyma of various organs for longer periods perhaps mainly due to the unique sizes and shapes, which enables to trace the flow movement in the parenchyma. For such studies, an essential equipment is the NIR fluorescent microscope. It is available now but needs more improvement to observe CNTs in individual cell. With the advances in the development of NIR fluorescent microscope as well as the CNT dispersion studies, CNT imaging probe could reveal the unknown phenomena in the body and contribute to reveal the mechanism of diseases, supporting the development of therapy methods.

[1] M. Yudasaka et al. Sci. Rep. 2017; 7: 44760.

Corresponding Authors: M. Yudasaka
E-mails: m-yudasaka@aist.go.jp

1S-2

Advanced STEM-EELS characterization of low-dimensional materials

○Ryosuke Senga[1]

[1] *Nanomaterial research institute, AIST, Tsukuba 305-8565, Japan*

The development of a monochromatic electron source for transmission electron microscopy (TEM) has pushed up the energy resolution to better than a few tens of millielectron volts, allowing us to identify the absorption peaks for optical and vibrational excitations involving the quantum effects by electron energy-loss spectroscopy (EELS) [1-4]. Therefore we can investigate the exciton behavior of a quantum object with a nanometer-scale resolution. In this study, the full range information of optical constants from an individual carbon nanotube with specific chirality has been successfully extracted by combining the optical absorption and EELS data [4]. The optical conductivity extracted from an electron energy-loss spectrum for a certain type of defect presents a characteristic modification near the lowest excitation peak (Fig. 1). The line-width of exciton peak shows a variety of broadening at different defect sites and suggests different degrees of shortening of its lifetime. Such local modulations of excitation behaviours at defects, which are the most essential factors for optoelectronic applications, have been discussed for long time but no experimental proof of the influence of different defects was available. Therefore our findings would be useful for further study to quantify the optoelectronic behaviors of nanoscale devices.

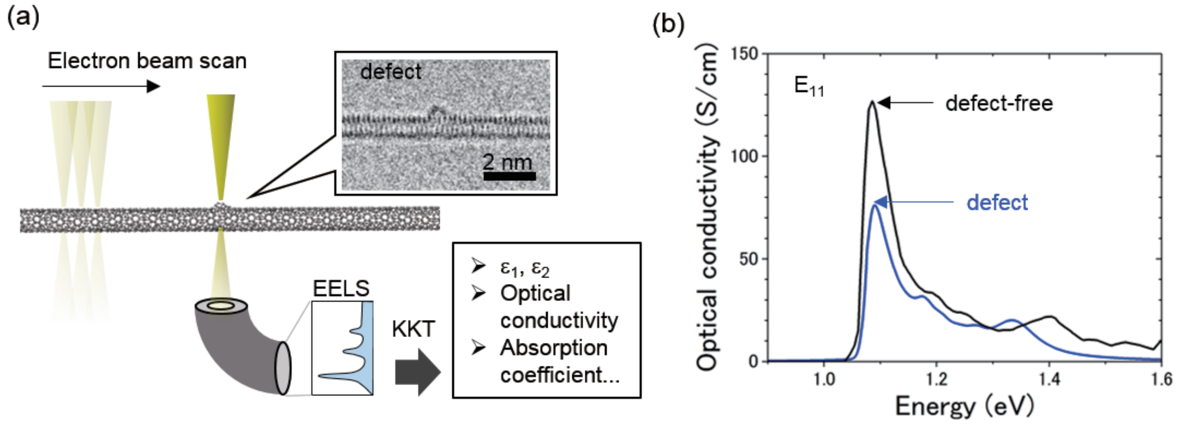

Fig. 1 High resolution EELS on an individual carbon nanotube. (a) Schematic of the experimental condition. The optical constants including optical conductivity as shown in (b) are extracted from EEL spectra obtained from individual defects through the Kramers-Kronig transformation (KKT).

[1] O. L. Krivanek *et al.*, Nature **514**, 209 (2014).
[2] R. Senga, T. Pichler and K. Suenaga, Nano Lett. **16**, 3661 (2016).
[3] F. S. Hage, T. P. Hardcastle, A. J. Scott, R. Brydson and Q. M. Ramasse, Phys. Rev. B **95**, 195411 (2017).
[4] R. Senga, T. Pichler, Y. Yomogida, T. Tanaka, H. Kataura and K. Suenaga, Nano Lett. **18**, 3920 (2018).

Corresponding Author: R. Senga
Tel: +81-29-862-6518
E-mail: ryosuke-senga@aist.go.jp

1S-3

Supramolecular doping of carbon nanotubes

○Yoshiyuki Nonoguchi[1,2]

[1] *Division of Materials Science, Nara Institute of Science and Technology, Ikoma 630-0192, Japan*
[2] *JST PRESTO, Kawaiguchi 332-0012, Japan*

Doping is a fundamental procedure in the ongoing investigation of the transport properties of conductors and semiconductors including carbon nanotubes. The carrier injection to carbon nanotubes modulates carrier concentration and polarity, which is essential for designing applications in carbon nanotube transistors, photovoltaics, and thermoelectrics. We have sought to elucidate the requirements for, and current challenges in, the doping of carbon nanotube films, particularly for studying their thermoelectric properties. This talk presents the elucidated principles for the chemical doping of carbon nanotubes and the stabilization of doped carbon nanotubes [1-7]. Supramolecular interactions are used for converting carbon nanotube films to their air-stable doped forms, and applying these doped films in the development of thermoelectric generators.

[1] Y. Nonoguchi *et al*. Sci. Rep., **3**, 3344 (2013).
[2] Y. Nonoguchi *et al*. Adv. Funct. Mater., **26**, 3021 (2016).
[3] Y. Nonoguchi *et al*. Chem. Asian J., **11**, 2423 (2016).
[4] Y. Nonoguchi *et al*. Small, **13**, 1603420 (2017).
[5] M. Nakano *et al*. Small, **13**, 1700804 (2017).
[6] Y. Nonoguchi *et al*. Chem. Commun., **53**, 10259 (2017).
[7] Y. Nonoguchi *et al*. J. Mater. Chem. A, DOI: 10.1039/C8TA03948H (2018).

Corresponding Author: Y. Nonoguchi
Tel: +81-743-72-6028, Fax: +81-743-72-6179,
Web: http://mswebs.naist.jp/LABs/kawai/index.html
E-mail: nonoguchi@ms.naist.jp

2S-4

Separation of single-wall carbon nanotubes by gel column chromatography and their applications.

○Takeshi Tanaka

Nanomaterials Research Institute, National Institute of Advanced Industrial Science and Technology (AIST), Tsukuba, Ibaraki 305-8565, Japan

Single-wall carbon nanotubes (SWCNTs) are promising material for various applications by their superior mechanical, electrical, optical properties. For the electrical and optical applications, separation of semiconducting SWCNTs from metallic ones is very important. We have developed the separation method of metallic/semiconducting and single-chirality semiconducting SWCNTs for the past decade. In this presentation, I will show the recent progress on the separation and scientific research and various applications using separated SWCNTs. Large-scale separation of single-chirality semiconducting SWCNTs was achieved using triple-mixed surfactant system on gel column chromatography [1]. This method could separate even enantiomers of single chiral semiconducting SWCNTs at high purity [2]. The separated SWCNTs enabled us to investigate excitonic band structure of semiconducting SWCNTs [2], enantiomeric purity of SWCNTs [3], and local optical properties of individual semiconducting SWCNT [4] as basic science. The separated semiconducting SWCNTs were also used for various applications, such as biological imaging [1,5], room-temperature single-photon emitter [6], and chemical sensors [7,8]. Details will be discussed in the presentation.

[1] Y. Yomogida, T. Tanaka, M. Zhang, M. Yudasaka, X. Wei, and H. Kataura, Nature Commun., **7**, 12056 (2016).

[2] X. Wei, T. Tanaka, Y. Yomogida, N. Sato, R. Saito, and H. Kataura, Nature Commun., **7**, 12899 (2016).

[3] X. Wei, T. Tanaka, T. Hirakawa, Y. Yomogida, and H. Kataura, J. Am. Chem. Soc. **139**, 16068 (2017).

[4] R. Senga, T. Pichler, Y. Yomogida, T. Tanaka, H. Kataura, and K. Suenaga, Nano Lett., **18**, 3920 (2018).

[5] M. Yudasaka, Y. Yomogida, M. Zhang, T. Tanaka, M. Nakahara, N. Kobayashi, Y. O. Ogura, K. Machida, K. Ishihara, K. Saeki and H. Kataura, Sci. Reports, **7**, 44760 (2017).

[6] X. He, N. F. Hartmann, X. Ma, Y. Kim, R. Ihly, J. L. Blackburn, W. Gao, J. Kono, Y. Yomogida, A. Hirano, T. Tanaka, H. Kataura, H. Htoon and S. K. Doorn, Nature Photonics **11**, 577 (2017).

[7] S. Ishihara, C. J. O'Kelly, T. Tanaka, H. Kataura, J. Labuta, Y. Shingaya, T. Nakayama, T. Ohsawa, T. Nakanishi, and T. M. Swager, ACS Appl. Mater. Interfaces **9**, 38062 (2017).

[8] S. Ishihara, J. Labuta, T. Nakanishi, T. Tanaka, and H. Kataura, ACS Sens. **2**, 1405 (2017).

Corresponding Author: T. Tanaka
Tel: +81-29-861-2903, Fax: +81-29-861-2786,
Web: https://staff.aist.go.jp/tanaka-t/index.html
E-mail: tanaka-t@aist.go.jp

2S-5

Determination of temperature distribution on a carbon nanotube by transmission electron microscopy

Michihiro Hashimoto[1], ○Kaori Hirahara[1, 2]

[1] *Department of Mechanical Engineering, Osaka University, Suita 565-0871, Japan*
[2] *Department of Physics, Graduate School of Science Tohoku University, Sendai 980-8578, Japan*

In previous studies, we focused on Joule-heating-assisted structural modulation of individual carbon nanotubes (CNTs) by in-situ transmission electron microscopy with a nanomanipulator system [1–6]. For example, plastic deformation of a CNT requires heat supply for cutting or reconnecting carbon–carbon bonds. Various type of processes, such as bending [1], cutting, sharpening [2], curing [3], superplastic elongation [4], and shrinking [5], have been carried out, and the results of those studies suggested that the amount of heat supplied is the one of the most important parameters governing the final structure of the product after the process. In addition, we have studied the filling process of metal nanoparticles in the hollow spaces of CNTs and found that the key factor controlling particle motion is the formation of a temperature gradient [6]. Therefore, it is essential to understand how this temperature gradient is formed for understanding the atomistic-level energetics of those processes. A few simple cases, for example, when a CNT is bridged between two large substances, have been discussed based on a model that describes the temperature distribution by using the one-dimensional equation of heat conduction assuming that both ends of the CNT are at room temperature. However, most practical cases are considerably more complicated. For example, it has been empirically shown that shorter CNTs are often difficult to process than longer ones. The degree of heat conductance at the interface between CNTs or at the CNT–substrate interface should be considered as well. In the metal loading process reported previously, a temperature gradient was created by connecting a CNT of diameter 2–4 nm to the tip of a thicker CNT of diameter ~20 nm. The maximum temperature is at the center of the thinner CNT [6], but it remained unclear as to how the gradient was formed in the actual system. In this study, we tried to visualize the temperature distribution of a single CNT during processing under heat supply by using metal nanoparticles as the thermometer. Multi-walled CNTs were supported on the edge of a thin silicon tip or on microgrids for TEM observation, and metal particles of diameter 5–20 nm were vacuum deposited on these CNTs. In the TEM, a platinum (or platinum-decorated silicon) probe was connected to the tip of a selected single CNT by operating the nanomanipulator. The bridged CNT was heated by Joule heating or by using a microheater equipped on the specimen stage, and structural changes in the CNT and metal particles with increasing temperature were monitored.

This work was supported by Research Grants in Natural Sciences of the Mitsubishi Foundation and JST CREST Grant Number JPMJCR1715, Japan.

[1] H. Somada *et al.*, Jpn. J. App. Phys. **46** 1055 (2007).
[2] H. Maruyama *et al.*, App. Phys. Ex. **3**, 0255101 (2010).
[3] S. Itaya *et al.*, Jpn. J. App. Phys. **51** 06FD22 (2012).
[4] K. Hirahara *et al.* App. Phys. Lett. **97**, 129903 (2010).
[5] K. Hirahara *et al.* Abstract of the 18th international microscopy congress (IMC 2014), MS-2-P-2898.
[6] R. Bekarevich, *et al.*, Nanoscale **8**, 7217 (2016); R. Bekarevich *et al.*, J. Phys. Chem C **121**, 9606 (2017).

Tel: +81-6-6879-7815, Fax: +81-6-6879-7815,
Web: http://www-ne.mech.eng.osaka-u.ac.jp/
E-mail: hirahara@mech.eng.osaka-u.ac.jp

2S-6

Growth of spin-capable MWCNT forest and application of aligned CNT assemblies

Yoku Inoue

Department of Electronics and Materials Science, Shizuoka University, Hamamatsu 432-8561, Japan

Dry-spin capability of carbon nanotube (CNT) forest has been attracting much interest because it enables very rapid unidirectional alignment of CNTs in large scale structures including yarns [1] and sheets [2]. Such CNT structures are expected to be used in wide variety of applications. We have been researching on the growth of dry-spin capable (spinnable) CNT forest and applications of the large scale CNT structures. The spinnable CNT forest requires strong van der Waals interaction between neighboring CNTs over a substrate. From such forest, continuous web is drawn out. Since all the CNTs are aligned in the drawn direction, fabricated yarns and sheets show high mechanical, electrical and thermal properties.

Our high density CNT forests are grown by catalytic chemical vapor deposition (CVD) on a substrate. $FeCl_2$ is used as a precursor of Fe catalyst nanoparticles [3]. The grown CNT has a multi-walled structure. Areal density is about $10^{10}cm^{-2}$ which allows all the CNTs bundled over the substrate and it results in high spinnability as shown in Fig.1. Several millimeter-long CNTs are connected each other and it forms a meter-long web. A CNT yarn was fabricated by twisting a CNT web in the same manner as conventional yarns. We found that those yarn properties are strongly influenced by CNT diameter, and smaller diameter CNTs result in higher electrical and mechanical properties in the yarns.

By stacking CNT webs, a unidirectionally aligned CNT sheet is formed (Fig.2). The sheet is robust and flexible, and acts as a preform for fabricating unique CNT-based applications, including structural and functional composite materials. On the other hand, when CNTs are composed in elastic polymer, it acts as a strain sensor [4]. Movements of nano-sized CNT-CNT contacts appear as variation of resistance of the composite. Highly aligned CNT structures by dry-spinning have been emerging as a key technology to bring CNT into industry.

[1] A. Ghemes *et al.*, Carbon **50**, 4579 (2012).
[2] Y. Inoue *et al.*, Carbon **49**, 2437 (2011).
[3] Y. Inoue *et al.*, Appl. Phys. Lett. **92**, 213113 (2009).
[4] K. Suzuki *et al.*, ACS Sensor **1**,817 (2016).

Corresponding Author: Y. Inoue
Tel: +81-53-478-1356
Web: http://cnt.eng.shizuoka.ac.jp/
E-mail: inoue.yoku@shizuoka.ac.jp

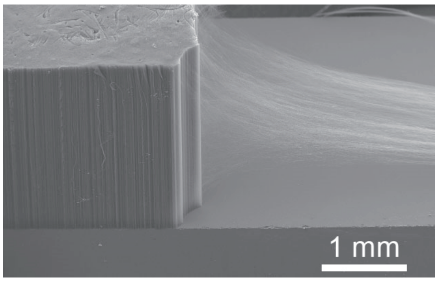

Fig. 1 CNT web is drawn from a dry-spin capable MWCNT forest.

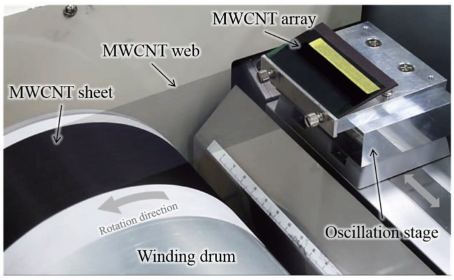

Fig. 2 Unidirectionally aligned CNT sheet is fabricated by stacking CNT webs.

Flexible and transparent energy harvesters with carbon nanotube thin films

Yutaka Ohno

Institute of Materials and Systems for Sustainability, Nagoya University, Nagoya 464-8603, Japan

Energy harvesting technologies, which harvest electricity from small energy sources existing in environment such as thermal energy, mechanical vibration, electromagnetic wave, fluidic energy, and so on, have been attracting much attention as the power source of the IoT devices distributed in various places. Carbon nanotubes (CNTs) are considered to be an important material for such energy harvesters, especially, for wearable self-powered device applications because of their excellent flexibility and stretchability. In this presentation, after reviewing the progress of energy harvesting technologies, recent results from our research on flexible/stretchable and transparent CNT-based energy harvesting sheets will be introduced.

Triboelectric generators, utilizing the contact electrification and electrostatic induction, are a kind of mechanical energy harvester. [1] By using carbon nanotube thin films that was covered with polydimethylsiloxane (PDMS), we have realized transparent and stretchable triboelectric generators. The output power as high as 8 W/m^2 was achieved by a surface treatment with CF_4 plasma. Some demonstrations such as driving 100 blue LEDs with a 5x5 cm^2 triboelectric generator, a generator-equipped gloves lighting with hand claps, and so on will be shown in the presentation.

Voltage generation from fluidic energy with a CNT thin film will also be presented. The generator consists of a CNT thin film formed on a plastic thin film and two electrodes formed on the both edge of the CNT thin film. When the droplets of the electrolyte solution moves on the CNT thin film, voltage generation takes place. The voltage generation phenomenon was previously reported with graphene. [2] Through the modeling of the voltage generation phenomenon, we found out that the thin film of purified semiconducting CNTs generates much higher output power than graphene does. A large area (15x15 cm^2) generator sheet fabricated with the spray coating technique demonstrated output power of 1 μW. We also demonstrated voltage generations from raindrops and waves, respectively.

Acknowledgment: The author thanks to Prof. H. Kataura of AIST, Prof. H. Ago of Kyusyu Univ., Prof. M. Ofuchi of Fujitsu Lab., collaborators of Nagoya Univ., and Meijo Nano Carbon Co., Ltd. for the fruitful collaborations and discussions. This work was supported by JST/CREST (JPMJCR16Q2).

[1] Z. L. Wang, *Mater. Today* **20**, 74 (2017).
[2] J. Yin *et. al.*, *Nat. Nanotechnol.* **9**, 378, (2014).

Corresponding Author: Y. Ohno
Tel & Fax: +81-52-789-5387
Web: http://qed63.qd.nuqe.nagoya-u.jp/
E-mail: yohno@nagoya-u.jp

3S-8

Nano-carbon terahertz imagers: Multi-view and super-resolution measurements and their applications to materials and biological non-destructive analysis

○Yukio Kawano

Laboratory for Future Interdisciplinary Research of Science and Technology, Department of Electrical and Electronic Engineering, Tokyo Institute of Technology, 2-12-1, Ookayama, Meguro-ku, Tokyo 152-8552, Japan

Sensing and imaging with terahertz (THz) waves have a great potential for the use in powerful non-destructive inspections. My talk will present our recent developments of two types of THz imaging methods: carbon-based THz flexible cameras [1-3] and plasmon-based near-field spectroscopic imagers [4-6]. Although most real objects have various three-dimensional curvatures, conventional THz imaging systems are mainly restricted to flat samples. We have developed a wideband, flexible and portable THz camera based on an array of carbon nanotube THz detectors, which has enabled multi-view THz inspections without using bulky systems. The latter part of my talk is devoted to explain plasmonic structures that are useful for evanescent-field detection and analysis in a subwavelength region. In spite of large availabilities, a main shortcoming of existing plasmonic devices is that they never show resonant frequency tunability for fixed structures. I introduce novel multi-frequency plasmonic structures and their applications to materials characterization and medical examination.

[1] D. Suzuki, S. Oda, and Y. Kawano, "A flexible and wearable terahertz scanner", *Nature Photonics* **10**, 809-814 (2016).

[2] D. Suzuki, Y. Ochiai, and Y. Kawano, "Thermal device design for a carbon nanotube terahertz camera", *ACS Omega* **3**, 3540–3547 (2018).

[3] D. Suzuki, Y. Ochiai, Y. Nakagawa, Y. Kuwahara, T. Saito, and Y. Kawano, "Fermi-level-controlled semiconducting-separated carbon nanotube films for flexible terahertz imagers", *ACS Applied Nano Materials* **1**, 2469–2475 (2018).

[4] Y. Kawano, "Chip-Based Near-Field Terahertz Microscopy", *IEEE Transactions on Terahertz Science and Technology* **6**, 356-364 (2016). (Invited paper)

[5] T. Iguchi, T. Sugaya, and Y. Kawano, "Silicon-immersed terahertz plasmonic structures", *Applied Physics Letters* **110**, 151105-1-4 (2017).

[6] X. Deng and Y. Kawano, "Surface Plasmon Polariton Graphene Mid-Infrared Photodetector with Multi-Frequency Resonance", *Journal of Nanophotonics* **12**, 026017-1-8 (2018).

Corresponding Author: Y. Kawano
Tel: +81-3-5734-3811, Fax: +81-3-5734-3811,
Web: http://diana.pe.titech.ac.jp/kawano/index.html
E-mail: kawano@ee.e.titech.ac.jp

3S-9

Ab Initio Study on Chemical and Optical Properties of Single-Wall Carbon Nanotubes Adsorbed by Atoms and Molecules

○Mari Ohfuchi[1]

[1] *Fujitsu Labs., Atsugi 243-0197, Japan*

Recently we can perform ab initio calculations for realistic models of chiral single-wall carbon nanotubes (SWCNTs). In the chirality separation experiments, for example, (5, 4) and (6, 4) nanotubes show a distinct red-shifted luminescence peak below E_{11}; however larger-diameter (8, 6) nanotubes have no pronounced peak at the level. This phenomenon is understood by studying the chemical reactions between O_2 molecules and SWCNTs with each chirality using ab initio methods. We found that the energy barrier from the physisorption of O_2 to the chemisorption is lower than that of the reverse reaction for (5, 4) and (6, 4) nanotubes, whereas the relation is opposite for (8, 6) nanotubes [1, 2]. One of the final products for the chemisorption gives slightly narrower band gap than that of pristine CNTs. For smaller-diameter (5, 4) SWCNTs, multiple emission peaks are also observed in addition to the original E_{11} peak in the photoluminescence spectrum.

The red-shifted E_{11} luminescence, called E_{11}*, is also observed from the SWCNTs exposed to ozone and light, and has attracted attention because of their greater luminescence quantum yield than that of pristine CNTs. In the recent bioimaging experiments, the E_{11}^{*-} emission whose energy is lower than that of E_{11}* increases its intensity with respect to E_{11}* as the ultraviolet (UV)/ozone irradiation time increases. To explain these experiments, we investigated the energetics and the optical transitions for complex O adsorption structures on (6,5) CNTs, including adsorption of two O atoms. We found two additional groups of optical transition levels for adsorption structures of two O atoms [3]. These results explain the multiple emission peaks and their irradiation time dependence in the photoluminescence (PL) spectra for CNTs oxidized by ultraviolet ozone, are also consistent with the PL measurements of SWCNTs oxidized by O_2 molecules during single chirality separation processes.

We also performed ab initio calculations for the adsorption of sodium dodecyl sulfate (SDS) surfactants onto (5, 5), (6, 5), and (10, 3) nanotubes to clarify the mechanism of metal/semiconductor separation of SWCNTs. How differently SDS surfactants behave on metallic and semiconducting CNTs is one of the fundamental questions in the science and application of CNTs. We found that dodecyl sulfate (DS) ions are more likely to adsorb onto SWCNTs than sodium (Na) ions or SDS molecules, whereas the adsorption energy of SDS molecules becomes stronger as the diameter of the SWCNTs increases, the adsorption energy of DS ions for metallic (5, 5) CNTs is much stronger than those for semiconducting (6, 5) or (10, 3) CNTs, causing a larger aggregation number of DS ions on metallic SWCNTs and a separation of SWCNTs by electronic type [4].

[1] M. Ohfuchi, J. Phys. Chem. C **119**, 13200 (2015).
[2] X. Wei *et al.*, J. Phys. Chem. C **120**, 10705 (2016).
[3] M. Ohfuchi and Y. Miyamoto, Carbon **114**, 418 (2017).
[4] M. Ohfuchi, J. Phys. Chem. C **122**, 4691 (2018).

Corresponding Author: M. Ohfuchi
Tel: +81-46-250-8194
E-mail: mari.ohfuti@jp.fujitsu.com

一般講演
General Lecture

1 – 1 ～ 1 – 12
2 – 1 ～ 2 – 7
3 – 1 ～ 3 – 10

1-1

Protein oxidation by carbon nanotubes is affected by metals originating from the catalyst

○Atsushi Hirano, Momoyo Wada, Takeshi Tanaka, Hiromichi Kataura

Nanomaterials Research Institute, National Institute of Advanced Industrial Science and Technology (AIST), Tsukuba, Ibaraki 305-8565, Japan

As-grown carbon nanotube (CNT) materials potentially induce oxidation of proteins; specifically, oxidation of protein sulfhydryl groups [1,2], leading to biotoxicity. However, effect of catalyst impurities contained in the CNT materials remains unclear. In this study, we found that the catalyst impurities along with CNTs induce oxidation of a sulfhydryl group, which were then ascribed to metals originating from the catalyst impurities. Numerical simulations of the oxidation indicate that the metal ions can mediates the redox reaction between CNTs and sulfhydryl groups, the rate of which is greater than that of the direct redox reaction between them. Both of CNTs and catalyst impurities are thus associated with their biological impacts in terms of oxidative stress on proteins.

We used cysteine (Cys) as a model compound with a sulfhydryl group to examine the oxidation by CNT (HiPco) samples. Fig.1a shows absorption spectra of the CNTs under the different conditions. Cys itself induced restoration of absorption spectrum, indicating reduction of the CNTs. However, the reduction was weakly but clearly suppressed in the presence of EDTA that is a chelating agent of metals. These results suggest that the reduction of the CNTs by Cys was mediated by coexisting metals. In fact, the addition of ferric ion led to obvious reduction of the CNTs in the presence of Cys even though ferric ion is oxidant. Consistent with the spectral measurement, time courses profiles showed a steep increase in absorbance at 1250 nm in the presence of Cys and ferric ion (Fig.1b). We proposed a kinetic reaction scheme for the reactions (Fig.2a). Time courses of the redox reaction of the CNTs were reproduced by numerical simulations on the basis of the reaction scheme (Fig.2b). Thus, the iron-mediated redox reaction is predominant over the direct redox reaction between CNTs and sulfhydryl groups.

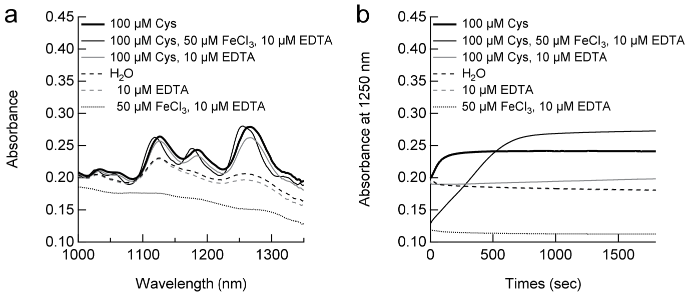

Fig. 1 Effect of iron ions on the redox reaction of the CNTs in the presence and absence of cysteine and EDTA. (a) Absorption spectra of the CNTs in the S_{11} region. (b) Time courses of absorbance values at 1250 nm.

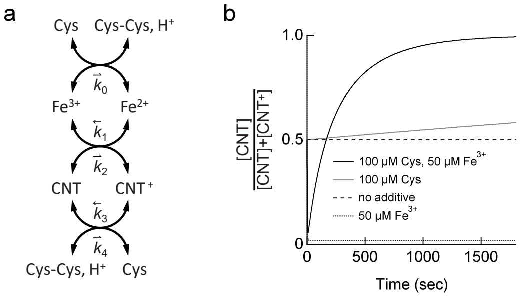

Fig. 2 Numerical simulations of the redox reactions of Cys with CNTs mediated by iron ions. (a) A proposed reaction scheme with reaction rate parameters (k). (b) Time courses of fractional concentrations of the reduced CNTs ([CNT]/([CNT]+[CNT$^+$])) under the different conditions.

[1] A. Hirano *et al.* J. Phys. Chem. Lett, **8**, 5216 (2017).

[2] A. Hirano *et al.* Nanoscale, **9**, 5389 (2017).

Corresponding Author: A. Hirano
Tel: +81-29-849-1064, Fax: +81-29-861-2786,
Web: https://staff.aist.go.jp/hirano-a/index.html
E-mail: hirano-a@aist.go.jp

Complete Degradation of Carbon Nanomaterials by Using Hypochlorite

Minfang Zhang[1*], Mei Yang[1], Hideaki Nakajima[1], Masako Yudasaka[1, 2],
Sumio Iijima[2], Toshiya Okazaki[1]

[1] National Institute of Advanced Industrial Science and Technology (AIST), 1-1-1 Higashi, Tsukuba, Ibaraki, 305-8565, Japan.

[2] Faculty of Science & Technology, Meijo University, 1-501 Shiogamaguchi, Tempaku-ku, Nagoya 468-8502, Japan.

Corresponding author: m-zhang@aist.go.jp

Carbon nanomaterials (CNM) containing carbon nanotubes (CNTs), carbon nanohorns and graphenes have been applied in a wide range of fields such as materials, electronics, energy storages, and biomedicine. More and more CNMs are produced and CNM-containing products are appearing in our daily life. It is estimated that the annual global market of only CNTs is the order of hundreds of tons now. With the increase of CNM industrialization, more and more CNM-contained wastewater would appear in many institute laboratories and industrial companies. On the other hand, the toxicity of CNM is still unclear and some adverse effects on human health have been reported. CNM-containing wastewater must be purified before being released into the environment and related rules or treatment process need to be urgently established. Unfortunately, no method has been reported so far. In this study, we have developed a simple method to eliminate CNM involved in industrial or laboratory wastewater using sodium hypochlorite. Hypochlorite has been considered to be a key oxidant in enzyme-catalyzed degradation of CNTs [1-2]. We have treated CNTs aqueous dispersions with sodium hypochlorite solution and found that CNTs can be degraded completely into carbon oxides. Since sodium hypochlorite is environmentally friendly and frequently used as a disinfectant or a bleaching agent in household cleaning, the method proposed here would be practically useful in the purification of CNM-contained industrial wastewater.

[1] B. L. Allen, G. P. Kotchey, Y. Chen, N. V. K. Yanamala, *et al*. J. Am. Chem. Soc. **131,** 17194 (2009).

[2] V. E. Kagan, N. V. Konduru, W. Feng, B. L. Allen, *et al.* Nature Nanotechnology 5, 354 (2010).

1-3

Brain Tissue Compatible Neural Probes Made from High Aspect Ratio (60:1) Free-Standing Carbon Nanotube Microelectrode Arrays

○Guohai Chen[1], Don N. Futaba[1], Robert C. Davis[2]

[1] CNT-Application Research Center, National Institute of Advanced Industrial Science and Technology (AIST), Tsukuba 305-8565, Japan
[2] Department of Physics and Astronomy, Brigham Young University, Provo, UT 84602, USA

Vertically aligned carbon nanotubes (VACNTs or forests) have obtained much attention due to its unique set of characteristics, such as long length, good alignment, and high specific surface area. As such, they have demonstrated numerous applications spanning from supercapacitors, dry adhesive, field emitters, through silicon vias, yarns, etc. Importantly, they have been shown as excellent candidates for electrodes/microelectrodes due to their combination of electrical conductivity, mechanical compliance, and surface area. However, due to mechanical requirements for VACNTs synthesis [1-2], directly growing high aspect ratio and free-standing VACNT posts (as microelectrodes) is challenging.

Here, we present the fabrication of a CNT-based neural probe using high aspect ratio (60:1) posts of CNT forests. The arrays of millimeter-tall, high aspect ratio, free-standing VACNT posts were synthesized through the assistance of a sacrificial CNT support structure (“hedge”). As a result, individual posts of millimeter-height and ~20 μm diameter were achieved. The electrochemical detection characterizations to both methyl viologen and dopamine were investigated using an individual VACNT post microelectrode [3]. In addition to the detection of the characteristic peaks, the VACNT microelectrode also showed fast-electrochemical response. Compared with conventional metal electrode post arrays, our CNT post arrays possess much more mechanical compliance with human tissue to avoid tissue damage/inflammation as well as higher surface to improve detection sensitivity. Our results represent one approach to overcome synthetic limitations to fabricate challenging structures.

[1] G.H. Chen *et al*. ACS Nano, **7** (11), 10218 (2013).
[2] G.H. Chen *et al*. Nanoscale, **8** (1), 162 (2016).
[3] G.H. Chen *et al*. ACS Biomater. Sci. Eng., **4** (5), 1900 (2018).

Corresponding Author: G.H. Chen
Tel: +81-29-861-4416
E-mail: guohai-chen@aist.go.jp

1-4

Formation and Photodynamic Behavior of Transition Metal Dichalcogenide–Fullerene Nanohybrids on Semiconducting Electrodes

○Tomokazu Umeyama[1], Baek Jinseok[1], Hiroshi Imahori[1,2]

[1] *Department of Molecular Engineering, Graduate School of Engineering, Kyoto University, Kyoto 615-8510, Japan*

[2] *Institute for Integrated Cell-Material Sciences (WPI-iCeMS), Kyoto University, Kyoto 606-8501, Japan*

Nanohybrid composites of C_{60} aggregates with transition metal dichalcogenide (TMD) nanosheets such as MoS_2 and WS_2 have been constructed by injecting a poor solvent, acetonitrile (MeCN), into the mixed dispersion of TMD and C_{60} in a good solvent, *N*-methylpyrrolidone (NMP). Furthermore, the composite films, where the TMD nanosheets are decorated with thin layers of C_{60} molecules, have been formed onto SnO_2 semiconducting electrodes by the electrophoretic technique using the composite aggregate dispersion in NMP/MeCN (Figure 1) [1].

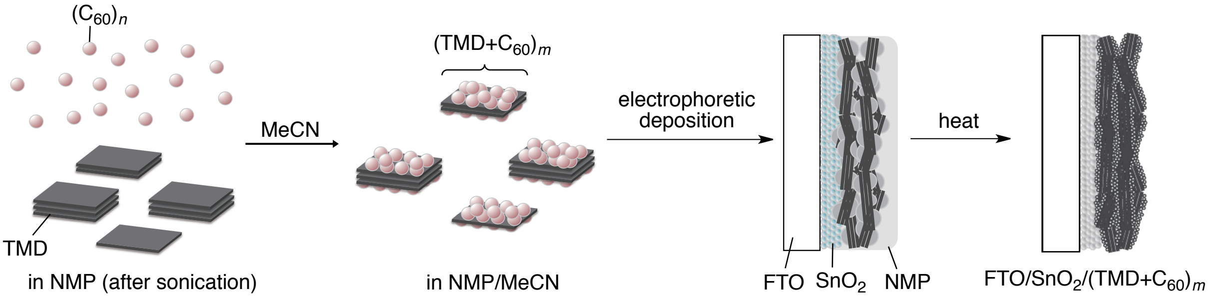

Figure 1. Formation and electrophoretic deposition of $(MoS_2+C_{60})_m$.

Time-resolved microwave conductivity (TRMC) measurements of the deposited materials revealed that photoexcitation of the composites exhibited much increased transient conductivities in comparison with single components of TMDs and C_{60}, indicating that the nanosized heterojunction structure of TMD and C_{60} promoted charge separation (CS). In addition, the decoration of the TMD nanosheets with C_{60} molecules hindered the undesirable charge recombination (CR) between an electron in the electrode and a hole in the TMD nanosheets. The accelerated CS between TMD and C_{60} and the suppressed CR due to the barrier effect of C_{60} thin layers significantly enhanced the photocurrent generation efficiencies in photoelectrochemical devices based on the MoS_2–C_{60} and WS_2–C_{60} composites up to 35% and 23% of incident photon-to-current (IPCE) values at 400 nm. The increment of IPCE in the device with the WS_2–C_{60} composite was smaller than that with MoS_2–C_{60} as a result of the inhomogeneous film structure originated from the strong interaction between WS_2 and C_{60}.

[1] J. Baek, T. Umeyama, W. Choi, Y. Tsutsui, H. Yamada, S. Seki, H. Imahori, *Chem. Eur. J.* **2018**, *24*, 1561.

Corresponding Author: T, Umeyama
Tel: +81-75-383-2568, Fax: +81-75-383-2571
Web: http://www.moleng.kyoto-u.ac.jp/~moleng_05/umeyama.html
E-mail: umeyama@scl.kyoto-u.ac.jp

1-5

Observation of Edge States of Graphene by FEM and FIM

Yahachi Saito[1]*, Yuhdai Watanabe[2], Tohru Hoshino[2], and Hitoshi Nakahara[2]

[1] Toyota Physical and Chemical Research Institute, Nagakute 480-1192, Japan
[2] Department of Applied Physics, Nagoya University, Nagoya 464-8603, Japan

Graphene is now attracting considerable attention as new material with two dimensionality and its peculiar electronic structures. Electronic states at graphene edges exhibit peculiar properties, e.g., localized states depending on the edge types (zigzag or armchair), and spin polarization (ferromagnetic order) at zigzag edge [1]. Field emission patterns from an open graphene edge show a striped pattern (or "lip pattern") consisting of an array of streaked spots; the direction of striation is perpendicular to the graphene sheet, and each stripe is divided into two wings by a central dark band running parallel to the graphene sheet. The "lip pattern" is considered to reflect the symmetry of π orbitals at a graphene edge. In addition to field emission microscopy (FEM), we have investigated graphene edges in atomic scale by field ion microscopy (FIM), which is complementary to FEM and gives higher spatial resolution than FEM.

Both FEM and FIM measurements are carried out using the same graphene edge. Typical FEM and FIM images of the same graphene emitter are shown in Figs. 1 (a) and (b), respectively. The FEM image (Fig. 1 (a)) exhibits a "lip pattern" characteristic to a graphene edge; array of two lobes elongated perpendicular to a graphene plane. The corresponding FIM image (Fig. 1 (b)) reveals more detailded structures because of higher spatial resolution; each streak in FEM is resolved into a pair of spots. The FIM image was taken using Ne as imaging gas. The direction of a line joining paired spots in FIM is perpendicular to the graphene plane, being similar to the case of FEM where streaks in FEM are elongated in the direction perpendicular to the graphene plane. Both of the FEM and FIM patterns show a mirror symmetry with a mirror plane along the central dark band (parallel to the graphene plane). Based on our previous studies on FEM of carbon emitters [2], the spacing between adjacent streaks in FEM and FIM is presumed to correspond with that of carbon atoms at the graphene edge. The image of paired bright spots extending to both sides of a graphene plane are considered to be formed by Ne atoms ionized in proximate to an unoccupied π*-orbital at the edge, as illustrated in Fig. 2. Thus, the FIM pattern is interpreted to represent a spatial distribution of the unoccupied edge states.

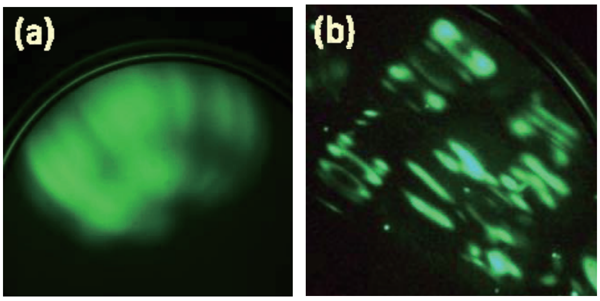

Fig. 1 (a) FEM and (b) FIM images of a graphene edge.

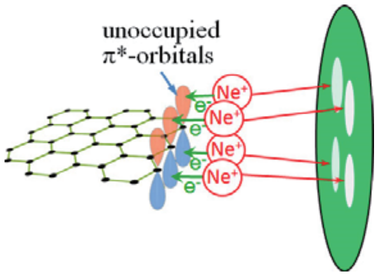

Fig. 2 Schematic illustrating the origin of FIM images of a graphene edge.

[1] M. Fujita, K. Wakabayashi, K. Nakada, and K. Kusakabe, J. Phys. Soc. Jpn. **65**, 1920 (1996)

[2] N. Yokoyama, K. Nakakubo, K. Iwata, K. Asaka, H. Nakahara, Y. Saito, Surf. Interface Anal. **48**, 1217 (2016)

*Tel: +81- 561-57-9616, Fax: +81- 561-63-6302, E-mail: ysaito@toyotariken.jp

Effective tube-length and density dependences on electric and mechanical properties of single-walled carbon nanotube fibers formed by wet-spinning

○Naoko Tajima[1], Takayuki Watanabe[1], Takahiro Morimoto[1], Kazufumi Kobashi[1],
Ken Mukai[1,2], Kinji Asaka[1,2], Toshiya Okazaki[1]

[1] *CNT Application Research Center, National Institute of Advanced Industrial Science and Technology (AIST), Tsukuba, Ibaraki 305-8565, Japan*
[2] *Inorganic Functional Materials Research Institute, National Institute of Advanced Industrial Science and Technology (AIST), Ikeda, Osaka 563-8577, Japan*

Among many applications of carbon nanotubes (CNTs), the production of fibers composed of CNTs offers a potential for high-strength and lightweight materials that are also thermally and electrically conductive. We have reported that the mechanical and electrical properties of CNT fibers by the wet spinning method are influenced by both the length of the constituent CNTs and the morphology of the fiber [1,2]. To elucidate the detailed mechanism, here we comprehensively investigate the CNT effective length and fiber density dependences on the electrical conductivity, fracture strength, and Young's modulus of CNT fibers.

We used single-walled CNTs synthesized by the enhanced direct-injection pyrolytic synthesis" method (eDIPS-CNTs) and dispersed them in a sodium taurodeoxycholate (TDOC) or a sodium-cholate (SC) aqueous solution. The eDIPS-CNT dispersions were prepared via three different dispersion methods: Homogenizer (a probe sonicator), Millser (Iwatani IFM-800DG), and Nanovater® (Yoshida Kikai NV C-ES008) [2].

CNT effective length, G/D value, and particle size (Stokes diameter) distribution were evaluated as CNT characteristics. The effective lengths are estimated according to the FIR spectra [3,4]. Particle size distribution of the "dispersion is measured using disk centrifuge (DC24000, CPS Instruments Inc.), which is based on differential sedimentation according to Stokes' law. The fiber density was obtained from the linear density and the cross-sectional area of the produced fibers.

The obtained electrical conductivities, fracture strengths and Young's moduli of the fibers were correlated well with the CNT effective lengths and the fiber densities, that is, CNT fibers having long effective length and high density show better properties. The quantitative analysis will be discussed in the symposium.

References
[1] X. Wu et al., J. Phys Chem. C 120, 20419 (2016).
[2] X. Wu et al., Appl. Phys. Exp. 10, 055101 (2017).
[3] T. Morimoto et al., ACS Nano, 8, 9897 (2014).
[4] T. Morimoto and T. Okazaki, Appl. Phys. Exp. 8, 055101 (2015).

Corresponding Author: Toshiya Okazaki
E-mail: toshi.okazaki@aist.go.jp

1-7

Control of chemical modification of graphene surfaces by substrate surface modification with self-assembled monolayers

Keiichiro Ikeda[1], ○Ryo Nouchi[1,2]

[1] Department of Physics and Electronics, Osaka Prefecture University, Sakai 599-8570, Japan
[2] PRESTO, Japan Science and Technology Agency, Kawaguchi 332-0012, Japan

Ultimate thinness of graphene is one of the most prominent features in its structure. The thinness enables us to change its characteristics by chemisorption of foreign atoms/molecules and to modulate an electron density in graphene by field-effect gating. Therefore, it is expected that the surface chemical modification of graphene can be controlled by such gating method. We have demonstrated that the degree of surface chemical modification of graphene is indeed controllable by electron density modulation of graphene [1,2]. In this study, we investigate on another methodology of field-effect gating, i.e., molecular gating by means of modification of the supporting substrate surface with a self-assembled monolayer (SAM). A local electric field generated by electric dipoles of the constituent molecules of SAMs [3] is found to control various chemical modification reactions of graphene.

We used two types of triethoxysilane molecules possessing antiparallel dipole moments. Single layer graphene was mechanically exfoliated on a SiO_2 substrate modified with SAMs of these molecules. Figure 1 shows results of molecular gate control of photochemical reactions based on benzoyl peroxide [4] deposited on graphene. In the Raman spectra acquired after UV irradiation, the *D* band, which is an indicator of the degree of chemical modification, was discernible only in the spectrum of graphene on the CH_3-SAM-modified substrate. Graphene on the CH_3 SAM should be more electron rich owing to the electrostatic effect (molecular gating effect) from the adjacent positive charge. Thus, graphene becomes more instable than the hole-rich one on the F SAM, leading to the higher reactivity. In the presentation, we will discuss other chemical modifications such as gas-phase photo-oxidation by atmospheric oxygen and liquid-phase modification by aryl diazonium salt.

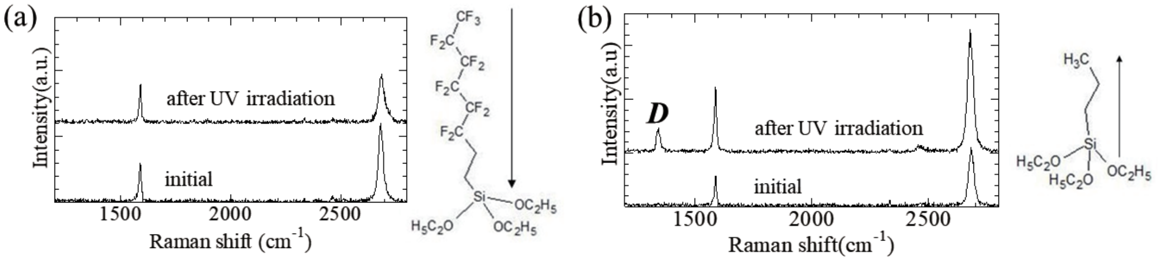

Fig. 1 Raman scattering spectra acquired before and after 10-min UV irradiation to graphene supported by SAM-modified SiO_2 substrates. The *D* band appeared only in graphene on CH_3-SAM-modified SiO_2 (b).

[1] X. Fan, R. Nouchi and K. Tanigaki, J. Phys. Chem. C **115**, 12960 (2011).
[2] N. Mitoma and R. Nouchi, Appl. Phys. Lett. **103**, 201605 (2013).
[3] K. Yokota, K. Takai and T. Enoki, Nano Lett. **11**, 3669 (2011).
[4] L. Haitao *et al.*, J. Am. Chem. Soc. **131**, 17099 (2009).

Corresponding Author: R. Nouchi
Tel: +81-72-254-8394, Fax: +81-72-254-8394,
Web: http://www.pe.osakafu-u.ac.jp/pe10/
E-mail: r-nouchi@pe.osakafu-u.ac.jp

1-8

Mesoscopic Thermoelectric Measurements of a 2D Metal-Organic Framework

Ryuichi Tsuchikawa[1], Neda Lotfizadeh[1], Shuwan Liu[1], Nabajit Lahiri[2], MacKenzie Lach[1],
Celine Slam[1], Janis Louie[2], Vikram Deshapnde[1]

[1]Department of Physics and Astronomy, University of Utah, USA
[2]Department of Chemistry, University of Utah, USA

Copper benzenehexathiol (Cu-BHT) is a hybrid compound categorized as two-dimensional (2D) metal-organic frameworks (MOFs), in which organic ligands are linked by metal ions to form a layered thin film. MOFs possess nanosized pores in the crystal, and applications to gas storage has been proposed due to a large surface to volume ratio. The freedom in choosing a different combination of metal ions and organic ligands allows us to design different MOFs using the same synthesis process [1,2]. Among MOFs, CuBHT is a unique MOF because it exhibits unusually high electrical conductivity [3]. We measured the thermal conductivity (κ), electrical conductivity (σ), and Seebeck coefficient (S) of thin flakes of Cu-BHT, and we found that the thermal conductivity of MOFs is intrinsically suppressed due to its high porosity. This selective suppression of phonons in a crystal can be utilized to improve the efficiency of thermoelectric energy conversion, i.e., to improve the thermoelectric figure of merit, $ZT = S^2\sigma T/\kappa$, where T is temperature. Along with its high electrical conductivity, CuBHT has a potential to be the next generation thermoelectric material.

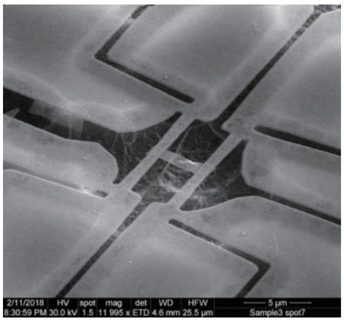

Figure 1: SEM image of the device used for the thermal conductivity measurement. A thin film of CuBHT is suspended

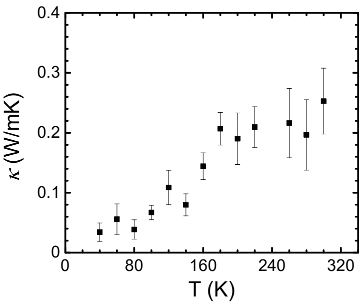

Figure 2: The temperature dependence of thermal conductivity of CuBHT

[1] H. Nishihara, et al., *J. Am. Chem. Soc.* **135**, 2462 (2013)
[2] N. Lahiri, N. Lotfizadeh, R. Tsuchikawa, V. V. Deshpande, J. Louie, *J. Am. Chem. Soc.* **139**, 19 (2017)
[3] X. Huang, et al., *Nat. commun.* **6**, 7408 (2013)

Corresponding Author: V. Deshpande
Tel: 801-581-6570
Web: https://sites.google.com/site/deshpandegrouputah/home
Email: vdesh@physics.utah.edu

1-9

In-situ measurement of WS_2 crystal growth with Au dot nucleation control

○Chao Li[1], Tomoya Kameyama[1], Toshiro Kaneko[1], Toshiaki Kato[1,2]

[1] *Department of Electronic Engineering, Tohoku University, Sendai 980-8579, Japan*
[2] *JST-PRESTO*

The discovery of graphene created a new era of two-dimensional (2D) material research because of the ultrathin thickness, high mechanical flexibility, and unprecedented novel optoelectronic properties. Nevertheless, the non-bandgap structure of graphene limits its practical applications as semiconductor devices [1]. Transition metal dichalcogenides (TMDs) known as another kind of 2D material, which possess monolayer structures as analogous atomic thickness as graphene. TMDs are expected to be applied on various kinds of semiconductor devices because of the tunable bandgap structure by layer number control. Especially, bright photoluminescence of TMDs makes them as the promising material for next generation optoelectrical applications. To fabricate the high performance optoelectrical devices, it is greatly urgent to synthesize high quality large size crystal [2]. However, the uncertain growth mechanism of TMDs makes it difficult to realize the ultra-large size synthesis of single crystal TMDs.

In our study, for the sake of the first stage of TMD growth mechanism elucidation, the quantitative estimation of TMD crystal growth was precisely conducted by introducing our unique nucleation control with Au-dot technology. As the result, in-situ measurement of WS_2 crystal growth has been successfully realized (Fig.1 (a) and (b)). From the results of in-situ measurements, the crystal growth speed at the initial growth stage is found to reach up to ~1.8×10^3 nm/s. It was also investigated that the growth speed attenuated with the crystal size increasing (Fig.1 (c)). The growth model was also created and the corresponding theoretical calculation was conducted. The result showed that the experimental result obtained from in-situ measurements was precisely fitted by the theoretical calculation (Fig.1 (d)), which means the validity of our established growth model.

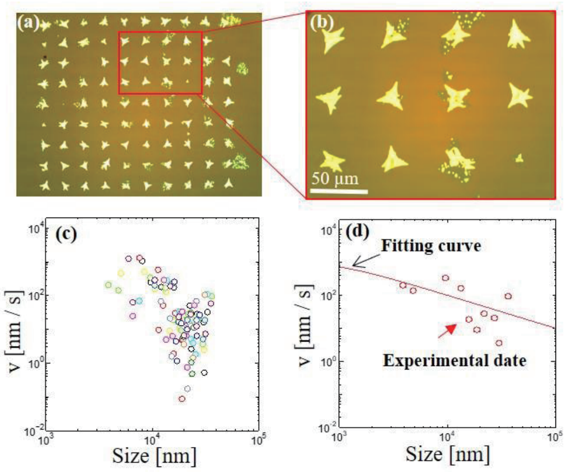

Fig. 1. (a) Low and (b) high magnification optical microscope image of WS_2 after CVD. (c) Plots of WS_2 growth speed (v) as a function of crystal size obtained by in-situ measurements. (d) Comparison of experimental data and theoretically obtained fitting curve.

[1] T. Kato and R. Hatakeyama: Nature Nanotechnology **7** (2012) 651.
[2] C. Li, Y. Yamaguchi, T. Kaneko, and T. Kato: Applied Physics Express **10** (2017) 075201.

Corresponding Author: C. Li
Tel: +81-22-795-7046, Fax: +81-22-263-9225,
E-mail: li15@ecei.tohoku.ac.jp

1-10

Extraordinarily stable supercapacitor electrodes with three-dimensional edge-free graphene walls

○Keita Nomura[1], Hirotomo Nishihara[1], Tomoya Shimura[1], Toshihiro Asada[2], Naoya Kobayashi[2], Takashi Kyotani[1]

[1] IMRAM in Tohoku University, Sendai 980-8577, Japan
[2] TOC Capacitors, Nagaoka 394-0035, Japan

Graphene is a two-dimensional (2D) material which has many fascinating features such as high theoretical surface area and chemical stability. However, graphene sheets are easily stacked by π–π interaction, resulting in the loss of such unique properties. Thus, assembling graphene sheets into 3D architectures especially equipped with mesopores without stacking has been a challenge. Our group has developed a unique mesoporous carbon, graphene mesosponge (GMS, Fig. 1) [1], consisting mostly of single-layer graphene walls. In this work, we demonstrate that GMS can be an extraordinarily stable electrode for supercapacitors.

GMS has been prepared according to the method previously reported [1]. As reference materials, activated carbon (YP50F) and reduced graphene oxide (rGO) were used. BET surface areas of GMS, YP50F, and rGO are 1800, 1650 and 450 m^2 g^{-1}, respectively. Fig. 2 shows the total amount of desorbed gases (H_2, CO, CO_2, and H_2O) during a temperature programmed desorption (TPD) run. In the TPD analysis, graphene edge sites which are terminated by hydrogen or oxygen-functional groups release the aforementioned gases, and therefore, the total gas evolution shown in Fig. 2 represents a measure of the amount of carbon edge sites. While YP50F and rGO have a large amount of edge sites and release a significant amount of gases, GMS does not, indicating the edge-free property of GMS. This is advantageous to achieve an excellent stability for electrochemical applications. The stability of GMS for supercapacitors was examined by using symmetrical two-electrode cells with a typical organic electrolyte (1.5 M Et_3MtNBF_4/PC). The cells were kept under a high voltage (3.5 V) and a high temperature (60 °C). This condition is really aggressive because general supercapacitors using activated carbon with organic electrolyte are easily collapsed over 3 V at room temperature. The capacitances of cells were monitored by temporarily stopping the durability test and measuring galvanostatic charge/discharge curves (5 mA/g) at 25 °C. The capacitance retention of GMS is much better than those of YP50F and rGO (Fig. 3). Thus, GMS is a promising material which enables a very high-voltage operation of supercapacitors.

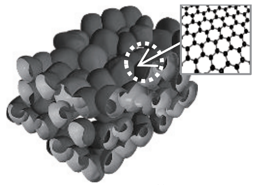

Fig. 1 Illustration of GMS.

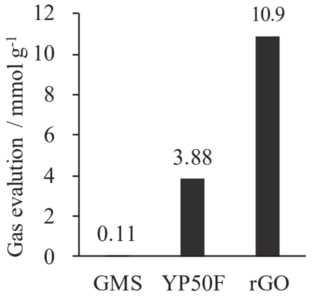

Fig. 2 The total gas evolution amounts of GMS, YP-50F and rGO during the TPD analysis up to 1800 °C.

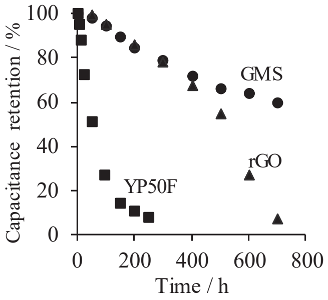

Fig. 3 Capacitance retention of GMS, YP-50F and rGO during the accelerated durability test under 3.5 V at 60 °C.

[1] Hirotomo Nishihara *et al.*, *Adv. Funct. Mater.*, **26** (2016), 6418-6427.

Corresponding Author: H. Nishihara
Tel: +81-22-217-5627, Fax: +81-22-217-5627,
Web: http://www.tagen.tohoku.ac.jp/labo/kyotani/index_e.html
E-mail: hirotomo.nishihara.b1@tohoku.ac.jp

1-11

Geometric and electronic structures of three-dimensional porous carbon networks

Y. Fujii[1], M. Maruyama[1], and S. Okada[1]
[1]*Graduate School of Pure and Applied Science, University of Tsukuba, 1-1-1 Tennodai,*
Tsukuba, Ibaraki305-8571, Japan

Physical properties of carbon allotropes and hydrocarbon materials are sensitive to their network topology arising basically from orbital hybridization of constituent C atoms. Diamond and graphene, which sorely consist of sp^3 and sp^2 C atoms, are an insulator and a zero-gap semiconductor, respectively. Mixing of C atoms with different orbital hybridizations endows the resultant covalent network with unique physical properties those are absent in the conventional allotropes or hydrocarbons. Indeed, our previous calculations demonstrated that two-dimensional covalent hydrocarbon networks consisting of sp^2 and sp^3 C atoms produce a Kagome band and Dirac cone at or near the Fermi level, depending on the shape and size of the sp^2 hydrocarbon networks inserted between adjacent sp^3 C atoms. In this work, we aim to theoretically design 3D covalent network of C and hydrocarbon, by assembling sp, sp^2, and sp^3 hybridized C atoms in the tetrahedral symmetry, as the possible structures of porous diamond networks, using the density functional theory with generalized grained approximation.

Figures 1(a) and 1(b) show 3D networks consisting of sp and sp^3 C atoms and sp^2 and sp^3 hydrocarbons, respectively. As for the networks consisting of sp and sp^3 C, the electronic structure strongly depends on the length of sp C chain. As for the hydrocarbon networks consisting of sp^2 and sp^3 C atoms, the networks are semiconductors with a direct bandgap, which depends on the length of sp^2 hydrocarbon units. In contrast, regardless of the chain length and hydrocarbons, they have the peculiar electronic structure near the Fermi level or band gap, which are characterized with a Dirac cone and two flat dispersion bands. Since these networks have the tetrahedral covalent networks, they are expected to possess high mechanical strength. However, owing to the sp or sp^2 C atoms bridging sp^3 C atoms, the network possess moderate or low Bulk modulus.

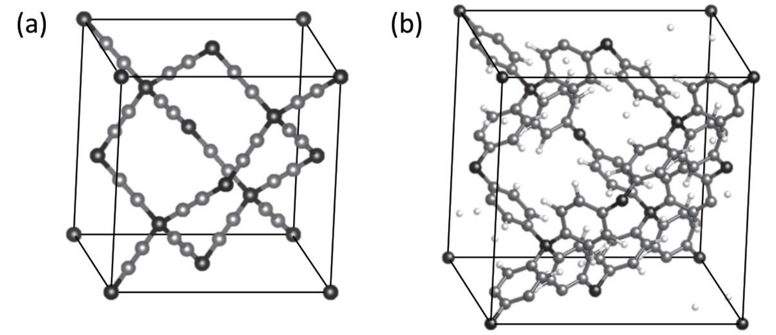

Fig. 1 Optimized structures of (a) a sp-sp^3 C network and (b) a sp^2-sp^3 hydrocarbon network. Dark gray, light gray, white spheres denote sp^3 C, sp/sp^2 C, and H atoms, respectively.

Corresponding author: Y. Fujii (yfujii@comas.frsc.tsukuba.ac.jp)

1-12

Development of combined ion trap ion mobility measurement system

Yudai Hoshino, Natsuki Terada, Fumiaki Uchiyama, Reona Miyamato, and ○Toshiki Sugai

Department of Chemistry, Toho University, Miyama 2-2-1 Funabashi, 274-8510, Japan

Ion mobility spectrometry (IMS) has been utilized to reveal novel structural information on nanomaterials[1]. To enhance the capability of IMS we have been working on an ion trap ion mobility (ITIMS) achieving long-term observation of nanomaterials up to 7 hours. However the information obtained by the method is restricted to structural one with low resolution. To get more information other measurement system should be combined together with higher structural resolution. Here we present newly developed combined ITIMS system to obtain optical and structural information with higher resolution.

The system consists of more than ten ion traps for high-resolution IMS, and one ionization laser and 4 excitation lasers with wavelengths 266, 405, 450, 532, and 650 nm with exchange stage for optical measurements. Nanomaterials such as graphene quantum dots and polystyrene particles with a diameters of 46 nm and fluorescent dye were ionized by the ionization laser and trapped in the system, and then were observed by a digital camera recording their emission induced by the excitation lasers on the exchange stage. Excitation and emission spectroscopy of the trapped nanomaterials were performed by changing the excitation laser and long-pass optical filter located in front of the camera.

Fig. 1 up shows observed trace image of the polystyrene particles through the long-pass filter with the various excitation lasers together with the dye excitation emission spectra. Apparently, when the excitation laser wavelength is within the scope of the dye excitation region (a, b) (Fig.1 down), the particle emission is observed whereas it is unobservable when out of the scope (c, d).

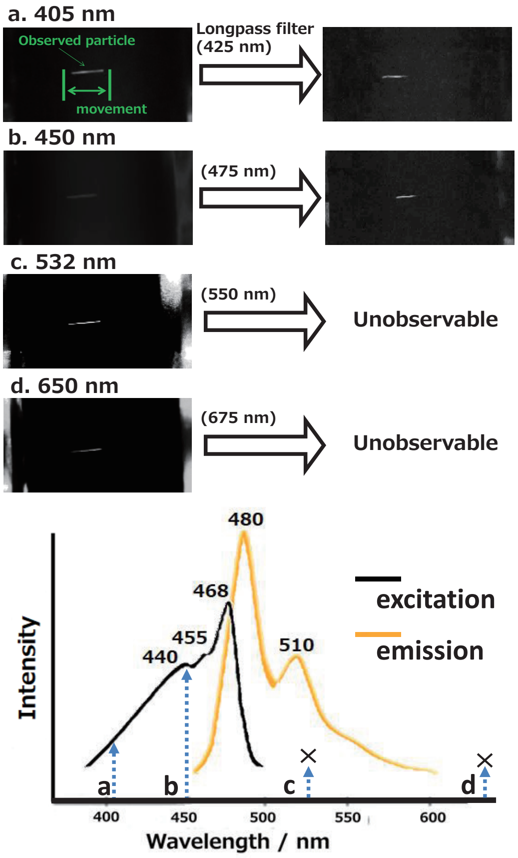

Fig. 1. Observed Emission of Polystyrene by Developed System and Excitation and Emission Spectra of 46 nm Polystyrene Particles with dye.

[1] T. Sugai *et al.*, *J. Am. Chem. Soc.* ***123***, 6427 (2001).

TEL: +81-47-472-4406, E-mail: sugai@chem.sci.toho-u.ac.jp

2-1

Controlled growth of multilayer h-BN using Ni-Fe alloy and its growth mechanism

○Yuki Uchida[1], Sho Nakandakari[1], Kenji Kawahara[2], Shigeto Yamasaki[1],
Masatoshi Mitsuhara[1], Hiroki Ago[1,2]

[1] *IGSES, Kyushu University, Fukuoka 816-8580, Japan*
[2] *Global Innovation Center (GIC). Kyushu University, Fukuoka 816-8580, Japan*

Multilayer h-BN has been widely recognized as an ideal substrate to bring out intrinsic properties of 2D materials [1,2]. Catalytic CVD method is expected to produce large-area h-BN films suitable for practical applications [3-5]. However, the uniform growth of multilayer h-BN is still a challenging issue, because it requires well controlled dissolution and segregation processes of B and N atoms. Recently, we have realized the uniform growth of multilayer h-BN using Ni-Fe alloy deposited on spinel by stabilizing the fcc structure and tuning the B, N solubilities (Figure 1) [6]. Moreover, our h-BN dramatically improved the optical property of WS_2.

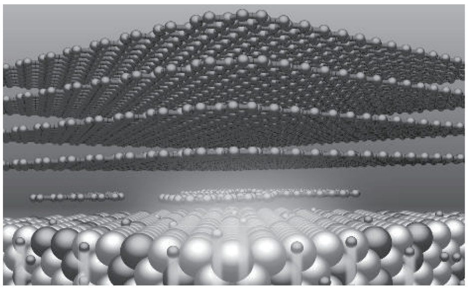

Fig. 1 Schematic growth model of multilayer h-BN on Ni-Fe alloy.

In this work, we systematically investigated the effect of crystal structure of Ni-Fe on the growth of h-BN. Interestingly, Ni-Fe/spinel(100) produced uniform multilayer h-BN, while multilayer h-BN was not observed on Ni-Fe/spinel(111) (Fig. 2a,b). The multilayer h-BN grown on the Ni-Fe/spinel(100) showed a well-defined layered structure with an interlayer distance of ~0.35 nm, corresponding to the h-BN structure (Fig. 2a inset). Based on electron back-scatter diffraction (EBSD) analysis, we found that introducing borazine ($B_3N_3H_6$) feedstock stimulates the conversion of crystal plane from fcc(100) to fcc(111) in the Ni-Fe/spinel(100), whereas Ni-Fe/spinel(111) shows no change of the crystal plane (Fig. 2c,d). We speculate that the packing density of the crystal plane before the $B_3H_6N_3$ supply is a key factor for the uniform segregation of multilayer h-BN. Our study presents that controlling surface crystal structure of the metal catalyst is necessary for the synthesis of uniform multilayer h-BN.

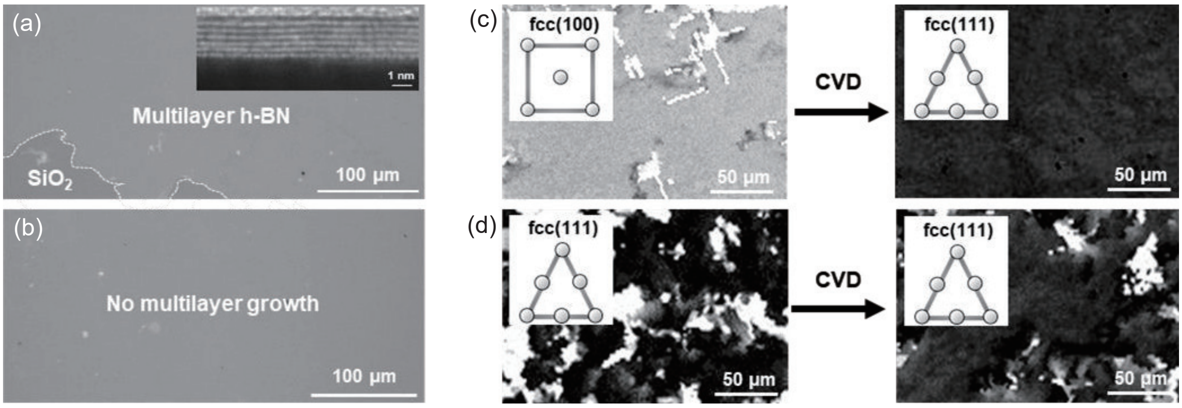

Fig. 2 Optical micrographs of h-BN transferred from Ni-Fe/spinel(100) (a) and (111) (b) to SiO_2/Si. Inset in (a) shows a cross-sectional TEM image of h-BN on Ni-Fe/spinel(100). EBSD images of Ni-Fe/spinel(100) (c) and (111) (d) before and after CVD.

[1] C. R. Dean *et al., Nat. Nanotechnol.*, **5**, 722 (2010). [2] M. Okada *et al., ACS Nano*, **8**, 8273 (2014). [3] Y. Uchida *et al., Phys. Chem. Chem. Phys.*, **19**, 8230 (2017). [4] H. Cho *et al., Sci. Rep.,* **5**, 11985 (2015). [5] S. M. Kim *et al., Nat. Commun.*, **6**, 8662 (2015). [6] Y. Uchida *et al., ACS Nano,* **12**, 6236 (2018).

2-2

Visualization of local defects affecting electrical transport properties of large area graphene films via lock-in thermography

○Hideaki Nakajima[1], Takahiro Morimoto[1], Yoshiue Ikuta[1], Yuki Okigawa[1],
Takatoshi Yamada[1], Kenji Kawahara[2], Hiroki Ago[2], and Toshiya Okazaki [1]

[1] *National Institute of Advanced Industrial Science and Technology, Tsukuba 305-8565, Japan*
[2] *Global Innovation Center, Kyushu University, Fukuoka 816-8580, Japan*

Large area graphene synthesis by chemical vapor deposition (CVD) method has rapidly progressed for realizing scalable device applications. Nevertheless, the existence of local defects seriously degrades its electrical transport properties. Although several experiments based on scanning tunneling microscopy have shown the influence of defects [1], only the limited area were investigated in those reports due to long measurement times. Recently, we have developed a novel measurement technique "lock-in thermography" (LIT) enabling fast and precise imaging of electrical characterization for large area carbon materials [2, 3]. Here, we demonstrate the visualization of local defects affecting electrical transport properties of large area CVD graphene films by LIT technique.

Figure (a) shows a fundamental concept of LIT. The bias voltage modulated at 25 Hz was applied to a single-layer CVD graphene with two electrodes, and the thermal radiation from sample was two-dimensionally imaged. By using lock-in detection, Joule heat component from the biased sample was detected separately from background heat storage.

An example of LIT image is indicated in Fig. (b). The white dashed lines correspond to edge of graphene, and domain boundary locations are identified as shown white arrows. The heat generation behaviors of LIT are strongly exhibited at boundary sites 1 and 2. Both boundaries show intense Raman D-bands (Fig. c), indicating that the observed thermal features are derived from boundary defects. In contrast, LIT shows a featureless thermal pattern at boundary site 3. Because of no D-band signature in the region, it is found that there is a seamless location. These results suggest that the LIT successfully images the electrical transport properties of domain boundaries over a mm-sized graphene film within a reasonable time frame (10 min.).

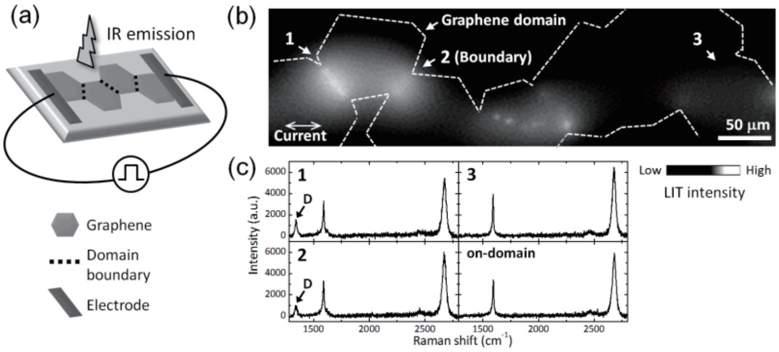

Figure (a) Schematic diagram of LIT. (b) LIT images with a single-layer CVD graphene epitaxially grown on a sapphire substrate. The sample was transferred onto a quartz substrate. (c) Raman spectrum at boundary locations 1-3.

[1] Q. Yu et al., Nat. Mater. **10**, 443 (2011). [2] T. Morimoto *et al.*, The 52nd FNTG General Symposium, 2-4 (2017).[3] H. Nakajima *et al.*, The 54th FNTG General Symposium, 3-8 (2018).

Corresponding Author: Toshiya Okazaki
Tel: +81-29-861-4173 / E-mail: toshi.okazaki@aist.go.jp

2-3

In Situ Study on Catalysts for Controlled Growth of Carbon Nanotubes

○Feng Yang, Yan Li
College of Chemistry and Molecular Engineering, Peking University, Beijing 100871, China

The structure-controlled growth of single-walled carbon nanotubes (SWNTs) is an important issue for their advanced applications. The catalysts play an essential role in controlling the structure of the SWNTs [1, 2]. Revealing the role of catalyst in the working environments is crucial for understanding the controlled growth mechanism. We developed a family of tungsten-based intermetallic compounds for chirality specific growth of SWNTs. The Co_7W_6 intermetallic compounds have high melting points (2400 °C) and very special crystal structure, acting as the structural templates with designed structures for growing SWNTs [3, 4].

Here, we demonstrated the structural and chemical stability of Co_7W_6 intermetallic catalysts at atomic level when feeding with carbon at high temperature (700-1100 °C). This was made possible by the use of using a state-of-the-art aberration-corrected environmental transmission electron microscope (ETEM) combined with *in situ* electron energy loss spectroscopy (EELS). We also established *in situ* synchrotron X-ray absorption spectroscopy (XAS) operated in the atmospheric-pressure CVD and demonstrated the stable local coordination structure of Co_7W_6. No carbide formation or carbon diffusion induced structural change was observed from these *in situ* characterization. Statistical *in/ex situ* measurements of the tube−catalyst interfaces showed that all the caps and SWNTs are perpendicular to the plane of the Co_7W_6 catalysts. These results demonstrate that Co_7W_6 catalysts act as the stable structure template for the chirality controlled growth of SWNTs.

Cobalt catalyzed the SWNT growth is generally believed to via a vapor–liquid–solid mechanism. Using Co as a model catalyst, we elucidated the synergetic role played by the cooperation of Co-Co_3C in catalyzing CVD growth of SWNTs. We recorded *in situ* and at the sub-angstrom level, the carburization of cobalt nanoparticle and formation of Co_3C play an essential role in the nucleation of carbon cap and consequent growth by ETEM. These findings are crucial for the rational design of catalysts for high efficiently catalyzing SWNTs.

[1] V. Jourdain and C. Bichara. Carbon, **58**, 2 (2013).
[2] M. Li, Y. Li *et al*. Top. Curr. Chem., **375**, 29 (2017).
[3] F. Yang, Y. Li *et al*. Nature, **510**, 522 (2014).
[4] F. Yang, Y. Li *et al*. Acc. Chem. Res., **49**, 606 (2016).

Corresponding Author: Yan Li
Tel: +86-10-62756773, Fax: +86-10-62756773,
Web: http://old.chem.pku.edu.cn/page/liy/
E-mail: yanli@pku.edu.cn

2-4

Narrow-band thermal exciton radiation in single-walled carbon nanotubes

○Taishi Nishihara[1,2], Akira Takakura[1,2], Yuhei Miyauchi[1,2,3], and Kenichiro Itami[1,2,4]

[1] *JST-ERATO, Itami Molecular Nanocarbon Project, Nagoya University, Nagoya 464-8602, Japan.*
[2] *Graduate School of Science, Nagoya University, Nagoya 464-8602, Japan.*
[3] *Institute of Advanced Energy, Kyoto University, Uji, Kyoto 611-0011, Japan.*
[4] *Institute of Transformative Bio-Molecules (WPI-ITbM), Nagoya University, Nagoya 464-8602, Japan.*

A number of intriguing photophysics arising from many-body quantum correlations have been discovered in single-walled carbon nanotubes (SWNTs). It has been experimentally revealed that excitons dominate the optical properties of SWNTs below room temperature. In contrast, thermal radiation, which is one of the fundamental optical properties, remains unclear because of some technical difficulties. The previous pioneering studies have reported light emission spectra consisting of broad peaks from individual SWNTs under Joule-heating conditions [1,2]. However, the carrier doping and current injection required to heat the nanotubes may considerably modify their one-dimensional quantum correlation effects [3], and the origin of the peak features (whether they are band-to-band or excitonic transitions) still remains debatable [1,2]. In addition, the possibility of competing electroluminescence mechanisms, including ambipolar carrier injection and impact excitation, further complicates the interpretation of light emission phenomena during current injection.

Here, we report the fundamental thermal radiation properties of intrinsic semiconducting and metallic SWNTs (S- and M-SWNTs) [4]. Individual SWNTs were suspended over an open slit in vacuum to suppress energy exchange with the surroundings. Continuous-wave laser irradiation was employed for heating SWNTs, which provided non-contact local heating while retaining the neutral charge balance of the SWNTs throughout the measurements. At 1,000–2,000 K, an intrinsic S-SWNT emitted linearly polarized, narrow-band near-infrared radiation (Fig. 1a), in contrast to its broadband radiation of a M-SWNT (Fig. 1b). We unambiguously confirmed that this narrow-band radiation is enabled by the thermal generation of excitons using the distinctive spectral difference between S- and M-SWNTs, and the simultaneous observation of the thermal radiation and the Rayleigh scattering spectra. In the presentation, universal features of thermal radiation of one-dimensional structures will be discussed.

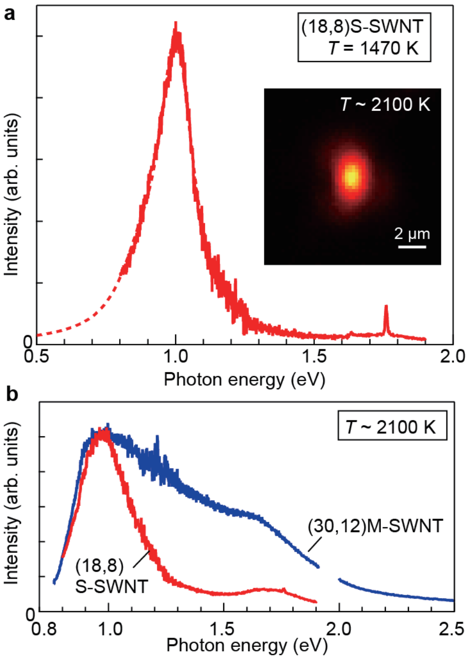

Fig.1 **a**, Thermal radiation of S-SWNT. **b,** Thermal radiation properties of S- and M-SWNTs.

[1] D. Mann, *et al.*, *Nat. Nanotech.* **2**, 33 (2007).
[2] Z. Liu, A. Bushmaker, M. Aykol, S. B. Cronin, *ACS Nano* **5**, 4634 (2011).
[3] Y. Miyauchi *et al.*, *Phys. Rev. B* **92**, 205407 (2015).
[4] T. Nishihara, A. Takakura, Y. Miyauchi, and K. Itami, *Nat. Commun.* accepted for publication.

Corresponding Authors: Y. Miyauchi, K. Itami Tel&Fax : +81-52-789-5916
E-mail: miyauchi@iae.kyoto-u.ac.jp, itami@chem.nagoya-u.ac.jp

Low-defective dispersion of SWCNTs by repetitive sonication process

○Hiromichi Kataura, Mayumi Tsuzuki, Mariko Kubota, Tomoko Sugita, Guowei Wang, and Takeshi Tanaka

Nanomaterials Research Institute (NMRI), AIST, Tsukuba 305-8565, Japan

Structural defects produced in single-wall carbon nanotube (SWCNT) have been crucial issue for developing high-mobility electronic devices. Since individually dispersed SWCNTs are inevitable for high-purity metal/semiconductor separation, we need to use strong sonication that quickly introduces serious defects on the SWCNT wall. At the previous FNTG symposium, we reported the effect of dissolved oxygen on the defect introduction to the SWCNT. In this presentation, we report the repetitive dispersion process which highly reduces the defect introduction. Recently, Noda *et al.* developed repetitive short-time dispersion and extraction process [1]. This process works well for the application of high-quality conducive film. However, it doesn't work for metal/ semiconductor separation because SWCNTs obtained are not individual. In this work, therefore, we have extended the method to obtain individually dispersed SWCNTs using strong sonication and ultracentrifugation process.

In this work, we used two different SWCNTs raw HiPco (D~1 nm, NanoIntegris) and raw EC1.5 (D~1.5nm, Meijo Nano carbon) without any purification. Soot of SWCNTs with concentration of 1 mg/ml was introduced to the 0.5 wt % sodium cholate aqueous solution. After short-time sonication, the solution was ultracentrifuged and collected upper 80% supernatant as individual SWCNTs. The sediment was collected and introduced in the sodium cholate aqueous solution and was sonicated and ultracentrifuged again for the second collection. This repetitive sonication-collection process was examined for different sonication time. Defects were monitored by Raman G/D ratio and photoluminescence intensity. AS a result, it was found that G/D value simply depends on the total sonication time. However, the total amount of individual SWCNTs obtained as supernatant was dependent on the number of ultracentrifugation. So that, shorter-time repetitive sonication process is better to get lower defective SWCNT solution. This result looks trivial but details were somewhat complicated and more interesting. We will show the latest results in the presentation.

Reference

[1] H. Shirae et al., Carbon 91 (2015) pp. 20 - 29.

Corresponding Author: Hiromichi Kataura
Tel: +81-29-861-2551
Web: http://kataura.html.xdomain.jp/index.html
E-mail: h-kataura@aist.go.jp

2-6

Electronic states of A_3C_{60} in the Mott boundary viewed from electrical transport

○**Katsumi Tanigaki**[1,2], **Yuki Matsuda**[2] **and Satoshi Heguri**[1]

[1] *AIMR, Tohoku University, Katahira 2-1-1, Aoba, Sendai, 980-8577, Japan*
[2] *Department of Physics, Graduate School of Science, Tohoku University, 6-3 Aramaki, Aoba-ku, Sendai 980-8578, Japan*

A similar Mott physics on unconventional superconductors, such as cuprates, Fe pnictides, and organic conductors is now claimed for expanded C_{60} superconductors, and electron-electron (e-e) interactions are thought to be very important origin of its high Tc superconductivity. On the other hand, the highest superconductivity surpassing the cuprates recently found in H_2S gives the discussion back to the electron-phonon (e-ph) mediated superconductivity for achieving high superconducting critical temperature (high T_c). The Fermi surface of A_3C_{60} (A=alkali metals) superconductors with expanded cell provides an intriguing research platform for both e-e and e-ph interactions. However, being different from other unconventional superconductors, electrical transport measurements had been very difficult for long years in expanded A_3C_{60} and made only for K_3C_{60} and Rb_3C_{60} with small cell size far apart from the Mott boundary, and hitherto important scientific discussion has been made based on only limited magnetic and optical probes. Here, we give intriguing first experimental results on accurate electrical resistivity ($\rho(T,P)$) for a variety A_3C_{60} with expanded under various temperature (T) and pressure (P). Electrical transport was carefully measured with straddling between the Mott insulator and the metallic/superconducting phase. A new phase diagram is proposed, which unambiguously shows an unprecedented new metallic state existing in the universal phase diagram.

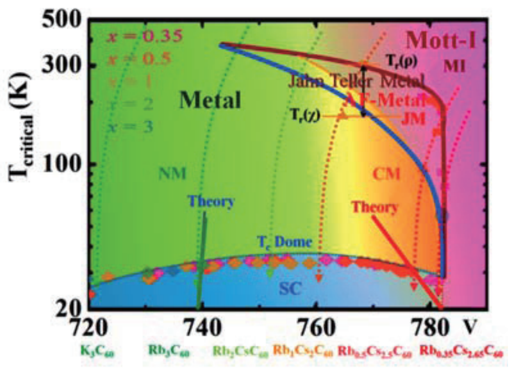

Fig. 1 A new phase diagram of A_3C_{60}.

[1]. S. Heguri and K. Tanigaki, Dalton Transactions, 47, 2881 (2018).

[2] Q. TN Phan, S. Heguri, H. Tamura, T. Nakano, Y. Nozue, K. Tanigaki, Phys. Rev. B 93, 075130 (2016).

[3] S. Heguri, N. Kawada, T. Fujisawa, A. Yamaguchi, A. Sumiyama, K. Tanigaki, M. Kobayashi, Phys. Rev. Lett. 114, 247201 (2015).

Corresponding Author: K. Tanigaki
Tel: +81-03-217--6166, Fax: +81-03-217-6167,
Web: http://sspns.phys.tohoku.ac.jp/
E-mail: tanigaki@tohoku.ac.jp

2-7

Achieving High Efficiency in Solution-Processed Perovskite Solar Cells using C_{60}/C_{70} Mixed Fullerenes

○Haosheng Lin [1], Il Jeon [1], Shigeo Maruyama [1], Yutaka Matsuo, [1,2]

[1] *Department of Mechanical Engineering, The University of Tokyo, Tokyo 113-8656, Japan*
[2] *Department of Chemistry, The University of Science and Technology of China, Hefei, Anhui, 230026, P. R. China*

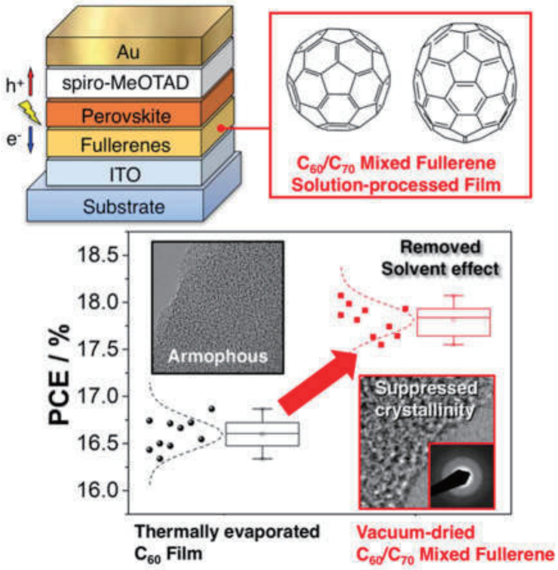

Fullerenes have attracted considerable interest as an electron transporting layer in perovskite solar cells. Fullerene-based perovskite solar cells produce no hysteresis and do not require high-temperature annealing. However, high power conversion efficiency can only be achieved when the fullerene layer is thermally evaporated, which is an expensive process. In this work, the limitations of a solution-processed fullerene layer have been identified as high crystallinity and the presence of remnant solvents, in contrast to a thermally deposited C_{60} film, which has low crystallinity and no remaining solvents. As a solution to these problems, a mixed C_{60} and C_{70} solution-processed film, which exhibits low crystallinity, is proposed as an electron transporting layer. The mixed-fullerene-based devices produce power conversion efficiencies as high as that of the thermally evaporated C_{60}-based device (16.7%), owing to improved fill factor and open-circuit voltage. In addition, by vacuum-drying the mixed fullerene film, the power conversion efficiency of the solution-processed perovskite solar cells is further improved to 18.0%. This improvement originates from the enhanced transmittance and charge transport by removing the solvent effect. This simple and low-cost method can be easily used in any type of solar cells with fullerene as the electron transporting layer.

Corresponding Author: Y. Matsuo
Tel: + 81-3-5841-0978,
E-mail: matsuo@photon.t.u-tokyo.ac.jp

Progress Review on Single-walled Carbon Nanotube Electrodes in Flexible Photovoltaics

○Il Jeon[1], Esko I. Kaupinnen[2], Yutaka Matsuo[1,3], Shigeo Maruyama[1.4]

[1] Department of Mechanical Engineering, The University of Tokyo, Tokyo 113-8656, Japan
[2] Department of Applied Physics, Aalto University School of Science, Aalto, FI-00076, Finland
[3] University of Science and Technology of China, Anhui 230026, China
[4] National Institute of Advanced Industrial Science and Technology, Ibaraki 305-8564, Japan

Energy is one of the biggest challenges that our society is facing. Global warming and energy crisis have prompted the society to look for pollution-free and infinitely renewable energy sources. Among the different renewable energies available, solar energy is by far the most abundant and clean energy source. It is no surprise that nature has taken advantage of this in the form of photosynthesis for the past billions of years. Photovoltaics, more generally known as solar cells, are semiconducting devices which convert solar energy to electricity, potentially meeting the demand of the world energy consumption while offsetting the carbon emissions. Solar cells have received much attention, especially in the last ten years due to emerging concerns about the energy crisis. Among different types of solar cells, thin-film solar cells are regarded to have the potential to lead the solar cell field with their power conversion efficiencies and flexible applications. However, they have problems of relying on inflexible and expensive indium tin oxide (ITO) transparent electrodes and metal electrodes.

Single-walled Carbon nanotubes (SWNTs) have emerged as materials for next-generation electrodes in thin-film solar cells, offering a possible alternative to the ITO and metal electrodes. SWNTs have excellent mechanical flexibility and are composed entirely of naturally abundant carbon. Therefore, SWNT conductive films in thin-film solar cells have been the subject of active research, which continues to this day. With the improvement on the properties of SWNTs in both synthetic and engineering levels, a remarkable advancement is expected to be made in the field of flexible thin-film solar cells.

In this presentation, we review the research progress made by our group in this area of research. We discuss different aspects that are key to successful substitution of the conventional electrodes by the next-generation SWNT electrodes.

Corresponding Author: S. Maruyama
Tel: + 81-3-5841-6421, Fax: + 81-3-5800-6983,
Web: http://www.photon.t.u-tokyo.ac.jp/~maruyama
E-mail: maruyama@photon.t.u-tokyo.ac.jp

3-2

Lightweight Copper-matrix/Carbon Nanotube Composites with Electrical Performances Rivalling Copper

Rajyashree Sundaram[1], Guohai Chen[1], Takeo Yamada[1], Don Futaba[1], Kenji Hata[1], ○Atsuko Sekiguchi[1]

[1] CNT-Application Research Center, National Institute of Advanced Industrial Science and Technology, Tsukuba 305-8565, Japan

We present lightweight copper-matrix carbon nanotube composites (Cu/CNT) with electrical performances competitive to Cu as next-generation Cu-substitutes. Our Cu/singlewall (SW)CNT, 2/3rd as light as copper, show room-temperature electrical resistivities (ρ) as low as 3.3×10^{-6} Ohm cm (~ × $2\rho_{Cu}$). The composite electrical resistivities are more stable to temperature than Cu with temperature coefficient of resistivity (TCR) values as low as 4.4×10^{-4} /K (~10% TCR_{Cu}). We note that the Cu/SWCNT electrical performances are markedly better than that of Cu/MWCNT composites we previously reported [1-3] with $\rho_{Cu/MWCNT} \sim 10\rho_{Cu}$ and $TCR_{Cu/MWCNT} \sim 50\%\ TCR_{Cu}$.

We fabricated Cu/SWCNT with these excellent electrical performances in different forms - as microscale pillars and macroscopic wires. We believe these composites have the potential to fulfill a growing need for lightweight electrically conducting Cu-substitutes. Our microscale Cu/CNT pillars could serve as better vertical interconnects than copper in electronic devices, aiding miniaturization with increased functionality. On the other hand, our macroscopic composite wires could replace heavy copper electrical wiring in aircrafts and automobiles for improved fuel efficiencies. The temperature-stable resistivity (low TCR) is particularly sought after for reliable high-temperature operation e.g., in motor windings.

[1] R. Sundaram *et al*. Sci. Rep., **7(1)**, 9267 (2017).
[2] R. Sundaram *et al*. Mater. Tod., Commun., **13**, 119 (2017).
[3] R. Sundaram *et al*. Jpn. J. Appl. Phys., **57(4)**, 04FP08 (2018).

Corresponding Author: A. Sekiguchi
Tel: +81-29-861-4551, Fax: +81-29-861-4851
Web: https://www.nanocarbon.jp/about/members/sekiguchi
E-mail: atsuko-sekiguchi@aist.go.jp

3-3

Flexible carbon nanotube ultraviolet sensing and memorizing array

Ting-Yu Qu[1], Yun Sun[1], Hui-Ming Cheng[1,2], ○Dong-Ming Sun[1,3]*

[1] Shenyang National Laboratory for Materials Science, Institute of Metal Research, Chinese Academy of Sciences, Shenyang 110016, China
[2] Tsinghua-Berkeley Shenzhen Institute, Tsinghua University, Shenzhen 518055, China
[3] Institute of Materials and Systems for Sustainability, Nagoya University, Nagoya 464-8603, Japan

Flexible non-volatile light sensing and memorizing functional device is a key component for future wearable electronics systems, however, such a device has not yet emerged up to date mainly constrained by two challenges in conventional nano-floating gate memory. One is the lacking of direct tunneling for charge trapping, the other is the existing of current leakage under a deformable environment. Here, we report a flexible carbon nanotube (CNT) non-volatile memory and ultraviolet detector using individual aluminum nanoparticles (Al NPs) as the nano-floating gate and ultra-thin oxidized alumina grown on the surface of each individual Al NPs as the tunneling layer. The fabricated memory exhibits a high on-off current ratio (> 10^5), a long-term extrapolated retention (> 10^8 s) and a durable flexibility at a 0.4% bending strain. In addition, a novel sensing and memorizing image system for ultraviolet illumination has been successfully demonstrated, showing a non-volatile photogenerated on-off current ratio up to 10^2 for an illumination time of 1 s and a sensing signal storage period up to 10 years. Our study will open up a new opportunity for future scalable manufacturing of flexible visual memories.

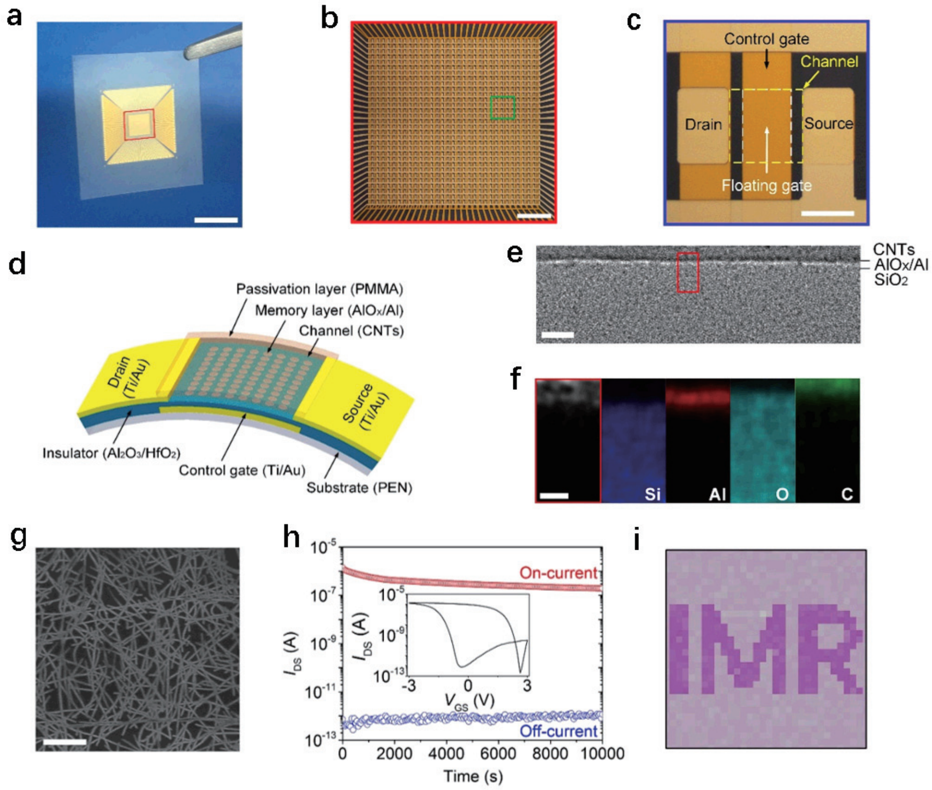

Fig. 1 Flexible CNT ultraviolet sensing and memorizing array. (a) Optical photograph of a chip (scale bar, 5 mm). (b) Micrograph of the 32 × 32 arrays (scale bar, 500 µm). (c) Single pixel (scale bar, 50 µm). (d) Schematics. (e) HRTEM image (scale bar, 10 nm). (f) HAADF-STEM and elemental mapping (scale bar, 3 nm). (g) SEM image of CNT channel (scale bar, 500 nm). (h) Retention and transfer characteristics. (i) Current distributions after an illumination.

[1] B. Wang *et al*. Adv. Mater., 1802057 (2018).
[2] Y, Chen *et al*. Adv. Sci., 1700965 (2018).
[3] T, Qu *et al*. In submission (2018).

Corresponding Author: D. Sun
E-mail: dmsun@imr.ac.cn

3-4

Molecular screening effects on exciton-carrier interactions in suspended carbon nanotubes

Takushi Uda[1,2], Shunsuke Tanaka[1,3], ○Yuichiro K. Kato[1,3]

[1] Nanoscale Quantum Photonics Laboratory, RIKEN Cluster for Pioneering Research,
Saitama 351-0198, Japan
[2] Department of Applied Physics, The University of Tokyo, Tokyo 113-8656, Japan
[3] Quantum Optoelectronics Research Team, RIKEN Center for Advanced Photonics,
Saitama 351-0198, Japan

Photoluminescence spectroscopy measurements are performed on suspended carbon nanotubes in a field-effect configuration, and the gate voltage dependence of photoluminescence spectra are compared for the pristine and the molecularly adsorbed states of the nanotubes [1]. We quantify the molecular screening effect on the trion binding energies by determining the energy separation between the bright exciton and the trion emission energies [2] for the two states (Fig. 1). The voltage dependence shows narrower voltage regions of constant photoluminescence intensity for the adsorbed states, consistent with a reduction in the electronic bandgap due to screening effects. The charge neutrality points are found to shift after molecular adsorption, which suggests changes in the nanotube chemical potential or the contact metal work function. The molecular screening effects allow for drastic spectral modifications, offering a new degree of freedom for nanoscale photonic devices [3,4].

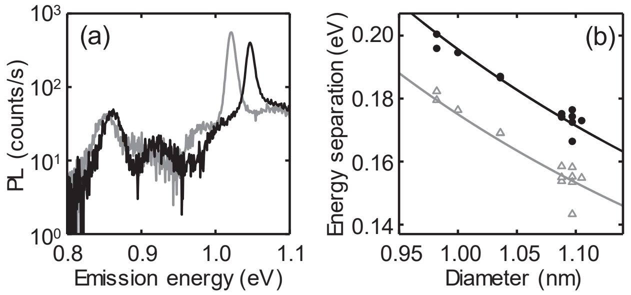

Fig.1 (a) PL spectra of a (10,5) tube in the pristine (black curve) and the adsorbed state (gray curve) taken under V_g = -1.5 V. (b) Diameter dependence of the energy separation between the exciton and the trion states for the pristine states (black dots) and the adsorbed states (gray triangles).

Work supported in part by JSPS (KAKENHI JP16H05962) and MEXT (Photon Frontier Network Program, Nanotechnology Platform). T.U. is supported by ALPS and JSPS Research Fellowship. We thank the Advanced Manufacturing Support Team at RIKEN for technical assistance.

[1] T. Uda, S. Tanaka, and Y. K. Kato, arXiv:1806.11239 (2018).
[2] M. Yoshida, A. Popert and Y. K. Kato, *Phys. Rev. B.* **93**, 041402(R) (2016).
[3] T. Uda, A. Ishii and Y. K. Kato, *ACS Photonics* **5**, 559 (2018).
[4] H. Machiya, T. Uda, A. Ishii and Y. K. Kato, *Appl. Phys. Lett.* **112**, 021101 (2018).

Corresponding Author: Yuichiro K. Kato
Tel: +81-48-462-1449
Web: http://katogroup.riken.jp/
E-mail: yuichiro.kato@riken.jp

3-5

Terahertz spectroscopy of individual carbon nanotube quantum dots

○Kenji Yoshida,[1] Takuma Tsurugaya, [1] Fumiaki Yajima,[2] Maki Shimizu,[2]
Yoshikazu Homma,[2] and Kazuhiko Hirakawa[1,3]

[1]*Institute of Industrial Science, University of Tokyo, Tokyo 153-8505, Japan*

[2]*Department of Physics and Research Institute for Science & Technology, Tokyo University of Science, Tokyo 162-8601, Japan*

[3]*Institute for Nano Quantum Information Electronics, University of Tokyo, Tokyo 153-8505, Japan*

Characteristic energies in carbon nanotubes (CNTs) lie in the terahertz (THz) frequency range. In addition, when a zero-dimensional quantum dot (QD) is formed in a CNT, other energy scales such as orbital quantization and vibrational excitation, also fall into the THz range. Therefore, THz spectroscopy is an ideal tool for investigating electronic structures and carrier dynamics of CNTs. However, most of the works on the THz spectroscopy have so far been performed on CNT films or bundles, which inevitably result in strong inhomogeneous broadening. Although a few attempts on THz response of individual CNTs were made in the past [1, 2], the THz properties of individual CNTs is still unclear.

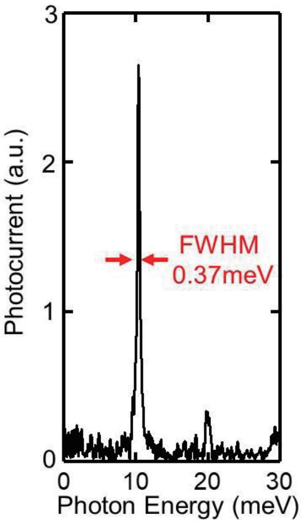

Fig. 1. A THz spectrum obtained from an individual carbon nanotube quantum dot.

We have investigated THz response of individual, short metallic CNTs of various lengths by using a transistor geometry and achieved THz-spectroscopy of CNTs at the individual level. By employing metal source-drain electrodes of a bow-tie antenna shape separated by a submicron gap, we efficiently focused broadband THz radiation radiation onto individual CNTs. Transport properties of the fabricated devices indicate that the CNTs act as QDs. We measured the spectra of THz-induced photocurrent generated in the CNT-QDs and found that there appears a sharp resonant peak. The photon energy of the peak shows a clear dependence on the CNT lengths and is in agreement with the bare quantum confined energies expected from the Fermi velocity in the metallic CNTs and their lengths; manybody correction in the intersublevel transition energy was not observed. The observed THz photocurrent peaks were as narrow as 0.3 meV, which is limited by the tunnel escape rates from the CNT-QDs to the contacting electrodes. The result demonstrated here is the first step toward THz-spectroscopic studies of other kinds of CNTs such as multi-walled CNTs and CNT-peapods at the individual level.

[1] Z. Zhong et al., Nat. Nanotech. 3, 201 (2008), [2] J. D. Chudow et al., Nano Lett. 16, 4909 (2016)

Corresponding Author: K. Yoshida, Tel: +81-(0)3-5452-6261, Fax: +81-(0)3-5452-6261
Web: http://thz.iis.u-tokyo.ac.jp/ E-mail: kyoshida@iis.u-tokyo.ac.jp

3-6

pH-dependent photoluminescence of monolayer transition-metal dichalcogenides in an aqueous solution

○Wenjin Zhang, Kazunari Matsuda, and Yuhei Miyauchi

Institute of Advanced Energy, Kyoto University, Uji, Kyoto 611-0011, Japan

Monolayer (1L) transition-metal dichalcogenides (TMDCs) MX_2, where M and X are a transition metal (typically Mo, W) and a chalcogen (typically S, Se, or Te), respectively, have recently attracted a great deal of attentions as a new class of two-dimensional (2D) direct gap semiconductors [1] promising for future electronics and optoelectronics applications. To date, various intriguing optical properties of atomically thin TMDCs in vacuum or ambient air conditions have been intensively studied using optical spectroscopy techniques [1-3]. However, knowledge on the optical spectra of these materials in aqueous solution with various pH values has still been quite limited, although variety of phenomena occurring at the interfaces of liquid and TMDCs may substantially modify their physical/chemical properties and affect their usefulness in applications. Thus, it is important to clarify the influence of the surface electrochemical phenomena in water on their optical properties.

Here we demonstrate a simple procedure for optical spectroscopic studies on mechanically exfoliated TMDCs immersed in a liquid, which will provide an excellent platform for examining impacts of various physical chemistry phenomena at the liquid/TMDC interface on their physical properties. 1L-TMDCs were prepared using mechanical exfoliation method, and transferred on transparent glass substrates. The substrate with the transferred 1L-TMDC was then tightly bonded with a glass tube to compose a liquid reservoir in which an enough amount of liquid can be kept over the sample during the measurements. The optical measurements were performed through the glass substrate using oil immersion objective lens and a home-made confocal optical measurement system.

Figure 1 shows PL spectra of 1L-MoS_2 in water and air conditions respectively. Considerable modifications in the PL intensity and spectral line shape (inset) were observed for the 1L-MoS_2 just by immersion in water [4]. Dependence of the PL spectra on pH and the mechanism of the spectral modulation will be discussed.

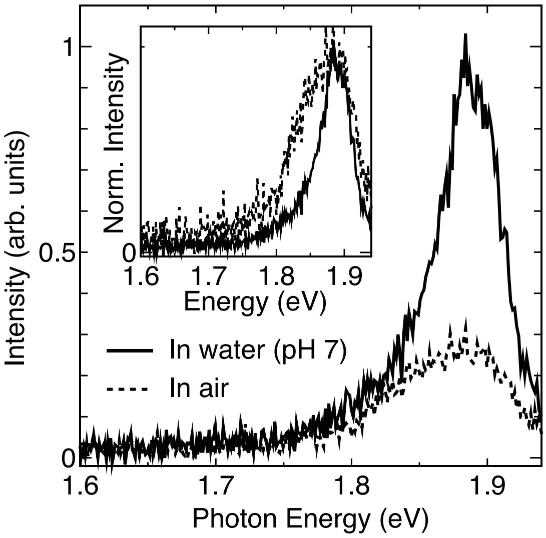

Fig. 1. PL spectra of 1L-MoS_2 in water (solid curve) and air conditions (dashed curve). Inset compares the PL spectra normalized by their intensities at the peak maxima.

[1] K. F. Mak, *et al.*, *Phys. Rev. Lett.* **105**, 136805 (2010).
[2] K. Matsuda, *J. Phys. Soc. Jpn.* **84**, 121009 (2015).
[3] S. Mouri, Y. Miyauchi, and K. Matsuda, *Nano Lett.* **3**, 5944 (2013).
[4] W. Zhang, K. Matsuda, and Y. Miyauchi, *J. Phys. Chem. C* **122**, 13175 (2018)

Corresponding Author: Y. Miyauchi
Tel/Fax: +81-774-38-3463/+81-774-38-4567
E-mail: miyauchi@iae.kyoto-u.ac.jp

3-7

Single-walled carbon nanotubes co-axially wrapped with mono- and few-layer boron nitride nanotubes and beyond

Rong Xiang[1,*], Taiki Inoue[1], Yongjia Zheng[1], Akihito Kumamoto[2], Yuichi Ikuhara[2], Ming Liu[1], Yang Qian[1], Shohei Chiashi[1], Esko I. Kauppinen[3], Shigeo Maruyama[1,4,*]

[1] *Departure of Mechanical Engineering, The University of Tokyo, Tokyo 113-8656, Japan*

[2] *Institute of Engineering Innovation, The University of Tokyo, Tokyo, Japan*

[3] *Department of Applied Physics, Aalto University School of Science, 15100, FI-00076 Aalto, Finland*

[4] *Energy Nano Engineering Lab., National Institute of Advanced Industrial Science and Technology (AIST), Ibaraki 305-8564, Japan*

We propose a conceptually new structure, in which mono- or few-layer hexagonal boron nitride (BN) seamlessly wrap around a single-walled carbon nanotube (SWCNT), and result in an atomically smooth coaxial tube consisting two different materials, as shown in Fig. 1. The structure is synthesized by chemical vapor deposition (CVD), and the length of the coaxial tubes can reach up to micrometers. As the reaction occurs on outer surface of the existing SWCNTs, we name this process conformal CVD. Various SWCNTs, e.g. vertically aligned array, horizontally aligned arrays, suspended SWCNTs, random networks and films, are employed as the starting material, and successful coating are achieved on all of them. TEM-EELS clearly demonstrated the BN-SWCNT coaxial structure in individual tube scale, while Raman, optical absorption, and cathode luminance spectra clearly confirm the existence of this structure in large scale. After coating, the SWCNTs can be fully coated and thermal stability significantly increases.

Our characterizations confirm that the outside BN coating started locally on the wall of a SWCNT and then merged into a BN nanotube on the curved surface of the SWCNT which served as a template. The thinnest inner SWCNT that can support the BN layer growth is found to be 0.6-0.7 nm. The number of walls can be tuned from 1 to few by controlling the CVD condition. The structure of inside SWCNTs are almost not effected by the conformal CVD, as evidenced by Raman and many other characterizations. The crystallization and cleanness of the starting SWCNT template are believed to be critical for the successful fabrication of outside walls. This structure is expected to have a broad interest and impact in many fields, which include but not limited in investigating the intrinsic optical properties of environment-isolated SWCNTs, fabricating BN-protected or gated SWCNT devices, and building more sophisticated 1D material systems.

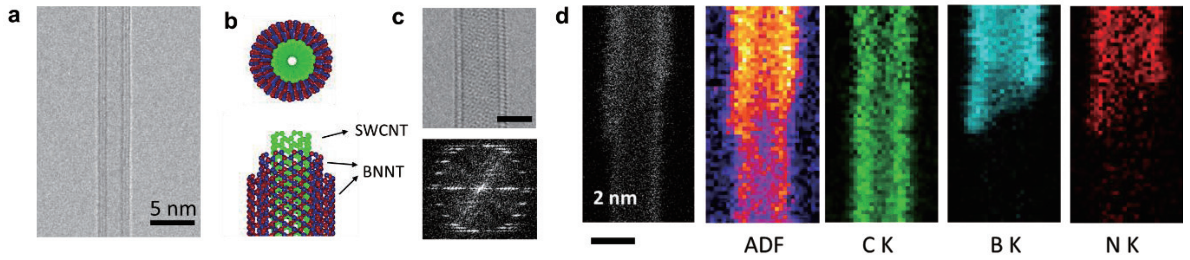

Figure 1 (a) TEM image and (b) atomic models of a SWCNT wrapped with two layers of BNNT; (c) cs-TEM image of a SWCNT-BN nanotube and its Fast Fourier Transform (FFT) pattern; (d) EELS mapping of a SWCNT partially wrapped with BN nanotube showing the inner is carbon and outer is BN.

[1] Rong Xiang et al., arXiv:1807.06154

Corresponding Author: xiangrong@photon.t.u-tokyo.ac.jp (RX); maruyama@photon.t.u-tokyo.ac.jp (SM)

3-8

Quantum Wells due to Electron-Phonon Interactions in Isotopically Layered Diamond Superlattices

○Yuki Bando[1], Masayuki Toyoda[1], Takashi Korestune[2], Susumu Saito[1]

[1] *Department of Physics, Tokyo Institute of Technology, Tokyo 152-8551, Japan*
[2] *Department of Physics, Tohoku University, Sendai 980-8578, Japan*

It has been known that electron-phonon interactions (EPIs) give rise to the band-gap renormalization in a semiconductor. Since the band-gap renormalization is mostly due to zero-point motions of phonons even at room temperature, EPIs can make differences in the electronic structure of isotopically different materials. Actually isotopic diamond superlattice (IDS), where ^{12}C and ^{13}C diamond layers are periodically stacked as shown in Fig. 1, has been produced by Watanabe *et al.* [1] and the confinement of photo-excited carriers in ^{12}C layers has been demonstrated experimentally. EPIs has been considered to have significant roles in this phenomenon, while the comprehensive understanding has not been achieved so far. In this work, we compute EPIs based on Allen-Heine-Cardona theory [2-4] with taking into account off-diagonal terms of self-energy [5] by using Wannier-based tight-binding Hamiltonian. We study in real ^{12}C/^{13}C IDS and virtual ^{6}C/^{24}C IDS for comparison. From the result of density of states (DOS), we have found that EPIs generate quantum wells (QWs) with a clear band offset around the valence-band top region in ^{6}C/^{24}C IDS for layer thickness of about 100 Å (Fig. 2). We also have confirmed the similar layer-thickness dependence of the QWs in ^{12}C/^{13}C IDS.

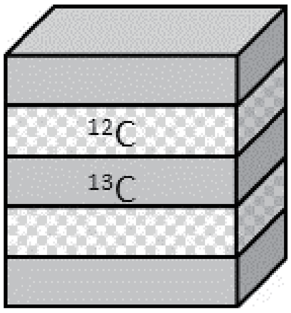

Fig. 1 Schematic figure of IDS.

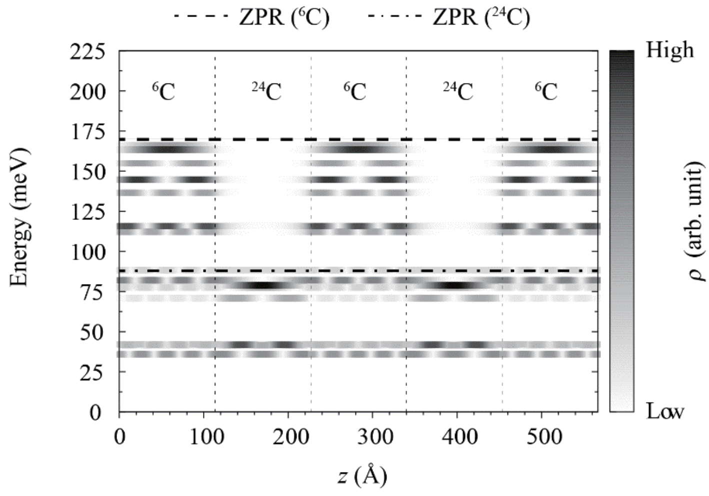

Fig. 2 Projection of DOS to stacking direction.

[1] H. Watanabe, H. Watanabe, C. E. Nebel, and S. Shikata, *Science* **324**, 1425 (2009)
[2] P. B. Allen and V. Heine, *J. Phys. C: Solid State Phys.* **9**, 2305 (1976)
[3] P. B. Allen, *Phys. Rev. B* **17**, 3725–3734 (1978)
[4] P. B. Allen and M. Cardona, *Phys. Rev. B* **23**, 1495–1505 (1981)
[5] M. van Schilfgaarde, T. Kotani, and S. Faleev, *Phys. Rev. Lett.* **96**, 226402 (2006)

Corresponding Author: Y. Bando
Tel: +81-3-5734-2387, Fax: +81-3-5734-2739,
Web: -
E-mail: y-bando@stat.phys.titech.ac.jp

3-9

Superior thermal conductivity enhancement of polymer composites with bioinspired graphene architecture

Dr. Cheng-Te Lin
Ningbo Institute of Material Technology & Engineering,
Chinese Academy of Sciences, China

Abstract

Based on the fast growth of the device performance, there has been an increasing demand for handling the issue of thermal management in electronic equipments. Therefore, it is of great significance to improve the thermal conductivity of the polymers, which are commonly used in electronic components. Due to the high intrinsic thermal conductivity, graphene exhibited great potential to be incorporated in the polymer matrix for the development of polymer composites with significant thermal conductivity enhancement. However, the difficulty of graphene dispersion and strong interfacial phonon scattering restrict the heat dissipation performance of graphene/polymer composites. The creation of bioinspired graphene architecture with controlled three-dimensional structure in the polymer matrix represents a promising solution for the issue of the difficulty of graphene dispersion, and leads to remarkable improvement of heat transfer capacity of the composites. Our works provide a path to develop a variety of highly thermally conductive polymer composites for use in heat dissipation and other thermal applications.

Biography

Dr. Cheng-Te Lin received his Ph.D. degree in Materials Science and Engineering at National Tsing Hua University (Taiwan) in 2008. In 2012, he was a postdoc in Prof. Jing Kong's group at Massachusetts Institute of Technology (MIT, USA), and undertook the investigation of graphene aerogel supercapacitors. Subsequently, he took part in the project of highly thermally-conductive polymer composites with Prof. Gang Chen (MIT, USA). From 2014 June, he is working as a full professor at Ningbo Institute of Material Technology and Engineering. He is the recipient of "1000 Young Talents Plan" from China's government (2015), "Hundred Talents Program" from Chinese Academy of Sciences (2014), and so on. Dr. Lin has 99 publications in *Nature Communications*, *Advanced Functional Materials*, *Chemistry of Materials*, *Journal of Materials Chemistry A*, and *Biosensors & Bioelectronics* etc. His research interests focus on the development of graphene-based applications, including CVD growth technique, functional composites, thermal interface materials, and biosensors. **E-mail:** linzhengde@nimte.ac.cn or chengte.lin@gmail.com

3-10

Visible-light-induced photodecarbonylation of α-diketone-type large acene precursors on Au(111) surface

○Hironobu Hayashi, Hiroko Yamada

Division of Materials Science, Nara Institute of Science and Technology (NAIST), 8916-5, Takayama-cho, Ikoma, Nara 630-0192, Japan

Recently, large acenes have gained great attention due to their potentials as functional organic semiconductors. The structure-property relationship of large acenes would be a good information for the effective design for next generation organic semiconducting and spintronics materials. Specifically, they could be used as model compounds to study chemical and physical properties of zig-zag type graphene nanoribbons. However, it is normally difficult to synthesize large acenes because of the low solubility and stability. On the other hands, we have developed photochemical precursor method to overcome these problems. Briefly, irradiation of α–diketone–type precursors at the n-π* absorption leads to the release of two molecules of CO, and the corresponding acenes can be prepared quantitatively in solutions or in films.[1,2]

Here, we report the synthesis of α–diketone–type heptacene and nonacene precursors. In addition, we also demonstrate the on-surface formation of heptacene and nonacene *via* visible-light-induced photodecarbonylation on Au(111) under ultrahigh vacuum conditions. Scanning tunneling microscopy (STM) and non-contact atomic force microscopy (nc-AFM) were used to investigate their chemical structures (Fig. 1). Furthermore, scanning tunneling spectroscopy (STS) measurements experimentally reveal HOMO-LUMO gaps of these large acenes.[3]

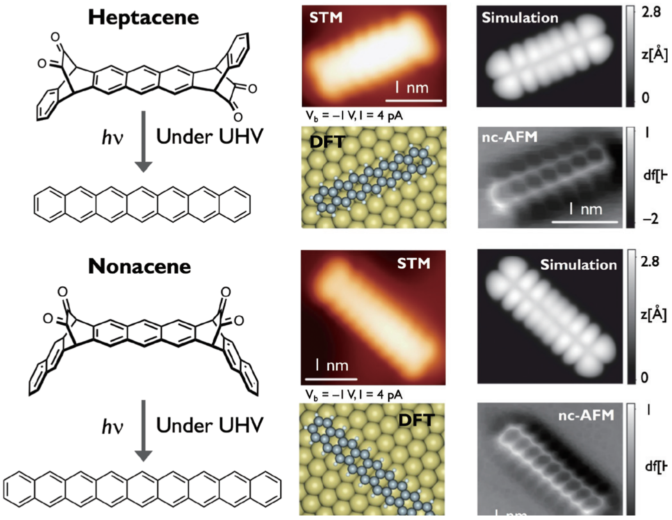

Figure 1. On-surface formation of heptacene and nonacene Au(111) under ultrahigh vacuum conditions. Acknowledgemen Dr. Urgel, J. I. and Prof. Fasel, R.@Empa.

[1] H. Yamada, Y, Yamashita, M. Kikuchi, H. Watanabe, T. Okujima, H. Uno, T. Ogawa, K. Ohara, N. Ono, *Chem.–Eur. J,* **11**, 6212 (2005).

[2] J. I. Urgel, H. Hayashi, M. D. Giovannantonio, C. A. Pignedoli, S. Mishra, O. Deniz, M. Yamashita, T. Dienel, P. Ruffieux, H. Yamada, F. Roman, *J. Am. Chem. Soc.*, **139**, 11658 (2017).

[3] The manuscript is under revision.

Corresponding Author: H. Hayashi
Tel: +81-743-72-6136, Fax: +81-743-72-6042,
Web: http://mswebs.naist.jp/LABs/env_photo_greenmat/
E-mail: hhayashi@ms.naist.jp

ポスター発表
Poster Preview

1P – 1 ～ 1P – 36
2P – 1 ～ 2P – 36
3P – 1 ～ 3P – 36

1P-1

Electronic and vibrational properties of boron-doped armchair graphene nanoribbons

○ M. S. Islam, Nguyen T. Hung, Ahmad R. T. Nugraha, Riichiro Saito
Department of Physics, Tohoku University, Sendai 980-8578, Japan

Graphene nanoribbons (GNRs), quasi-one-dimensional materials, are two-dimensional stripes of graphene having potential applications in future nanoelectronic and optoelectronic devices [1]. The energy bandgaps of armchair graphene nanoribbons (AGNRs) are inversely proportional to their ribbon widths [2]. For 7-AGNR, the experimentally observed energy bandgap is 2.3 eV [3]. Recently, A. Grüneis *et al.*, experimentally measured the Raman spectra for both undoped and boron doped 7-AGNR [4]. They found some new peaks in the Raman spectra in the boron doped case that are absent in undoped case. However, the origin of these peaks are not clear. We expect that the electronic band structures of AGNRs not only depend on ribbons width but also depend on doping and position of doping atom. In this study, we investigate how the energy bandgaps of the boron doped AGNRs are affected by the ribbons width, number of dopants and dopants position. We also explore to understand which atoms are responsible for the new Raman peaks.

In order to reproduce the experimental results, we theoretically calculate the band structures and nonresonance Raman intensities at Γ point, for both undoped and boron-doped case by using density functional theory (DFT). We find that the boron atoms along the backbone of an AGNR have clear effect on the energy bandgap of the ribbon.

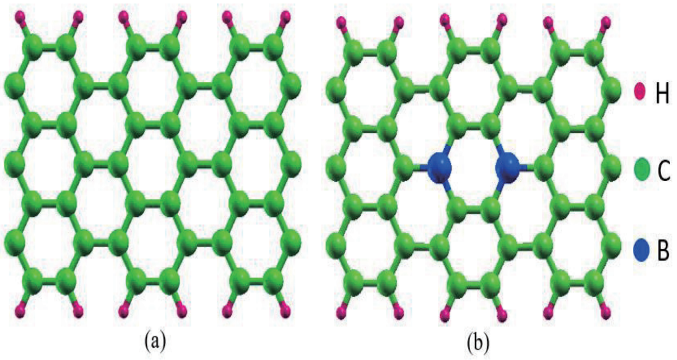

Fig. 1: (a) 7-AGNR, (b) Boron doped 7-AGNR

[1] A. Kimouche *et al*., Nat. Commun. **6,** 10177 (2015)
[2] Y. W. Son *et al*., Phys Rev. Lett. **97,** 216803 (2006)
[3] P. Ruffieux *et al*., ACS Nano. **6 (8),** 6930–6935 (2012)
[4] A. Grüneis *et al.,* unpublished

Corresponding Author: Md Shafiqul Islam
E-mail: islam@flex.phys.tohoku.ac.jp

1P-2

High yield fabrication of quantum device made of graphene nanoribbon

○Wakana Okita[1], Hiroo Suzuki[1], Toshiro Kaneko[1], Toshiaki Kato[1,2]
[1]Department of Electronic Engineering, Tohoku University, Sendai 980-8579, Japan
[2] JST-PRESTO

Graphene is one of the topical nanomaterials attracting attentions as next generation electronic materials due to its superior electrical conductivity, mechanically flexible structure and high optical transparency. While graphene has 2-dimensional sheet structure and shows metallic like behaviour, it has been discovered that graphene nanoribbon (GNR) has finite bandgap, which can be obtained by making graphene into 1-dimensional structure. This discovery made GNR conspicuous material mainly in semiconductor device field around the world.

One of our significant achievement so far is that we succeeded in integrated synthesis of suspended GNR for the first time [1-3] by unique plasma CVD process [4] combining with a creative idea, using nanobar structure as a catalyst. Heading towards implementation of practical application of suspended GNR grown by our method, it is essential to comprehend its detailed electrical property. For this purpose, we prepare a narrow (~20 nm) GNR (Fig.1 (a)) and carried out transport measurement at low temperature (~15 K). As a result, almost perfectly periodic Coulomb diamonds property was observed, which can be caused by quantum confinement effect (Fig.1 (b)). However, in previous research the probability that Coulomb diamonds can be observed was exceptionally low, which makes it difficult to realize integrated quantum devices with GNRs. Therefore, it is very valuable subject to tackle how to improve fabrication yield for quantum device made of suspended GNR grown by plasma CVD.

In this research, it is aimed to increase fabrication yield for quantum device by optimization of plasma CVD process and original nanobar structures. Consequently, fabrication yield for quantum device turned out to be increased by using short nanobar. Furthermore, it has been revealed that decreasing carbon supply amount while plasma CVD can also contribute to improving fabrication yield of GNR quantum devices. Decrease of carbon supply amount may provide thinner layer GNR and higher tunnel barrier, which is enough to induce quantum confinement effect. This research possesses very useful results to realize future integrated-quantum devices with GNRs.

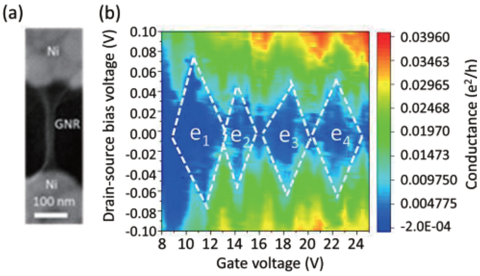

Fig. 1: (a) Typical scanning electron microscope image of GNR after CVD. (b) Typical Coulomb diamonds features of GNR device.

[1] T. Kato and R. Hatakeyama: Nature Nanotechnology **7** (2012) 651.
[2] H. Suzuki, T. Kaneko, Y. Shibuta, M. Ohno, Y. Maekawa and T. Kato: Nature Communications **7** (2016) 11797.
[3] H. Suzuki, N. Ogura, T. Kaneko, and T. Kato: Scientific Reports (2018) *in press*.
[4] T. Kato and R. Hatakeyama: ACS Nano **6** (2012) 8508.

Corresponding Author: W. Okita
Tel:+81-22-795-7046,
E-mail:wakana.okita.r5@dc.tohoku.ac.jp

1P-3

Epitaxial growth of large monolayer h-BN and its application to gas barrier layer

○Alexandre Budiman Taslim[1], Hideaki Nakajima[2], Yung-Chang Lin[3], Yuki Uchida[1],
Kenji Kawahara[4], Takahiro Morimoto[2], Toshiya Okazaki[2], Kazu Suenaga[3], Hiroki Hibino[5],
Hiroki Ago[1,4]

[1] *Interdisciplinary Graduate School of Engineering Sciences, Kyushu University, Fukuoka 816-8580*
[2] *CNT Application Research Center, AIST, Tsukuba 305-8565*
[3] *Nanomaterials Institute, AIST, Tsukuba 305-8565*
[4] *Global Innovation Center (GIC), Kyushu University, Fukuoka 816-8580*
[5] *School of Science and Technology, Kwansei Gakuin University, Hyogo 669-1337*

A structural analog of graphene, hexagonal boron nitride (h–BN) has been reported to be an ideal substrate for graphene and related 2D materials due to its flat surface without dangling bond [1]. Furthermore, h–BN is promising for gas barrier application, because h-BN is more chemically and thermally stable than graphene and its insulating property prevents galvanic corrosion that occurs in graphene coating [2]. Chemical vapor deposition (CVD) has been commonly used to grow h-BN on various metal catalysts, such as Cu, Cu-Ni alloy, and Fe [3-5]. However, due to relatively small size and random orientation of h–BN grains, high density of grain boundaries was formed, which will deteriorate the barrier property of h–BN [2]. Thus, the growth of large area h–BN grain, with good crystallinity and alignment is necessary in order to improve the barrier property. Here, we present epitaxial growth of monolayer h-BN on a Ni(111) thin film and its application as a gas barrier layer.

The growth of h–BN was performed by flowing borazine $(HBNH)_3$ precursor on Ni(111) thin film deposited on c-plane sapphire. By optimizing the growth conditions, we have obtained large h-BN grains as large as 0.5 mm (Figure 1). This grain size is among the largest size reported so far [4,5]. Additionally, as we can see from Figure 1 inset, low-energy electron diffraction (LEED) confirmed the epitaxial nature of the h–BN on Ni(111). Thus, a low defect density can be expected due to possible stitching between merged grains. We have investigated the gas barrier property of our h-BN grains. The metallic Ni was well preserved even after heating in air at 500 ºC for 15 min (see Figure 1), demonstrating the high stability of the h-BN. The boundary between merged grains was not damaged by this high temperature process. As graphene starts to be oxidized at 250 °C in air [2,6], h-BN is more promising for gas barrier application.

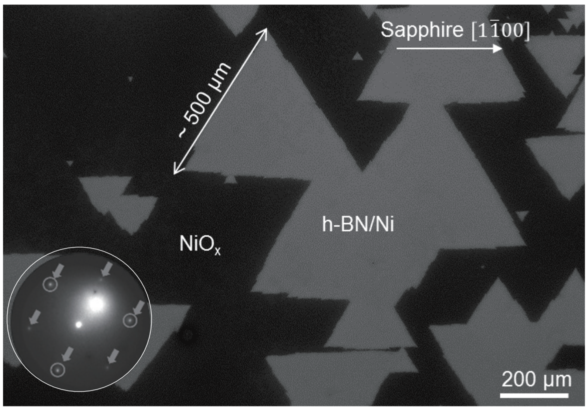

Fig. 1 Optical image of Ni surface after oxidation at 500 °C for 15 min. Inset shows the LEED patterns of h–BN (circles) and Ni (arrows) before oxidation.

[1] C. R. Dean *et al.*, Nat. Nanotechnol. **5**, 722 (2010)
[2] L.H. Li & Y. Chen, Adv. Funct. Mater. **26**, 2594 (2016)
[3] K. K. Kim *et al.,* Nano Lett. **12**, 161 (2012)
[4] G. Lu *et al.*, Nat. Commun. **6**, 6160 (2015)
[5] S. Caneva *et al.,* Nano Lett. **15**, 1867 (2015)
[6] D. Ding *et al.*, J. Phys. Chem. C **122**, 902 (2018)

Corresponding Author: H. Ago Tel: +81-92-583-8815, E-mail: h-ago@gic.kyushu-u.ac.jp

1P-4

Reduction of the temperature dependence of the resonance frequency shift in nano-electro-mechanical resonator with a van der Waals heterojunction

○Taichi Inoue, Yuta Mochizuki, Kuniharu Takei, Takayuki Arie, Seiji Akita

Department of Physics and Electronics, Osaka Prefecture University, Sakai 599-8531, Japan

Nano-electro-mechanical resonators are expected for highly sensitive force sensor or oscillator owing to their high frequency and controllability [1]. However, the reduction of the heat-induced frequency shift is one of the challenges for practical applications. Here, we reduce the heat-induced frequency shift in mechanical resonator (MR) by MoS_2/graphene van der Waals heterojunction, which have the different signs of thermal expansion coefficients (TECs) [2].

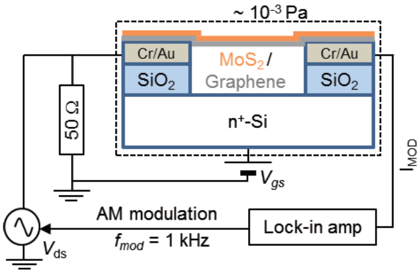

Fig. 1 Measurement setup.

We measured the resonance frequency of graphene and stacked MoS_2/graphene MRs under the vacuum of ~ 10^{-3} Pa (Fig. 1). The suspended area of the MR is treated as a field effect transistor channel. The vibration was driven by applying alternative current source drain voltage V_{ds}. The resonance was detected by amplitude modulation (AM) down mixing. Also, the resonance frequency can be tuned upward by increasing gate voltage V_{gs}, which increases electrostatic force between MR and the substrate.

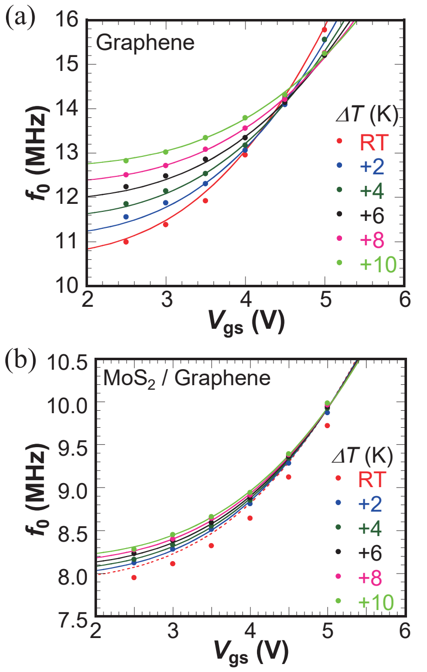

Fig. 2 The V_{gs} and ΔT dependence of f_0 for (a) graphene and (b) MoS_2/graphene MRs.

Fig. 2 shows V_{gs} and temperature change ΔT dependence of resonance frequency f_0 for (a) graphene and (b) MoS_2/graphene MRs. In graphene MR, the shift is modulated from positive to negative as increasing V_{gs}. This result originates from strain by V_{gs} [3]. The TEC of graphene MR was estimated to -1.6×10^{-6} K^{-1} by the vibration model, which is close to previous research (-7.0×10^{-6} K^{-1} [3]). In MoS_2/graphene MR, however, the shift was suppressed for all V_{gs}. This is due to the stack of the positive and negative TECs of MoS_2 and graphene, which makes the apparent TEC of MoS_2/graphene α_{app} close to 0 as follows.

$$\alpha_{app} = \frac{E_{gra}\alpha_{gra}n_{gra} + E_{MoS_2}\alpha_{MoS_2}n_{MoS_2}}{E_{gra}n_{gra} + E_{MoS_2}n_{MoS_2}} \quad \begin{pmatrix} E\text{: Young's modulus} \\ \alpha\text{: TEC} \\ n\text{: Number of layers} \end{pmatrix}$$

By analyzing the vibration model, the whole TEC of the MoS_2/graphene MR was calculated as -5.9×10^{-7} K^{-1}, which was 1/3 smaller than that of the graphene MR.

Acknowledgements: This work was partially supported by KAKENHI Grant Number JP15H05869, J16H00920, 16K14259, 16H06504, and 17H01040.

Reference: [1] T. inoue *et al.* ACS Omega **2**, 5792 (2017) [2] T. Inoue *et al.*, *arXiv*, 1805.03835 (2018) [3] V. Singh *et al.*, *Nanotechnology* **21**, 209801 (2010)

Corresponding Author: T. Inoue, Tel: +81-72-254- 9261, E-mail: t_inoue-4@pe.osakafu-u.ac.jp

Development of fabrication method for high quality hBN-encapsulated TMD device

○Takato Hotta [1], Keiji Ueno [2], Kenji Watanabe [3], Takashi Taniguchi [3],
Hisanori Shinohara [1], Ryo Kitaura [1]

[1] Department of Chemistry, & Institute for Advanced Research, Nagoya University, Nagoya 464-8602, Japan
[2] Department of Chemistry, Saitama University, Saitama 338-8570, Japan
[3] National Institute of Materials Science, Tsukuba 305-0044, Japan

Transition metal dichalcogenides (TMDs) and its heterostructures provide fascinating opportunities for exploration of physics and chemistry in the realm of two-dimensional systems. Recent works on TMDs have clearly demonstrated that hBN-encapsulated structures are essential to address intrinsic properties of TMDs and TMD-based heterostructures. Now, the bottleneck in the fundamental research of TMDs is the fabrication of high-quality hBN-encapsulated devices. During the device fabrication process, impurities are easily encapsulated between hBN and TMDs, which leads to degradation of the quality of the devices. For further exploration of fundamental properties of TMD and TMD-based heterostructures, development in a fabrication method of high-quality devices is indispensable. In this work, we have focused on development of high-quality hBN-encapsulated devices based on the nano-squeeze method [1].

Figure 1 shows hBN-encapsulated $MoSe_2/WSe_2$ ($hBN/MoSe_2/WSe_2/Graphene/hBN$). We have applied picking-up-based dry transfer method for the fabrication of the heterostructure. During the fabrication process, bubble formation has occurred as shown in Figure 1a. We have removed the bubbles by the nano squeeze method, where bubbles are removed through sweeping the surface of the sample with an AFM tip. As shown in the figure, after sweeping the surface, most of bubbles are removed, and height between $MoSe_2$ and WSe_2 significantly decreased from 2.0 to 1.1 nm. In the presentation, optical and electronic properties of fabricated devices will be discussed in detail.

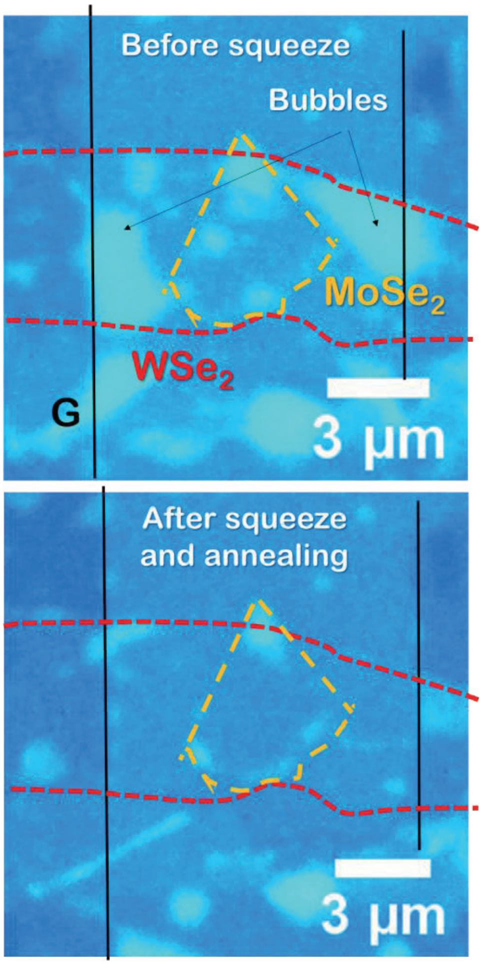

Fig. 1 An optical microscope image of the fabricated $MoSe_2/WSe_2$ heterostructure with graphene electrode. Top is the image before sweeping and bottom is the image after sweeping and annealing.

[1] M. R. Rosenberger, et. al., ACS Appl. Mater. Interfaces 10, 10379-10387 (2018).

Corresponding Author: H. Shinohara and R. Kitaura
Tel: +81-52-789-3660, Fax: +81-52-747-6442,
E-mail: noris@nagoya-u.jp and r.kitaura@nagoya-u.jp

1P-6

Synthesis of small-diameter, high-crystallinity single-wall carbon nanotubes (SWCNTs) using Ni-Al-O nanopowder

○Bozhi Chen[1], Toshihiro Sato[1], Hisashi Sugime[2], Eleni Temeche[3], Richard M. Laine[3], Suguru Noda[1, 4]

[1] *Department of Applied Chemistry, School of Advanced Science and Engineering, Waseda University, 3-4-1 Okubo, Shinjuku-ku, Tokyo 169-8555, Japan*
[2] *Waseda Institute for Advanced Study, Waseda University, 1-6-1 Nishi Waseda, Shinjuku-ku, Tokyo 169-8050, Japan*
[3]*Department of Materials Science and Engineering and the Macromolecular Science and Engineering Center, University of Michigan*
[4]*Waseda Research Institute for Science and Engineering, Waseda University, Tokyo 169-8555, Japan.*

Single-wall carbon nanotubes (SWCNTs) with small diameter and high crystallinity are important in various applications such as transparent conductive films and thin film transistors. Preparation of small diameter catalyst particles is crucial, so we focused on $[NiO]_{0.5}[Al_2O_3]_{0.5}$ spinel nanopowder which is synthesized by liquid-feed flame spray pyrolysis (LF-FSP) [1]. Ni nanoparticles (NPs) can be formed on the surface of the spinel by annealing at high temperature under reductive atmosphere, and the diameter of Ni NPs is controllable with the annealing condition. In addition, large specific surface area of the spinel nanopowder is advantageous for future mass production of SWCNTs.

The nanopowder was sonicated and dispersed in C_2H_5OH, drop-casted on SiO_2/Si substrates, and then dried at ambient condition. The substrates were loaded into a hot-wall chemical vapor deposition (CVD) apparatus, and the temperature was ramped up under Ar flow (100–900 sccm) at ambient pressure. After reaching the reaction temperature, CH_4 was added as both reductant and carbon source to grow CNTs. Unlike common CVD processes where the reduction of the catalyst is carried out under H_2 atmosphere, in this study, the catalyst was reduced with CH_4 which enabled the formation of small catalyst NPs followed by immediate SWCNT growth. The growth time was fixed to 10 min, and the concentration of CH_4 was changed from 10–90 vol% with the total flow rate of 1000 sccm. After the growth, CH_4 was stopped and the samples were cooled down under Ar flow. The as-grown samples were analyzed by SEM, Raman (excitation wavelength: 488 nm), and TEM. The SWCNTs with small diameter (1–2 nm) and high crystallinity ($I_G/I_D > 20$ in Raman spectrum) were obtained (Fig. 1). The I_G/I_D ratio is comparable to the high quality SWCNTs grown from C_2H_5OH [2,3].

[1] R. M. Laine, et al, *Nature Materials* **5**, 710 (2006).
[2] S. Maruyama, et al., *Chem. Phys. Lett.* **360**, 229 (2002).
[3] Y. Murakami, et al., *Jpn. J. Appl. Phys* **43**, 1221 (2004).

Corresponding Author: S. Noda
Tel: 03-5286-2769
E-mail: noda@waseda.jp

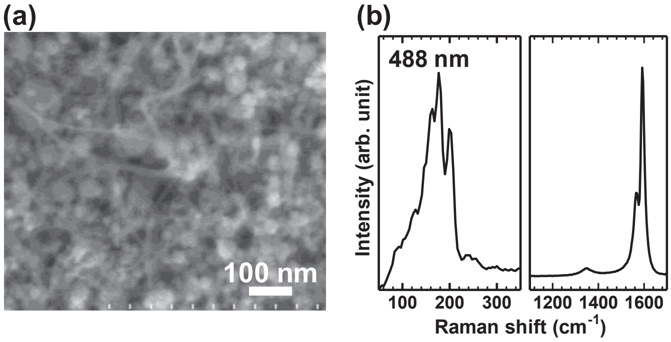

Fig 1. (a) SEM image and (b) Raman spectrum of SWCNTs grown from CH_4 using $[NiO]_{0.5}[Al_2O_3]_{0.5}$ nanopowder at 850 °C for 10 min.

Carrier density control of SWCNTs for electric power generation

○Guowei Wang, Takeshi Tanaka, Atsushi Hirano, and Hiromichi Kataura

Nanomaterials Research Institute, National Institute of Advanced Industrial Science and Technology (AIST), Tsukuba, Ibaraki 305-8565, Japan

By moving electrolyte droplet on an ultra-thin conductive film, an electric power can be generated, which is useful for IoT sensing devices. Now we are preparing semiconducting single-wall carbon nanotube (SWCNT) thin films for this purpose. To achieve high efficiency, we need to control the carrier density of the SWCNT film precisely. For the electronic device applications, external chemical doping has been widely used to control the SWCNT carrier density. To ensure high stability of chemical doping in the environment, however, we need to encapsulate dopant molecules inside the SWCNTs for this purpose [1].

In this study, *N,N'*-bis(3-pentyl)perylene-3,4,9,10-bis(dicarboximide) (PBI) and 2,4-bis[4-(*N,N*-diphenylamino)-2,6-dihydroxyphenyl]squaraine (DPSQ) were selected as n- and p-type dopant molecules, respectively. Before doping, endcaps of SWCNTs (EC1.5, Meijo Nano Carbon, unsorted) were removed by heating in air. Subsequently, the SWCNTs were refluxed in 1,4-dioxane for 4 h with dopant molecules pre-dissolved therein. After the reflux process, the SWCNTs were washed for many times to remove excess dopant molecules outside the SWCNTs. The PBI and DPSQ molecules encapsulated in SWCNTs were characterized by optical absorption spectra (Fig. 1). The absorption peaks of PBI and DPSQ after reflux process show clear red-shifts that suggest the successful encapsulation. We will control the amount of dopant molecules, namely the number of carriers, as the next step.

This work was supported by JST CREST Grant Number JPMJCR16Q2, Japan.

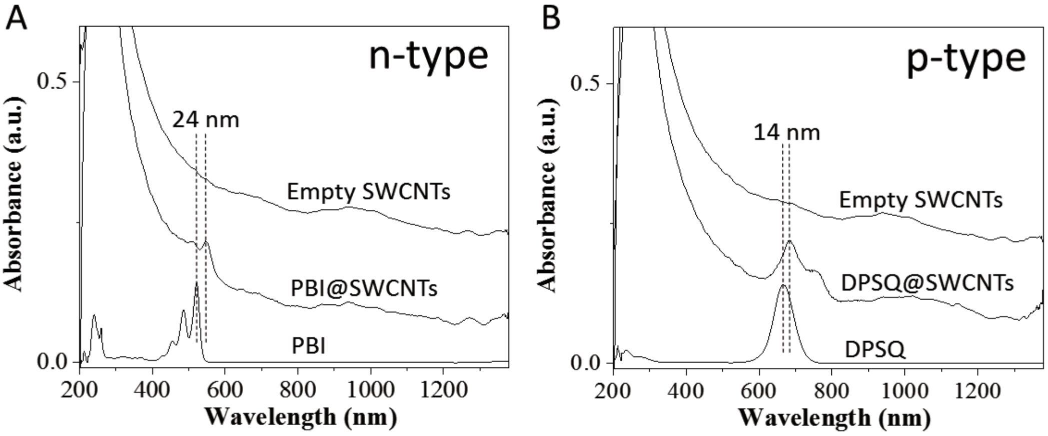

Fig. 1. Optical absorption spectra of (A) empty SWCNTs, PBI@SWCNTs, and PBI dissolved in 1,4-dioxane, (B) empty SWCNTs, DPSQ@SWCNTs, and DPSQ in 1,4-dioxane.

[1] T. Takenobu et al. Nat. Mater. 2, 683 (2003).

Corresponding Author: H. Kataura
Tel: +81-29-861-2551, Fax: +81-29-861-2786,
E-mail: h-kataura@aist.go.jp

Triboelectric generator with carbon nanotube thin film for wearable electronics

○Masahiro Matsunaga[1], Jun Hirotani[2], Shigeru Kishimoto[2], Yutaka Ohno[2,3]

[1]Venture Business Laboratory, Nagoya University, Nagoya 464-8603, Japan
[2]Department of Electronics, Nagoya University, Nagoya 464-8603, Japan
[3]Institute of Materials and Systems for Sustainability, Nagoya University, Nagoya 464-8603, Japan

With rapid growth of the field of the internet of things, energy harvesting devices have been attracting attention for an alternative way of battery to drive electronics. Recently, triboelectric generator (TEG), which is a kind of mechanical energy harvesters, is attracting interests for highly-efficient energy harvester [1]. The working mechanism of the TEG is a combination of contact electrification and electrostatic induction. The TEG has a potential for wearable electronics using stretchable materials such as carbon nanotube (CNT) thin film [2]. In this study, we fabricated transparent and stretchable TEG toward wearable energy harvester, using a CNT thin film as an electrode.

The TEG was composed of a carbon nanotube thin film covered with polydimethylsiloxane (PDMS) as shown in Fig. 1. After spin-coating PDMS onto a plastic substrate, a CNT film was formed on the PDMS surface by the transfer process based on the floating catalyst chemical vapor deposition or by the spray coating of CNT ink. After connecting Cu wire with silver paste, the top PDMS was spin-coated to cover the CNT thin film. We then applied CF_4 plasma to modify the PDMS surface to be fluorinated surface for an enhancement of the output power.

Figure 2 shows a photograph of the fabricated TEG, which is transparent and stretchable. We applied mechanical contacts by hand tapping with nitrile glove, and measured voltage through the load resistance. The instantaneous peak power reached over 8 W/m^2 at the load resistance of 30 MΩ. The power was sufficient to drive 100 blue LEDs connected in series. We also demonstrated energy harvesting from human motions such as elbow's motion and hand claps.

Acknowledgment: This work was supported by JST/CREST (JPMJCR16Q2).

[1] Z. L. Wang, Mater. Today **20**, 74 (2017).
[2] N. Fukaya *et al*., ACS Nano **8**, 3285 (2014).

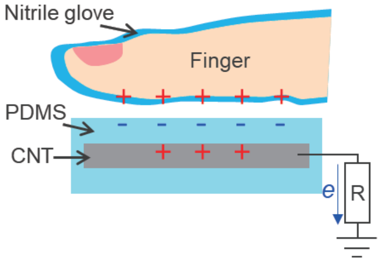

Fig. 1. Schematic of triboelectric generator and measurement setup.

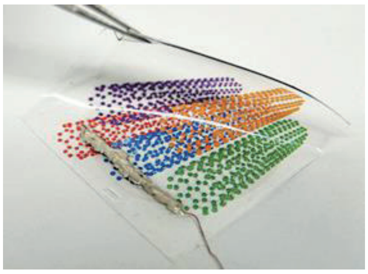

Fig. 2. Photograph of fabricated triboelectric generator.

Corresponding Author: Y. Ohno
Tel & Fax: +81-52-789-5387, E-mail: yohno@nagoya-u.jp

Photoluminescence properties of *meta*-linked bis-aryl-modified single-walled carbon nanotubes

○Boda Yu[1], Tomohiro Shiraki[1,2], Tsuyohiko Fujigaya[1,2,3,4]

[1] Graduate School of Engineering, Kyushu University, Fukuoka 819-0395, Japan
[2] WPI-I^{2}CNER, Kyushu University, Fukuoka 819-0395, Japan
[3] JST-PRESTO, Saitama, 332-0012, Japan
[4] Center for Molecular Systems (CMS), Kyushu University, Fukuoka 819-0395, Japan

Semiconducting single-walled carbon nanotubes (SWNTs) show near infrared (NIR) photoluminescence (PL) from E_{11} transition, which is applicable to bio imaging and telecommunication devices. The PL properties such as wavelengths are usually determined by chiral indices of SWNTs. Recently, however, local chemical functionalization of SWNTs has been reported to produce new PL, E_{11}*, that has red-shifted and higher quantum yields compared to the original E_{11} PL [1]. Regarding the locally functionalized SWNTs (lf-SWNTs), we reported a newly designed bis-aryldiazonium salt that induced largely red-shifted PL of $E_{11}{}^{2*}$ transition compared to E_{11}* PL of lf-SWNTs through the chemical modification [2]. Therein, theoretical calculations indicated that the band gaps of the $E_{11}{}^{2*}$ PL were influenced by the positional difference of the secondary aryl binding. Recently, Doorn et al. reported that hydrogen attachment, which occurs after a reaction of SWNTs with a mono-aryl diazonium salt, induced remarkable spectral shifts of E_{11}* [3]. Here, we newly design methylene-linked bis-aryldiazonium salts bridged at the *meta* positions of the aryl groups for further modulation of the $E_{11}{}^{2*}$ PL.

The *meta*-linked bis-aryldiazonium salts having different methylene chain lengths were synthesized (*m*Cn-Dz; n is the number of methylene units) and reacted with solubilized SWNTs in a micellar D_2O solution (*m*Cn-lf-SWNTs). By UV/vis/NIR absorption spectroscopy, a slight decrease of absorbance was observed after the chemical reaction for *m*C3-lf-SWNTs, indicating local chemical functionalization of the tubes. In contrast, the PL spectrum of *m*C3-lf-SWNTs showed a remarkable change compared to that of the pristine SWNTs; that is, a new PL peak appeared at 1260 nm. Interestingly, *m*C5-lf-SWNTs showed PL at 1246 nm. It is considered that the observed dependence of the resulting $E_{11}{}^{2*}$ PL wavelength on the methylene chain lengths of bis-aryldiazonium compounds can be varied between *para* and *meta* linkage systems, indicating creation of positional differences in the two point attachment structures based on the molecular designs of modifiers. Other structural factors will be discussed at the symposium.

[1] Y. Piao, B. Meany, L. R. Powell, N. Valley, H. Kwon, G. C. Schatz, Y. Wang, Nat. Chem, **5**, 840 (2013).
[2] T. Shiraki, T. Shiraishi, G. Juhász, N. Nakashima, Sci. Rep, **6**, 28393 (2016).
[3] S. K. Doorn *et al*. ACS. Nano, **11**, 10785 (2017).

Corresponding Author: T. Fujigaya
Tel: +81-092-802-2840, Fax: +81-092-802-2840,
Web: http://www.chem.kyushu-u.ac.jp/~fifth/jp/
E-mail: fujigaya.tsuyohiko.948@m.kyushu-u.ac.jp

1P-10

Photoluminescence energy shift of locally functionalized single-walled carbon nanotubes by effects of solvent molecules

○Yoshiaki Niidome[1], Tomohiro Shiraki[1,2], Tsuyohiko Fujigaya[1,2,3,4]

[1] Department of Applied Chemistry, Kyushu University, Fukuoka 819-0395, Japan
[2] WPI-I2CNER, Kyushu University, Fukuoka 819-0395, Japan
[3] JST-PRESTO, Honcho, Kawaguchi, Saitama 332-0012, Japan
[4] CMS, Kyushu University, Fukuoka 819-0395, Japan

Single-walled carbon nanotubes (SWNTs) show photoluminescence (PL) due to unique electronic structures based on the one dimensional nanoarchitechtures. The PL properties are known to be sensitively changed by microenvironmental effects of surrounding surfactants and solvent molecules [1]. As a new characteristic, recently, local chemical functionalization of SWNTs is reported [2][3]. Namely, the locally functionalized SWNTs (lf-SWNTs) emit new PL (E_{11}*) that has lower band-gap energy over 100 meV and higher quantum yields compared to those of original PL (E_{11}) of the pristine SWNTs.

In this study, we examine microenvironment effects on the PL properties of lf-SWNTs to investigate the effect for exciton at locally functionalized site and at the pristine sites. We synthesized nitroaryl lf-SWNTs (lf-SWNTs-NO_2) that were solubilized in D_2O by using a surfactant, to which o-dichlorobenzene (oDCB) was mixed. Finally, the resultant aqueous layer was collected for optical measurements.

Fig. 1 shows PL spectra of lf-SWNTs-NO_2 before and after mixing of oDCB. Interestingly, the E_{11}* PL showed larger energy shifts than that of the E_{11} PL. The result indicates that interactions of oDCB with the nanotubes would be different between the local functionalized sites and the pristine sites. Similar energy shift were observed when other solvents were mixed. Detail results and mechanisms of the systems will be presented at the poster.

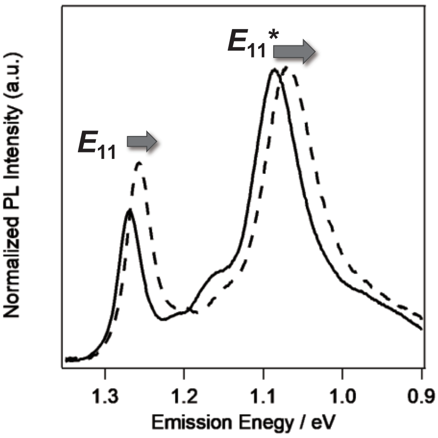

Fig. 1 PL spectra of lf-SWNT-NO_2 before (solid line) and after (dashed lines) mixing oDCB.

[1] Y. Miyauchi. J. Mater. Chem. C, **1**, 6499 (2013)
[2] Y. Wang *et al.* Nat. Chem. **5**, 840 (2013)
[3] T. Shiraki *et al.* Nanoscale. **9**, 16900 (2017)

Corresponding Author: T. Fujigaya
Tel/Fax: +81-92-802-2842,
Web: http://www.chem.kyushu-u.ac.jp/~fifth/jp/
E-mail: fujigaya.tsuyohiko.948@m.kyushu-u.ac.jp

1P-11

Spontaneous Assembly of Chevrel-Phase Mo_6Te_6 Nanowires Inside Carbon Nanotubes

○Masataka Nagata[1], Yusuke Nakanishi,[1, 2] Shivani Shukla,[3] Zheng Liu,[4, 5] Yung-Chang Lin,[5]
Kazu Suenaga,[5] and Hisanori Shinohara[1, 2]

[1]Department of Chemistry, Nagoya University, Nagoya 464-8602, Japan
[2]Institute for Advanced Research, Nagoya University, Nagoya 464-8602, Japan.
[3]Department of Materials Science and Engineering, Carnegie Mellon University, Pittsburgh, USA.
[4]National Institute of Advanced Industrial Science and Technology (AIST), Nagoya 463-8560, Japan.
[5]National Institute of Advanced Industrial Science and Technology (AIST), Tsukuba 305-8565, Japan.

Transition-metal chalcogenides (TMCs) are low-dimensional materials that demonstrate morphology-dependent properties and functions, and hence are regarded as one of the most promising candidates for ‘post-nanocarbon’ materials. In contrast to 0D and 2D TMCs, much less is known about 1D TMCs due to ineffective techniques for the precise control over the nano-structures. Chevrel-phase nanowires are well-defined 1D Mo_6X_6 compounds (X= chalcogen), which allow for future innovations such as electron channels and building blocks for integrated nano-electronics. Although the nanowires has previously been fabricated by employing top-down methods [1] and chemical reactions [2], length limitations (<0.1 μm) and bundled structures pose barriers for further exploring their properties and application.

In this work, we report a method for the bulk production of long, single Mo_6Te_6 nanowires by using the CNT-templated reaction that we have developed over the last decade [3]. The structure of Mo_6Te_6 nanowires was determined by transmission electron microscopy (Fig. 1). Our CNT-templated reaction enables their bottom-up growth, allowing for bulk production of long (>1 μm) Chevrel-phase nanowires isolated by CNTs and possessing ideal diameters. Current Raman and X-ray photoelectron spectroscopic analyses reveal the growth mechanism and novel properties of these 1D nanowires. Our results should open a new route for the bulk production of exceptionally long and isolated 1D TMCs, leading to investigation of their electronic and optical properties as well as application.

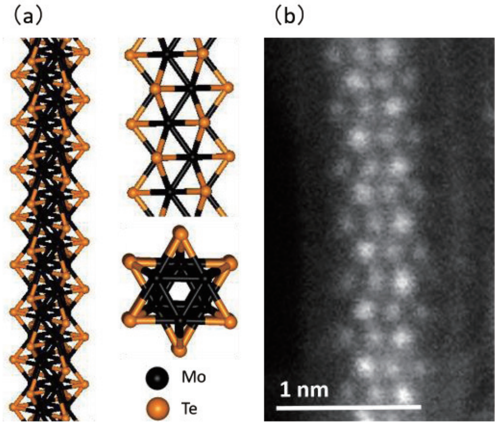

Fig.1 (a) Atomic structural model and (b) a scanning transmission electron micrograph of a single Mo_6Te_6 nanowire.

[1] J. Lin *et al.*, ***Nat. Nanotech.,*** 9, 436, (2014).
[2] J. Kibsgaard *et al.*, ***Nano Lett.,*** 8, 11, 3928 (2008).
[3] H. Shinohara, ***Jpn. J. Appl. Phys.,*** 57, 020101 (2018).

Corresponding Author: Y. Nakanishi and H. Shinohara
Tel: +81-52-789-3660
Web: http://nano.chem.nagoya-u.ac.jp/japanese/
E-mail:nakanishi.yusuke@g.mbox.nagoya-u.ac.jp; noris@nagoya-u.jp

1P-12

Basic Physico-Chemical Properties of C_{2V}-Symmetrical Octasubstituted Fullerene Derivatives

○Yue Ma[1], Hiroshi Ueno[2], Hiroshi Okada[3], Koya Uchiyama[4], Hiroshi Moriyama[4], Yutaka Matsuo[1,2,3]

[1] *Hefei National Laboratory for Physical Sciences at Microscale, University of Science and Technology of China, 96 Jin-zhai Road, Hefei, Anhui 230026, China*
[2] *School of Chemistry, Northeast Normal University, Changchun, Jilin 130024, China*
[3] *Department of Mechanical Engineering, School of Engineering, The University of Tokyo, Bunkyo-ku, Tokyo 113-8565, Japan*
[4] *School of Chemistry, Graduate School of Science, Toho University, Miyama, Funabashi, Chiba 274-8510, Japan*

Intensive research has been applied on chemical functionalization of fullerenes over the past decades, aiming at utilizing their broad availabilities in various research fields. Compared with the numerous kind of mono-functionalized fullerenes that have been deeply taken into investigation, however, only a few rational approaches towards fullerene multiadducts are reported due to the difficulty of regioselective synthesis, efficiently isolation, and unambiguous characterization. Although we reported the new synthetic approach towards novel C_{2V}-symmetrycal octa–substituted fullerenes recently[1], systematic evaluation of their basic properties is still insufficient yet.

In this work, the aggregation behaviour as well as electrochemical properties has been systematically studied for this series of octa–substituted fullerene derivatives (Figure 1a). These samples could exist as monomer in both nonpolar toluene and middle polar dichloromethane (Figure 1b) while high polar DMF rendered the molecule forming 100 nm aggregates. Cyclic voltammetry measurements reveals not only their stable redox properties but also indicated their LUMO levels can be widely and precisely tunable. The details will be shown on the poster.

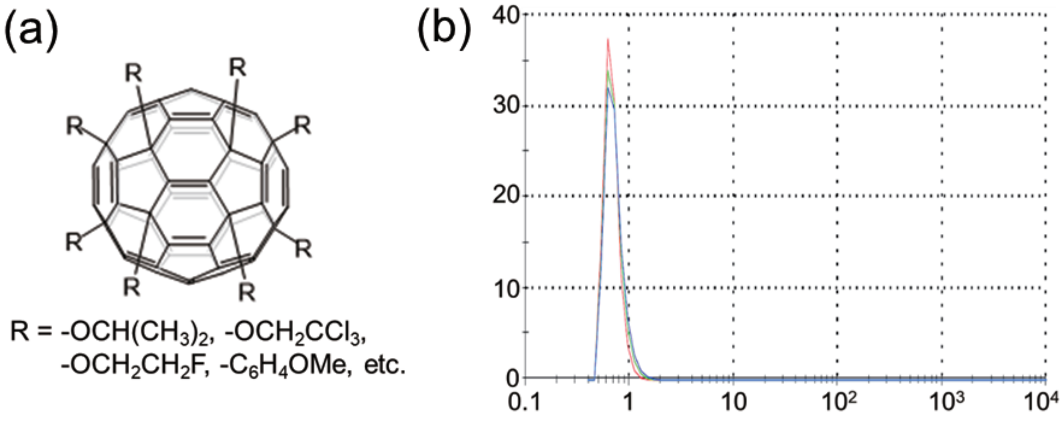

Figure 1. (a) Structure of C_{2V}-symmetrycal octasubstituted fullerenes. (b) Particle size distribution of $C_{60}(OCH(CH_3)_2)_8$ in dichloromethane.

[1] H.Ueno *et al.*, *J. Org. Chem.*, in revision.

Corresponding Author: Y. Matsuo
Tel: +81-3-5841-0978, E-mail: matsuo@photon.t.u-tokyo.ac.jp

1P-13

Evaluation of thermal conductance of single-wall carbon nanotube thin film by time domain thermo-reflectance method

○Hiroyuki Matsuo [1], Yohei Yomogida [1], Takashi Yagi[2], Kazuhiro Yanagi [1]

[1] *Department of Physics, Tokyo Metropolitan University, Hachioji, Tokyo 192-0397, Japan*
[2] *Department of Physics, National Institute of Advanced Industrial Science and Technology, Tsukuba, Ibaraki,305-8563, Japan*

In recent years, organic conductive polymers and carbon nanotubes have attracted a lot of interest as thermoelectric materials. For this purpose, it is important to evaluate their thermal conductance in their thin film form. There are various approaches to evaluate the thermal conductance of thin films, such as steady heat conduction analysis, 3ω method, laser flash method, periodic heating method, and so on. In this study, we investigated thermal conductance of single-wall carbon nanotube (SWCNT) thin films by Time-Domain Thermoreflectance method (TDTR), which can evaluate thermal conductance in the direction perpendicular to the surface, [1] because this method is expected to be applicable for FET device structures.

SWCNT films (MEIJO nano carbon ARCSO, Unpurified: metal / semiconductor mixed sample) were formed on the surface of an aluminum thin film (thickness 33nm). The thickness of SWCNT thin film was adjusted to be about 200nm. TDTR measurements were performed by irradiating pump light (1550nm, pulse width 0.5ps) and probe light (775nm, pulse width 0.5ps) from the Al side. The modulation on pump light at a cycle of 200kHz was applied, and then the phase change of reflectivity of the Al film was evaluated by the lock-in amplifier. As shown in Fig. 1, there are significant difference in phase change between Al without SWCNTs and Al with SWCNTs. As shown in Fig. 2, we were able to reproduce the phase change by analyzing the two-layer model; "SWCNT layer / Al layer / glass substrate" with the SWCNT layer set at 200 nm. Based on the analysis results, a thermal conductivity of the thin film was evaluated to be 0.08W m^{-1} K^{-1}. In contrast, according to the results obtained by periodic heating method, the thermal conductance was evaluated to be 13.5W m^{-1} K^{-1}, which is lateral thermal conductivity in the thin films. This means that the thermal conductivities of the perpendicular and lateral directions in the films are different, reflecting the anisotropy of thermal conductivity of SWCNTs in the thin films.

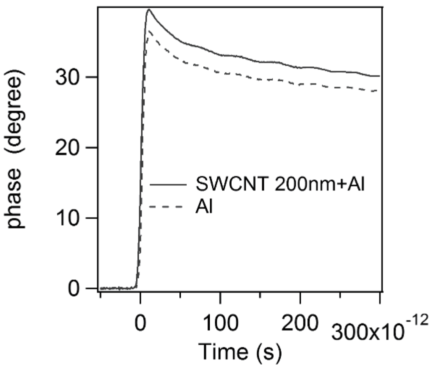

Figure1 ：Phase change of reflectivity of Al with SWCNTs and Al without SWCNTs.

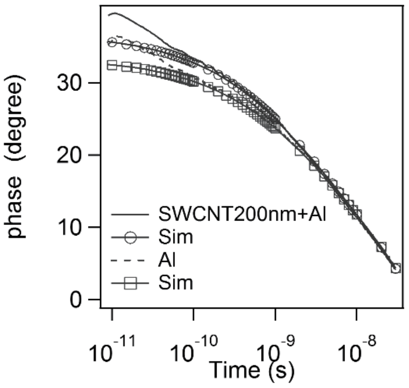

Figure2: Analysis result of the two-layer one-board model of "SWCNT layer / Al layer / glass substrate"

[1]. Kajita et al., Jpn. J. Appl. Phys. 55, 056203 (2016)

Corresponding Author: K. Yanagi, Tel: ＋81-42-677-2494,
E-mail: yanagi-kazuhiro@tmu.ac.jp

1P-14

Chemical reactions at local modified sites of single-walled carbon nanotubes for photoluminescence modulation

○Tomohiro Shiraki[1,2], Tamehito Shiga[1], Naotoshi Nakashima[2], Tsuyohiko Fujigaya[1,2,3,4]

[1] Department of Applied Chemistry, Kyushu University, Fukuoka, 819-0395, Japan
[2] WPI-I2CNER, Kyushu University, Fukuoka, 819-0395, Japan
[3] PRESTO-JST, Saitama 332-0012, Japan
[3] CMS, Kyushu University, Fukuoka 819-0395, Japan.

Single-walled carbon nanotubes (SWNTs) show photoluminescence (PL) in the near infrared (NIR) region, by which development of a wide range of applications including optoelectronic devices and imaging/sensing materials is expected. Recently, local chemical functionalization of SWNTs has been reported to create new PL (E_{11}*) that is redshifted with enhanced quantum yields compared to the original PL (E_{11}) of the pristine SWNTs.[1-3] The E_{11}* PL emerges by the formation of new emissive sites that have narrower band gaps and trap excitons generated on the tubes by photo-excitation. We have been synthesizing molecularly-designed modifiers to modulate the E_{11}* PL properties and, have succeeded in a selective E_{11}* wavelength shift of the locally functionalized SWNTs (lf-SWNTs) based on binding of specific molecules on the local modified sites through molecular recognition.[2,3]

In this study, a new approach based on molecular systems is devised using chemical reactions at the local modified sites of the lf-SWNTs for E_{11}* PL modulation. Here, we employ imine bond formation, which is a condensation reaction between aldehyde and amine groups, at the modified sites of aromatic aldehyde-modified lf-SWNTs (lf-SWNTs-CHO). The reactions were conducted by mixing with various aniline derivatives and then, PL spectral measurements were carried out. Fig. 1 shows PL spectra of the pristine SWNTs and the lf-SWNTs-CHO. For the lf-SWNTs-CHO, a PL peak appeared at 1140 nm (E_{11}*) which is red-shifted than the E_{11} PL (980 nm). When *p*-methylaniline, *p*-bromoaniline or *p*-nitro aniline was mixed with lf-SWNTs-CHO, the E_{11}* PL provided different wavelength shift values $\Delta\lambda$ (= $\lambda(E_{11}*) - \lambda(E_{11})$) of 154, 163, and 165 nm, respectively. The results indicate that the wavelength shift occurs with strong dependence on the chemical structures of the bound aniline derivatives in the imine bond formation process. Furthermore, reverse reactions and an additional reaction on the imine-formed sites were found to realize multistep wavelength shifts in this material.

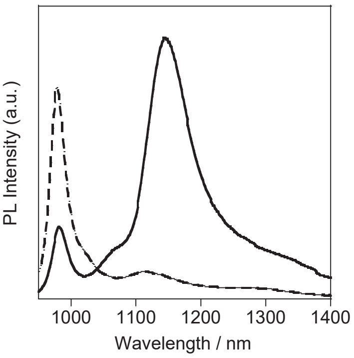

Fig. 1 PL spectra of the pristine SWNTs (dashed line) and the lf-SWNTs-CHO (solid line). λ_{ex} = 570 nm.

[1] Y. Piao, B. Meany, L. R. Powell, N. Valley, H. Kwon, G. C. Schatz, Y. Wang, Nat. Chem., **5**, 840 (2013).
[2] T. Shiraki, H. Onitsuka, T. Shiraishi, N. Nakashima, Chem. Commun., **52**, 12972 (2016).
[3] H. Onitsuka, T. Fujigaya, N. Nakashima, T. Shiraki, Chem. Eur. J., **24**, 9393 (2018).

Corresponding Author: T. Fujigaya
Tel: +81-092-802-2840, Fax: +81-092-802-2840
Web: http://www.chem.kyushu-u.ac.jp/~fifth/jp/
E-mail: fujigaya.tsuyohiko.948@m.kyushu-u.ac.jp

1P-15

Theory of circular dichroism in single wall carbon nanotubes including the depolarization effect

○Yuya Iwasaki and Riichiro Saito

Department of Physics, Tohoku University, Sendai 980-8578, Japan

Physical properties of a single wall carbon nanotubes (SWNT) are known to depend on its geometrical structure, which is defined by a set of integers (n,m) corresponding to a chiral vector (or chirality) for rolling up a graphene layer into a nanotube. The direction of rolling up of graphene layer (whether clockwise or anticlockwise) will determine the handedness of the SWNT, which means that chirality (n,m) may also have its equivalent counterpart (n+m,-m). Recently, the different handedness of SWNT for a particular chirality can be observed by using circular dichroism (CD) spectroscopy, in which the CD is defined as the difference of the optical absorption due to the left- and right-handed circularly polarized light [1,2]. Sato, *et al.* [3] shows numerical calculations of CD spectra of SWNT based on electron-photon interaction by the tight binding method, in which they explained the chirality dependence of CD spectra. Their calculation results are in good agreement with the experiment in the case of perpendicular incidence to the nanotube axis. However, the contribution of parallel incidence to the nanotube axis does not reproduce the experimental results well.

To solve the problem of CD in the case of parallel incidence, we expect that the depolarization field cancels out the applied electric field, and total electric field is suppressed [4,5]. This phenomenon is known as the depolarization effect and we should consider it to calculate the optical absorption quantitatively. In this work, we calculate the CD spectra and dynamical conductivity by the tight binding method. We will show numerical calculated results and consider how much the optical absorption can be suppressed by the depolarization effect.

[1] X. Wei *et al.*, Nat. Comm. **7**,12899 (2016)
[2] G. Ao *et al.*, JACS **138**, 16677 (2016)
[3] N. Sato *et al.*, Phys. Rev. B. **95**, 155436 (2017)
[4] S. Uryu and T. Ando, Phys. Rev. B. **74**, 155411 (2006)
[5] K. Sasaki, Phys. Rev. Applied. **9**, 034018 (2018)

Corresponding Author: Yuya Iwasaki
Tel: +81-22-795-6442, Fax: +81-22-795-6447,
E-mail: iwasaki@flex.phys.tohoku.ac.jp

Free-Standing Single-Walled Carbon Nanotube Thin Films Fabricated by Wet Process with narrow bundle thickness distribution

○Yuichi Kato, Atsuko Sekiguchi, Kazufumi Kobashi, Takeo Yamada, Kenji Hata

National Institute of Advanced Industrial Science and Technology (AIST), Central 5, 1-1-1 Higashi, Tsukuba 305-8565, Japan

Carbon nanotube (CNT)-based free-standing thin films are in high demand as switching or sensing elements in MEMS devices, ultrafiltration membranes, etc. The fundamental issue with fabricating them is regulating bundle thickness homogeneity, which is inherently difficult due to the high proclivity for CNTs to bundle and entangle[1]. In general, uniform structure reduces microscopic stress concentration in material and produce high mechanical strength. Here we demonstrate the fabrication of macroscale (2-cm-diameter) free-standing thin single-walled CNT films with thicknesses as low as 200 nm (**Fig. 1**) by wet-processing.

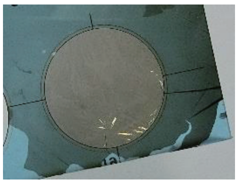

Fig. 1 Photograph of a free-standing CNT film.

We prepared single-walled CNT suspensions by ultrasonication using different liquid media shown in **Table 1** to control bundle thickness distribution of the films. We prepared CNT films (***film-I*, *-II***) by blade-coating of the CNT suspensions. We used identical CNT starting materials and processing methodology.

Film-I shows maximum tensile strength of 166 MPa, which is higher than that of ***film-2*** (33 MPa).

We compared bundle thickness distribution of the films. ***Film-I*** shows narrower bundle thickness distributions (uniform structure) than the other samples, which could contribute to the observed high mechanical strengths.

To study the origin of the uniformity difference, we measured size of CNT aggregates in parent suspensions by flow image analyzer. We found that well-stabilized suspensions using surfactants with higher fractions of smaller aggregates lead to CNT films with uniform structures that exhibit high mechanical performances.

Our work presents a bottom-up approach of tailoring ultrathin freestanding CNT films by wet-processing, a versatile and potentially scalable fabrication methodology.

Table 1. Prepared CNT films, tensile strength, and bundle thickness distribution.

Name	Solvent, Surfactant	Tensile Strength [MPa]	Bundle thickness 10^{th} -90^{th} percentile [nm]
film-I	toluene, FC12	166	7-11
film-II	propylene glycol	33	19-109

FC12:10-dodecyl-7,8-dimethyl-10*H*-benzo[g]pteridine-2,4-dione

[1] K. Kobashi *et al.* Chem. Sci. 4, 727 (2013)

Corresponding Author: Atsuko Sekiguchi
Tel: +81-29-861-4611, Fax: +81-029-861-4851,
Web: http://www.nanocarbon.jp/
E-mail: atsuko-sekiguchi@aist.go.jp

1P-17

Modification of multi-walled carbon nanotubes with photoreactive silane coupling agent: application for highly adhesive surface coating

○Tomoya Takada, Seisyu Takakuwa, Yuichiro Kitamura

Department of Applied Chemistry and Bioscience, Chitose Institute of Science and Technology,
Chitose 066-8655, Japan

Fabrication of hybrid materials containing carbon nanotubes (CNTs) has been paid much attention from an industrial viewpoint. Coating of CNTs onto transparent substrates such as glass reveals preparation of novel transparent conductive materials. Especially, immobilization of CNTs on the substrate surface through chemical bond is expected to be a promising tool for fabrication of weatherable CNT coatings. In this work, photoinduced modification of multi-walled CNTs (MWCNTs) with photoreactive silane coupling agent was examined and the modified MWCNTs were employed to fabricate chemically immobilized MWCNT coating on glass surface (Fig. 1). Benzyl-type radicals have been known to smoothly generate by photochemical bond scission of benzyl halide derivatives such as chloride. This reaction can be used to make sidewall modification of MWCNTs; it has been known that organic radicals smoothly attack CNT surface to form covalent bonds.

Materials used were MWCNTs provided by Nanocyl, Belgium and p-(chloromethyl)phenyltrimethoxysilane (PCMPS) provided by Alfa Aesar, USA. Firstly, PCMPS and MWCNTs were mixed in methanol and irradiated with ultraviolet light from a xenon light source under continuous stirring at room temperature. Then soda-lime glass pieces were dipped into the mixture. The PCMPS attached on MWCNT surface was hydrolyzed by adding aqueous acetic acid solution to convert -OCH_3 to -OH. The -OH groups generated by the hydrolysis can form hydrogen bonds with silanol groups on glass surface; MWCNTs can be attached on the glass surface through the interaction. The glass pieces coated with MWCNTs were then dried at 65 ºC, washed with methanol and heated with a muffle furnace to form -Si-O-Si- linkages between MWCNT surface and glass surface. The fabricated samples were characterized by means of X-ray photoelectron spectroscopy (XPS), Raman spectroscopy, and so on. Adhesiveness of the MWCNTs coating was examined with scotch-tape test.

The firmly attached MWCNT layer were successfully fabricated on the glass surface by the method described above. The layer was not taken away even after several scotch-tape adhesion-peeling cycles. Other results of characterization will be shown at the symposium.

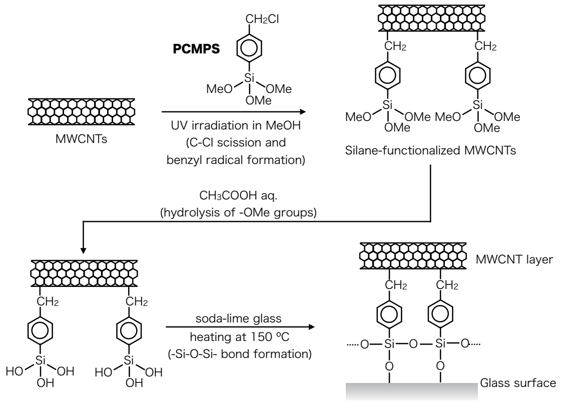

Fig. 1. Process for fabrication of MWCNT layer on glass surface.

Corresponding Author: T. Takada
Tel: +81-123-27-6056, Fax: +81-123-27-6056,
Web: http://www.geocities.jp/takada719/cisttakada/index.html
E-mail: t-takada@photon.chitose.ac.jp

1P-18

Determination of association constants of pyrene- and porphyrin-based nanotweezers and nanocalipers with SWNTs

○ Alejandro López-Moreno, and Naoki Komatsu

Graduate School of Human and Environmental Studies, Kyoto University, 606-8501 Kyoto

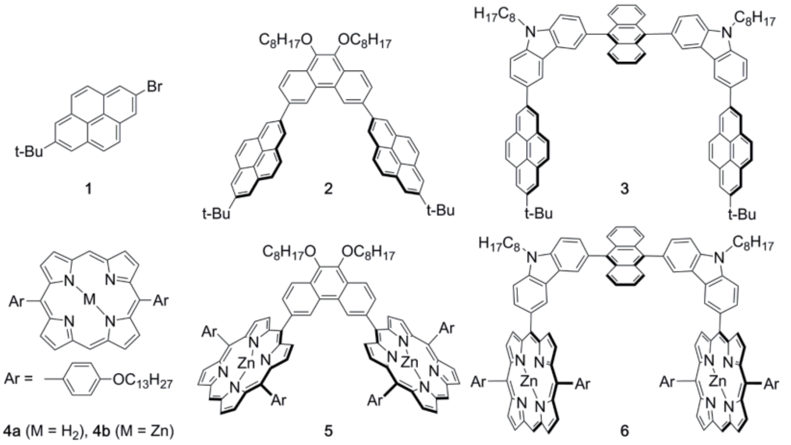

Figure 1 Structures of pyrene **1**, pyrene-based nanotweezers **2**, pyrene-based nanocalipers **3**. porphyrin **4**, phorpyrin-based nanotweezers **5**, and porphyrin-based nanocalipers **6**.

Association constants between soluble molecules and insoluble carbon nanotubes can be determined using a quantitative thermogravimetric method reported recently [1]. Here, we applied this method to determine the association constants of SWNTs with pyrene (**1**), porphyrin (**4**), and their derivatives including nanotweezers (**2**, **5**) and nanocalipers (**3**, **6)** shown in **Figure 1** [2]. The association constants (K_a) determined in DMF are shown in **Table 1**. The nanotweezers (**2** and **5**) and nanocalipers (**3** and **6**) exhibit much higher association constants than the monomers (**1** and **4**) by two and three orders of magnitude, respectively. This can be interpreted qualitatively by the number of interactions between the host molecules with SWNT surface to stabilize the complexes. Porphyrin-based nanotweezers and nanocalipers (**5** and **6**) showed ten times larger association constants than pyrene-based ones (**2** and **3**), though the constants of porphyrins (**4**) are hundred times larger than those of pyrene (**1**). The difference between porphyrin and pyrene is considered to be caused by higher flexibility and wider π-conjugated system in the porphyrins than pyrenes [3].

Table 1 Association constants (M^{-1}) of **1 – 6** with SWNTs in DMF

	(6,5) CoMoCat	**HiPCO**
Pyrene **1**	12.6 ± 0.6	9 ± 1
Nanotweezers **2**	$(4 \pm 2) \times 10^3$	$(2.0 \pm 0.4) \times 10^3$
Nanocalipers **3**	$(5 \pm 2) \times 10^4$	$(6 \pm 2) \times 10^4$
Porphyrin **4a**	$(3.3 \pm 0.9) \times 10^3$	$(2.4 \pm 0.8) \times 10^3$
Porphyrin **4b**	$(4 \pm 1) \times 10^3$	$(4.2 \pm 0.5) \times 10^3$
Nanotweezers **5**	$(7 \pm 3) \times 10^4$	$(5 \pm 2) \times 10^4$
Nanocalipers **6**	$(4 \pm 2) \times 10^5$	$(4 \pm 1) \times 10^5$

[1] A. de Juan, A. López-Moreno, J. Calbo, E. Ortí, E. M. Pérez, *Chem. Sci.* **6**, 7008 (2015); J. Calbo, A. López-Moreno, A. de Juan, J. Comer, E. Ortí, E. M. Pérez, *Chem. Eur. J.* **23**, 12909 (2017); A. López-Moreno, N. Komatsu, the 54th FNTG general symposium, 1-4 (2018).

[2] G. Liu, A. F. M. M. Rahman, S. Chaunchaiyakul, T. Kimura, Y. Kuwahara, N. Komatsu, *Chem. Eur. J.* **19**, 16221 (2013); G. Liu, F. Wang, S. Chaunchaiyakul, Y. Saito, A. K. Bauri, T. Kimura, Y. Kuwahara, N. Komatsu, *J. Am. Chem. Soc.* **135**, 4805 (2013).

[3] G. Liu, Y. Miyake, N. Komatsu, *Org. Chem. Front.*, **4**, 911 (2017).

Corresponding Author: A. López-Moreno
Tel: +75-753-7871, E-mail: lopez.alejandro.74a@st.kyoto-u.ac.jp

1P-19

Chemical reaction analysis of cobalt oxide clusters with ethanol by FT-ICR mass spectrometer

○Ryohei Yamada[1], Kaoru Hisama[1], Ken Mizutani[1], Shohei Chiashi[1], Shigeo Maruyama[1,2]

[1] *Department of Mechanical Engineering, The University of Tokyo, Tokyo 113-8656, Japan*
[2] *Energy NanoEnginerring Lab. National Institute of Advanced Industrial Science and Technology (AIST), Ibaraki. 305-8564, Japan*

Single-walled carbon nanotubes (SWCNTs) are expected as useful materials of various devices and chemical vapor deposition (CVD) method is one of the most common methods to produce SWCNTs. In CVD method, SWCNTs are grown from metal catalyst by supplying gas molecules containing carbon atoms. Although the growth mechanism has been investigated, the reactions between the catalyst and the carbon source gas are still unclear. The reactivity of nano-particles is different from that in bulk, and it is regarded as a key point of SWCNT growth. In addition, the reactivity varies depending on the oxidation state. However, it is difficult to reveal the chemical reactions on the nano-particles. Alcohol catalytic CVD (ACCVD) method is one of the CVD methods. In ACCVD method, cobalt and ethanol are often used as the catalyst and carbon source, respectively.

Fourier transform ion cyclotron resonance (FT-ICR) mass spectrometer makes it possible to analyze the chemical reactions between atom clusters and gas molecules. Cobalt non-oxide clusters reacted with ethanol, and "simple chemisorption" and "dehydrogenated chemisorption" were observed [1]. In this study, the chemical reactions between cobalt oxide clusters and ethanol were observed by FT-ICR mass spectrometer. Clusters were trapped in the FT-ICR cell, and reaction was observed after oxygen and ethanol were injected. Cobalt oxide clusters ($Co_nO_m^+$) with different n and m were observed after oxidization of cobalt, and $Co_3O_3^+$ cluster was one of the most generated clusters. The spectra in Fig. 1 shows the reaction of $Co_3O_3^+$. H_2 adsorption and C_2H_6 adsorption were observed. Reaction between $Co_3O_3^+$ and ethanol resulted in H_2 adsorption. As ethanol reaction proceeded, $Co_3O_3(C_2H_6)^+$ were generated and the number of $Co_3O_3H_2^+$ decreased. It indicated that ethanol adsorption with dehydration probably occurred on $Co_3O_3H_2^+$. These results show that reactivity of cobalt oxide clusters is different from that of non-oxide clusters since main reaction of non-oxide clusters is "simple chemisorption" [1].

In addition, the other reactions were observed on $Co_3O_3^+$. For example, $Co_3O_3^+$ and six ethanol molecules reacted, and three H_2O and one CH_4O are desorbed. This reaction resulted in $C_8H_{20}O$ adsorption.

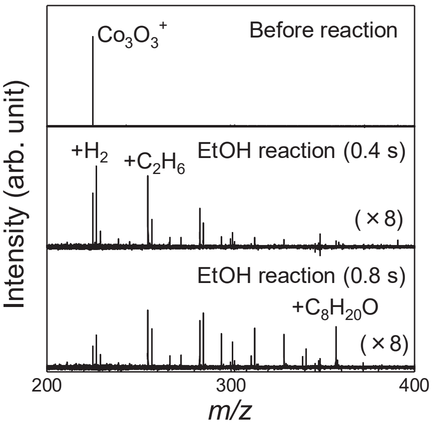

Fig. 1 Spectra of $Co_3O_3^+$ cluster and products resulted in ethanol reaction.

[1] S. Inoue *et al. Jpn. J. Appl. Phys.*, **47-4**, 1931-1936 (2008).

Corresponding Author: S. Maruyama
Tel: +81-3-5841-6421, Fax: +81-3-5841-6983,
Web: http://www.photon.t.u-tokyo.ac.jp/index-j.html
E-mail: maruyama@photon.t.u-tokyo.ac.jp

1P-20

Fractal analysis of self-organized carbon nanotube forest structure

○Adam Pander[1, 2], Takatsugu Onishi[1], Fumiya Nagamine[1], Sachio Hayashi[1], Akimitsu Hatta[1, 2], Hiroshi Furuta[1, 2]

[1] Dep. of Electronic and Photonic Systems Engineering, Kochi Univ. of Tech., Kochi 782-8502, Japan
[2] Center for Nanotechnology, Kochi Univ. of Tech., Tosayamada, Kami, Kochi, 782-8502, Japan

A dependence between optical properties of carbon nanotube (CNT) forest and its structure is generally known. In CNT forest, local regions of different density of CNTs exist and are the main reason behind the variation of properties throughout the forest. Local fluctuations of the formation process result in the variation of the agglomeration of a catalyst material and give rise to a diverse distribution of catalyst sizes and densities throughout the single sample. Under certain conditions, the formation of small catalyst particles occurs, implying a smaller distance between each grain, which results in a higher areal density, while the agglomeration of bigger particles requires more of the catalyst material, thus, the distance between individual particles increases. The size and density of catalyst particles are closely correlated to the diameter and density of CNTs within the forest [1]. Despite this fact, the self-correlation between the distribution of low and high-density areas in CNT forest, and the local properties remains unknown. To quantify the degree of CNT forest density and resultant properties, a scale dependent parameter named fractal dimension was used.

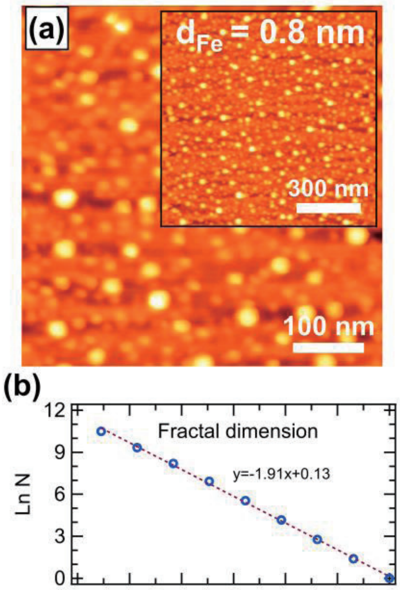

Figure 1. (a) AFM image of catalyst surface after annealing and calculated fractal dimension.

Fractals are complex geometric designs that repeat themselves or their statistical properties on many scales, and because of that are “self-similar”. Also, in the CNT field, fractal geometry was used for the quantitative description of the morphology of CNTs [2, 3]. This approach was adapted before to study the conductance and thermoelectric properties of CNTs and to investigate the adsorption of gases in CNTs.

The purpose of this work is to study the self-correlation and self-similar organization between the size and density of catalyst nanoparticles and CNTs, and the local fluctuations of properties. In the presented study, the fractal dimension and lacunarity are measured and the fractality is determined. The study of the self-correlation and the variation between areas with different density offers a new and important explanation of the diversity of optical properties of CNT forest.

This work was supported by KAKENHI No. 17K06205, 24560050, and the joint research project of Inst. of Laser Eng., Osaka University (2017B1-FURUTA).

[1]. Pander, A., Hatta, A. & Furuta, H., Appl. Surf. Sci. 371, 425–435 (2016).
[2]. Smajda, R., Kukovecz, Á., Kónya, Z. & Kiricsi, I., Carbon N. Y. 45, 1176–1184 (2007).
[3]. Sun, C.-H., Li, F., Ying, Z., Liu, C. & Cheng, H.-M., Phys. Rev. B 69, 33404 (2004).

Corresponding Author 1: H. Furuta
Tel: +81-(0)887 572 211
E-mail: furuta.hiroshi@kochi-tech.ac.jp

Corresponding Author 2: A. Pander
Tel: +81-(0)80 2983 4051
E-mail: adam.michal.pander@kochi-tech.ac.jp

1P-21

Effects of catalysts and growth conditions on growth process of individual SWNTs studied by digital isotope labeling

○Shun Yamamoto[1], Keigo Otsuka[2,3], Bunsho Koyano[1], Taiki Inoue[1], Rong Xiang[1], Shohei Chiashi[1], Shigeo Maruyama[1,4]

[1] Department of Mechanical Engineering, The University of Tokyo, Tokyo, 113-8656, Japan
[2] Quantum Optoelectronics Research Team, Riken Center for Advanced Photonics, Wako, 351-0198, Japan
[3] Nanoscale Quantum Photonics Laboratory, Riken Cluster for Pioneering Research, Wako, 351-0198, Japan
[4] Energy NanoEngineering Lab, National Institute of Advanced Industrial Science and Technology (AIST), Tsukuba, 305-8564, Japan

Single-walled carbon nanotubes (SWNTs) is highly expected toward the applications of electronic devices. Researchers have studied the nucleation and growth rates of SWNTs experimentally [1] for realizing chirality-controlled and high-density growth of SWNT arrays. In addition, recently we reported a new method for tracing time-resolved growth profiles of individual SWNTs by embedding digitally-coded isotope labels [2]. We introduced the different ratio of ^{13}C ethanol as labels in a pulsed manner (Fig. 1(a)) and detected labels by Raman mapping measurement (Fig. 1(b)).

In this report, we studied the effects of catalysts and temperature on growth profiles of SWNTs by a CVD method on r-cut quartz substrates. We utilized iron and cobalt as catalysts and changed temperature between 750 – 850 °C. All SWNTs from both catalysts were grown by the base-growth mode. The growth rates of SWNTs were faster and final lengths of them were longer at higher growth temperature. As for the incubation time, the SWNTs from iron catalysts had large variety, but many SWNTs from cobalt catalysts started growing just after introducing ethanol (Fig. 1(c,d)). Moreover, the SWNTs from cobalt catalysts had shorter lifetime than those from iron catalysts.

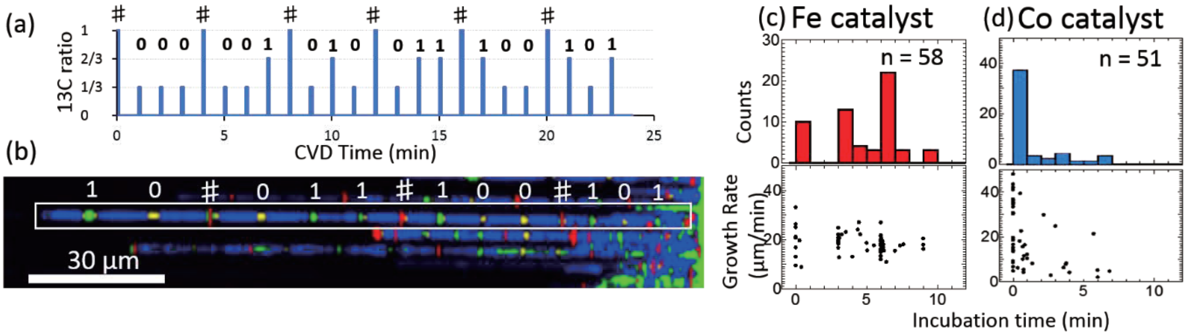

Fig. 1 (a) Introduction of labels by ^{13}C ethanol. (b) Raman mapping image colored by the shifts of G-band peaks. (c,d) Growth rates and incubation time of SWNTs grown at 850 °C from iron and cobalt catalysts.

[1] R. Rao *et al., Nat. Mater.* **11**, 213 (2012). [2] K. Otsuka, S. Yamamoto *et al., ACS Nano* **12**, 3994 (2018).

Corresponding Author: S. Maruyama Tel: +81-3-5841-6408, Fax: +81-3-5841-6408,
E-mail: maruyama@photon.t.u-tokyo.ac.jp

1P-22

Local structure and properties of polycyclic aromatic hydrocarbon molecule encapsulated in single-walled carbon nanotubes studied by molecular dynamics simulations(III)

○Ryo Nagai[1], Yosuke Kataoka[3] and Hironori Ogata [1,2]
[1] *Graduate School of Sci. and Engin., Hosei University, Koganei, 184-8584, Japan*
[2]*Research Center for Micro-Nano Technology, Hosei University, Koganei, 184-0003, Japan*
[3]*Research Center for Computing and Multimedia Studies, Hosei University, Koganei, 184-8584, Japan*

Carbon nanotubes (CNTs) are one of the most promising materials due to their superior electronic, thermal and mechanical properties. Single-walled carbon nanotubes (SWNTs) have hollow spaces of about several nm in diameter. Various functional molecules such as fullerenes can be encapsulated in the hollow space, and it is expected that new functions will be developed by capsulation. It has been reported that columnar layered polycyclic aromatic hydrocarbon(PAH) molecules such as coronene encapsulated in SWNTs can exhibit unique luminescence properties depending on their molecular orientations. We have been investigated the local structures and properties of various kinds of PAH molecules encapsulated in SWNTs systematically. In this study, molecular dynamics simulations were performed to clarify the packing structures of encapsulated perylene molecules in different chiral SWNT. Figure 1 shows the snapshots of the orientation structure of perylene molecules encapsulated in SWNT of equal diameter with different chirality at 298 K. It was found that the difference in chirality of SWNT caused a difference in the orientation of the encapsulated perylene molecules. Detailed results will be discussed in the conference.

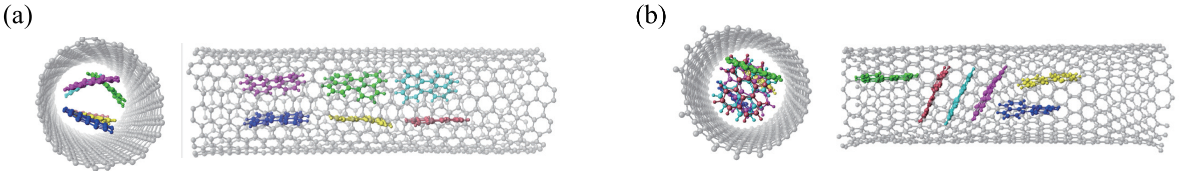

Figure 1. Snapshots of (a) perylene@(12,9)SWNT and (b)perylene@(18,1)SWNT at 298 K.

References:

[1] A. V. Talyzin *et al., Nano Lett.* **11**(2011)4352-4356.

[2] Miho Fujihara, *et al*., *J. Phys. Chem.* C **116**(2012)15141−15145.

[3] Alexander I. Chernov *et al., Phys. Status Solidi* B **251**(2014)2372–2377.

[4] Y. Sakane, *et al., AIP ADVANCES* **5** (2015)117113.

[5] Y.Joko, *et al., Phys. Chem. Chem. Phys.***19**(2017)27704-27715.

[6] T.Koyama, *et al., J.Phys. Chem. C* **122**(2018)5805-5812.

Corresponding Author: H. Ogata
Tel: +81-42-387-6229, Fax: +81-42-387-6229, E-mail: hogata@hosei.ac.jp

1P-23

Analysis of graphene-h-BN heterostructure growth mechanism from ethanol and ammonia borane

○Hayato Arai[1], Naomasa Ueda[1], Daisuke Ito[1], Taiki Inoue[1], Rong Xiang[1], Shohei Chiashi[1], Shigeo Maruyama[1, 2]

[1] Department of Mechanical Engineering, The University of Tokyo, Tokyo 113-8656, Japan
[2] Energy Nanoengineering Lab, National Institute of Advanced Industrial Science and Technology(AIST), Ibaraki 305-8564, Japan

Graphene has been attracting a wide attention as a promising materials for electronic devices due to its prominent properties, such as carrier mobility[1]. In addition, its thickness of one atom can open up a possibility to realize smaller devices than before. However, properties of graphene are easily degraded by impurities or dangling bonds of substrates because of its surface sensitivity. To suppress such effects, hexagonal boron nitride (h-BN) has been expected as a substrate or protective material for graphene devices. It has been reported that carrier mobility of graphene on h-BN was higher by one order of magnitude compared to that on SiO_2[2]. Although there are some reports about successful growth of graphene and h-BN heterostructure[3,4], controllable growth of them is still challenging. Catalyst substrates [3] or precursor gases [4] sometimes etches away atomic layers grown on substrates.

In this work, we performed sequential CVD growth of h-BN and graphene on copper substrates. We used ammonia borane and ethanol as precursors of h-BN and graphene, respectively. For h-BN growth, CVD furnace was heated up to 1050 °C. To supply precursor of h-BN, ammonia borane was heated at 60 °C for 10 min. After h-BN growth, the temperature of the CVD furnace was cooled down quickly to 900 °C. When the temperature reached to 900 °C, we began to supply ethanol to grow graphene. Figure 1(a) shows SEM image of h-BN and graphene grown on copper. Merged triangular flakes and darker circular flakes on them are regarded as h-BN and graphene, respectively. Raman spectrum from the heterostructure was shown in Fig. 1(b).

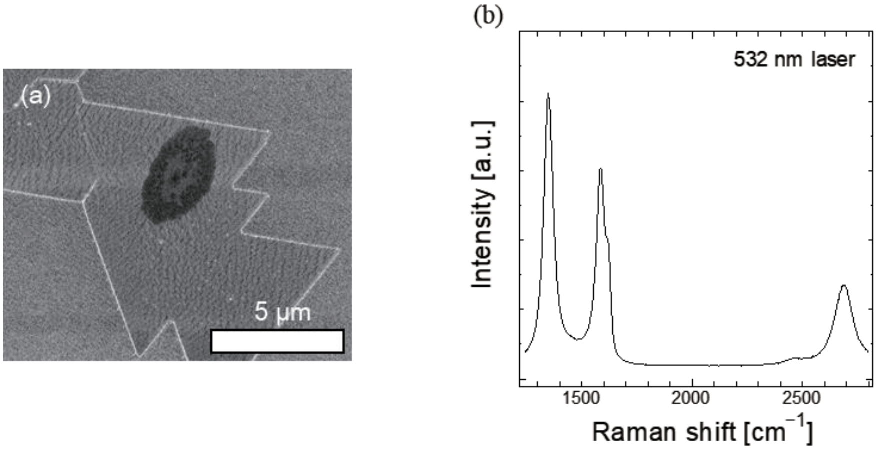

Fig. 1 (a) SEM image of h-BN and graphene. (b) Raman spectrum from heterostructure.

[1] J. H. Chen, *et al*., *Nat. Nanotechnol.,* **3**, 206 (2008).
[2] C. R. Dean, *et al.*, *Nat. Nanotech.*, **5**, 722 (2010).
[3] G. Kim, *et al*., *Nano Lett.,* **15**, 4769 (2015).
[4] T. Gao, *et al.*, *Nat. Com.*, **6**, 6835 (2015).

Corresponding Author: S. Maruyama
Tel: +81-3-5841-6421, Fax: +81-3-5841-6421,
Web: http://flex.phys.tohoku.ac.jp/japanese
E-mail: maruyama@photon.t.u-tokyo.ac.jp

1P-24

Mechanically coupled graphene drum-type mechanical-resonators

○Keisuke Akazawa, Yuta Mochizuki, Taichi Inoue, Daiki Yoshikawa, Kuniharu Takei,
Takayuki Arie, Seiji Akita

Department of Physics and Electronics, Osaka Prefecture University,
Sakai 599-8531, Japan

Graphene is suitable for high performance mechanical resonator (MR) because of extremely low mass and high Young's modulus. Coupled mechanical resonators are one of emerging components for ultralow power information processing mimicking the superposition of states. Here, we demonstrate the coupled MRs consisting of two drum-type graphene MRs (G-MRs) connected with a graphene bridge.

Monolayer graphene was transferred onto the SiO_2 (500 nm)/Si substrate and was etched by O_2 plasma to form the graphene stripe with the width of 2 μm. Next, the SiO_2 layer underneath of the graphene stripe was etched by buffered HF, and dried by using supercritical drying. Figure 2 shows the G-MRs coupled with a graphene bridge with a width of 2 μm, where the radii of the fabricated G-MRs was 3 μm. One of G-MRs was driven by the photothermal method using intensity modulated laser with a wavelength of 660 nm as indicated by a pink arrow in Fig. 2. The resonance properties of each G-MR were individually measured using another laser with a wavelength of 521 nm as indicated by green arrows in Fig. 2.

Figures 3 shows the resonance curves of G-MR A and G-MR B, where only the G-MR A was actuated. The resonances of both of G-MRs were successfully observed even under this actuation condition. The resonance frequencies of G-MR A and B are 11.8 and 12.1 MHz, respectively, where the quality factors for both G-MRs are ~ 200. In addition, we observed complicated coupled resonances at higher frequency around 12.9 MHz. Similar resonance curves were also observed under the actuation of the G-MR B. These indicate that the two G-MRs are mechanically coupled through the graphene bridge.

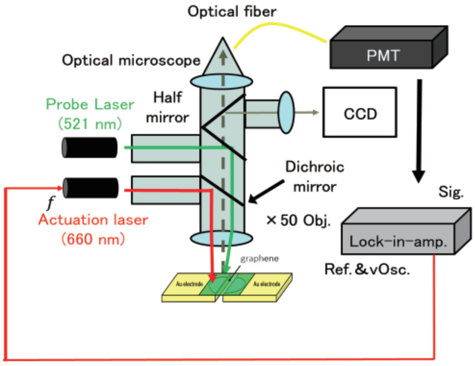

Fig. 1 Measurement setup

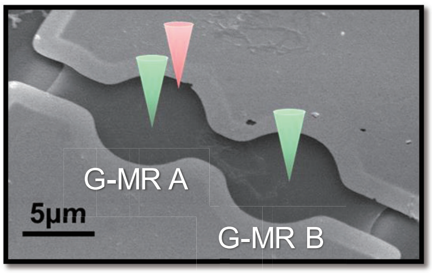

Fig. 2 SEM image of the graphene resonator and the laser position

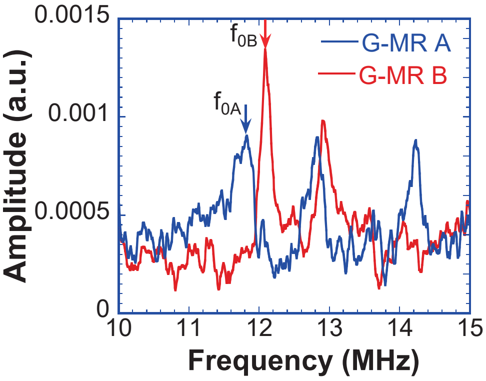

Fig. 3 Resonance curves of G-MR A and G-MR B, where the G-MR A is actuated.

Acknowledgements This work was partially supported by KAKENHI Grant Numbers 15H05869, 16H00920, 16K14259, 16H06504, and 17H01040.

Corresponding Author: K. Akazawa, Tel: +81-72-254- 9261, E-mail: akazawa-4@pe.osakafu-u.ac.jp

1P-25

Graphene mechanical resonator decorated with quantum-dots

○Masashi Hori, Yuta Mochizuki, Taichi Inoue, Daiki Yoshikawa, Kuniharu Takei
Takayuki Arie, Seiji Akita

Department of Physics and Electronics, Osaka Prefecture University,
Sakai 599-8531, Japan

Graphene is widely applied to nano-mechanical resonator (MR) because of its excellent electrical and mechanical properties. In order to append additional functionality, decoration of graphene with functional nanoparticle such as quantum dot (Q-dot) is one of promising routes. However, the suspended G-MR is very fragile, so that it is hard to decorate G-MR with Q-dot as shown in Fig. 1. Especially, the wet process destroy the suspended structure because of the surface tension of the liquid. Here, we demonstrate the fabrication of G-MR decorated with Q-dot through floating mist particles including the Q-dot generated by a nebulizer.

Figure 2 shows a fluorescence image of a drum G-MR decorated with Q-dots. A few Q-dots are observed on the G-MR region, where the number of particles on G-MR can be roughly controlled by the time for attachment process. Figure 3 shows a resonance curve of the Q-dot decorated G-MR. Resonance frequency and its quality factor are 6.88MHz and 341, respectively. Thus, we have successfully attached Q-dots on G-MR without breaking. We believe that the proposed fabrication process is applicable for loading other nanoparticles on nano-MR consisting of atomically thin materials.

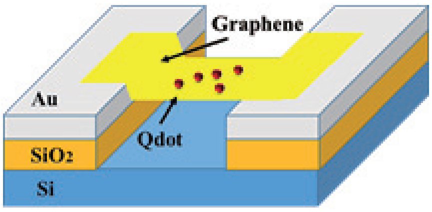

Fig. 1 Graphene resonator decorated with Q-dot.

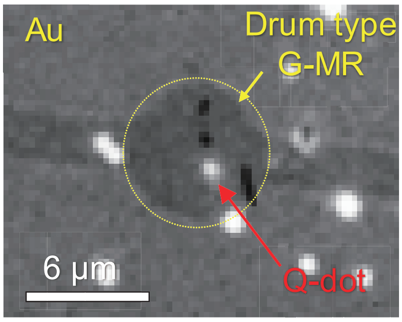

Fig. 2 Fluorescence microscope image of Q-dot on the G-MR

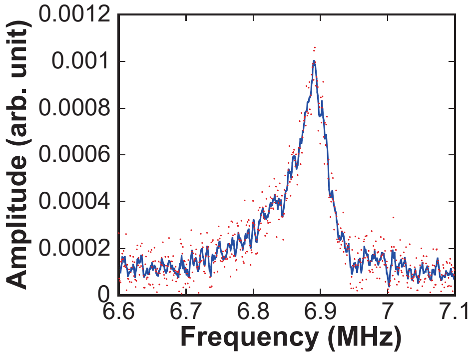

Fig. 3 Resonance curve of the G-MR decorated with Q-dot measured in vacuum.

Acknowledgements This work was partially supported by KAKENHI Grant Numbers 16H00920, 16K14259, 16H06504, and 17H01040.

Corresponding Author: M. Hori, Tel: +81-72-254-9261, E-mail: hori-4@pe.osakafu-u.ac.jp

1P-26

Reduction reaction kinetics of individual graphene oxide sheet studied by Twilight fluorescence microscopy

○Katsuki Kanazawa, Masahito Sano

Department of Organic Materials Science, Yamagata University, Yonezawa 992-8510, Japan

Twilight fluorescence (TwiF) microscopy can image individual single-layer graphene sheet floating in a solution [1]. A highly concentrated dye solution is added to a graphene solution and is placed on a glass plate. An excitation beam is incident on the glass/solution interface at a near total internal reflection angle. Because the beam is rapidly absorbed by the concentrated dye, fluorescence emission is localized to within a sub-micrometer distance from the glass interface. If there is a difference between the fluorescence from the free dye in solution and one from the dye interacting with the graphene sheet, the sheet can be visualized in real time.

Graphene oxide (GO) can be made in mass quantities and is readily dispersible in various solvents. GO has been used as an ink and a precursor for composite materials. In many instances, GO is reduced to recover some of the lost properties of graphene for final applications. Thus, it is important to understand how the reaction proceeds for maximizing efficiency. In this study, the reduction reaction of single-layer GO sheet by vitamin C is followed at an individual sheet-level in a reacting solution by TwiF microscopy.

With the present experimental condition, GO appeared darker as the reaction proceeded. Because the imaged GO sheets were away from the glass interface, the contrast was mainly due to the increasing light absorption. We used three kinds of dyes (2 green, 1 red) in two different solvents at various vitamin C concentrations. For nearly all cases, the best fit was obtained by a logarithmic function. This implies that the transmittance decreases logarithmically, regardless of the dye, solvent, and concentration. A logarithmic kinetics is known as the Elovich model and is often found in heterogeneous chemisorption systems under a condition that the activation energy increases with the surface coverage.

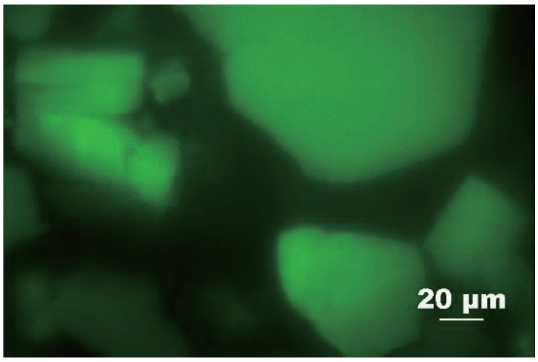

Fig. 1 TwiF image of GO sheets before reaction.

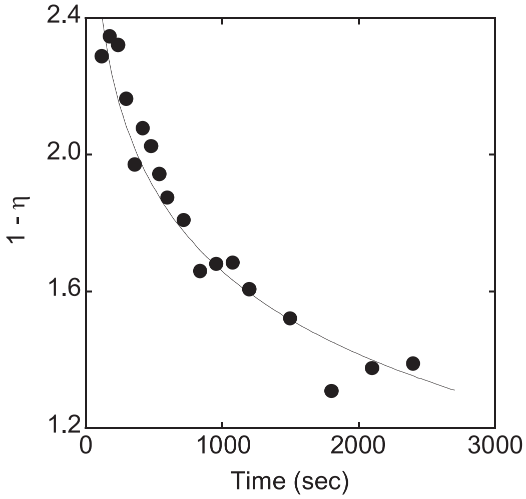

Fig. 2 Temporal change of contrast of a single GO sheet. A curve is the least-squared log function.

[1] Y. Matsuno, Y. Sato, H. Sato, M. Sano, *J. Phys. Chem. Lett.* **2017**, *8*, 2425-2431.

Corresponding Author: M. Sano
Tel: +81-238-26-3072,
Web: http://sanolab.yz.yamagata-u.ac.jp/
E-mail: mass@yz.yamagata-u.ac.jp

1P-27

Synthesis and Photophysical Properties of Covalently Linked Polycyclic Aromatic Hydrocarbon-Porphyrin Systems

○Hiroki Yamada[1], Takuma Hanaoka[1], Tomokazu Umeyama[1], Jaehong Park[1],
Hiroshi Imahori[1,2]

[1] *Graduate School of Engineering, Kyoto University, Kyoto 615-8530, Japan*
[2] *Institute for Integrated Cell-Material Sciences, Kyoto University, Kyoto 615-8510, Japan*

Recently, photofunctionalization of graphenes using π-aromatic units has attracted much attention due to their potential for the applications in artificial photosynthesis and solar energy conversion. Polycyclic aromatic hydrocarbons (PAHs) including hexa-*peri*-hexabenzocoronene (HBC) are partial structures of graphene and can be regarded as model molecules of graphene. In this study, we utilized two nanographene molecules with different sizes, i.e., a HBC and a PAH molecules with graphene nanoribbon oligomer (GNRO) structure consisting of 114 sp^2 carbons, to be linked with two zinc porphyrin (ZnP) units through a *p*-phenylene spacer at the periphery as model systems to elucidate the fundamental photophysical properties of nanographenes.

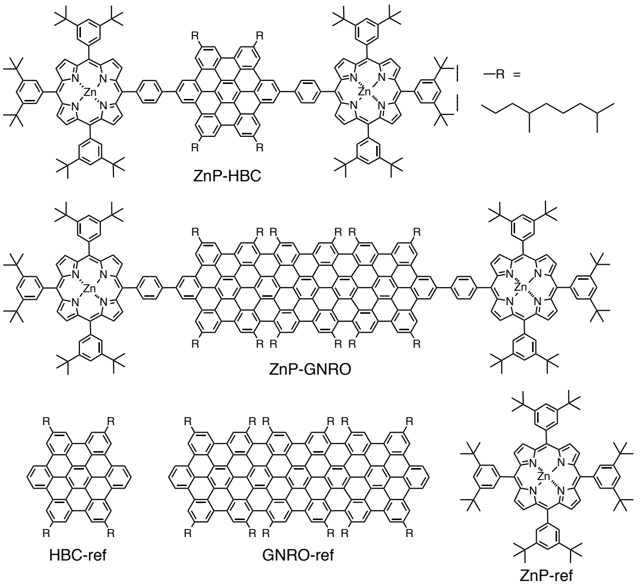

Figure 1. Structures of ZnP-HBC, ZnP-GNRO, HBC-ref, GNRO-ref and ZnP-ref.

The fluorescence spectrum of ZnP-HBC excited at 360 nm, where the absorption intensity ratio of ZnP and HBC is 1 : 7, exhibited two broad peaks at 604 and 656 nm. This spectrum coincided well with that of ZnP-ref, suggesting the occurrence of energy transfer (EnT) from the singlet excited state of HBC (^{1}HBC*) to ZnP in ZnP-HBC. On the other hand, the shape and intensity of the fluorescence spectrum of ZnP-GNRO with the excitation at porphyrin Soret band (422 nm) born a remarkable resemblance to those of GNRO-ref, indicating that the efficient EnT from the singlet excited state of ZnP (^{1}ZnP*) to GNRO occurs in ZnP-GNRO. The narrowed optical bandgap of the GNRO moiety due to the expanded π-conjugation system switched the EnT direction. To get deep insight into the interaction between nanographenes and ZnP in the excited states, time-resolved transient absorption (TA) spectra measurements were conducted. When the HBC moiety in ZnP-HBC was mainly excited, TA spectra at 100 ps and 2.1 ns matched well with those of ZnP-ref, corresponding to the singlet and triplet excited states of ZnP. On the other hand, the shapes of the TA spectra of ZnP-GNRO largely resembled those of GNRO-ref. These results were in good accordance with the results of steady-state fluorescence.

Corresponding Author: H. Imahori
Tel: +81-75-383-2566, Fax: +81-75-383-2571,
Web: http://www.moleng.kyoto-u.ac.jp/~moleng_05/
E-mail: imahori@scl.kyoto-u.ac.jp

1P-28

Moiré superlattices of graphene on Cu (111)

○Yui Ogawa and Yoshitaka Taniyasu

NTT Basic Research Laboratories, NTT Corporation, Atsugi 243-0198, Japan

Moiré superlattices appear in graphene on a metal substrate due to the lattice mismatch and stacking rotation between graphene and the substrate. The Moiré superlattices are valuable to tune electrical band structure. In this study, we analyze moiré superlattices in graphene grown on Cu (111) grown observed by scanning tunneling microscopy (STM).

Graphene was grown on pre-growth annealed Cu foil having mainly (111) plane by micro-wave plasma chemical vapor deposition method with methane gas. STM measurements were performed with VT-STM (Omicron) with Pt-Ir tip at room temperature below 6.0×10^{-10} Torr after cleaning the sample surface at 500 ˚C for 20 min.

We observed several moiré superlattices with the periodicities (moiré length, L) of 3.0 – 4.2 nm. The moiré angle φ is the angle of moiré unit cell respect to Cu (111).Fig. (a) is one of STM topography image with 3.5 nm moiré length. Fig. (b) shows a correlation map of Moiré length and angle as a function of rotation angle of graphene lattice against to Cu (111) adapted from an analysis method theoretically proposed by P. Zeller *et al* [1]. The correlation were calculated regarding typical three type of reciprocal lattice vectors of moiré in k-space: R0-moiré $\vec{K}_{\text{Moiré}} = (0,1)_{\text{gra}} - (0,1)_{\text{Cu}}$, R30-moiré $\vec{K}_{\text{Moiré}} = (1,1)_{\text{gra}} - (0,2)_{\text{Cu}}$, and R18.5-moiré $\vec{K}_{\text{Moiré}} = (1,2)_{\text{gra}} - (0,3)_{\text{Cu}}$. The plotted experimental data on the Fig. (b) matched well to the calculated correlation in case of R0- moiré, so that the observed moiré superlattices can be assigned as R0- moiré. Our result suggested that P. Zeller *et al*'s analysis can be great use in a characterization of experimentally observed moiré in graphene on the metal substrate.

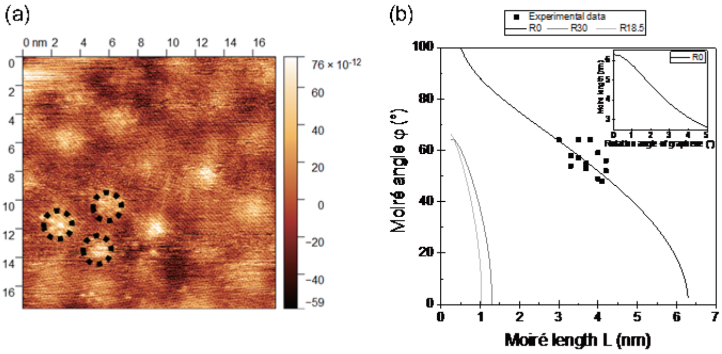

Fig. (a) STM topography image of graphene on Cu (111). Moiré superlattice is marked by dotted circles. (b) Correlation map of moiré length and angle of R0- (black), R30-(gray), and R18.5-(light gray) moiré for graphene on Cu (111). The inset of (b) is the moiré length of R0- moiré as a function of rotation angle of graphene against to Cu (111).

[1] P. Zeller *et al., New. J. Phys.* **16**, 083028 (2014).

Corresponding Author: Y. Ogawa
Tel: +81-46-240-3423, Fax: +81-46-240-4718
Web: http://www.brl.ntt.co.jp/group/shitsuko-g/index-j.html, E-mail: ogawa.yui@lab.ntt.co.jp

1P-29

Site-dependence of relationships between photoluminescence and applied electric field in monolayer and bilayer molybdenum disulfide

○Junji Nozaki[1], Hiroyuki Nishidome[1], Mina Maruyama[2], Susumu Okada[2], Satoshi Kusaba[3], Koichiro Tanaka[3], Keiji Ueno[4], Yohei Yomogida[1], and Kazuhiro Yanagi[1]

[1] Department of Physics, Tokyo Metropolitan University, Hachioji, Tokyo 192-0397, Japan
[2]Graduate School of Pure and Applied Sciences, University of Tsukuba, Tsukuba, Ibaraki 305-8571, Japan
[3]Department of Physics, Graduate School of Science, Kyoto University, Sakyo-ku, Kyoto 606-8502, Japan
[4]Department of Chemistry, Graduate School of Science and Engineering, Saitama University, Sakura-ku, Saitama 338-8570, Japan

Understanding of the optical properties at a specific site in 2D materials is important for future applications [1] [2]. Here, we investigated the site-dependence of the relationship between the photoluminescence spectrum and an electric field in exfoliated monolayer and bilayer molybdenum disulfide (MoS_2) using a technique combining scanning near-field optical microscopy (SNOM) and a bias voltage application from the cantilever as shown in Fig. 1(a) (EF-SNOM) [3]. We found clearly different behaviors between PL at monolayer sites and bilayer sites with the application of a bias voltage. At the monolayer sites, a decrease of the A-peak intensity was observed with the positive shift of the bias voltage, and the PL intensity exhibited a strong site dependence. At the bilayer sites, we clarified that carrier injection at a site in the bilayer region induces an increase in the A-peak intensity and a decrease in the I peak (Fig. 1(b-d), which was consistent to the results of our DFT calculations.

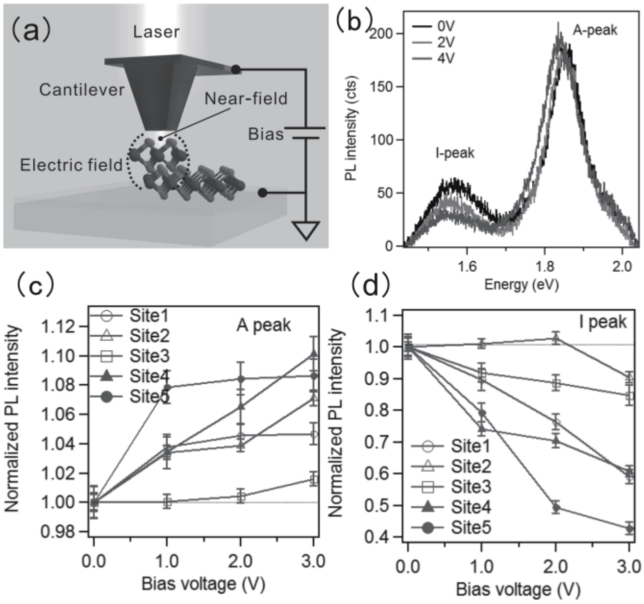

Fig. 1 (a) A schematic illustration of EF-SNOM measurements of monolayer and bilayer MoS_2. (b) Typical changes in the PL spectrum at a bilayer site upon application of a bias voltage. The relationship between normalized PL and bias voltage for the (b) A peak and (c) I peak at five different sites in bilayer regions.

As shown in this study, our EF-SNOM technique is a very powerful tool to understand the background of site-dependent optical properties of 2D materials.

[1] X. Yin *et al., Science* **344**, 488 (2014). [2] Y. M. He *et al., Nat. Nanotechnol.* **10**, 497 (2015).

[3] J. Nozaki *et al., Sci Rep* **7**, 46004 (2017).

Corresponding Author: K. Yanagi
Tel: +81-(0)42-677-2809, Fax: +81-(0)42-677-2483 E-mail: yanagi-kazuhiro@tmu.ac.jp

1P-30

Competition between electron and hole doping by hydrazine molecular adsorption on MoS_2

○N.Kodama[1], Y.Ishiguro[2], K.Takai[1,2]

[1]*Graduate school of Science and Engineering, Hosei University, Tokyo 184-8584, Japan*
[2]*Department of Chemical Science and Technology, Hosei University, Tokyo 184-8584, Japan*

The carrier injection to 2D-materials by molecular adsorption is one of important strategy to control its properties. Especially the study of electron doping is important however those reports are few. A tunable electron doping by hydrazine aqueous is known for graphene through the precise controlling of the hydrazine concentration and the adsorption time [1, 2]. Molecular doping is also effective for MoS_2 which has similar structure to graphene and sensitive to surrounding environment. In this study, MoS_2 mono layer adsorbed with hydrazine is investigated in order to clarify the kinetics of doping by Raman and PL measurements.

Hydrazine aqueous was dropped on MoS_2 mono layer prepared by mechanical exfoliation on 90 nm SiO_2/Si substrate, followed by drying by air blow and immediate Raman and PL measurements with an excitation wavelength of 532 nm at room temperature. The same operation was repeated while varying the adsorption time or concentration of hydrazine.

The FWHM of A_{1g} of Raman spectrum for MoS_2 mono layer is sensitive to its doping level [3]. As shown in Fig. 1, the kinetics of A_{1g} FWHM for 10 % is shorter than that for 1 %, indicating good tunability of the kinetics of doping by the hydrazine concentration in spite of the opposite behavior for 0.1% similar to 0 % (water adsorption). Change in the compositions of the exciton and trion peak in PL spectra shown in Fig.2 indicates successful electron doping for 10 % and 1 % but hole doping for 0.1 % and 0 %. Here it should be noted that molecular doping proceeds through the electrochemical process, so doping using aqueous solution involves the simultaneous doping by surrounding species. These suggests hole doping by oxygen in ambient air might occur at the same time due to the presence of water [2]. Tunable doping by hydrazine aqueous concentration is accompanied with the competition between electron doping by hydrazine and hole doping by oxygen in ambient atmosphere.

This project was supported by JSPS and RFBR under the Japan - Russia Research Cooperative Program.

[1] Z.Chen *et al.*, *APPLIED PHYSICS LETTERS* 106, 091602 (2015), [2] T.Umehara *et al.*, FNTG (2015)
[3] B.Chakraborty *et al.*, *PHYSICAL REVIEW* B 85, 161403(R) (2012)

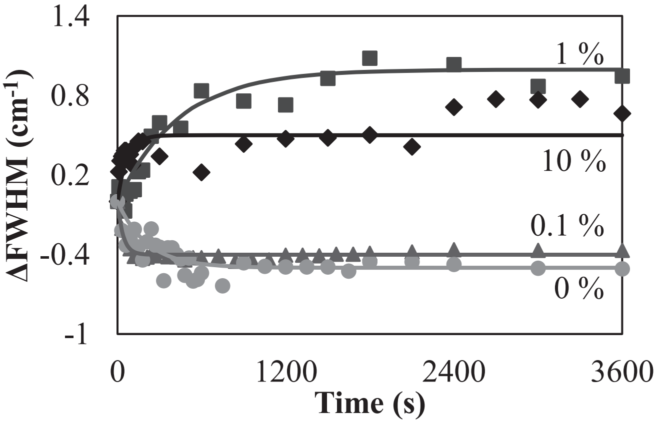

Fig.1 Kinetics of A_{1g} of Raman spectra for MoS_2 adsorbed with various concentration of hydrazine

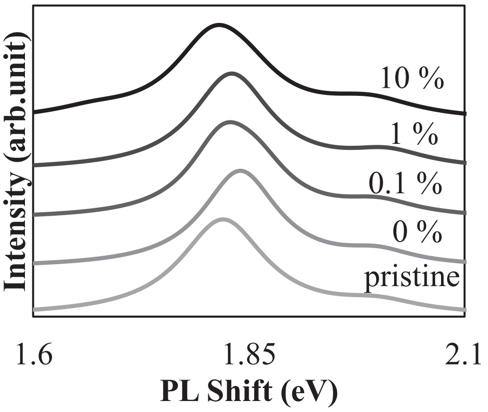

Fig.2 PL spectrum for MoS_2 pristine and adsorbed with various concentration of hydrazine at 3600 s

Corresponding Author: Kazuyuki Takai
Tel: +81-42-387-6138, Fax: +81-42-387-7002

1P-31

Carrier transport properties of WS_2 nanotubes obtained from solvothermally synthesized $W_{18}O_{49}$ nanowires

○Yohei Yomogida and Kazuhiro Yanagi

Department of Physics, Tokyo Metropolitan University, Tokyo 192-0397, Japan

Tungsten disulfide (WS_2) nanotubes are cylindrical multiwall nanotubes with various diameters. WS_2 nanotubes exhibit unique tunability of band gap and carrier mobility, and moreover, they have great advantages for semiconductor applications compared to carbon nanotubes because WS_2 nanotubes exhibit only semiconducting characteristics regardless how they are rolled [1]. Previously, we have investigated carrier transport properties of WS_2 nanotube networks using a chemical vapor deposition (CVD)-grown commercial sample [2]. Although we tried to prepare thin WS_2 nanotubes that attract much attention for their low dimensionality by structure sorting [3], that sample was not suitable due to its small content of thin nanotubes. To obtain thin WS_2 nanotubes, in this study, we performed synthesis of WS_2 nanotubes via sulfidation of solvothermally systhesized tungsten oxide ($W_{18}O_{49}$) nanowires [4].

$W_{18}O_{49}$ nanowires were synthesized via solvothermal reaction of WCl_6 in ethanol, carried out in a teflon-lined stainless-steel autoclave at 180 °C for 24 h. The obtained nanowires were reacted with sulfur at 840 °C for 2 h in N_2 flow to allow formation of WS_2 nanotubes. Fig. 1 shows the typical TEM image of the obtained WS_2 nanotubes. We successfully obtained WS_2 nanotubes with mean diameter of about 20 nm. This mean diameter is smaller than that of the sorted CVD-grown sample (33 nm) [2].

Carrier transport properties of the obtained WS_2 nanotubes were evaluated by ionic-liquid gating approaches. As shown in Fig. 2, the WS_2 nanotube networks exhibited ambipolar carrier transport. This result indicates thin WS_2 nanotubes obtained from solvothermally synthesized $W_{18}O_{49}$ nanowires are useful for semiconductor applications.

[1] G. Seifert et al, Solid State Commun. 114, 245-248 (2000). [2] M. Sugahara et al, Appl. Phys. Express 9, 075001 (2017). [3] Y. Yomogida et al, ACS Omega, accepted (2018). [4] Y. Chen et al, Mater. Res. Lett. 5, 508-515 (2017).

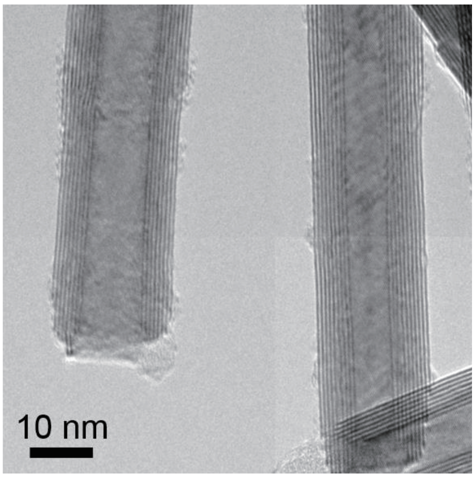

Fig. 1 TEM image of WS_2 nanotubes synthesized from solvothermally synthesized $W_{18}O_{49}$ nanowires

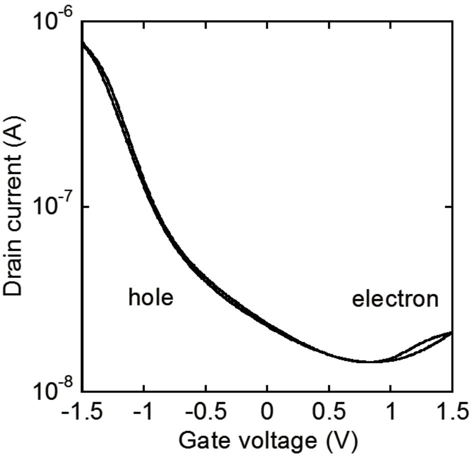

Fig. 2 Transistor characteristics of ionic-liquid gated WS_2 nanotube networks

1P-32

Gate-induced potassium intercalation to exfoliated MoS_2 flakes.

○Ryotaro Okada[1], Yohei Yomogida[1], and Kazuhiro Yanagi[1]

[1] *Department of Physic, Tokyo Metropolitan University, Hachioji, Tokyo 192-0397, Japan*

Molybdenum disulfide (MoS_2) belongs to semiconducting transition metal dichalcogenides (TMDCs) and attracts interest because of its remarkable physical characteristics such as superconducting transition. MoS_2 is known to show superconducting transition by various methods including chemical doping [1, 2] or ionic liquid gating [3, 4]. However, the resistance doesn't become zero. It is said that the residual resistance is caused by the inhomogeneous distribution of the superconducting state within the channel [3]. We expect that the inhomogeneity is due to the presence of local states on the surface of the sample such as defects because charge carriers can be accumulated only on the surface of materials in ionic liquid gating. On the other hand, in various TMDCs except for MoS_2, the technique of gate-induced alkali metal intercalation can lead TMDCs to superconducting state with zero resistance [5]. In this technique, we expect that the superconducting channel can be formed inside the layer. Therefore, by applying this technique to MoS_2, we investigate whether zero resistance appears or not in the exfoliated MoS_2 flakes.

We exfoliated a synthesized MoS_2 crystals (2D Semiconductors) and transferred that flake onto Si/SiO_2 substrate. Then, Ti/Au electrodes were deposited with shadow mask and potassium ion electrolyte was dropped.

Insulator-metal transition was observed from 3 V to 9 V of gate voltage (V_G). At $V_G = 12$ V, the resistance decreased drastically in low temperature region. We confirmed that this drop was due to superconducting transition by observing the disappearance of superconductivity at critical magnetic field. But as shown here, zero resistance was not observed. The resistance didn't become zero even at higher V_G, and superconducting phase-transition was clearly suppressed by over-doping at $V_G = 16$ V. In conclusion, gate-induced potassium intercalated MoS_2 could show superconductivity but could not show zero resistance. This result suggests the existence of inhomogeneity inside layer structure of the MoS_2 flake.

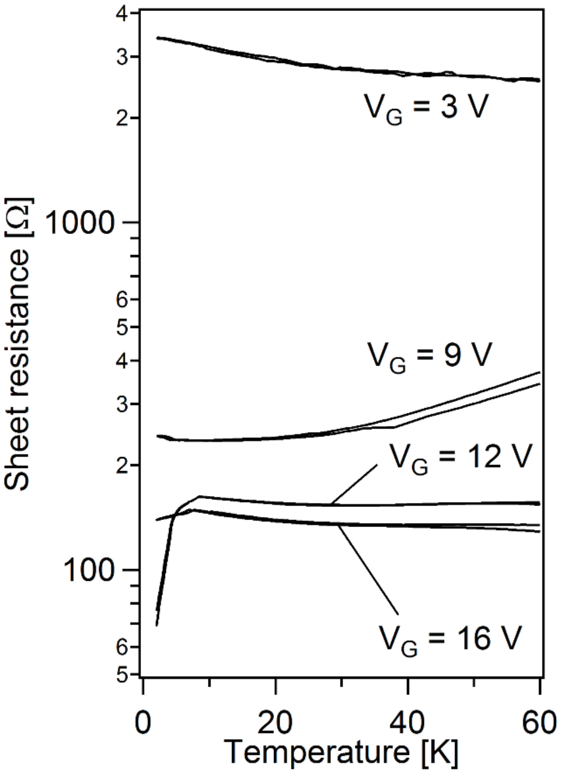

Fig. 1 Temperature dependence of the channel sheet resistance at various gate voltages (V_G).

[1] J. A. Woollam *et al.* Phys. Rev. B, **13**, 3843 (1976).
[2] J. A. Woollam *et al.* Mat. Sci. Eng., **31**, 289 (1977).
[3] K. Taniguchi *et al.* Appl. Phys. Lett., **101**, 042603 (2012).
[4] J. T. Ye *et al.* Science, **388**, 1193 (2012).
[5] W. Shi *et al.* Sci. Rep., **5**, 12534 (2015).

Corresponding Author: K. Yanagi
Tel: +81-42-677-2809
Web: http://www.comp.tmu.ac.jp/nano2/
E-mail: yanagi-kazuhiro@tmu.ac.jp

1P-33

Photoluminescence weakening and overlayer deposition of WS_2 induced by van der Waals interaction

°Hyun Goo Ji[1], Adha Sukma Aji[1], Kazunari Matsuda[2], and Hiroki Ago[1,3]

[1]Interdisciplinary Graduate School Engineering Science, Kyushu University, Fukuoka 816-8580
[2]Institute of Advanced Energy, Kyoto University, Kyoto 611-0011
[3]Global Innovation Center (GIC), Kyushu University, Fukuoka 816-8580

Recently, transition metal dichalcogenides (TMDCs) have attracted a great interest due to their unique electronic and optical properties. Chemical vapor deposition (CVD) has been regarded as the most promising method to synthesize large-area TMDCs with high reproducibility.[1,2] Having similar hexagonal crystal structure with many TMDCs, c-plane sapphire is commonly utilized as a growth substrate in the CVD growth.[3] However, few studies have been reported on the influence of sapphire substrate on growth behavior and physical properties of TMDCs.[4] Therefore, it is worthwhile to investigate in more detail.

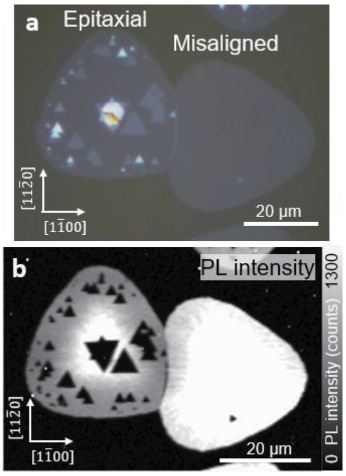

Fig. 1. (a) Optical image and (b) PL intensity mapping image of as-grown WS_2 grains on sapphire substrate. The crystal axes of sapphire are also shown.

In this work, we demonstrate that higher strain is induced in the epitaxially grown WS_2 grains via van der Waals interaction with sapphire as compared with misaligned WS_2 grains. Figure 1 shows the optical image of as-grown WS_2 grains and their photoluminescence (PL) mapping image. It is clearly seen that the epitaxial grain shows weaker PL intensity and a preferential multilayer growth. The van der Waals interaction on epitaxial grain is attributed to induce a structural distortion and electronic disorder, resulting in multilayer formation.[5] Figure 2 shows PL spectra of (a) as-grown and (b) transferred WS_2 grains measured at different temperatures. In as-grown WS_2, the epitaxial grain showed weaker and broader PL which became almost comparable with misaligned grain after transfer. It reflects strong van der Waals interaction between as-grown epitaxial grain and sapphire substrate. Moreover, no significant difference was observed in the electrical transport properties of transferred WS_2 grains (Figure 2c), indicating the strong coupling with sapphire does not cause severe crystal defects in the epitaxially grown grains. We believe our work gives new understanding of the influence of sapphire on the growth behavior of TMDCs.[6]

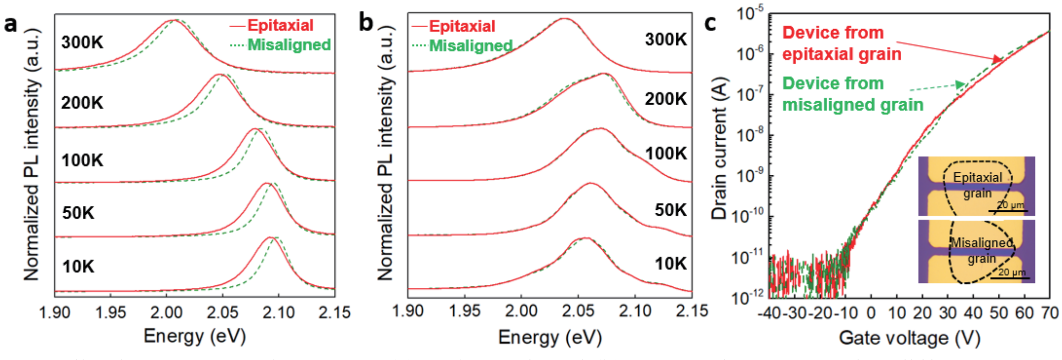

Fig. 2 Normalized PL spectra of as-grown (a) and transferred (b) WS_2 grains measured at different temperatures. (c) Transfer curves of aligned and misaligned WS_2 grains which were measured after the transfer on SiO_2/Si substrate for back-gate geometry (V_d = 1V). The insets show optical images of fabricated FET devices.

References: [1] S. J. Yun *et al.*, *ACS Nano,* **2015**, *9*, 5510. [2] H. G. Ji *et al.*, *Chem. Mater.*, **2018**, *30*, 403. [3] D. Dumcenco *et al.*, *ACS Nano*, **2015**, *9*, 4611. [4] Y. Hoshi *et al.*, *Phy. Rev. Mater.*, **2018**, *2,* 064003. [5] H. J. Conley *et al.*, *Nano Lett.,* **2013**, *13*, 3626. [6] H. G. Ji *et al.*, submitted.

Correspondence: H. Ago (Tel&Fax: +81-92-583-8815, E-mail: h-ago@gic.kyushu-u.ac.jp)

1P-34

Edge controllable growth of hexagonal boron nitride crystals by atmospheric pressure chemical vapor deposition

○ Kamal P Sharma[1,2], Aliza Khaniya Sharma[1], Golap Kalita[3], Masaki Tanemura[3], Takahiro Maruyama[1,2]

[1] Department of Applied Chemistry, Meijo University, Nagoya 468-8502, Japan
[2] Nanomaterials Research Center, Meijo University, Nagoya 468-8502, Japan
[3] Department of Physical Science and Engineering, Nagoya Institute of Technology, Nagoya 466-8555, Japan

Hexagonal boron nitride (h-BN) shows a structural analog of graphene and is a wide band gap 2D insulator consisting of alternating sp^2–bonded boron and nitrogen atoms [1]. h-BN is also realized as a promising substrate for pristine functionality of other 2D materials (graphene, MoS_2, WS_2, etc.) and widely used in different electronic and optoelectronics applications [2]. Nowadays, chemical vapor deposition (CVD) technique is adopted to grow large area h-BN on various transition metals. However, due to complexity in growth mechanism, single domain size has been limited to a few micro meters [3]. Herein, we tackled the controllable synthesis of h-BN larger than 25µm in edge length.

For h-BN crystals synthesis, a bare Cu foil was loaded into the horizontal tubular furnace and heated at 10.5ºC/min from room temperature to 1050ºC with 100 sccm Ar. After annealing the Cu foil for 30 min with Ar:H_2=100:17 sccm, h-BN source (Ammonia borane (AB, H_3BNH_3)) was evaporated for 62min (largest crystals of 25µm) with Ar:H_2=100:2 sccm. Subsequently, the growth furnace was rapidly cooled down to room temperature within 30min. As synthesized h-BN crystals were analyzed by optical microscopy (OM), SEM, XPS, AFM and TEM.

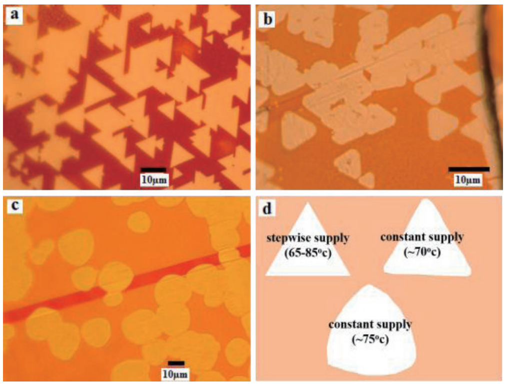

Fig. 1. OM images of h-BN crystals with (a) stepwise heating, and (b), (c) constant temperature heating of AB at 70ºC and 75ºC respectively. (d) Schematics representation of observed crystal shapes.

Fig. 1(a) shows the OM image of regular shaped (N-terminated) triangular h-BN crystals grown by stepwise decomposition of AB. However, on constantly heating AB at 70 and 75ºC, truncated [Fig. 1(b)] and Reuleaux [Fig. 1(c)] shaped triangular h-BN crystals were synthesized, respectively. Thus, we achieved controllable synthesis of h-BN crystals.

[1] K. K. Kim et al., Nano Lett. 12, 161 (2012).
[2] F. Withers et al., Nat. Mater. 14, 301 (2015).
[3] R. Y. Tay al., Nanoscale 8, 2434 (2016).

Corresponding Author: Takahiro Maruyama
E-mail: takamaru@meijo-u.ac.jp

1P-35

Electronic structure of thin films of hydrocarbon molecules under an external electric field

○Manaho Matsubara[1] and Susumu Okada[1]

[1] *Graduate School of Pure & Applied Sciences, University of Tsukuba, Tsukuba 305-8571 Japan*

Hydrocarbon molecules are representative materials for various functional devices, because of their tunable electronic properties by controlling the molecular shapes and conformations. Indeed, it has been demonstrated that condensed structures of hydrocarbons can be utilized in photovoltaic, thermoelectric, and electronic devices, as for the promising materials to endow the devices with remarkable flexibility. In such devices, carrier accumulation in hydrocarbons by the electrode and counter molecules/atoms is essential for their functionalities. However, microscopic insight into the distribution of accumulated carrier in condensed structures of hydrocarbons are not addressed to date, because of their complex geometries of surfaces and interfaces with respect to the electrode or counter materials arising from van der Waals spacing around the molecules. Thus, in this work, we aim to investigate the influence of the molecular conformations of hydrocarbons on the carrier accumulation under an external electric field, using the density functional theory combined with the effective screening medium method. To simulate the carrier accumulation in hydrocarbon complexes, we consider naphthalene thin films in the field-effect transistor structure where the electrode is simulated by using the effective screening medium method. In the thin film, naphthalene has flat, undulated, or staggered conformations with respect to the electrode.

Our calculations show that distribution of accumulated carrier depends on molecular arrangement to the electrode. Fig.1 shows the bird-eye-views of accumulated carriers in the naphthalene films with various molecular arrangements with respect to the electrode. In the thin film with the flat molecular arrangement to the electrode, the carrier is uniformly injected into the thin film. In contrast, as for the thin film in which the molecules possess undulated or staggered arrangements to the electrode, the injected carriers exhibit inhomogeneous distribution on the particular plane parallel to the electrode. These facts imply that the molecular arrangements of the hydrocarbon in their thin films seriously affect their transport properties with FET structures.

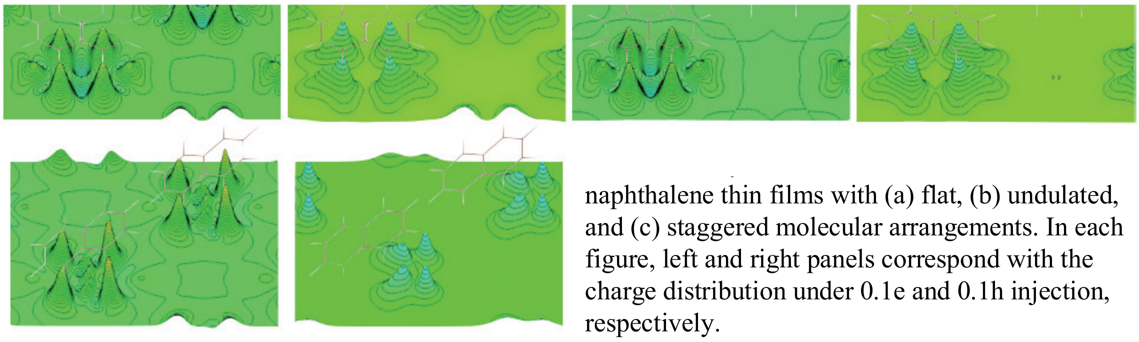

naphthalene thin films with (a) flat, (b) undulated, and (c) staggered molecular arrangements. In each figure, left and right panels correspond with the charge distribution under 0.1e and 0.1h injection, respectively.

Corresponding Author: M. Matsubara
Tel: +81-29-853-5921,
E-mail: mmatsubara@comas.frsc.tsukuba.ac.jp

1P-36

Direct Exfoliation of Graphene and h-BN with Various Photosensitizers in Water Aiming at Cancer Phototherapy

Ahmad Tayyebi, Naoko Ogino, Naoki Komatsu*
Graduate School of Human and Environmental Studies, Kyoto University, Kyoto 606-8501

Photodynamic therapy (PDT) and photothermal therapy (PTT) are noninvasive treatments for cancer. Recently, our group reported on the direct and simple approach for water-dispersable graphene-chlorine e6 (G-Ce6) composites [1]. The composite shows significant cytotoxicity under light irradiation. In this paper, we extend this approach to various combination of 2D nanosheets and photosensitizers, and investigate the stability of composites and phototherapeutic efficacy for cancer cells.

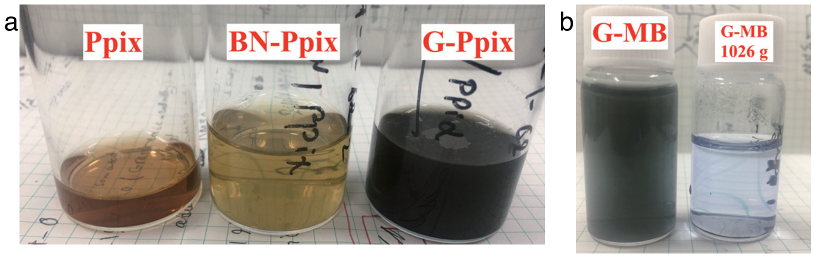

Figure 1: Images of Ppix, BN-Ppix and G-Ppix in water (a), and G-MB before and after centrifugation (b).

To prepare the composites, bulk 2D material (graphite or hexagonal boron nitride (h-BN)) and photosensitizer (protoporphyrin ix (Ppix) or methylene blue (MB)) were bath-sonicated in 20 mL water for 36 h. The resulting suspensions were centrifuged at 1026*g*. Ppix with graphite and h-BN gave stable aqueous dispersions (Figure 1a), implying the composite formation of 2D nanosheet with Ppix (G-Ppix and BN-Ppix, respectively) as in the case of G-Ce6. However, MB cannot form stable dispersion, because of no blackish dispersion after centrifugation (Figure 1b).

To confirm the complexation, the absorption spectra were measured as shown in Figure 2. It is shown that the Soret bands of Ppix are red-shifted in both G-Ppix and BN-Ppix. Large upward baseline shift is observed in the case of G-Ppix due to the absorption of graphene. On the other hand, BN-Ppix exhibits large upward baseline shift only at the shorter wavelength probably because of the scattering from the h-BN nanosheet.

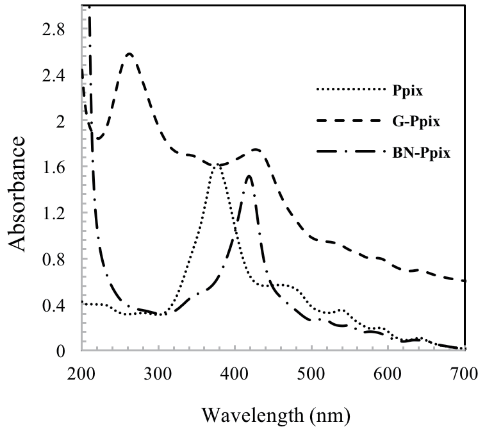

Figure 2: Absorption spectra of Ppix solution and, G-Ppix and BN-Ppix dispersions in water.

We will continue to investigate the structure and aqueous stability of these composites and evaluate the phototherapeutic efficacy.

[1] G. Liu, H. Qin, T. Amano, T. Murakami, and N. Komatsu, *ACS Appl. Mater. Interfaces*, **7**, 23402 (2015).

Corresponding Author: N. Komatsu
Tel, Fax: +81-75-753-6833 E-mail: komatsu.naoki.7w@kyoto-u.ac.jp

2P-1

General Method for the Synthesis of Transition-metal Dichalcogenide Nanoribbons Inside Carbon Nanotubes

○Motoki Aizaki,[1] Ellen Park,[1] Zheng Liu,[2] Kazu Suenaga,[2] Yusuke Nakanishi,*[1,3] and Hisanori Shinohara*[1,3]

[1] *Department of Chemistry, Nagoya University, Nagoya 464-8602, Japan.*
[2] *National Institute of Advanced Industrial Science and Technology (AIST), Tsukuba 305-8565, Japan.*
[3] *Institute for Advanced Research, Nagoya University, Nagoya 464-8602, Japan.*

Transition-metal dichalcogenides (TMDs) have emerged as another important class of 2D materials with unique physical properties, after the discovery of graphene. When reduced to nanoribbon geometries, the inherently different nature of TMDs is likely to provide more complexities in comparison to their graphene counterparts. However, exploration of 1D TMDs' exotic electronic [1] and magnetic [2] properties has been hindered due to challenges with synthesizing high-quality samples with precise width and thickness at the atomic level. The inner hollow spaces of carbon nanotubes (CNTs) can serve as nano-reactors for the synthesis of well-defined TMD nanoribbons [3]. Although there have been a few reports of syntheses of TMD nanoribbons inside CNTs, limited success has been achieved in fabricating MoS_2 and WS_2 nanoribbons that are several tens of nanometers in length [4].

Here we report the CNT-templated syntheses of a series of TMD nanoribbons based on the vapor-phase reaction of a highly reactive metal chloride and chalcogen. We have utilized this bottom-up reaction to achieve the first synthesis of $NbSe_2$/WSe_2 nanoribbons with a sub-nanometer width. Precise atomic-level nanoribbon structures synthesized in experiments were confirmed by high-resolution electron microscopy (HRTEM). In particular, MoS_2 nanoribbons have a smooth zigzag edge (Fig 1) and a length of over 100 nm. The present simple reaction, in principle, can be applied to fabricate various TMD nanoribbons, depending on the corresponding metal chlorides and chalcogen. Our results will lead to the experimental studies of the physical properties of TMD nanoribbons.

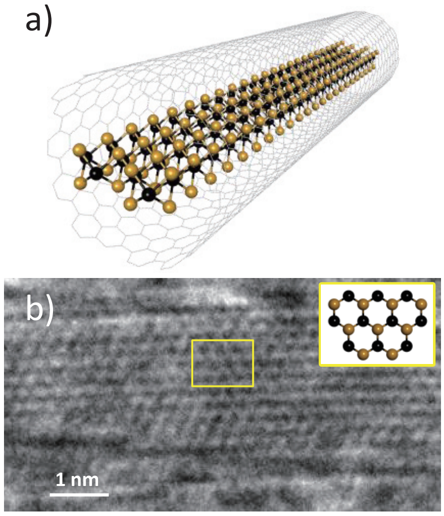

Fig.1. (a) Schematic and (b) HRTEM images of an individual MoS_2 nanoribbon confined within a single-walled CNT.

[1] Y. Cai *et al., J. Am. Chem. Soc.*, **136**, 6269 (2014)
[2] Y. Li *et al., J. Am. Chem. Soc.*, **130**, 16739 (2008); P. Cui *et al., Nano Lett.*, **17**, 1097 (2017)
[3] H. Shinohara, *Jpn. J. Appl. Phys.*, **57**, 020101 (2018)
[4] Z. Wang *et al., J. Am. Chem. Soc.,* **132**, 13840 (2010); A. Botos *et al., J. Am. Chem. Soc.*, **138**, 8175 (2016)

Corresponding Author: Y. Nakanishi and H. Shinohara
Tel: +81-52-789-3660, Fax: +81-52-747-6442
Web: http://nano.chem.nagoya-u.ac.jp/
E-mail: nakanishi.yusuke@g.mbox.nagoya-u.ac.jp, noris@nagoya-u.jp

2P-2

Morphology-dependent Thermal Transport of Single-walled Carbon Nanotube Films

○Takuya KITANO[1], Tsuyoshi KAWAI[1], Yoshiyuki NONOGUCHI[1,2]

[1] *Graduate School of Materials Science, Nara Institute of Science and Technology, NAIST, 8916-5 Takayama Ikoma Nara*
[2] *JST PRESTO, 4-1-8 Honcho, Kawaguchi, Saitama 332-0012, Japan*
E-mail : kitano.takuya.kk1@ms.naist.jp : nonoguchi@ms.naist.jp

[Introduction]

The thermal conductivity of single-walled carbon nanotubes (SWNTs) has been reported to span from ~10^1 W m^{-1} K^{-1} for buckypapers to ~10^3 W m^{-1} K^{-1} for a single nanotube.[1-3)] Such discrepancy could be considered to stem from interface thermal resistance between SWNTs, where the control of nanotube bundle morphology is crucial for exploiting the tunability of SWNTs' thermal conductivity. Here we examine the thermal conductivity of films made from well-dispersed, and chemically-aggregated SWNTs.

[Method]

We used o-dichlorobenzene (o-DCB) as a good solvent to disperse SWNTs. Then o-xylene, a poor solvent, was added to the uniform dispersion in order to intentionally aggregate SWNTs. Finally, we fabricated 30 um-thick SWNT films by filtering the dispersion onto 0.2um-pore membranes

[Result and discussion]

We successfully fabricated the films made from the SWNTs of averaged bundle diameters ranging from 13±0.8 nm to 65±5 nm (Fig. 1 (a)). In this range, SWNT films showed tunable thermal conductivity (Fig. 1 (b)). Aggregated SWNT films showed the apparently mono-component time profile of heat detection in the Xenon flash method, where the thermal diffusivity of less than 50 mm^2 sec^{-1} was estimated. Similar film diffusivity has been reported in the many literatures. On the other hand, films composed of the most exfoliated SWNTs exhibited the fastest, and subsequent components thereafter. The fastest one yields the thermal diffusivity exceeding 2000 mm^2 sec^{-1}. Importantly, we found that the contribution of several components relies on the SWNT bundle diameters, that is, morphological dispersibility.

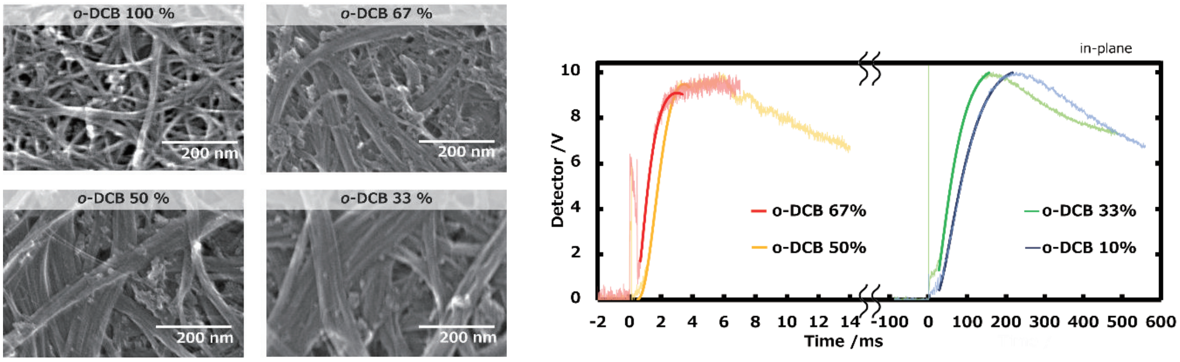

(a) (b)

Fig 1. (a) Scanning electron microscope photographs (b) Xenon flash profiles (Red : o-DCB 67%, Yellow : o-DCB 50%, Green : o-DCB 33%, o-DCB 10%)

1) Ya Feng. *et al*. Appl. Phys. Lett. 112, 191904 (2018)
2) J. Hone. *et al.* APL 77, 666 (2000).
3) Philippe Gonnet. *et al.* Curr. Appl. Phys. 6, 119 (2006).

2P-3

Tuning the electronic properties of single-walled carbon nanotubes by defluorination-assisted nitrogen doping and defect formation for efficient oxygen reduction electrocatalysis

○Koji Yokoyama[1], Yoshinori Sato[2], Masashi Yamamoto[2], Tetsuo Nishida[2],
Kenichi Motomiya[1], Kazuyuki Tohji[1], Yoshinori Sato[1,3]

[1]Graduate School of Environmental Studies, Tohoku University, Sendai 980-8579, Japan
[2]Stella Chemifa Corporation, Osaka 595-0075, Japan
[3]Institute for Biomedical Sciences, Interdisciplinary Cluster for Cutting Edge Research, Shinshu University, Matsumoto 390-8621, Japan

Recently, nitrogen-doped and non-doped defective carbon nanotubes (CNTs) have been reported to be metal-free, durable, and highly efficient oxygen reduction reaction (ORR) electrocatalysts as alternatives to platinum [1,2]. However, the roles of nitrogen species and defects in CNTs for the ORR catalytic activity are still under debate. Theoretical reports suggest that nitrogen species and defects in CNTs alter their electronic properties and hence facilitate the ORR [3,4]. Meanwhile, the experimental relationship between the electronic property and ORR catalytic activity has not been fully investigated. Here, we synthesized nitrogen-doped and non-doped defective single-walled CNTs (SWCNTs) by defluorination-assisted nitrogen doping [5] and defect formation. Moreover, we evaluated their ORR catalytic activities [6], and correlated them with their electronic properties including work function (WF) and conductivity.

Highly crystalline SWCNTs synthesized by the arc-discharge method were fluorinated at 250 °C using 20% F_2/N_2 gas for 4 h. N-SWCNTs were prepared by annealing the fluorinated SWCNTs at 500 °C for 30 min in a gas flow of 1% NH_3/N_2. The N-SWCNTs were further annealed at 1000 °C for 3 h in a N_2 flow to synthesize AN-SWCNTs. To prepare non-doped defective SWCNTs (AF-SWCNTs), the fluorinated SWCNTs were annealed at 1000 °C for 3 h in a N_2 flow. The ORR catalytic activities of the prepared samples were evaluated by electrochemical measurements using RDE in 0.5 M H_2SO_4. The WF and conductivity were measured by ultraviolet photoelectron spectroscopy and four-probe method, respectively.

Judged from the onset potential (E_{onset}) and number of electrons transferred per oxygen molecule (n) involved in the ORR, the AN-SWCNTs exhibited the highest ORR catalytic activity (Fig. 1). The AN-SWCNTs contained 0.8 at% nitrogen consisting of enriched graphitic-type species. The WF of the AN-SWCNTs was lower than those of the hc-, N-, and AF-SWCNTs, while the conductivity of the AN-SWCNTs was higher than those of the N- and AF-SWCNTs. These results suggest that low WF and high conductivity observed in the AN-SWCNTs can contribute to excellent ORR catalytic activity.

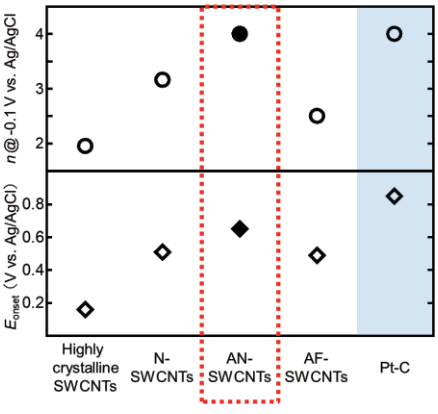

Fig. 1 E_{onset} and n @ -0.1 V (vs. Ag/AgCl) involved in ORR for the highly crystalline, N-, AN-, and AF-SWCNTs, and Pt-C.

[1] K. Gong *et al.*, Science **323**, 760 (2009).
[2] K. Waki *et al.*, Energy Environ. Sci. **7**, 1950 (2014).
[3] S. Ni *et al.*, Nanoscale **4**, 1184 (2012).
[4] S. Jiang *et al.*, Nanoscale **6**, 14262 (2014).
[5] K. Yokoyama *et al.*, Carbon **94**, 1052 (2015).
[6] K. Yokoyama *et al.*, J. Mater. Chem. A **4**, 9184 (2016).

Corresponding Author: Y. Sato
Tel & Fax: +81-22-795-3215,
E-mail: yoshinori.sato.b5@tohoku.ac.jp

2P-4

Local strain control for realization of low-voltage operable, highly-stretchable carbon nanotube thin-film transistors

○Yuya Nishio[1], Jun Hirotani[1], Shigeru Kishimoto[1], and Yutaka Ohno[1,2]

[1]*Department of Electronics, Nagoya University, Nagoya 464-8603, Japan*
[2]*Institute of Materials and Systems for Sustainability, Nagoya University, Nagoya 464-8603, Japan*

Stretchable devices can closely contact with stretchable free-form surface, and they are expected for wearable devices to realize continuous monitoring of human activities and health conditions. Many approaches such as deformable serpentine bridge designs [1] and stretchable devices using random network of out-of-plane wrinkles [2] have been reported. However, they showed low-stretchability and constraints in terms of circuit design. Although stretchable carbon nanotube thin-film transistors (CNT TFTs) have also been reported, they showed degradation of electrical performance with applied strain. [3] Recently, intrinsically stretchable transistors were reported, however, they needed to be operated at high gate voltage because low dielectric constant polymer is used as a gate dielectric layer. [4] In this work, we have realized the CNT TFTs which provides low-voltage operation and high stretchability simultaneously by introducing the local strain control layer.

We fabricated CNT TFTs with a channel of a semiconducting-CNT thin film, transparent electrodes of a CNT thin film, and a 50 nm-thick Al_2O_3 gate dielectric layer on a stretchable poly(dimethylsiloxane) (PDMS) film. In order to suppress the influence of applied strain, local strain control layer composed of a rigid polymer was introduced on top of the channel region of the CNT TFTs.

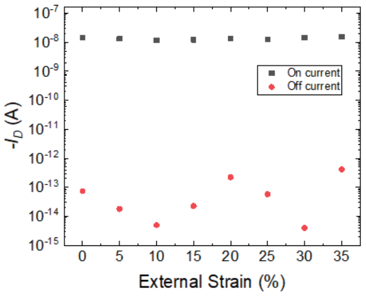

Fig. 1 ON and OFF currents as a function of externally applied tensile strain.

The fabricated CNT TFTs exhibited typical p-type transistor characteristics with a carrier mobility of 6.8 cm^2/Vs and on/off ratio of about 10^5, and was operable at gate voltage of less than 2 V. They also showed the robust electrical performances against applied strain as shown in Figure 1. Figure 2 shows the measured strain induced in the channel region during stretching cycle perpendicular to the channel direction. By introducing strain control layer, only 1.5 % of externally applied tensile strain was induced in the channel region, clearly showing the effectiveness of the strain control technique.

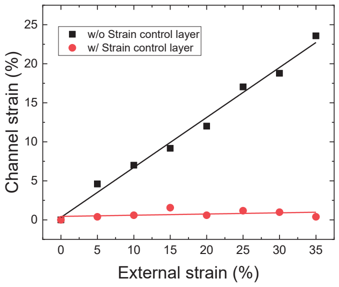

Fig. 2 Measured strain induced in the channel region as a function of externally applied tensile strain.

[1] D.-H. Kim *et al.*, Proc. Natl. Acad. Sci., **105**, 18675 (2008).
[2] M. Kaltenbrunner *et al.*, Nature **499**, 458 (2013).
[3] D.-M. Sun *et al.*, Nat. Commun. **4**, 2302 (2013).
[4] S. Wang *et al.*, Nature **555**, 83 (2018).

Corresponding Author: Y. Ohno
Phone & Fax: +81-52-789-5387, E-mail: yohno@nagoya-u.jp

2P-5

Ratchet-free solid-state inertial rotation of a guest ball in a tight tubular host

○Taisuke Matsuno[1], Yusuke Nakai[2], Sota Sato[1], Yutaka Maniwa[2], Hiroyuki Isobe[1]

[1] Department of Chemistry, The University of Tokyo and JST ERATO, Bunkyo-ku, Tokyo 113-0033, Japan
[2] Department of Physics, Tokyo Metropolitan University, Hachioji, Tokyo 980-8578, Japan

Solid-state dynamics of [60]fullerene (C_{60}) is controlled by intimate intermolecular face-to-face contacts and results in restricted motions at low temperatures [1]. Manipulation of the solid-state dynamics of fullerene molecules is thus an interesting yet challenging problem.

We have previously synthesized a finite (12,8)-helical carbon nanotube molecule called [4]CC, that binds C_{60} to form a peapod-like host-guest complex ([4]CC$\supset$$C_{60}$, Fig. 1 and 2a) [2]. Here we report that this tubular host liberates the solid-state dynamics of C_{60} from the motional restrictions. Variable-temperature crystallographic analyses indicated that the electron density of C_{60} more evenly distributed at higher temperature, indicating the liberated degree of freedom (Fig. 2b). The solid-state dynamics has been quantitatively unveiled by solid-state ^{13}C NMR (Fig 2c). The line-shape and relaxation time analyses revealed a small energy barrier of +2 kcal mol^{-1} for the reorientation. This value is unexpectedly small, because the association between the tube and C_{60} is a large energy gain of –14 kcal mol^{-1}. The solid-state rotational motions reached a non-Brownian, inertial regime with an extremely rapid rotational frequency of 213 GHz at 335 K [3].

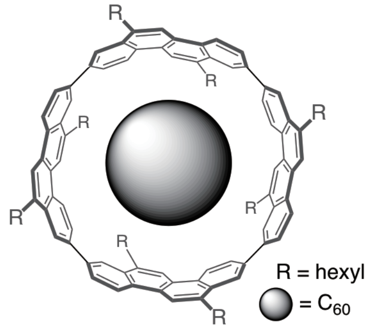

Fig. 1. Chemical structure of the host-guest complex [4]CC$\supset$$C_{60}$.

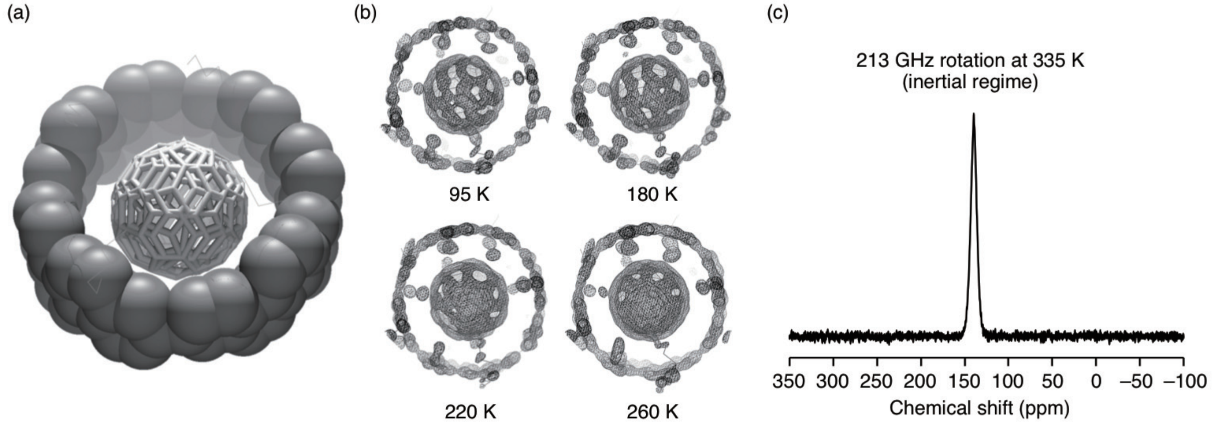

Fig 2. Structures and dynamics of [4]CC$\supset$$C_{60}$. (a) Side view of the crystal structure at 295 K. (b) Temperature-dependent electron density mappings with $2F_o–F_c$ (RMSD: 1.5σ). (c) Solid-state ^{13}C NMR spectra of C_{60} in [4]CC indicating rapid free rotation.

[1] Johnson, R. D.; Yannoni, C. S.; Dorn, H. C.; Salem, J. R.; Bethune, D. S. *Science* **1992**, *255*, 1235-1238.

[2] Isobe, H.; Hitosugi, S.; Yamasaki, T.; Iizuka, R. *Chem. Sci.* **2013**, *4*, 1293-1297.

[3] Matsuno, T.; Nakai, Y.; Sato, S.; Maniwa, Y.; Isobe, H. *Nat Commun.* **2018**, *9*, 1907.

Corresponding Author: H. Isobe
Tel: +81-(0)3-5481-4777, Fax: +81-(0)3-5841-4162
Web: http://www.chem.s.u-tokyo.ac.jp/users/physorg/
E-mail: isobe@chem.s.u-tokyo.ac.jp

2P-6

Repeated synthesis of vertically-aligned CNTs via reduction-CVD-oxidation treatment of Co-Al-O catalyst layer

○Toshihiro Sato[1], Hisashi Sugime[2], Richard M. Laine[3], Suguru Noda[1, 4]

[1] Department of Applied Chemistry, School of Advanced Science and Engineering, Waseda University, 3-4-1 Okubo, Shinjuku-ku, Tokyo 169-8555, Japan
[2] Waseda Institute for Advanced Study, Waseda University, 1-6-1 Nishi waseda, Shinjuku-ku, Tokyo 169-8050, Japan
[3]Department of Materials Science and Engineering and the Macromolecular Science and Engineering Center, University of Michigan
[4]Waseda Research Institute for Science and Engineering, Waseda University, Tokyo 169-8555, Japan.

It is well known that the catalyst nanoparticles (NPs) get coarsened through Ostwald ripening [1] during chemical vapor deposition (CVD), resulting in growth termination of vertically-aligned carbon nanotubes (VA-CNTs). We here propose and develop an approach for repeated CNT synthesis via oxidation and dissolution of the coarsened Co NPs to the Al_2O_3 underlayer and reduction and segregation of Co NPs from the $CoAl_2O_4$ layer (Fig. 1).

We prepared the Co/Al_2O_3 catalyst layer on a SiO_2/Si substrate with a wide thickness range (0.20–20 nm) using the combinatorial masked deposition method (0.20–20 nm) [2]. The substrate was annealed at 900 °C in O_2/N_2 to form $CoAl_2O_4$ layer, and then was reduced at 800 °C in $H_2/CO_2/Ar$ to form Co NPs. CNTs were grown by CVD by flowing $C_2H_2/CO_2/H_2/Ar$ at 800 °C, and were detached from the substrate using a scotch tape. The substrate was then annealed under O_2/N_2 at 800 °C to dissolve the coarsened Co NPs in the Al_2O_3 layer. We repeated the reduction-CVD-oxidation treatment for three cycles, and confirmed similar CNT growth keeping ~200 μm height for ~20 nm thick Co layer (Fig.2).

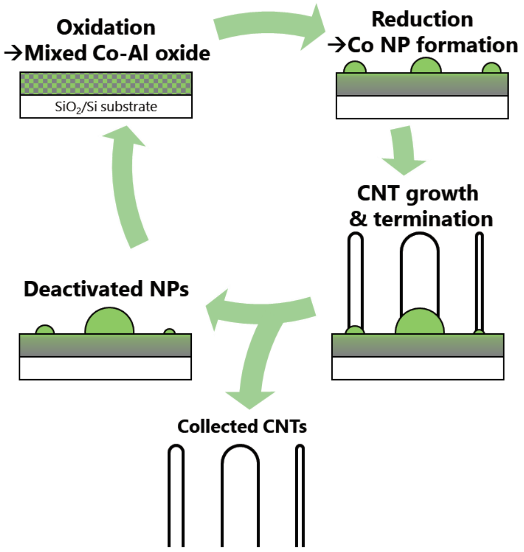

Fig. 1 Schematics of the method resetting Co NPs with reduction-oxidation treatment

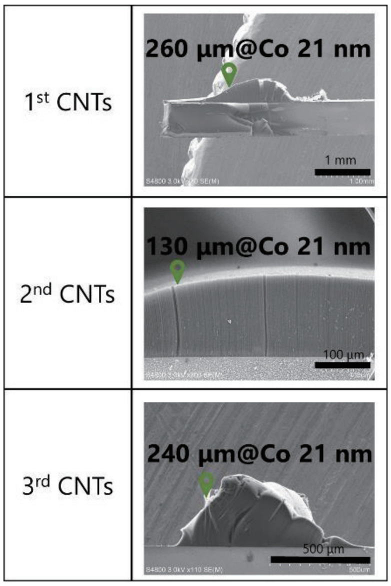

Fig.2 Repeated VA-CNT synthesis on sputtered CoO and Al_2O_x

[1] K. Hasegawa, S Noda, *Carbon* **49**, 4497 (2011).
[2] S. Noda et al., Carbon **44**, 1414 (2006).

Corresponding Author: S. Noda, Tel: 03-5286-2769, E-mail: noda@waseda.jp

2P-7

Performance improvement of transparent solar cell using few-layered transition metal dichalcogenide by Schottky barrier control

○Y. Yamaguchi[1], W. Okita[1], C. Li[1], T. Kaneko[1], and T. Kato[1,2]

[1]*Department of Electronic Engineering, Tohoku University, Sendai 980-8579, Japan*
[2] *JST-PRESTO*

Layered transition metal dichalcogenide (TMD) is one of the most attractive materials for future transparent and flexible optoelectrical devices due to their atomically thin structure, band gap in visible light range, and high optical transparency. Although the solar cell of TMD has been widely investigated by many groups, those are based on the pn junction type solar cell. Since complicated structures are required to form pn junction structures in TMD such as dual gate electrodes or position selective doping, the device size of pn junction solar cell with TMD is limited within very small region (few μm). In spite of the outstanding advantages of TMD, those merits of TMD have not been applied for transparent and flexible solar cell, which is attracted intense attention as a next-generation energy harvesting technology.

Recently, we have developed a new fabrication process of TMD-based solar cell [1]. In our process, Schottky type device configuration is utilized, which can be simply formed by asymmetrically contacting electrodes and TMD. The power conversion efficiency (PCE) clearly depended on the work function difference between two electrodes (ΔWF). A higher efficiency could be obtained with higher ΔWF (Pd-Ni), which is consistent with our concept. Based on the optimizations of electrodes and distance, the PCE can be reached up to 0.7 %, which is the highest value for solar cell with similar TMD thickness [1].

In our previous study, we used conventional metals such as Ni and Pd to tune the Schottky barrier height between electrode and TMD. To improve the transparency of whole device, however, it is required to use transparent electrodes. In this study, we use indium tin oxide (ITO) as an electrode and form transparent and flexible solar cell. Since controlling ΔWF is a key to improve the PCE in our device, the surface of ITO was functionalized by various plasma treatments with hydrogen, nitrogen and oxygen as reactive species. It is found that the work function of ITO can be controlled by changing plasma species and treatment time (Fig. 1). After controlling the ΔWF of ITO electrodes with plasma treatments, clear power generation can be observed. It is also found that the PCE increases with ΔWF controlled by N_2 plasma treatment (Fig. 2). Since our simple fabrication process includes high potential for large scale fabrication, this achievement is very important for realizing the industrial application of TMD as a transparent and flexible solar cell.

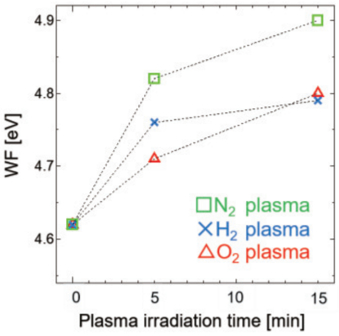

Fig. 1. WF variation of ITO after different plasma treatments.

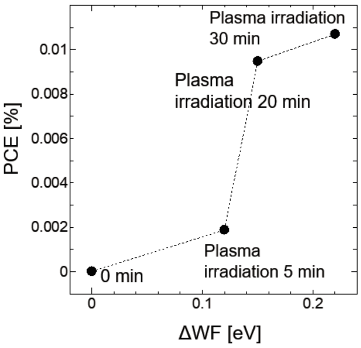

Fig. 2. PCE as a function of ΔWF between ITO electrode pairs.

[1] T. Akama, W. Okita, R. Nagai, C. Li, T. Kaneko, and T. Kato: Sci. Reports **7** (2017) 11967.

Corresponding Author: Y. Yamaguchi

Tel: +81-22-795-7046, Fax: +81-22-263-9225, E-mail: yoshiki.yamaguchi.t5@dc.tohoku.ac.jp

2P-8

Universality in Transition Metal Dichalcogenide Light-Emitting Devices

○Hirofumi Matsuoka[1], Juliette Tempia [1], Tomoyuki Yamada [1], Tomohiro Ogura [1],
Lain-Jong Li [2], Tomo Sakanoue [1], Jiang Pu [1], and Taishi Takenobu [1]
[1] Department of Applied Physics, Nagoya University, Nagoya 464-8603, Japan
[2] Physical Science and Engineering, KAUST, Thuwal, 23955-6900, Kingdom of Saudi Arabia

Transition Metal Dichalcogenide (TMDC) monolayers have attracted much interest as active materials for light-emitting devices due to their atomically thin thickness, direct bandgap, and spin-valley coupled electronic structure [1-3]. However, most relevant TMDC light-emitting devices are made using tiny samples and it is highly required to fabricate devices using large-area TMDC monolayers for practical applications. Recently, we proposed a novel device structure, in which two electrodes were deposited on a TMDC film and cover them with an electrolyte. We successfully achieved light emission from large-area WSe_2 and MoS_2 polycrystalline films [4]. Although we observed clear electroluminescence (EL) images of these devices (Figs. (a), (b) and (c)), the position of the recombination zone was strongly sample dependent and the detailed operational mechanism is still an open questions. Here, to understand the behind mechanism of these light-emitting devices, we fabricate several devices using various TMDC monolayers and try to find the universality among them.

We fabricated electrolyte-based transistors of centimeter-scale polycrystalline WSe_2, $MoSe_2$, and WS_2 monolayers using ion gels, a mixture of an ionic liquid and a triblock co-polymer. Firstly, we operated these devices as light-emitting devices using two electrodes on TMDC films. As shown in Figs. (a), (b), and (c), just by applying voltages, we observed the clear EL images between the two electrodes through a microscope and a CCD camera, suggesting the formation of p-i-n junction due to electric double layer carrier doping. Based on these high-resolution images, we determined the exact position of recombination zone and derived the length ratio between the p-doped regime and the n-doped regime. Next, we also measured both hole and electron carrier mobilities in the same devices using transistor configurations. Finally, to search for the hidden universality in TMDC light-emitting devices, we carefully compared the relationship between the p/n length ratio of EL images and mobility ratio of transistor measurements. As a result, we found the obvious universality between these two parameters, which is an important milestone to understand the behind mechanism of these light-emitting devices.

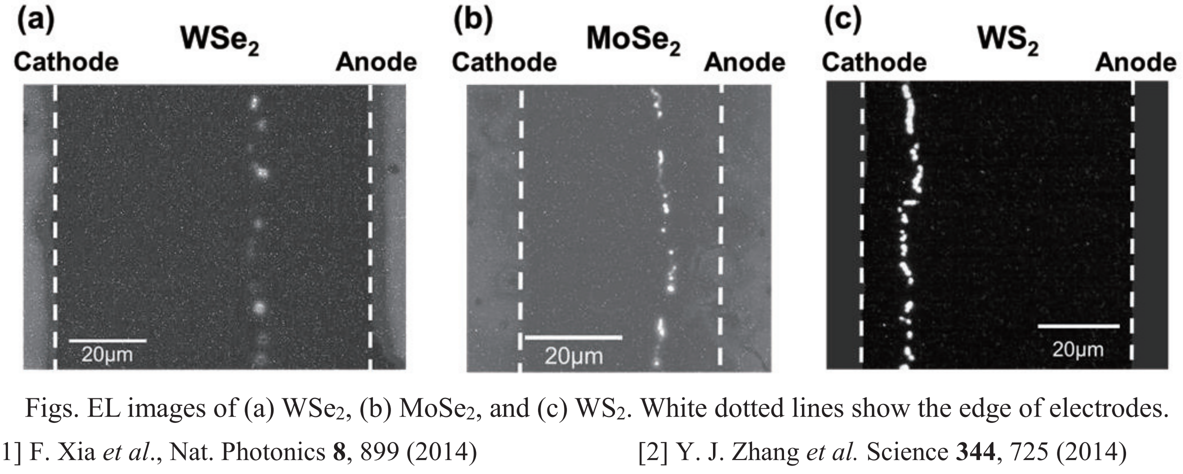

Figs. EL images of (a) WSe_2, (b) $MoSe_2$, and (c) WS_2. White dotted lines show the edge of electrodes.

[1] F. Xia *et al*., Nat. Photonics **8**, 899 (2014)
[2] Y. J. Zhang *et al.* Science **344**, 725 (2014)
[3] J. Pu, T. Takenobu Adv. Mater. **30**, 1707627 (2018)
[4] J. Pu *et al*. Adv. Mater. **29**, 1606918 (2017).

Corresponding Author: T. Takenobu. Tel: +81-52-789-5173 E-mail: takenobu@nagoya-u.jp

2P-9

Ab Initio Calculations of the Influence of Surface Water on Graphene

○Yusei Kioka[1], Yuki Maekawa [2], Kenji Sasaoka [3], Takahiro Yamamoto [1,2,3]

[1] *Department of Electrical Engineering, Tokyo University of Science, Tokyo, 125-8585, Japan*
[2] *Department of Liberal Arts, Tokyo University of Science, Tokyo, 125-8585, Japan*
[3] *Water Frontier Science & Technology Research Center, RIST, Tokyo University of Science, Tokyo, 125-8585*

It had long been believed that water molecules cannot adsorb on graphene because it is a hydrophobic material. However, the previous theoretical studies based on classical molecular dynamics (MD) simulations showed that single or double water layers are formed on a graphene surface, depending on number of water molecules [1,2]. Before the results obtained from these simulations, Homma *et al*. discovered the existence of the similar water molecular layers around a carbon nanotube by both photoluminescence measurements and classical MD simulations [3]. While the layer structure perpendicular to a graphene surface has been systematically and rigorously researched, the microscopic structure parallel to the surface has not yet been fully clarified, so that this means that the hydrogen bonding network in the water layers on graphene is not understood enough. Moreover, the influence of surface water on the electronic states of a graphene remains to be elucidated yet.

In this work, we constructed the microscopic structure of surface water on a free-standing graphene and a graphene on hexagonal boron nitride substrate using classical MD simulations. For the obtained structures, we investigated the influence of surface water on the electronic states of a graphene using *ab initio* calculations based on the density functional theory. Our MD simulations reproduced that the surface water exhibits single or double layered structures on graphene depending on the water vapor pressure in the spite of presence or absence of the substrate. In addition, we clarified the two-dimensional hydrogen-bond network is formed on the water layers on graphene surface [4]. We explain that the structure of surface water and the electronic states of water adsorbed graphene at poster session.

[1] T. A. Ho and A. Striolo, J. Chem. Phys. **138**, 054117 (2013).

[2] A. Akaishi, T. Yonemaru, and J. Nakamura, ACS Omega **2**, 2184 (2017).

[3] Y. Homma, *et al.*, Phys. Rev. Lett. **110**, 157402 (2013).

[4] Y. Maekawa, K. Sasaoka and T. Yamamoto, Jpn. J. Appl. Phys. **57**, 035102 (2018).

Corresponding Author: Takahiro Yamamoto,
Tel&FAX: +81-3-5213-0990,
E-mail: takahiro@rs.tus.ac.jp

2P-10

Theoretical Analysis on Thermoelectric Effects of Bilayer Graphene in Vertical Electric Field

○Hikaru Horii[1], Kenji Sasaoka[2], Takahiro Yamamoto[1,2], Hidetoshi Fukuyama[3]

[1] *Faculty of Engineering, Tokyo University of Science, Tokyo 125-8585, Japan*
[2] *RIST, Tokyo University of Science, Chiba 278-8510, Japan*
[3] *Tokyo University of Science, Tokyo 162-8601, Japan*

Thermoelectric generation is a potential key technology for recovering energy from waste heat. To obtain high thermoelectric (TE) performance, it is required that both the electrical conductivity and the Seebeck coefficient are high. Enhancement of TE performance is an important issue for material science and engineering, but it is not easy to develop the high-performance TE materials due to the trade-off relation between the conductivity and the Seebeck coefficient. For this reason, various materials has been investigated and improved by band engineering. Recently, carbon nanotube has especially attracted attention as a potential material for exhibiting high TE performance and flexibility [1].

In this study, we focused on the bilayer graphene, whose band-edge structure can be modulated by the vertical electric field as shown in Fig. 1 [2]. To validate TE performance of the bilayer graphene, we have investigated TE response using thermal Green's function methods and Kubo formula [1] to calculate TE properties in bandgap and band-edges exactly.

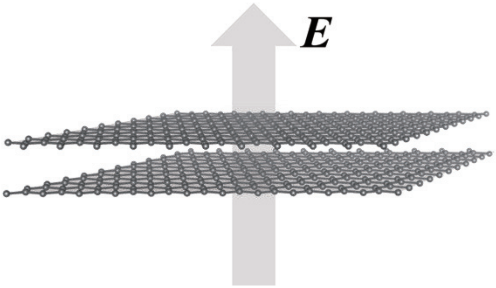

Fig. 1 Bilayer Graphene in Vertical Electric Field

As a result, we found that Seebeck coefficient and TE power near the band-edges became large due to the peak of the density of states and that the chemical potential with maximum TE power can be controlled by adjusting the electric field to modulate the band-edges. Therefore, we can improve the TE performance of bilayer graphene by applying the proper electric field.

Although this method is not suitable for energy hearvesting because of using an external electric source for the band engineering, this problem can be solved by the method of electric field effect using spontaneous polarization of ferroelectrics, which we presented in FNTG53 and FNTG54. We have already known that bandgap of bilayer graphene opens when it is touched with ferroelectrics. Thus, the bilayer graphene can be a powerful and flexible TE material by using with ferroelectrics controlled spontaneous polarization of ferroelectrics.

[1] T. Yamamoto and H. Fukuyama, *J. Phys. Soc. Jpn.* **82**, 024707 (2018).
[2] T. Ohta et al. , *Science* **313**, 951 (2006).

Corresponding Author: T. Yamamoto
Tel: +81-3-5876-1492
E-mail: takahiro@rs.tus.ac.jp

2P-11

Novel 2D Heterostructures of Monolayer WS_2 and 2D Perovskite

○Ufuk Erkılıç[1], Hyun Goo Ji[1], Kazunari Matsuda[2], Hiroki Ago[1,3,*]

[1] *Interdisciplinary Graduate School of Engineering Sciences, Kyushu University,*
Fukuoka 816-8580, Japan
[2] *Institute of Advanced Energy, Kyoto University, Gokasho, Uji, Kyoto 611-0011, Japan*
[3] *Global Innovation Center (GIC), Kyushu University, Fukuoka 816-8580, Japan*

Recently, organic-inorganic hybrid perovskites have attracted great attention thanks to their exceptional properties, such as long carrier diffusion lengths, high optical absorption, strong luminescence, and bandgap tunability through chemical composition [1]. Thus, integration of the perovskites with 2D materials offers a new opportunity to obtain unique properties. However, because of their vulnerability to common solvents, conventional wet transfer processes are not applicable to perovskites to create new heterostructures [2]. In this study, we demonstrate preferential vapor deposition of lead iodide (PbI_2) onto monolayer WS_2 and successive vapor-phase conversion to perovskite (methyl ammonium lead iodide ($MAPbI_3$))/WS_2 heterostructure. Preferential growth of PbI_2 via vapor deposition allowed us to obtain large area and uniform perovskite/WS_2 heterostructures.

We synthesized monolayer WS_2 by CVD on c-plane sapphire and vapor-deposited PbI_2 onto WS_2. Afterwards, PbI_2 was converted to perovskite ($MAPbI_3$) by vapor phase intercalation of methyl ammonium. Figure 1a shows a schematic illustration of perovskite/WS_2 heterostructure. The optical image of perovskite with different thicknesses on WS_2 is given in Figure 1b. Photoluminescence (PL) spectra have been taken from pristine $MAPbI_3$, pristine WS_2, and the heterostructure (Fig. 1c). The thick pristine $MAPbI_3$ showed an intense PL peak at ~1.65 eV, while WS_2 showed a moderate PL peak at ~2.0 eV. In the case of the heterostructure, PL peaks from both $MAPbI_3$ and WS_2 were significantly quenched. It is known that $MAPbI_3$/WS_2 interface exhibits type-II band alignment which is desirable for photonic devices, such as solar cells, photodetectors, and light emitting diodes [3]. Considering the type-II band alignment, PL quenching can be attributed to charge transfer or interlayer exciton formation at the interface. Details of the experimental conditions and temperature dependent PL studies will be discussed in the symposium.

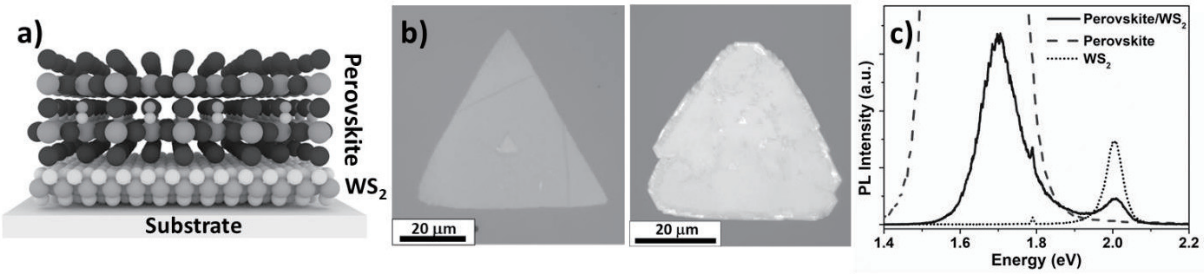

Fig. 1: a) Schematic illustration of perovskite/WS_2 heterostructure. b) Optical image of a thin (left) and thick (right) layer of perovskite grown on WS_2. c) PL spectra of WS_2, $MAPbI_3$, and $MAPbI_3$/WS_2 heterostructure.

[1] B. R. Sutherland *et al*. Nature Photon., **10**, 295 (2016). [2] H.-C. Cheng *et al*. Nano Lett., **16**, 367 (2016).
[3] C. Ma *et al*., Adv. Mater., **28**, 3683 (2016).

Corresponding Author: Hiroki Ago

Tel and Fax: +81-92-583-8852

E-mail: h-ago@gic.kyushu-u.ac.jp

2P-12

Variation of excited-state dynamics in trifluoromethyl functionalized C_{60} fullerenes

○Jaehong Park[1]

[1] *Department of Molecular Engineering, Graduate School of Engineering, Kyoto University,*
Kyoto, 615-8510, Japan

As the C_{60} fullerene and its derivatives have shown their competence as electron acceptors in solar energy conversion applications, many fullerene derivatives have been introduced to modulate the physical, chemical, electrochemical, and optoelectrical properties of the fullerene family.[1,2] Various trifluoromethyl (CF_3) group-substituted fullerenes (TMFs) have been synthesized and their structures have been characterized.[2] In general, these CF_3 substitutions on fullerenes have shown a one-electron reduction potential ($E^{0/-}_{1/2}$) shift toward a more positive energy with respect to $E^{0/-}_{1/2}$(C_{60}), due to their electron-withdrawing CF_3 groups.[3] Despite the various molecular engineering strategies, how CF_3 groups perturb the intrinsic excited-state dynamics of fullerenes, which can play an important role on photoinduced charge-generation and recombination, remain elusive.

Here, we report on electronically excited-state dynamics of three different TMFs ($C_{60}(CF_3)_n$: **C60/4-1**, **C60/6-2**, and **C60/10-1**, featuring four, six, and ten trifluoromethyl groups, respectively; Fig. 1) using optical spectroscopy as well as ultrafast pump/probe transient absorption spectroscopy.[4] **C60/4-1** and **C60/6-2** dissolved in toluene solvent show near-unit $S_1 \rightarrow T_1$ intersystem crossing quantum yield (Φ_{ISC}), ca. 1 ns S_1-state lifetimes, and microsecond-timescale T_1-state lifetimes, which are typical of the fullerene class. On the other hand, **C60/10-1** exhibits a dominant sub- nanosecond nonradiative $S_1 \rightarrow S_0$ relaxation mechanism and negligible Φ_{ISC}, therefore decreasing the average excited-state lifetime (τ_{avg}) by about 5 orders of magnitude compared to that of **C60/4-1** and **C60/6-2** ($\tau_{avg} \approx 17$ μs and 54 μs for **C60/4-1** and **C60/6-2**, respectively, whereas ($\tau_{avg} \approx 100$ ps for **C60/10-1**). These excited-state characteristics of **C60/4-1** and **C60/6-2** are preserved in polymer matrix, suggesting that fullerene/polymer interactions do not modulate intrinsic photophysics of trifluoromethyl-substituted fullerenes. The contrasting excited-state study results of **C60/4-1** and **C60/6-2** to that of **C60/10-1** infer that intrinsic optical properties and excited-state dynamics can be affected by the substitution on the fullerene.

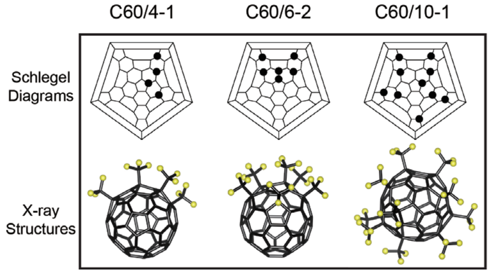

Fig. 1 Schlegel diagrams, X-ray structures of **C60/4-1**, **C60/6-2**, and **C60/10-1**.

[1] G. Yu, *et al.* Science, **270**, 1789 (1995); Y. Matsuo *et al.* Adv. Funct. Mater., 19, 2224 (2009).

[2] O. V. Boltalina *et al.* Chem. Rev., **115**, 1051 (2015).

[3] A. A. Popov *et al.* J. Am. Chem. Soc., **129**, 11551 (2007).

[4] J. Park *et al.* PCCP, **18**, 22937 (2016).

Corresponding Author: J. Park
Tel: +81-075-383-2549, Fax: +81-075-383-2556,
Web: https://park-group.wixsite.com/park-group
E-mail: j.park@moleng.kyoto-u.ac.jp

2P-13

Optical Properties of Carbon Nanotube Forest metamaterials

○Hiroshi Furuta[1], Adam Pander[1],
Keisuke Takano[2], Akimitsu Hatta[1], Makoto Nakajima[3]

[1]Department of Systems Engineering, Kochi Univ. Technol., Kochi, 7820003, Japan,
[2]Shinshu University, Nagano, 3908621, Japan, [3]Osaka University, Osaka, 5650871, Japan

CNT forest of high emissivity, nearly ideal "black-body absorber[1]", would be a strong candidate material for the future application in high-sensitive sensor, thermal energy storage device[2], and so on. Recently, metamaterials, electro-magnetic circuit to the incident EM-wave, opened a method to design desired optical properties. We recently reported CNT forest metamaterial in infrared and visible region in order to increase optical and thermal absorbance utilizing FIB nanofabrication [3, 4].

In this presentation, optical properties of metamaterials composed by 1D anisotropic material of CNTs, and their patterning of resonator shapes are discussed. Figure 1[6] shows calculated UV-Vis-IR spectra of vertical- and parallel-aligned metal-nanorod CNT forests to the Electric field (Ez) of incident EM wave propagating in the x direction, showing good correspondence to the experimental results[5] in Fig. 2(a-d). Components of perpendicularly aligned CNTs, which were parallel to the Ez of EM wave, increased reflectance in longer wave length region. Alignment of CNTs had an important role to improve absorption on the metamaterial patterns. Patterning shape effect of CNT forest metamaterials[3-5] will be also discussed in detail.

This work was supported by JSPS KAKENHI Grant Number JP 17K06205 and JP 24560050.

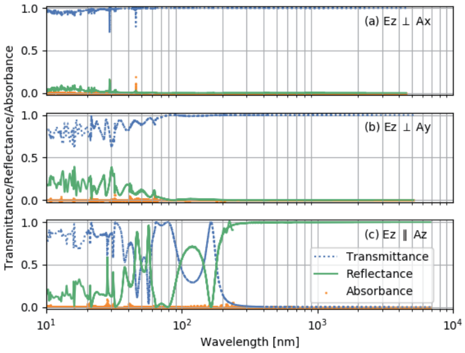

Fig. 1 (a-c) Calculated Transmittance, reflectance and absorbance spectra by meep FDTD program for the ideal-metal-nanorod CNT forests. Ez of EM wave was perpendicular to (a) x-axis and (b) y-axis of CNT alignment, and (c) parallel to z-axis of CNT alignment. [6]

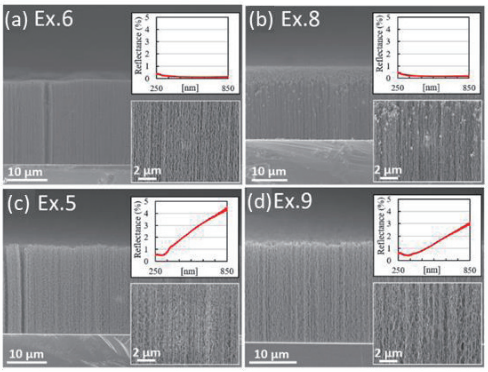

Fig. 2 (a, b) Highly vertically aligned CNT forests exhibiting low reflectance in 10-degree specular reflectance [5]. (c, d) Low-degree aligned, wavy CNT forests showing higher reflectance in longer wavelength [5].

[1] K. Mizuno *et al.*, PNAS 106(15), 6044-6047 (2008)
[2] H. Furuta, JSPS KAKENHI Grant Number JP 17K06205.
[3] A. Pander *et al.*, Nano-Micro Lett. 9:44 (2017).
[4] H. Miyaji *et al.*, Dia. Rel. Mat. 83, 196-203 (2018)
[5] A. Pander, et al., Vacuum 154, 285-295(2018).
[6] H. Furuta *et al.*, WONTON2018 (Hakone, 2018).

Corresponding Author: H. Furuta
Tel: +81-887-57-2211
Web: http://gecko.eng.kochi-tech.ac.jp
E-mail: furuta.hiroshi@kochi-tech.ac.jp

2P-14

Analysis on carbon nanotube dispersibility by using differential centrifugal sedimentation

○Taiyo Shimizu, Takeo Yamada, Ken Kokubo, Kenji Hata

CNT-Application Research Center, National Institute of Advanced Industrial Science and Technology (AIST), Tsukuba 305-8565, Japan

Dispersibility of carbon nanotube (CNT) is a critical issue for achieving advanced nanocomposite materials making the efficient use of CNTs' superior properties. Poor dispersion of CNTs results in poor enhancement, or even deterioration of the properties such as mechanical strength. In the case of solution-mixing fabrication, mechanical debundling of CNT in a dispersing media is generally adopted, and good dispersion of CNT before mixing with the matrix of composite should be achieved in order to prepare well-dispersed CNT nanocomposites.

In this study, we propose a new method for providing a clue to determine the "degree of debundling" for various CNTs in a dispersing solvent. Differential centrifugal sedimentation (DCS) analysis provides a particle size (Stokes diameter) distribution calculated from detected settling velocity of the particles in a suspension/dispersion under centrifugal force (Fig. 1a). Although this method has recently turned out to be more useful than other analytical techniques, such as dynamic light scattering, to estimate the size and dispersibility of CNTs with dispersant (e.g. surfactant), we found that DCS analysis can also be applied to suspensions of CNT agglomerates without any dispersant.

Stable suspensions of several CNTs were prepared by using a high-pressure homogenizer [1] . Agglomerate size distributions of CNT suspensions obtained from DCS analysis are shown in Fig 1b, and each CNT was classified into three groups, A to C, according to its peak position. Concerning morphology in a nanometer scale, while CNT group A, for instance, displayed straight bundles with thick and relatively homogeneous width, curved and debundled structures were observed in CNT group C (Fig. 2). Each CNT group displayed different morphology, and CNTs in the same group showed the similar degrees of debundling. Although elucidation of detailed mechanism is still being addressed, size distributions of agglomerates from DCS are related to the degree of debundling. The DCS analysis can thus provide useful information on the morphology of the agglomerates in CNT suspensions, from which we can easily estimate the degree of debundling for individual CNT suspensions.

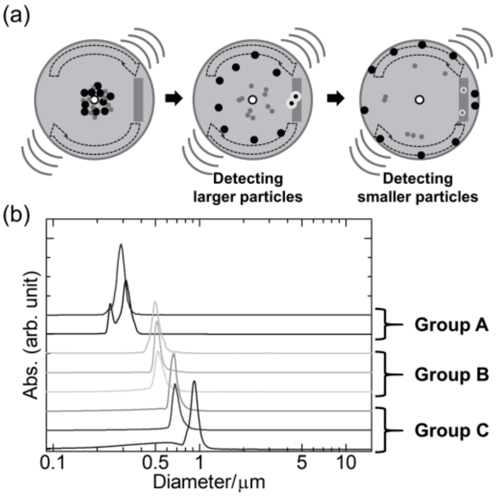

Fig. 1 (a) Schematic of DCS analysis and (b) size distributions of CNT agglomerates.

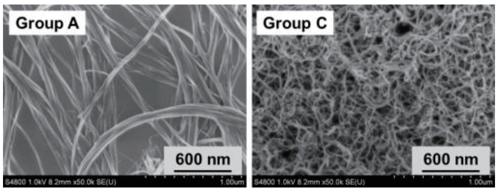

Fig. 2 Scanning electron microscopy images of typical CNT agglomerates.

[1] K. Kobashi *et al*. Chem. Sci., **4**, 727 (2013)

Corresponding Author: T. Shimizu
Tel: +81-29-861-5712 Web: http://www.nanocarbon.jp
E-mail: shimizu-t@aist.go.jp

2P-15

Diameter variation effects on electrical transport in semiconducting carbon nanotube thin film

○Masaaki Tsukuda[1] and Takahiro Yamamoto[1]

[1] Department of Electrical Engineering, Tokyo University of Science,
Niijuku 6-3-1, Katsushika-ku, Tokyo 125-8585, Japan

Although carbon nanotube (CNT) thin films are expected as flexible and transparent transistors, the physical origin of their high electric performance remains to be clarified yet because individual variations in nanotube length and diameter are involved in nanotube network. In addition, its electrical conductivity also depends on geometrical network structure such as nanotube density and alignment. Therefore, understanding various properties of CNT thin film has been the subject of controversy over the last few years.

In order to understand relation between the network structure with the nanotube densities, alignment, length and diameter, and their electrical transport property, we have done computational study on electrical transport in CNT thin films, using a numerical stick-percolation-based model. Especially, we have thoroughly explored how nanotube diameter variation affects electrical transport properties of CNT thin films.

In the present study, we conducted an electrical transport simulation for CNT network consisted of semiconducting CNTs with a fixed film length of 5 μm and film width of 5 μm(seen in Fig1). CNT network is transformed into effective resistor network composed of the junction resistance between CNT pairs. Then, we applied a nodal analysis method to calculate a current value flowing in a film.

To investigate diameter variation effects on electrical transport in CNT network, nanotube diameter is determined by diameter distribution in experimental HiPco and eDIPS samples [1][2]. We will discuss the detail of the obtained results in the presentation.

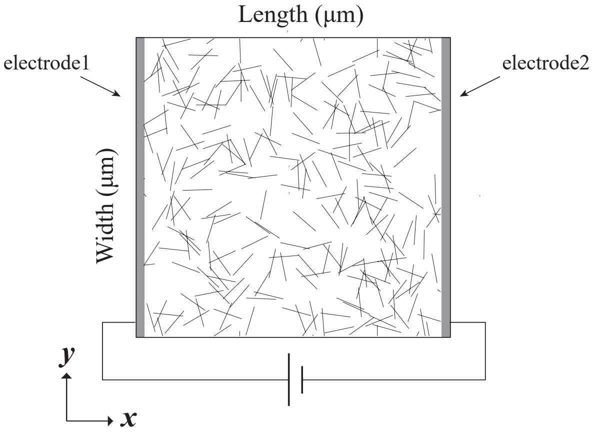

Fig1. Schematics of a random network consisting of CNTs

[1] Z. Luo, L. D. Pfefferle, G. I. Haller, and F. Papadimitrakopoulos, J. Am. Chem. Soc. **128**, 15511 (2006).
[2] T.Saito, S.Ohmori, B. Shukla, M.Yumura, and S.Iijima, Appl. Phys. Express **2**, 095006 (2009).

Corresponding Author: T. Yamamoto
Tel: +81-3-5876-1492
E-mail: takahiro@rs.tus.ac.jp

2P-16

Mechanical properties of carbon nanotubes under the uniaxial strain

○Kazufumi Yoneyama and Susumu Okada

Graduate School of Pure and Applied Sciences, University of Tsukuba, Tsukuba 305-8571, Japan

Because of tubular covalent networks of sp^2 C atoms, carbon nanotubes (CNTs) are known to exhibit remarkable mechanical properties, allowing them constituents for flexible devices and composite materials. Indeed, CNTs possess the high Young's modulus of about 1 TPa. On the other hand, although the electronic properties of CNTs are known to strongly correlate with their diameter and chirality, a little is known about the mechanical properties of CNTs with respect to their microscopic geometries. In particular, quantitative discussion about the correlation between the mechanical properties and network topologies are absent. Thus, in this work, we aim to elucidate the mechanical properties of CNTs with the diameter of about 0.95 nm in terms of their chiral angles, using the density functional theory with the generalized gradient approximation. In particular, we provide the mechanical toughness of carbon nanotubes against the tensile strain in terms of their chiral angles.

For the above purpose, we consider (12,0), (10,4), and (7,7) CNTs as the representative zigzag, chiral, and armchair CNTs with similar diameters, allowing us to make quantitative investigation of the mechanical properties of CNTs with respect to their chirality. Our calculations show that the Young's modulus is 0.741, 0.748, and 0.754 TPa for (12,0), (10,4), and (7,7) CNTs, respectively, indicating that the Young's modulus is insensitive to the tube chirality. In contrast, mechanical toughness against the tensile strain strongly depends on the CNT chirality. The mechanical toughness is inversely proportional to the chiral angle. (7,7) CNT exhibits higher mechanical toughness against the tensile strain than the other two CNTs, retaining its tubular structure up to 40 % tensile strain, while (12,0) CNT shows the least toughness among three CNTs. The calculated critical breakdown tension is 170.82, 195.56, and 200.84 nN for (12,0), (10,4), and (7,7) CNTs, respectively.

Corresponding Author: K. Yoneyama
E-mail: kyoneyama@comas.frsc.tsukuba.ac.jp

2P-17

SWNT films doped with Trifluoromethanesulfonic acid as durable electrode in perovskite solar cells

○ Ahmed Shawky[1], Il Jeon[1], Esko I. Kauppinen[2], Yutaka Matsuo[1,3], Shigeo Maruyama[1,4,*]

[1] Departure of Mechanical Engineering, The University of Tokyo, Tokyo 113-8656, Japan
[2]Aalto University School of Science, Aalto, FI-00076, Finland
[3] Hefei National Laboratory for Physical Sciences at Microscale, University of Science and Technology of China, 96 Jinzhai Road, Hefei, Anhui 230026, China
[4] Energy Nano Engineering Lab., National Institute of Advanced Industrial Science and Technology (AIST), Ibaraki 305-8564, Japan

In perovskite solar cells (PCS), there is a much attention regarding easy fabrication and stability issues. Easing fabrication comes to elimination of the vacuum deposition of noble metal electrodes like Au and Ag as well as reducing cost. Stability issues is recently addressed as these metals can interact with the perovskite layers and suppress degradation of the whole PCS device [1]. Alternatively, single-walled carbon nanotubes (SWNT) represent a great candidate to replace the metal electrodes. SWNT is a favorable electrode material, owing to its hydrophobic nature, earth-abundance, and mechanical robustness. The application of SWNT grasps good stability and versatility in PCS [2]. The aerosol-synthesized SWNT top electrode replacing metals in PSCs has shown the most promising potential. The application of SWNT as the top electrode substantially enhances the stability of PSCs by removing the ion migration and drastically reduces the fabrication cost as it can be easily deposited onto devices by a simple mechanical transfer. As a step to increase robustness of SWNT electrodes, we showed that sulfonic acids like Trifluoromethanesulfonic acid (TFMS) and Nafion® showed longest doping durability compared to well-known HNO3 [3].

In this regard, we apply the TFMS mixed with polar solvent as durable dopant of SWNT to increase both electrical conductivity and hole extraction ability of SWNT. SWNTs were laminated on the normal $CH_3NH_3PbI_3/SnO_2$/ITO system as electrodes in this device. The TFMS-doped SWNT showed an increase of the photoconversion efficiency (PEC) by 20% compared to the SWNT-based PCS. Further analysis will be shown on this system in the symposium. We expect that TFMS doped-SWNT-based PCS can withstand the humid air for more than a year with negligible loss in PCE.

[1] N. N. Shlenskaya et al., J. Mater. Chem. A, 2018,6, 1780-1786.
[2] T. Sakaguchi et al., MRS Communications, 2018, DOI:10.1557/mrc.2018.142
[3] I. Jeon et al., J. Mater. Chem. A, 2018, DOI:10.1039/C8TA03383H

Corresponding Author: Prof. S. Maruyama
TEL: +81-3-5841-6421
Web: http://www.photon.t.u-tokyo.ac.jp/
E-mail: maruyama@photon.t.u-tokyo.ac.jp

2P-18

Mechanical properties of CNT spun yarn reinforced by polymer infiltration and chemical binder

°T. Kina, M. Karita, T. Nakano, Y. Inoue

Department of Electronics and Materials Science, Shizuoka Univ., Hamamatsu 432-8561, Japan

Since the discovery of dry spinning phenomenon from a carbon nanotube (CNT) forest [1], a dry-spun CNT yarn has been an attractive material as the structural material. One of good things of the dry-spinning is that large-scale and highly aligned CNT structures are uniformly formed. However, since the CNTs are connected by van der Waals force, the spun yarn fails by relative sliding of CNTs, and its high mechanical properties are far inferior to those of individual CNT. Further improvement of mechanical properties was required in order to application of CNT yarn to structural material. In this work, we focused on suppression of relative sliding of CNTs by polymer infiltration and chemical binder.

Dry-spin capable multi-walled CNT forests were grown on oxidized Si wafer by chloride mediated CVD method and mist catalyst CVD method. CNT yarns were fabricated by spinning the CNT forests. CNT yarns were immersed in the solution of polymer or chemical binder. After a certain period of time, the solution was removed from the CNT yarn.

Stress-strain curves of pristine and polyvinyl alcohol (PVA) reinforced CNT yarns are shown in Fig.1. By reinforcing with PVA, compared to pristine, the tensile strength of CNT yarns increased from 600 to 1200 MPa, and the Young's modulus from 30 to 93 GPa. Scanning electron microscopy (SEM) images of PVA reinforced and pristine CNT yarn are shown in Fig.2. In the case of pristine CNT yarn, there are spaces between CNTs. On the other hand, the spaces between CNTs are filled with PVA (Fig.2b). These results indicate that CNT are connected by PVA and it suppresses relative sliding of CNTs, leading to a strong and stiff yarn.

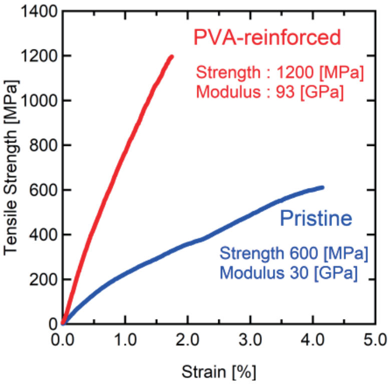

Fig.1 Stress-strain curves before and after reinforcing CNT yarn.

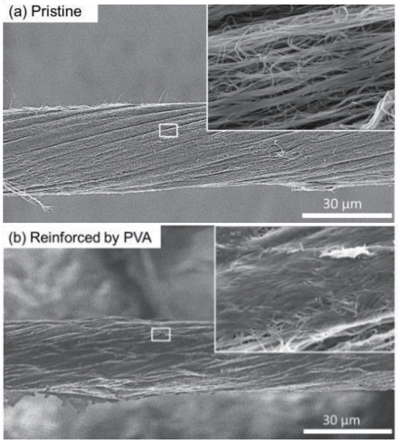

Fig.2 SEM images of (a) pristine and (b) PVA-reinforced CNT yarns.

[1] K. Jiang *et al.* Nature, **419**, 801 (2002).

Corresponding Author: Y. Inoue
Tel: +81-53-478-1356, Fax: +81-53-478-1356
E-mail: inoue.yoku@shizuoka.ac.jp

2P-19

Dependence of field emission from carbon nanotube tip on the size of the counter electrode

○Keita Funayama[1], Jun Hirotani[2], Yutaka Ohno[2,3], Keiichi Shimaoka[1], Hiroya Tanaka[1], Yukihiro Tadokoro[1]

[1] *Toyota Central Research & Development Laboratory, Inc., Nagakute 480-1192, Japan*
[2] *Department of Electronics, Nagoya University, Nagoya 464-8603, Japan*
[3] *Institute of Materials and Systems for Sustainability, Nagoya University, Nagoya 464-8603, Japan*

The phenomenon of field emission has been widely used in various applications[1,2]. It is well-known fact that the resulting tunnel current is described by Fowler-Nordheim (F-N) theory; for the field intensity ξ_{ex} around the emitter, the current is given as $I = C_1 S(\beta\xi_{ex})^2 exp[-C_2/\beta\xi_{ex}]$ where S is the emitting area, C_1 and C_2 are the constants. This equation has been obtained under the assumption that the anodic electrode is infinite plate, and the key parameter, enhancement factor β, is determined only by the shape of the emitter[3].

In nanoscale systems fabricated on the wafer by micro process, however, it is easily supposed that the anodic electrode is not an infinite plate but a thin film and its size is very confined to fabricate on the narrowed area. Owing to the effect of the finite size of the anodic electrode, it is expected that the current does not follow the existing F-N theory. In that case, the accurate performance estimation of nanoscale systems, one of the examples is nano-mechanical resonator with single MWCNT, will be difficult. The current from the emitter, tip of the CNT, is used to detect the motion of the resonator. We fabricated such system on the wafer by electron-beam(EB) lithography and EB deposition as shown in Fig.1 to demonstrate that the influence of the finite-anode can be described by the additional enhancement factor.

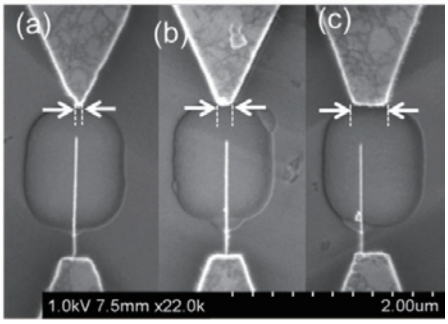

Fig. 1 SEM images of the nano-emitter made of MWCNT. Electrode width is (a) 50nm, (b)100nm, and (c)300nm

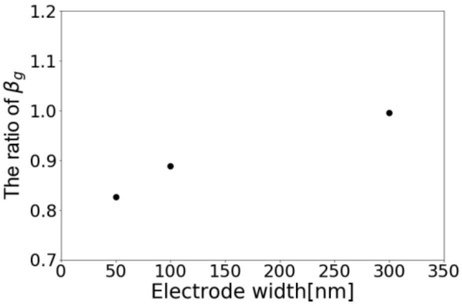

Fig. 2 The ratio of β_g depended on the electrode width.

In this work, the introduced enhancement factor has two terms, β_g and β_0, which describe the influence of the size of the anode and the shape of the emitter, respectively. Now we have $\beta = \beta_g\beta_0$. Simply, $\beta_0 = L/d$ where L is the length and d is the diameter of the CNT[3]. For three patterns of the anode width, 50nm, 100nm, 300nm, the current was measured, and based on the F-N theory with the introduced β, the value of β_g was calculated. Fig.2 shows the averaged ratio to the case with the width 300 nm. It was observed that the current depends on the anode size, which indicates that the size should be considered in the modelling of the current in nanoscale systems.

[1] J. Moser, *et al.*, *Nature Nanotech.*, **8**, 493 (2013). [2] S. K. Georgantzinos, *et al.*, *Sensor Review*, **34**, 319 (2014). [3] G. S. Bocharov, *et al.*, *Nanomaterials*, **3**, 393 (2013).

Corresponding Author: K. Funayama
Tel: +81-561-71-7421, Fax: +81-561-63-6948, E-mail: funayama@mosk.tytlabs.co.jp

Study of the growth of MWCNT forest by chloride-mediated CVD

○Kota Komastsubara, Tatsuhiro Hayashi, Motoyuki Karita, Takayuki Nakano, Yoku Inoue

Department of Electronics and Materials Science, Shizuoka University, Hamamatsu 432-8561

Carbon nanotubes (CNTs) are expected to be used for many applications in various fields because of their great characteristics. Vertically aligned CNT forests on substrates have been receiving a lot of attention including researches for electrodes in energy storage, thermal interface materials, LSI inter connects. We have been studying the growth of multi-walled CNT (MWCNT) forest by chloride-mediated chemical vapor deposition (CM-CVD) which uses iron chloride ($FeCl_2$) as the catalyst precursor [1]. This growth method enables to deposit iron thin film on a substrate and to grow MWCNT forest in the same furnace. Therefore, it does not require thin film deposition of catalyst. Moreover, the CM-CVD MWCNT forest has high growth rate, dense and long CNTs, and high dry-spin capability. In this study, to investigate CNT growth mechanism, we observed very substrate surface area of the CNT forest focusing on the morphology of iron catalyst nanoparticles.

We used oxidized Si substrate for CNT growth. The CNT growth conditions are as follows; growth temperature: 820 °C, pressure: 20 Torr, $FeCl_2$: 120 mg, C_2H_2: 200 sccm, Ar: 300 sccm, growth time: 2-6 min. We observed the cross-sectional images of MWCNT by transmission electron microscopy, and analyzed substrate surface area including the iron catalyst nanoparticles.

Figure 1 shows the scanning electron microscopy (SEM) images of MWCNT forest grown by CM-CVD method. The substrate was cleaved, and cross-sectional observation was carried out. We found that the catalyst nanoparticles were diffused into SiO_2 layer (shown in Fig. 2). The iron diffusion is pronounced in the CM-CVD rather than conventional Fe-catalyst CVD. Further, we found that additional supply of Cl_2 gas in CM-CVD made the catalyst diffusion deeper. We will present the behavior of nanoparticles in the present CVD process.

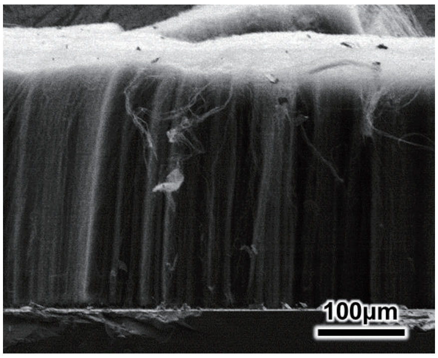

Fig.1 Vertically aligned MWCNT forest grown by CM-CVD method.

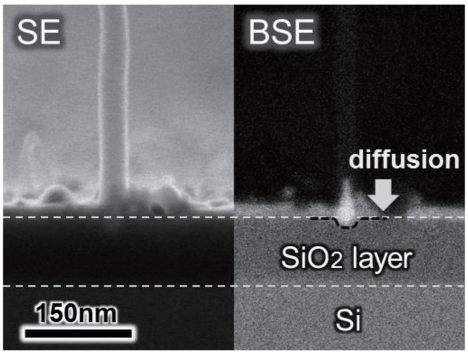

Fig.2 Cross-sectional secondary and backscattered electron images of MWCNT. Fe nanoparticles are diffused in the SiO_2 layer.

[1] Y. Inoue, et al, Appl. Phys. Lett. 92, 213113 (2008).

Corresponding Author: Yoku Inoue
Tel: +81-53-478-1107, Fax: +81-53-478-1356
Web: http://cnt.eng.shizuoka.ac.jp/
E-mail: inoue.yoku@shizuoka.ac.jp

2P-21

Growth of Multi-Millimeter-Tall Single-Wall Carbon Nanotube Forests Using Fe/Gd/Al Catalysts

○ Rei Nakagawa[1], Toshihiro Sato[1], Suguru Noda[1], Hisashi Sugime[2]*

[1]*Department of Applied Chemistry, Waseda University*
[2]*Waseda Institute for Advanced Study, Waseda University*

Single-wall carbon nanotube (SWCNT) forests hold great possibilities for their unique structure including vertical alignment, high density and specific surface area, and large length, however their application is still very limited due to the challenges it faces in their production. Chemical vapor deposition (CVD) is one the most commonly used method for SWCNT synthesis, and a major problem it has is the growth termination caused by the deactivation of the catalysts. Several papers reported that the deactivation of the catalyst is closely related with the coarsening of the catalyst nanoparticles during the growth. In general, it is more difficult to maintain small catalyst nanoparticles than the larger ones as the mobility of the nanoparticle is larger and/or the stability is lower. In the past, to combat these challenges Cho et al. reported the enhanced synthesis using Fe-Gd catalyst and achieved a 21.7 mm-tall multi-walled carbon nanotube (MWCNT) forest through a 13-hour synthesis with a growth rate of 27 μm/min [1]. However, the possibility of using Gd for SWCNT growth was not discussed in detail.

In this work, we applied the Gd/Al underlayers to the growth of SWCNT forests, and systematically studied the mechanism behind the enhanced growth. By optimizing the catalyst condition, we have achieved a 3 mm-tall CNT array in 45 min at 800 °C with 885 sccm Ar, 5 sccm CO_2, 10 sccm C_2H_2, and 100 sccm H_2 at 1 atm. It was found that Gd layer with the thickness of less than 1 nm was effective when it was deposited between Fe and Al layers. The Raman spectra showed the radial breathing mode (RBM) peaks from the top to bottom of the CNT forests, which suggests the continuous synthesis of SWCNT. The mechanism behind the prolonged synthesis of SWCNT was investigated using the TEM-EDS.

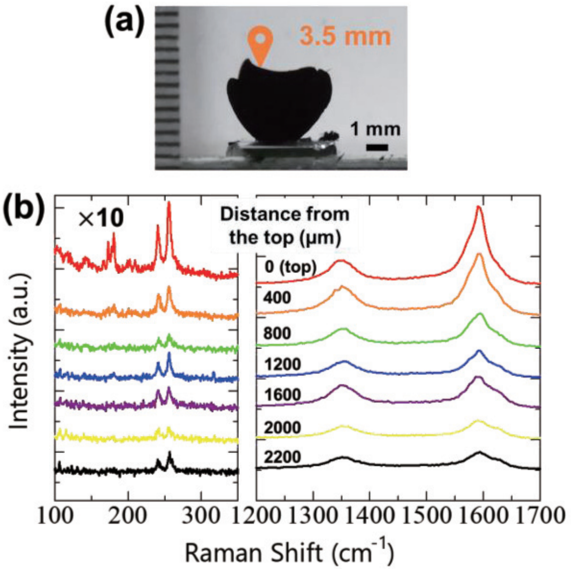

Fig. 1 (a) CNT forest synthesized using the Gd/Al underlayer. (b) Raman spectra (488 nm) obtained from the synthesized CNT forest

[1] W. Cho et al., *Carbon* **72**, 264 (2014).

Corresponding Author: H. Sugime
Tel&Fax:+81-3-5286-2769
E-mail: sugime@aoni.waseda.jp

2P-22

Increasing ethylene conversion efficiency using pre-catalytic treatment prior to single-walled carbon nanotube synthesis

○Naoyuki Matsumoto[1], Sachiko Ishizawa[1], Michiko Irie[1], Megumi Hirano[1],
Kenji Hata[1], Don N. Futaba[1]

*[1] National Institute of Advanced Industrial Science and Technology (AIST),
Central 5, 1-1-1- Higashi, Tsukuba, Ibaraki, 305-8565, Japan.*

Over the past 25 years, since the discovery of the single-walled carbon nanotube (SWCNT), the field has taken great strides in the development of SWCNT-based and carbon nanotube (CNT)-based applications, such as composite materials, strain sensors, and fibers. Utilizing their unique structural characteristics, such as diameter, density, and chirality, many of these applications benefit from their high aspect ratio, i.e. long length. One of the most common ways to efficiently grow long CNTs is to grow them as a vertically aligned assembly, often called a "forest". In this way, the catalysts, which are deposited onto a substrate can grow in bulk up to the millimeter-scale, and have served as the basis for mass production, which is essential for the development of the CNT industry. Therefore, the development of high efficiency and large throughput methods for SWCNT synthesis is important for realizing the practical use of SWCNT applications.

Highly efficient SWCNT synthesis has been demonstrated with a wide range of carbon sources, e.g. ethylene, butane, acetylene, etc. as well as by appropriately "pre-heating" carbon sources [1,2]. However, the carbon efficiency (percentage of carbon feedstock converting into CNTs) remains only about 1-5%, which leaves the majority of the carbon source unused to form carbonaceous impurities adsorbed onto the CNTs as well as volatile organic compounds in the exhaust gases. Acetylene has demonstrated exceptionally high carbon efficiency [2], however does not represent a viable large scale solution to this problem as it also represents a significant explosive hazard. To address this, we demonstrate an approach for high yield and high conversion efficiency synthesis of SWCNTs using the heterogeneous catalysis of ethylene using catalysts prior to the substrate (denoted "Pre-Cat"). Importantly, this catalytic reaction only requires low temperature to proceed thereby not requiring any complex heating equipment. We achieved the high efficiency SWCNT growth by using Pre-Cat CVD method (CNT length: 1575 µm in 10 min growth time at 800 ºC) with reduced ethylene concentration. The level of synthetic yield was similar to the normal growth (without Pre-Cat growth). In TEM observation, the CNTs grown in Pre-Cat process were SWCNTs (the average wall number; 1.2 and the diameter; 2.9 nm), whose structures were the same as SWCNTs in normal growth.

This work was supported by JSPS Grant-in-Aid for Young Scientists (B) Grant Numbers JP17K14091.

[1] H. Kimura *et al.* ACS Nano, **7**, 3150 (2013).
[2] N. Matsumoto *et al*. Nanomaterials **5**, 1200 (2015).

Corresponding Author: N. Matsumoto
Tel & Fax: +81-29-861-4654
Web: http://www.nanocarbon.jp/
E-mail: matsumoto-naoyuki@aist.go.jp

Preparation Conditions for Carbon Nanobrushes: Influence of Catalyst Types

○Ryota Yuge[1], Fumiyuki Nihey[2], Kiyohiko Toyama[1], and Masako Yudasaka[3, 4]

[1]*System Platform Research Laboratories, NEC Corporation, Tsukuba 305-8501, Japan,*
[2]*Data Science Research Laboratories, NEC Corporation, Tsukuba 305-8501, Japan,*
[3]*Nanomaterials Research Institute, National Institute of Advanced Industrial Science and Technology (AIST), Tsukuba, 305-8565, Japan*
[4]*Graduate School of Science and Technology, Meijo University, Nagoya 468-8502, Japan*

Fibrous aggregates of single-walled carbon nanohorns, named as carbon nanobrushes (CNBs), were recently discovered [1]. The CNBs are drawing attention as electrode materials for various devices such as nanocarbon-polymer actuators, electric double layer capacitors, and fuel cells since they show high electrical conductivity, high dispersibility in solutions, and large specific surface areas. Although the CNBs are easily prepared by CO_2 laser ablation of Fe-containing carbon targets [1], their yield is low and the major products are the spherical single-walled carbon nanohorn aggregates (CNHs). To increase the yield of CNBs, various preparation conditions such as the Fe concentration in carbon targets, target rotation speed, laser power density, and density of carbon target itself have been examined [2-3]. In this study, we tried to prepare CNBs by using carbon target containing different catalysts other than Fe such as Co and Ni. The structures of obtained samples were also studied in detail.

A CO_2 laser ablated the catalyst-containing carbon targets at room temperature under ambient pressure. The CO_2 laser was operated at the power of 3.2 kW in the continuous-wave mode. The target of 30 mm in diameter and 50 mm in length was rotated at 1 rpm for 30 second during the laser ablation. The gas pressure in the growth chamber was kept at 700-800 Torr by controlling the evacuation rate while the buffer gas of nitrogen was kept at a flow rate of 10 L/min. The carbon targets containing Fe (3 at. %, 1.44 g/cm^3), Ni (3 at. %, 1.48 g/cm^3), and Co (3 at. %, 1.45 g/cm^3) were used in our experiments.

From scanning electron microscopy and scanning transmission electron microscopy observations, CNBs were prepared effectively when the Fe catalyst was used. The CNB quantities prepared at 3 at. % of Fe concentration was much larger than that at 1 at. %. On the other hand, CNBs were hardly prepared by using the Ni or Co catalyst. The CNHs of seed, bud, and dahlia types were mainly prepared for Ni catalyst and CNHs of petal-dahlia type for Co catalyst. Therefore, we found that Fe catalyst is essential for CNB formation. The details will be discussed in the presentation.

[1] R. Yuge *et al*. Adv. Mater. **28**, 7174 (2016).

[2] R. Yuge *et al*. The 52th FNTG General Symposium, 3P-24 (2017).

[3] R. Yuge et al. The 54th FNTG General Symposium, 3P-19 (2018).

Corresponding Author: R. Yuge, Tel: +81-29-850-1566, Fax: +81-29-856-6137, E-mail: r-yuge@bk.jp.nec.com

2P-24

Direct growth of graphene by low-pressure CVD
--- Effect of crystal orientation of sapphire surface ---

○Yuki Ueda[1], Jumpei Yamada[1], Taishi Ono[1], Takahiro Maruyama[2], and Shigeya Naritsuka[1]

[1] Department of Materials Science and Engineering, Meijo University, Nagoya 468-8502, Japan
[2] Department of Applied Chemistry, Meijo University, Nagoya 468-8502, Japan

Large-size single-crystalline graphene is usually obtained on copper-based catalyst by chemical vapor deposition (CVD). However, the transfer process, which is mandatory for the device fabrication, largely deteriorates the grown graphene. Direct growth of graphene on a dielectric substrate is the best answer to solve the problem. C-plane sapphire is conventionally used as a substrate [1], while very few studies are reported on the optimization of crystal orientation of sapphire surface. In this study, we use a-plane, r-plane and c-plane sapphires to study their effects on the graphene growth.

Graphene was directly grown on sapphires using low pressure CVD without metal catalyst. Mixture gas of nitrogen, hydrogen, and diethylacetylene (C_6H_{10}: 3-Hexyne) was flown to a reactor for the growth of graphene. Growth temperature was systematically changed between 1090 °C and 1210 °C.

Figure 1(a) shows Raman spectra of samples grown at 1210 °C. D, G and G' peaks were observed both on a-plane and r-plane samples. The peak intensities on r-plane sample were stronger than those on a-plane sample. On the other hand, no Raman signal was observed on c-plane sample. In the case of the c-plane and a-plane samples, graphene was found to grow only in the pits, formed on the surface of the sapphires during CVD. The phenomenon is similar to the case of Saito et al. [2], in which Al-rich surface was reported to appear inside the pits and to show a catalytic effect for the graphene growth. In our case of r-plane sapphire, the graphene was found to grow simply in 2D nucleation mode. This is because the surface of r-plane sapphire has a catalytic effect, and enhances the decomposition of growth species. Consequently, the use of r-plane sapphire successfully brings a fast and smooth direct growth of graphene, as shown in Fig.1 (b).

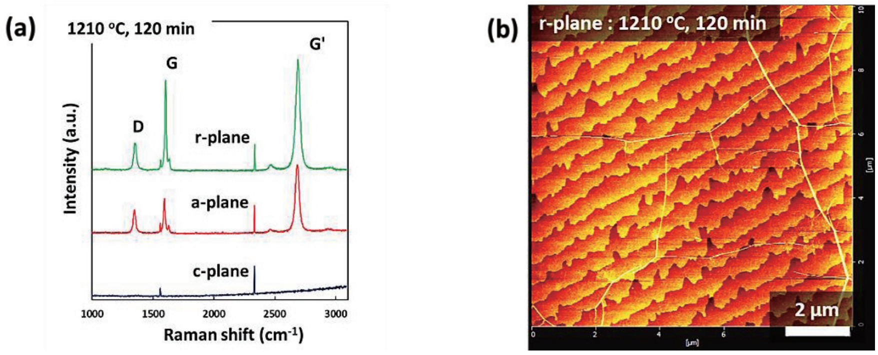

Fig. 1 (a) Effect of crystal orientation of sapphire surface on Raman spectra, and (b) AFM image of sample grown on r-plane sapphire at 1210 °C.

Acknowledgement: This work was supported in part by JSPS KAKENHI Grant Numbers 15H03558, 26105002.

[1] M. A. Fanton et al., ACS Nano 5, 8062 (2011).
[2] K. Saito and T. Ogino, J. Phys. Chem. C 118, 5523 (2014).

Corresponding Author: Y. Ueda, Tel: +81-52-838-2387, E-mail: 173441501@ccalumni.meijo-u.ac.jp

2P-25

Measurement of scattering time and electrical properties for graphene using THz time-domain spectroscopy

○Takashi Fujii[1,3], Kohei Soda[1], Shinichiro Mouri[1], Tsutomu Araki[1], Yuki Ueda[2],
Shigeya Naritsuka[2], Toshiyuki Iwamoto[3]

[1] Department of Electrical and Electronic Engineering, Ritsumeikan University, Kusatsu 525-8557, Japan
[2] Department of Materials Science and Engineering, Meijo University, Nagoya 468-8502, Japan
[3] Nippo Precision Co., Ltd, Nirasaki 407-0175, Japan

THz time-domain spectroscopy (THz-TDS) has been developed for technology characterizing the complex permittivity, $\tilde{\varepsilon}(\omega)$, with THz frequency region [1]. THz-TDS is the pulsed Fourier spectroscopy using the femto-second laser and the amplitude of electric field of electromagnetic wave can be detected along the time-domain region, ranging with pico-second. $\tilde{\varepsilon}(\omega)$ can be calculated by using Fourier transformed results without Kramers-Kronig relations because the amplitude of electric field was measured in THz-TDS.

It is well-known that the scattering time (τ) of electrons and holes in most 3-dimensional semiconductor materials is ranging between femto- and pico-seconds. Then, it was possible to characterize the electrical properties, such as the conductivity, the carrier concentration and the mobility, applying the Durde model by measuring $\tilde{\varepsilon}(\omega)$ in THz frequency region.

We tried to analyze τ and the electrical properties of the graphene using THz-TDS. The THz-TDS has the advantage of measurements for the electrical properties without making the electrodes on the sample.

The graphene grown on sapphire substrate, of which growth temperature was systematically varied, were prepared by using low-pressure chemical vapor deposition (CVD) method. After the transmitting properties were measured by THz-TDS, the transmittance and the phase delay were calculated using Fast Fourier Transform. They were analyzed by Fresnel's formula of two layers case. First layer was sapphire substrate and second layer was graphene with assuming its thickness of 0.3nm.

Formula 1 shows $\tilde{\varepsilon}(\omega)$ of graphene through the medium of τ and sheet carrier concentration (N_g) with assuming the Durde model for 3-dimensional semiconductor, where ε_b is background dielectric constant and v_F is Fermi velocity. [2,3].

$$\tilde{\varepsilon}(\omega) = \varepsilon_b - \frac{e^2 v_F \sqrt{N_g}}{\varepsilon_0 \hbar} \times \frac{1}{\omega(\omega - i/\tau)} \qquad (1)$$

We determined τ from the measuring results, as shown in table 1.

Table 1. Growing temperature via scattering time (τ).

Growing temperature (°C)	1090	1130	1170	1210
τ (femto-second)	23	34	51	85

[1] T. Fujii *et al*. Journal of the European Ceramic Society **26**, 1857 (2006).
[2] Kin Fai Mak *et al*. Solid State Communications **152**, 1341 (2012)
[3] T. Fujii *et al*. The65th JSAP Spring Meeting 2018, 18p-C202-8

Corresponding Author: T. Fujii
Tel: +81-77-561-2884, Fax: +81-77-561-3994,
E-mail: tafujii@fc.ritsumei.ac.jp

2P-26

Quantum description of excitation of surface plasmon by light in graphene

M. Shoufie Ukhtary, Riichiro Saito
Department of Physics, Tohoku University, Sendai 980-8578, Japan

Surface plasmon (SP) is electromagnetic (EM) wave propagating on the surface of a material. SP is associated with the collective oscillation of charges on the surface of material. SP is interesting due to the potential applications, such as optical switching devices, biosensors and wave guide based on the excitation of SP. The strength of EM field decreases in the perpendicular direction to the surface, making the SP confined. It is well-known that the excitation of SP by external EM wave requires the matching between energy-momentum of external EM wave and SP or resonance conditions. It is also assumed that the resonance conditions will cause an enhancement of EM wave absorption by the material which is shown by the peak of absorption spectrum. However, the explicit physical explanation of the SP excitation is not understood clearly within only the classical electromagnetism. Furthermore, the contribution of SP excitation to the optical spectra is also not clearly understood as far as we know.

Due to the confinement nature of SP, the quantum treatment of SP is possible, where the SP is considered as a quasiparticle travelling on the surface. In this work, we study how the SP can be quantized as an oscillator harmonic, similar to the quantization of photon [1, 2]. In this study, we use the quantization scheme given by Archambault et al [1], where they quantized the energy of electromagnetic wave on the surface by introducing creation-annihilation operators. By quantizing the SP, we can explain why the excitation of SP requires the resonance conditions by deriving the matrix element of photon-plasmon interaction. We therefore show that the peak on the absorption spectrum comes from the SP excitation by calculating the absorption spectrum of SP. We show that the total absorption spectrum comes from the contribution of SP and single particle excitation. In the point of view of application, the quantum description of the interaction between light and SP in graphene can be useful for the case that requires the matrix element of interaction in quantum mechanics, such as surface enhanced Raman spectroscopy with surface plasmon in graphene.

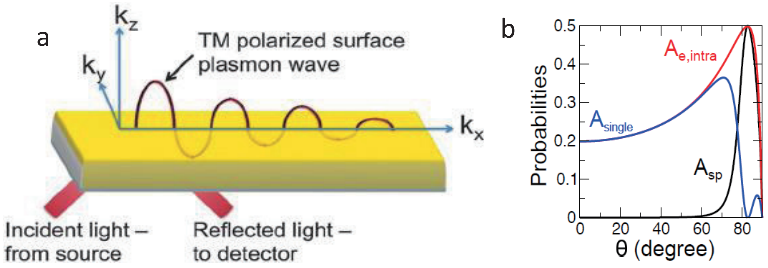

(a) Excitation of SP by light. (b) The optical spectra (Ae,intra) consists of SP (Asp) and single particle (Asingle) contributions

References:
[1] Archambault et al. PRB 82 035411 (2010)
[2] Finazzi et al. PRB 86 035428 (2012)

Corresponding Author: M. Shoufie Ukhtary, E-mail: shoufie@flex.phys.tohoku.ac.jp

2P-27

New refrigeration systems based on elastic nanosponges consisting of graphene

○Hirotomo Nishihara[1], Keita Nomura[1], Masanori Yamamoto[1], Masashi Ito[2], Masanobu Uchimura[2], Takashi Kyotani[1]

[1] Institute of Multidisciplinary Research for Advanced Materials, Tohoku University, 2−1−1 Katahira, Aoba, Sendai 980−8577, Japan
[2] Advanced Materials Laboratory, Research Division, Nissan Motor Co., Ltd., 1 Natsushima-cho, Yokosuka, Kanagawa 237−8523, Japan

Refrigeration is a thermodynamic process, during which heat is transferred from a low-temperature reservoir to a high-temperature one. Air conditioners represent typical refrigeration systems based on the reverse Carnot cycle utilizing the latent heat of a fluid called refrigerant (Fig. 1a). However, conventional halocarbon-based refrigerants cause ozone depletion and global warming; therefore, it is highly desirable to replace them with environmentally friendly media (such as water). Refrigeration systems containing porous adsorbents such as zeolites allow using water as the refrigerant; however, their sizes are relatively large. In this work, we propose a unique concept of refrigeration based on the reversible phase transition of a green refrigerant (water or alcohol) occurring in elastic nanosponge materials consisting of single-graphene walls [1-3], as shown in Fig. 1b. Its theoretical coefficient of performance (COP) is inversely proportional to the Young's modulus of a nanosponge material and comparable or even potentially superior to those of conventional air conditioners (Fig. 1c). Moreover, we demonstrate for the first time the reversible phase transition of water achieved by mediating the mechanical force applied to the real nanosponge materials. By 'squeezing' a nanosponge containing liquid water, its vapor is released, whereas the opposite process occurs during the free expansion of the nanosponge.

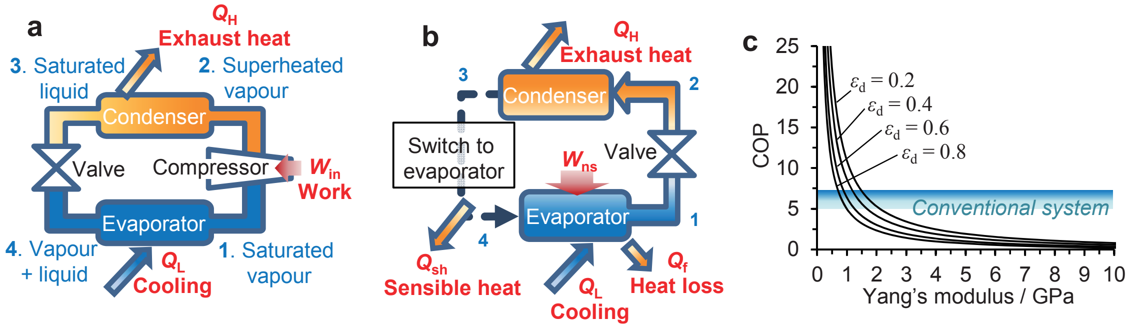

Fig. 1 (a) Schematic of the conventional refrigeration systems. The refrigerant undergoes four different phase transformations described by the numbers 1–4. (b) Schematic of the proposing new refrigeration systems. (c) Approximate relations between the COP and Young's modulus of the nanosponge, which were obtained at various strains of nanosponge (ε_d). Decreasing ε_d increases the magnitude of COP and overall nanosponge volume, making the entire system more bulky.

[1] Z. X. Ma, T. Kyotani, A. Tomita, Chem. Commun., 2365 (2000).
[2] H. Nishihara, et al. Carbon, 129, 854 (2018).
[3] H. Nishihara, et al. Adv. Funct. Mater., 26, 6418 (2016).

Corresponding Author: H. Nishihara
Tel: +81-22-217-5627, Fax: +81-22-217-5626,
Web: http://www.tagen.tohoku.ac.jp/labo/kyotani/nishihara/nishihara_e.html
E-mail: hirotomo.nishihara.b1@tohoku.ac.jp

Contrast mechanism of graphene oxide in Twilight fluorescence microscopy

○Yu-uki Ishikawa, Masahito Sano

Department of Organic Materials Science, Yamagata University, Yonezawa 992-8510, Japan

Twilight fluorescence (TwiF) microscopy is a newly developed microscopy that is capable of imaging individual single-layer graphene sheet floating in a liquid [1]. The microscope utilizes a total internal reflection (TIR) configuration. A graphene solution mixed with a highly concentrated dye solution is placed on the glass surface. An excitation beam is incident on the glass/solution interface from below at a near TIR angle. Not only the evanescent field by TIR, but the weak refracted ray is transmitted to the solution phase to excite the dye as well. Due to strong absorption by the concentrated dye, the refracted ray diminishes rapidly as it travels (the inner filter effect, IFE). Thus, the region of fluorescence is localized to within a sub-micrometer distance from the glass interface. The TwiF contrast η is given by a difference between the fluorescence from the free dye in solution I_0 and one from the dye interacting with the graphene sheet I as $\frac{I_0-I}{I_0}$. In this study, we examine the contrast quantitatively.

(1) GO attached to the glass surface

We treat the case that graphene oxide (GO) appears darker than the surrounding solution. In this case, the contrast η of the n-layer GO sheet is given by a form

$$\eta = 1 - aT^{2n}$$

where a is a constant related with Förster resonance energy transfer (FRET) and T is a transmittance of a single-layer GO assumed to be independent of a wavelength. We measured η from TwiF image of a GO sheet and a height t from AFM image of the identical GO sheet. Multi-layer sheets with clear steps were selected. Most data points follow the theoretical curve well with n replaced by t. We will also discuss FRET contribution by changing the dye and its concentration.

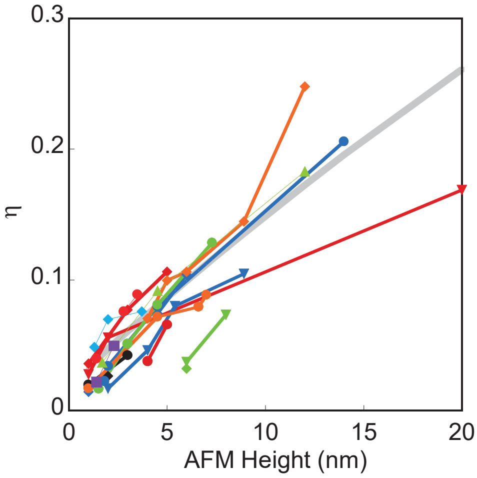

Fig. 1 TwiF contrast and AFM height of identical GO sheets.

(2) Floating GO away from the glass surface

Far away from the glass surface, the evanescent field from TIR is negligible and the dye is excited by the diminishing refracted ray by IFE. It is important to know a decay constant β for the refracted ray of a form $e^{-\beta z}$ at a distance z from the glass surface, for it is used in evaluating the contrast η in most observations of floating sheets. We will report a value of β determined by analyzing a rotating GO sheet in solution.

[1] Y. Matsuno, Y. Sato, H. Sato, M. Sano, *J. Phys. Chem. Lett.* **2017**, *8*, 2425-2431.

Corresponding Author: M. Sano
Tel: +81-238-26-3072,
Web: http://sanolab.yz.yamagata-u.ac.jp/
E-mail: mass@yz.yamagata-u.ac.jp

2P-29

Exciton-phonon coupling in MoS_2 by resonance Raman Scattering

○ Toshiya Shirakura[1], Riichiro Saito[1]

[1]Department of Physics, Tohoku University, Sendai 980-8578, Japan

Excitonic effects are expected to be very strong for two dimension materials such as the MoS_2 transition metal di-chalcogenides (TMDs). Resonance Raman spectroscopy is a very useful tool to study excitonic transitions and exciton-phonon interactions in semiconductors. Exciton is the bound states between electron and a hole. To make exciton wave function, electron and hole wave functions should be mixed to each other. Then we can make exciton wave function that is localized in the real space.In this work, we calculate the exciton Raman scattering for the transition metal di-chalcogenides. We show that the A_{1g} phonon mode is enhanced when the excitation laser is in resonance with A and B excitons (optical transition energies are 1.88 eV and 2.03 eV respectively) [1] of MoS_2, while the E^1_{2g} phonon mode is shown to be enhanced when the excitation laser is close to C exciton (optical transition energy is 2.7 eV). We show from the symmetry analysis of the exciton-phonon interaction that the mode responsible for the E^1_{2g} resonance is identified as the high energy C exciton recently predicted by experiment [2]. In the calculation, exciton-phonon matrix element is evaluated by resonance Raman scattering. In order to obtain the exciton-phonon matrix element, we need to solve the exciton wave function by Bethe-Salpeter equation (BSE). In the BSE, the direct Coulomb interaction and exchange interaction. By using maximally localized Wannier function (MLWF) [3].

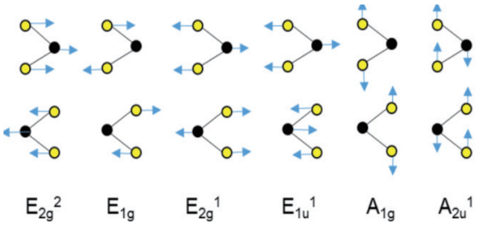

Fig.1 Atomic displacements of the A1g and E^1_{2g} phonon mode. Yellow (black) circle is corresponding to Mo and S atom.

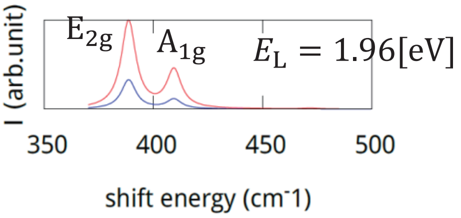

Fig.2 Resonance Raman intensity for different polarized light. The incident photon energy is 1.96 eV. There are two peak. One is the E_{2g} phonon mode resonance. The other one is A_{1g} phonon mode contribution.

[1] K. F. Mak, *et al.*, Phys. Rev. Lett. **105**, 136805 (2010).
[2] D. Y. Qiu, *et al.*, Phys. Rev. Lett. **111**, 216805 (2013).
[3] N. Marzari, *et al.*, Phys. Rev. B. **56**, 12847 (1997).

Corresponding Author: T. Shirakura,
E-mail: shirakura@flex.phys.tohoku.ac.jp

Alkali metal-assisted growth in metal-organic chemical vapor deposition of two-dimensional layered chalcogenides

○Yu Kobayashi[1], Shoji Yoshida[2], Toshifumi Irisawa[3], Naoya Okada[3], Lim Hong En[1],
Kenji Watanabe[4], Takashi Taniguchi[4], Yutaka Maniwa[1], Osamu Takeuchi[2],
Hidemi Shigekawa[2], Yasumitsu Miyata[1,*]

[1] *Department of Physics, Tokyo Metropolitan University, Hachioji, Tokyo 192-0397, Japan,*
[2] *Faculty of Pure and Applied Sciences, University of Tsukuba, Tsukuba, Ibaraki 305-8573, Japan,*
[3]*Nanoelectronics Research Institute, National Institute of Advanced Industrial Science and Technology (AIST), Tsukuba, Ibaraki 305-8568, Japan,*
[4]*National Institute for Materials Science, 1-1 Namiki, Tsukuba, Ibaraki 305-0044, Japan*

Metal organic chemical vapor deposition (MOCVD) is one of the most powerful ways to prepare large-scale and uniform transition metal dichalcogenide (TMDC) atomic-layers and their heterostructures[1-3]. So far, the progress in vapor phase growth have been achieved by the use of metal organic precursors and additional growth promoters such as alkali metal halides. Although several works have been reported, the roles of the promoter remain unclear. It is therefore crucial to understand and control the effects of promoter to achieve better growth.

Here, by using alkali metal compounds as promoters, we report a high-quality TMDC growth with MOCVD. We found that the introduction of alkali metals improves various parameters, which includes grain size, uniformity of layer number, nucleation density, and defect density of TMDCs such as MoS_2, WS_2, $MoSe_2$, and WSe_2 monolayers. Besides, the alkali metal promoters work also on the exfoliated graphite and hexagonal boron nitride, the van der Waals surfaces, in addition to SiO_2 and sapphire. Our results suggest that the alkali metals may play a role in aiding the formation of intermediate products composed of alkali metals and transition metals rather than dehydration and/or substrate surface modification. The present findings pave way for the simple and rapid preparation of large scale, high quality TMDCs, and TMDC-based heterostructures.

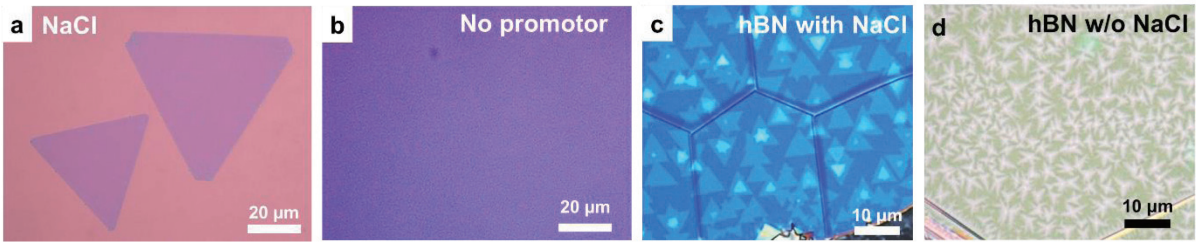

Figure 1. Optical images of MOCVD grown WS_2 (a) with and (b) without NaCl on SiO_2/Si, and (c) with and (d) without NaCl on hBN.

[1] K. Kang *et al*. Nature, **520**, 656-660 (2015). [2] H.-K. Kim *et al*. Nano Lett., **17**, 5056–5063 (2017).
[3] S. Xie *et al.* Science, **359**, 1131–1136 (2018)

Corresponding Author: Y. Miyata, Tel: +81-42-677-2508,
Web: http://www.comp.tmu.ac.jp/miyata/index.html, E-mail: ymiyata@tmu.ac.jp

2P-31

Electric double layer light emitting diode of WS_2/MoS_2 in-plane heterostructures

○Yuhei Takaguchi[1], Jiang Pu[2], Hirofumi Matsuoka[2], Yu Kobayashi[1],
Taishi Takenobu[2], Yutaka Maniwa[1], Yasumitsu Miyata[1]

[1] *Department of Physics, Tokyo Metropolitan University, Hachioji 192-0397, Japan*
[2] *Department of Applied Physics, Nagoya University, Nagoya 464-8603, Japan*

Heterostructures of transition metal dichalcogenides (TMDCs) are an attractive system to realize high-performance devices including light-emitting diodes and tunnel field-effect transistors. To maximize their potential, we have developed growth processes of various in-plane heterostructures based on TMDC monolayers [1]. Recently, Pu *et al.* reported a simple way to generate light emitting diodes in a semiconductor using electric double layer [2]. By using this technique, several groups including us have demonstrated the electric double layer light emitting diodes (EDLEDs) of TMDC-based in-plane heterostructures [3,4]. In our previous study, the $MoSe_2$/WSe_2 EDLED shows point-like electroluminescence (EL) around the heterointerface, which suggests low crystallinity of the interface. In this study, we report an improved growth process and the observations of linear EL from the interface of in-plane heterostructures based on TMDC monolayers.

WS_2/MoS_2 in-plane heterostructures was grown on sapphire substrates by using two-step, salt-assisted chemical vapor deposition (CVD) processes. First, monolayer WS_2 was grown using WO_3 and Sulfur, and then, monolayer MoS_2 was grown from the edge of WS_2 with MoO_2 and Sulfur. Cr/Au electrodes were then deposited on the samples by using a shadow mask or photolithography. To fabricate EDLEDs, Cr/Au electrodes were then deposited, and then, ion gel was spin coated on the sample [2]. An illustration of device is shown in Fig.1a. As shown in Fig.1b, the device shows linear light emission from the interface by applying voltage at two electrodes. We also found that the EL spectrum showed the same peak as the photoluminescence (PL) of the WS_2 and MoS_2 monolayers, and additional peaks were observed around 1.5 eV (Fig.1c). In the presentation, we will show the details of sample preparation and discuss a mechanism of EL in the present EDLEDs.

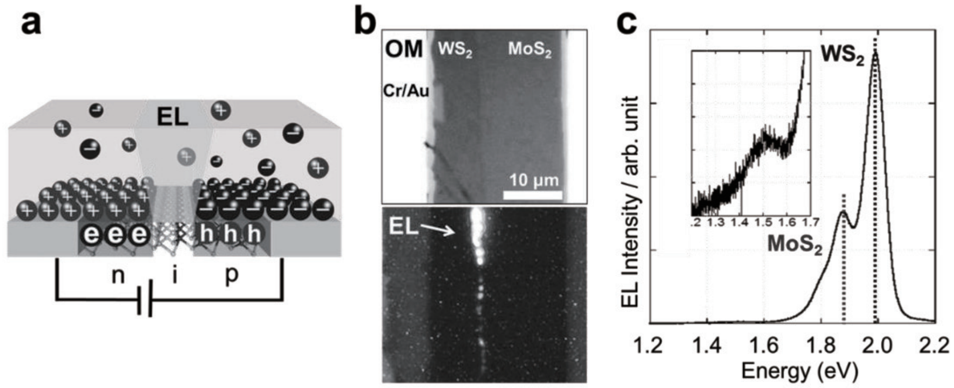

Fig.1 (a) Illustration and (b) optical and electroluminescence (EL) images of WS_2/MoS_2-based EDLED device. Arrows indicate the observed EL. (c) EL spectrum of the EDLED device

[1] Y. Kobayashi *et al.,* ***Sci. Rep.***, 6, 31223 (2016). [2] J. Pu *et al.,* ***Adv. Mater.*** , 29, 1606918 (2017).

[3] M. Li et al., ***Adv. Func. Mater.*** 28, 1706860 (2018) [4] Y. Takaguchi et al., 53th FNTG symposium.

Corresponding Author: Yasumitsu Miyata, Tel: 042-677-2508, E-mail: ymiyata@tmu.ac.jp

2P-32

Layer-number-controlled synthesis of WS_2 integrated by Au dot technology

○Tomoya Kameyama[1], Chao Li[1], Toshiro Kaneko[1], Toshiaki Kato[1,2]

[1]Department of Electronic Engineering, Tohoku University, Sendai 980-8579, Japan
[2] JST-PRESTO

Recently, two-dimensional (2D) materials such as graphene have attracted enormous attention due to its intriguing electronic and optical properties [1]. Nonetheless, the metallic property of graphene limits its semiconductor application because of the zero-bandgap structure [2]. Transition metal dichalcogenide (TMD) is also known as one subset of 2D materials, which possesses monolayer thickness as similar as graphene. Furthermore, their semiconductor band structure can be precisely changed from indirect transition to direct transition by tuning layer number from multilayers to monolayer, which makes them become one of the most prospective candidates in many applications, such as transistors, sensors, and solar cells [3].

In our previous research, we explored an effective method to control the nucleation site of TMD with Au dot as nucleation center. Highly-integrated synthesis of monolayer TMD has been realized with this method. To use this unique growth method in practical applications, it is necessary to control the structure of integrated TMD, especially layer number has to be controlled to improve the performance of optoelectrical devices.

Then, in this study, we attempted to control the layer number of highly-integrated tungsten disulfide (WS_2) by controlling the Ar flow rate during the thermal chemical vapor deposition (CVD) synthesis with Au-dot nucleation. As the result, multilayer WS_2 can be synthesized with low Ar flow rate. On the contrary, monolayer WS_2 can be obtained with high Ar flow rate (Fig. 1). To elucidate the critical effect of Ar flow rate during WS_2 synthesis, quadrupole mass analyzer (Q-mass) instrument was introduced to measure the precursor change at the crystal growth region around the growth substrate during all the synthesis process. As the result, it is found that the amount of sulfur (S) in vapor phase seems to correlate with the final product, i.e. the layer number and size of WS_2, denoting the balance of W and S supply may be one of the critical element to decide the layer number of WS_2 grown from Au dot.

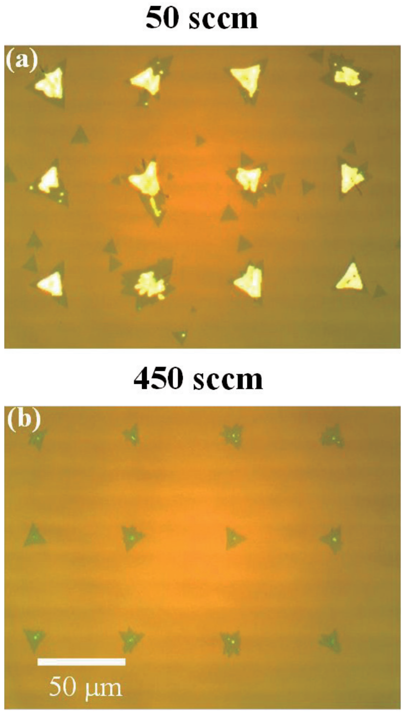

Fig. 1 Optical microscope image of (a) multilayers and (b) monolayer WS_2 synthesized at 50 sccm and 450 sccm of Ar flow rate, respectively.

[1] T. Kato and T. Kaneko: ACS Nano **8** (2014) 12777.
[2] T. Kato and R. Hatakeyama: Nature Nanotechnology **7** (2012) 651.
[3] T. Akama, W. Okita, R. Nagai, C. Li, T. Kaneko, and T. Kato: Scientific Reports: **7** (2017) 11967.

Corresponding Author: T. Kameyama
Tel: +81-22-795-7046, Fax: +81-22-263-9225,
E-mail: tomoya.kameyama.r1@dc.tohoku.ac.jp

Asymmetric carrier accumulation in bilayer van der Waals heterostructures of TMDC under an external electric field

○ Mina Maruyama, Susumu Okada

Graduate School of Pure and Applied Sciences, University of Tsukuba, Tsukuba 305-8571, Japan

Transition metal dichalcogenides (TMDCs) are representative semiconducting layered materials in which each layer is bound via weak van der Waals (vdW) interaction as the case of graphite. Thus, they are attracting much attention as for the staring materials for designing vdW heterostructures by layer-by-layer stacking. Because of the substantial wavefunction overlap between layers, the vdW heterostructures of TMDCs exhibit versatile electronic structure, depending on the constituent layers and their stacking sequence [1]. In this work, we investigated carrier accumulation in vdW heterostuctures of TMDCs under an external electric field for providing a guiding principle to design the field-effect transistor (FET) of TMDC vdW heterostructure using the density functional theory combined with the effective screening medium methods.

Figure 1 shows the structural model and distribution of accumulated carriers in the vdW heterostructures consisting of MoS_2 and WS_2. Our calculations showed that the distribution of the accumulated electrons by the field exhibit asymmetric nature with respect to the mutual arrangement of the vdW heterostructure to the electrode. For the arrangement that the electrode is situated at the MoS_2 side, the injected electron is mostly injected into a MoS_2 layer, indicating localized nature [Fig. 1(a)]. In contrast, for the opposite TMDC arrangement, the injected electron is relatively extended to the second layers of TMDCs [Fig. 1(b)]. This fact implies that the carrier accumulation in the TMDC-FET with vdW heterostructure strongly depend on the stacking sequence of their constituent TMDCs.

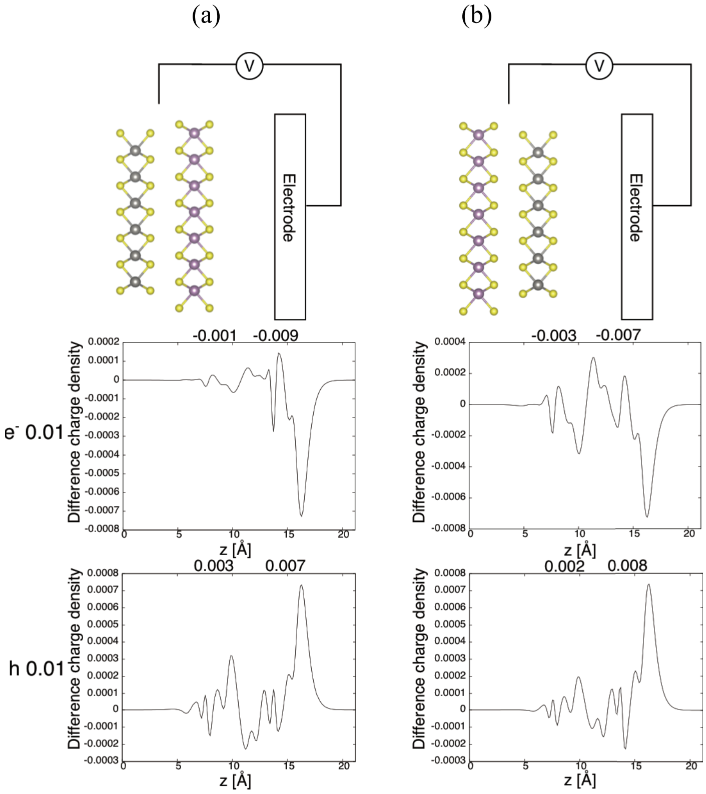

Fig. 1: Structural models and distribution of accumulated carriers of (a) WS_2/MoS_2/electrode and (b) MoS_2/WS_2/electrode structures.

[1] A. K. Geim and I. V. Grigorieva, Nature **499**, 419 (2013).

Corresponding Author: M. Maruyama
Tel: +81-29-853-5921, Fax: +81-29-853-5924,
E-mail: mmaruyama@comas.frsc.tsukuba.ac.jp

2P-34

Facile Production of MoS_2 Nanosheets by Ball Milling: Optimization of Operating Parameters

○Naoko Ogino, Ahmad Tayyebi , Naoki Komatsu

Graduate School of Human and Environmental Studies, Kyoto University
Sakyo-ku, Kyoto 606-8501, Japan

The production of 2D nanomaterials such as molybdenum disulfide (MoS_2), tungsten disulfide (WS_2) and graphene have been attracting extensive interest due to their characteristic optical and electronical properties. We recently reported that MoS_2 and WS_2 were exfoliated in the presence of sodium cholate (SC) through ball milling and resulting powder was readily dispersed in water [1]. Herein, we studied the conditions of ball milling thoroughly to obtain high-yield of the 2D nanosheet and control its size and thickness.

To prepare MoS_2 nanosheet and its aqueous dispersion, bulk MoS_2 and SC were ball milled and the resulting black powder was suspended in water. On the ball milling, the following parameters were investigated; ball volume ratio (φ (%) = V_{ball} / $V_{\text{container}}$), material weight ratio (SC / MoS_2), milling speed, ball diameter, and milling duration. After centrifugation of the suspension at 6000 rpm, the stable aqueous supernatant was subjected to UV-vis and AFM analyses to determine the yield, length and layer numbers of the MoS_2 nanosheet. [2]

As shown in Fig. 1a, the material ratio giving the best yield (%) decreased from 2 to 0.5 and 0.75, as the ball volume ratio increased from 10% to 80%. The best yield (65%) was obtained at φ = 50% and SC / MoS_2 = 0.75. The yield was improved to 94%, when milling speed increased from 300 rpm (Fig. 1a) to 600 rpm at φ = 50% and SC / MoS_2 = 0.75. Under the conditions optimized above, both length and layer numbers of MoS_2 decreased as the ball milling duration increased (Fig. 1b).

We are going to apply these results to the production of various 2D nanosheets.

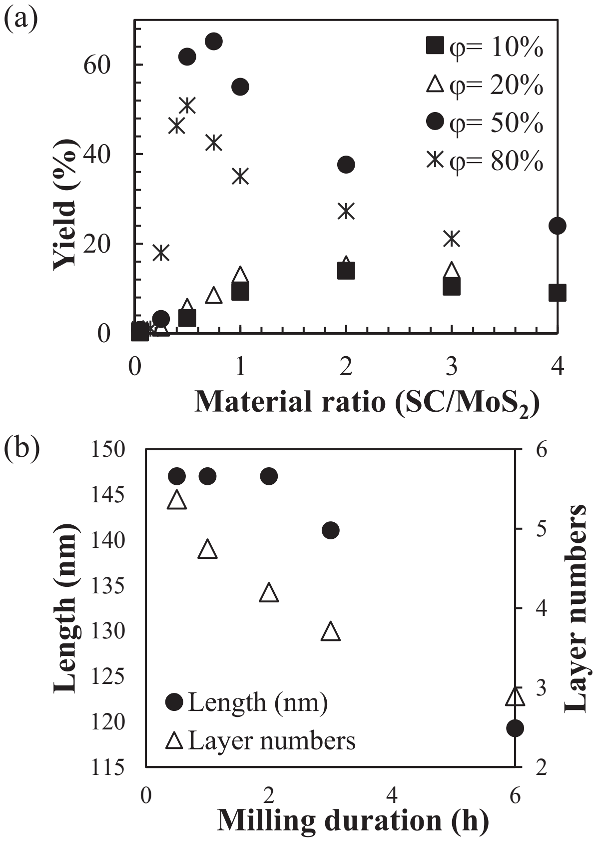

Fig. 1. (a) Yield of MoS_2 as a function of material weight ratio of SC / MoS_2 at 10, 20, 50, 80% ball volume ratio. The milling speed and duration are 300 rpm and 6 h, respectively. (b) Length and the layer numbers of MoS_2 as a function of milling duration (φ = 50%, SC / MoS_2 = 0.75, and milling speed = 300 rpm).

[1] G. Liu et al. *ChemNanoMat*. **2**, 500 (2016)

[2] C. Backes et al. *Nat. Comumn.* **5**, 4576 (2014)

Corresponding Author: Naoki Komatsu
Tel, Fax: +91-75-753-6833
Email: komatsu.naoki.7w@kyoto-u.ac.jp

2P-35

Laser Induced Phosphorescence of Polyyne Molecules at 20 K

○Tomonari Wakabayashi[1], Kazunori Ozaki[1], Hal Suzuki[1], Yusuke Morisawa[1],
Urszula Szczepaniak[2]

[1]*Department of Chemistry, Kindai University, Higashi-Osaka, Osaka 577-8502, Japan*
[2]*Laboratory for Physical Chemistry, ETH Zürich, Zürich 8093, Switzerland*

Cyanopolyyne is known for its radio-frequency detection in the interstellar space in the late 70's. Molecules up to HC_9N have been confirmed, while the observation of $HC_{11}N$ in the molecular cloud TMC-1 [1] was recently negated [2]. Hydrogen-end-capped polyyne could be a candidate for possible interstellar molecules, though its detection was thwarted by the selection rule of the rotational transition for the centrosymmetric linear molecule [3]. Recently, phosphorescence was observed in the laboratory for cyanopolyyne molecules, HC_5N, HC_7N, HC_9N, isolated in solid rare-gas matrices [4-6]. In this work, hydrogen-end-capped polyyne was isolated in solid hexane at 20 K and laser induced phosphorescence was measured.

Sample molecules, $H(C{\equiv}C)_nH$ (n = 4−6), were prepared by laser ablation of graphite in liquid hexane, followed by separation using HPLC techniques [7]. The solution containing size-selected polyyne molecules was condensed on a copper slab cooled at 20 K in vacuum. The solid matrix sample was irradiated by the second harmonic of OPO laser (GWU VersaScan, 213−302 nm) to record optical emission spectra on a polychromator with a CCD array detector (PI320, PyLoN OE256).

The phosphorescence spectrum of C_8H_2 in solid hexane at 20 K shows vibrational progression for the symmetric stretching ν_2 mode of the *sp*-carbon chain (~2190 cm^{-1}) at 532, 603, 694, 815, and 988 nm for the 0−ν bands of ν = 0−4 (Fig. 1). The lifetime was ~30 ms for the $a^3\Sigma_u^+ \rightarrow X^1\Sigma_g^+$ transition (inset in Fig. 1). The excitation spectrum of C_8H_2 in the UV (215−255 nm) contains at least two components, one following the absorption spectrum in the solution at ambient temperature and the other red-shifted.

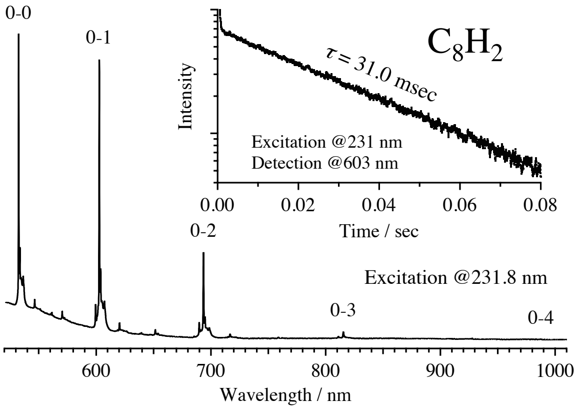

Fig. 1. Phosphorescence spectra and temporal decay (0-1 band) of C_8H_2 in solid hexane at 20 K.

[1] M. B. Bell *et al.* Astrophys. J. **483**, L61 (1997).
[2] R. A. Loomis *et al.* Mon. Not. Roy. Astron. Soc. **463**, 4175 (2016).
[3] J. August *et al.* Astrophys. Space Sci. **128**, 411 (1986).
[4] M. Turowski *et al.* J. Chem. Phys. **133**, 074310 (2010).
[5] I. Couturier-Tamburelli *et al.* J. Chem. Phys. **140**, 044329 (2014).
[6] U. Szczepaniak *et al.* J. Phys. Chem. A **121**, 7374 (2017).
[7] T. Wakabayashi *et al.* Carbon **50**, 47 (2012).

Corresponding Author: T. Wakabayashi
Tel: +81-4307-3408, Fax: +81-6723-2721,
Web: http://www.chem.kindai.ac.jp/stphys/kouzou/
E-mail: wakaba@chem.kindai.ac.jp

Correlation between Pore Size Distribution and Hydrogen Production in Thermal Catalytic Decomposition of Methane using Carbon Catalysts

○Dai miyamoto[1], Yoshito Umeda[2], Hiroaki Hamaguchi[3], Masashi Suzuki[3], Toru Harigai[1],
Tsuyoshi Tanimoto[1], Hirofumi Takikawa[1], Yoshiyuki Suda[1]

[1] *Department of Electrical and Electronic Information Engineering, Toyohashi University of Technology, Toyohashi, Aichi 441-8580, Japan*
[2]*Toho Cryogenics Co., Ltd, Nagoya, Aichi 456-0004, Japan*
[3]*Aichi Center for Industry and Science Technology, Toyota, Aichi 470-0356, Japan*

Thermo-catalytic decomposition (TCD) of methane is the attractive hydrogen production process to mitigate CO_2 emissions commonly associated with the conventional processes. However, the problem of the process is catalyst deactivation by carbon deposition [1]. In the previous study, we showed that activated carbon had a high specific surface area but the catalytic activity was lost immediately [2]. The purpose of this study is to investigate the correlation between the catalysts pore structure and deactivation of catalysts by using four carbon catalysts with different structures. The four carbon catalysts tested in this study were as follows: coconut-shell activated carbon (AC), mesoporous carbon (MC), carbon black (CB) and carbon nanofiber (CNF). Experiments were carried out in a fixed-bed reactor using 1.7 g of the catalysts and the flow rate of methane gas was 50 ml/min. The reaction temperature was 1173 K. The produced gas was analyzed by a hydrogen detector and gas chromatography. Carbon catalysts before and after the experiments were analyzed by Raman spectroscopy. The methane conversion ratio was derived from the following formula using the hydrogen concentration obtained by gas analysis [2].

$$Methane\ \ conversion\ \ ratio = \frac{Produced\ \ H_2\ \ concentration}{2 - Produced\ \ H_2\ \ concentration} \quad (1)$$

Temporal change of the methane conversion ratio of all the catalysts was examined. The period for which the methane conversion ratio of 25% or higher lasted was 80 min for AC, 200 min for MC and 550 min for CB. The methane conversion ratio of CNF was low.

Table 1. Properties of the carbon catalysts.

Catalyst	Specific surface area [m^2/g]	Total pore volume [cm^3/g]	Micropoore volume [cm^3/g]	Mesopore volume [cm^3/g]	Particle size [μm]
AC	1712	0.816	0.781	0.171	6.5
CB	1469	1.562	0.527	1.102	0.002
MC	1577	3.147	1.165	3.020	5
CNF	270	—	—	—	—

Table 1 shows the properties of the carbon catalysts. MC and CB had a larger mesopore volume than AC. CB also had a small particle size compared to MC. It is thought that a large mesopore volume as well as small particle size is effective for TCD of methane.

Acknowledgements

A part of this work was supported by “Development project of near-term hydrogen economy forming technology” for priority of research project of Knowledge Hub Aichi. The authors would like to thank K. Asato for emeritus Prof. of Gifu Univ. and H. Yamashita for emeritus Prof. of Nagoya Univ. with discussion about correlation between produced carbon and methane conversion.

[1] Lee Eun Kyoung, *et al*, Carbon., **42**, 12-13, 2641-48 (2004)
[2] Haruki Nishii, *et al,* submitted

Corresponding Author: Y. Suda, Tel: +81-532-44-6726, E-mail: suda@ee.tut.ac.jp

Dynamic Behavior of a Single *but* Hydrogen-Bonded Water Molecule inside a Hydroxy Open-Cage Fullerene C_{60} Derivative

○Shota Hasegawa, Yoshifumi Hashikawa, Yasujiro Murata

Institute for Chemical Research, Kyoto University, Uji 611-0011 Japan

Hydrogen-bonded (H-bonded) H_2O molecule participates in a variety of field such as protein folding, drug delivery, catalyst, and so forth.[1] However, there have been no experimental example to see dynamic behavior of a H-bonded single H_2O molecule because it is difficult to isolate the H-bonded single H_2O molecule from Hydrogen-bonding (H-bonding) network. Thus, we designed an open-cage C_{60} derivative $H_2O@$**2** with a large inner space and a multiply hydroxylated opening. We expected dynamic behavior of the encapsulated H_2O molecule through H-bondings between the encapsulated H_2O molecule and the OH groups on the orifice.

$H_2O@$**2** was synthesized from $H_2O@$**1**[2] by the selective reduction of carbonyl groups on the rim of the opening in 75% yield (Scheme 1). The single crystal X-ray structure analysis demonstrated that $H_2O@$**2** has a strong intramolecular H-bonding network on the opening as well as an intermolecular H-bondings leading to dimerization (Figure 1). In addition, positional disorders of the encapsulated H_2O molecules were observed at positions of the center and off-center closer to the opening with the occupancy ratio of 0.11(2) and 0.81(2), respectively, indicative of the translational motion of the confined H_2O. The ^1H NMR measurements displayed that **2** dimerizes in the solution state. Additionally, the ^1H NMR measurements, which were performed at a low concentration to prevent the dimerization (0.91 mM, ODCB-d_4), exhibited a downfield shift of the encapsulated H_2O molecule by decreasing the temperature due to the formation of H-bondings with OH groups on the opening. Noticeably, this phenomenon was supported by the long ^1H NMR relaxation time of the encapsulated H_2O molecule inside **2**, reflecting the restricted rotational motion. In the solid state, all of the OH groups on the opening were reversibly exchangeable with D_2O. However, the confined H_2O molecule was inactive against the H/D exchange with the OD groups on the opening within 2 days. Thus, it would be concluded that the encapsulated H_2O molecule is less basic and less acidic than bulk H_2O.

Scheme 1. Synthesis of $H_2O@$**2**

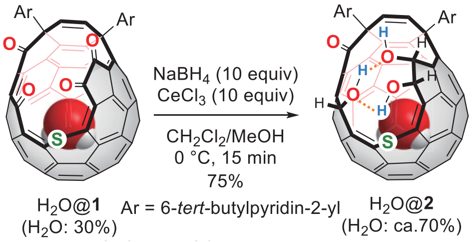

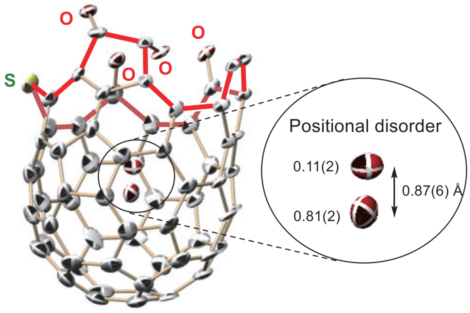

Figure 1. X-ray structure of $H_2O@$**2**. Solvent molecules, hydrogen atoms and aryl groups were omitted for clarity. Thermal elipsoids are set in 50% probability.

[1] Mahadevi, A. S.; Sastry, G. N. *Chem. Rev.* **2016**, *116*, 2775–2825.

[2] Futagoishi, T.; Murata, M.; Wakamiya, A.; Murata, Y. *Org. Lett.* **2013**, *13*, 2750–2753.

Corresponding Author: Y. Murata
Tel: +81-774-38-3172, Fax: +81-774-38-3178
Web: http://www.scl.kyotou.ac.jp/~kouzou/index.html
E-mail: yasujiro@scl.kyoto-u.ac.jp

Functionalization of single-walled carbon nanotube with dendrons: Control of functionalization degree and infrared photoluminescence properties

○Yui Konno[1], Michio Yamada[1], Yutaka Maeda[1], Pei Zhao[2,3], Xiang Zhao[2], Masahiro Ehara[3], Shigeru Nagase[4]

[1] Department of Chemistry, Tokyo Gakugei University, Koganei, Tokyo 184-8501, Japan
[2]Institute for Chemical Physics & Department of Chemistry, State Key Laboratory of Electrical Insulation and Power Equipment, Xi'an Jiaotong University, Xi'an 710049, China
[3]Research Center for Computational Science, Institute for Molecular Science, Okazaki, Aichi 444-8585, Japan
[4]Fukui Institute for Fundamental Chemistry, Kyoto University, Kyoto, 606-8103, Japan

Single-walled carbon nanotubes (SWNTs) are expected for numerous applications because of their outstanding mechanical and electrical properties. Weisman et al. has reported near-infrared (NIR) photoluminescence (PL) appearance from individually dispersed semiconducting SWNTs.[1] These NIR PL between 1000 to 1400 nm, which is known as a second NIR window, are very useful for biological imaging materials because of its bio-permeability. Recently, conspicuous appearance of bright, red-shifted PL peaks arised from SWNTs functionalization such as oxidation and arylation using ozone and aryl diazonium compounds has been focused.[2,3] We have reported that new, red-shifted PL around 1200 nm (E_{11}**) was emerged selectively by two-step reactive alkylation using alkyllithium and alkyl bromide as well as by reductive alkylation using sodium naphthalenide and 1,2-dibromomethylbenzene.[4,5] On the other hand, both the new, red-shifted PL peaks, corresponding to E_{11}* with the peak top at around 1100 nm and and E_{11}**, were emerged by reductive alkylation using sodium naphthalenide and benzyl bromide. Akizuki et al. has recently reported the new localized states of functionalized SWNTs could act as an excited state in up-conversion PL (UCPL).[6] The E_{11}* state has an advantage in UCPL efficiency compared to the E_{11}** state.[5] Herein, we report new methodology for control of functionalization degree and emergence of new PL properties of SWNTs by reductive alkylation using alkyl bromides bearing dendrons.

Functionalization of (6,5)-enriched SWNTs was conducted according to a reported procedure.[4] Briefly, the SWNTs were treated with sodium naphthalenide, and then three generations of dendron-appended alkyl bromide were added to the resulted SWNT anion, respectively. Functionalization degree of the functionalized SWNTs was estimated from Raman spectra. The optical properties of the functionalized SWNTs were characterized by absorption and photoluminescence spectra. The influence of the generation of dendrons on their degree of functionalization and optical properties will be discussed in this presentation.

[1] M. J. O'Connell *et al. Science* **297**, 593 (2002). [2] S. Ghosh *et al. Science* **330**, 1656 (2010). [3] S. Diao *et al. Nat. Chem.* **5**, 840 (2013). [4] Y. Maeda *et al. Chem. Commun.* **51**, 13462 (2015). [5] Y. Maeda *et al. Nanoscale* **8**, 16916 (2016). [6] N. Akizuki *et al. Nat. Commun*. **6**, 8920, (2016)

Corresponding Author: Y. Maeda
Tel: +81-42-329-7512 E-mail: ymaeda@u-gakugei.ac.jp

3P-3

Investigation on mechanism of voltage generation by continuous flow of fluid on surface of carbon nanotube thin film

°Yuzuki Ando[1], Ryohei Nishi[1], Shigeru Kishimoto[1], Hiromichi Kataura[2], and Yutaka Ohno[1,3]

[1] *Department of Electronics, Nagoya University, Nagoya 464-8603, Japan*
[2] *National Institute of Advanced Industrial Science and Technology, Tsukuba 305-8565, Japan*
[3] *Institute of Materials and Systems for Sustainability, Nagoya University, 464-8603, Japan*

Recently, the voltage generation from fluidic energy with graphene and carbon nanotubes (CNTs) is attracting much attention in the field of the energy harvesting. [1-3] Among them, the energy harvesting from continuous flow of fluid [2, 3] is considered to provide more opportunities in various environments. The mechanism of the voltage generation by continuous flow is, however, unclear, and understanding the physics is the most important point for increasing output power. In this work, we have investigated the mechanism of the voltage generation with CNT thin film by using various device structures and fluids.

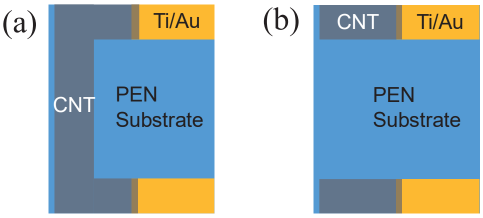

Fig. 1 Schematic structure of generator devices, (a) Type 1, (b) Type 2.

Figure 1(a) shows a schematic structure of a generator device consisting of a CNT thin film and Au electrodes on a polyethylenenaphthalate (PEN) substrate, named Type 1. We used semiconducting CNTs separated by gel-chromatography [4]. In the voltage generation experiments, the fluid flows on the CNT thin film from the top to bottom of the figure. To investigate the role of the CNT thin film, we also fabricated the device, Type 2, where is no CNT thin film in between two electrodes as shown in Fig. 1(b). Figure 2 shows a schematic of the experimental setup. The generator device was inserted into a silicone tube, and the output voltage generated by the flow of fluid was measured by a semiconductor device parameter analyzer. Since a power-driven pump can be a noise source, the fluid is driven by the gravity. Figure 3 shows the voltage waveform measured when deionized water was used as the fluid. The flow velocity was ~70 cm/s. We connected a load resistance of 100 MΩ to stabilize the potential of the electrodes for Type 2. The voltage generations of ~30 mV for Type 1 and ~80 mV for Type 2 were observed. This suggests that the CNT thin film between the electrodes in Type 1 is not essential, but the electrodes at both ends dominantly contributes to the voltage generation by continuous flow of the fluid.

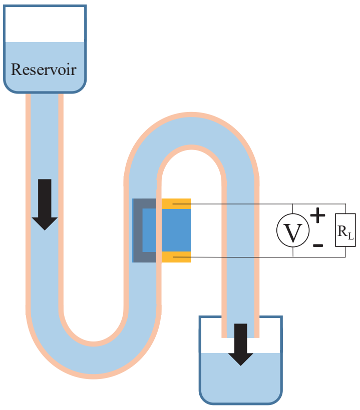

Fig. 2 Experimental setup.

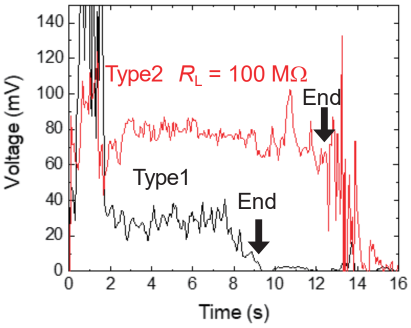

Fig. 3 Voltage waveforms.

Acknowledgment: This study was partially supported by JST/CREST (JPMJCR16Q2).

[1] J. Yin *et. al.*, Nat. Nanotechnol. **9**, 378, (2014).
[2] P. Dhiman *et. al.*, Nano Lett. **11**, 3123, (2011).
[3] S. Ghosh *et. al.*, Science **299**, 1042 (2003).
[4] T. Tanaka *et al.*, Anal. Chem. **87**, 9467 (2015).

Corresponding Author: Y. Ohno
Phone & Fax: +81-52-789-5387
E-mail: yohno@nagoya-u.jp

3P-4

Design and fabrication of carbon nanotube analog integrated circuits

○Taiga Kashima[1], Jun Hirotani[1], Shigeru Kishimoto[1], and Yutaka Ohno[1,2]

[1]*Department of Electronics, Nagoya University, Nagoya 464-8603, Japan*
[2]*Institute of Material and Systems for Sustainability, Nagoya University, Nagoya 464-8603, Japan*

Carbon nanotube thin-film transistors (CNT TFTs) are promising active component for flexible electronics because of high carrier mobility and excellent mechanical flexibility [1]. In recent years, high-yield and reproducible fabrication of CNT TFTs have become possible by using purified semiconductor CNTs. This opens a possibility to realize functional integrated circuits with CNT TFTs. Although digital circuits such as adders and CPU [2, 3] are reported, the analog integrated circuits have not been realized yet. In this work, we have designed and fabricated the differential amplifier, which is the fundamental analog circuits, using the design tools with the CNT TFT model we built recently [4].

The devices were fabricated on a polyethylene naphthalate (PEN) substrate. Purified semiconducting CNTs were used as the channel. The gate oxide of Al_2O_3 (45 nm) layer was deposited by atomic layer deposition. By using self-align process, the parasitic capacitances between the gate and source/drain electrodes were minimized. The channel length of transistors was set to be 20 μm, balancing the ON/OFF ratio and the cutoff frequency.

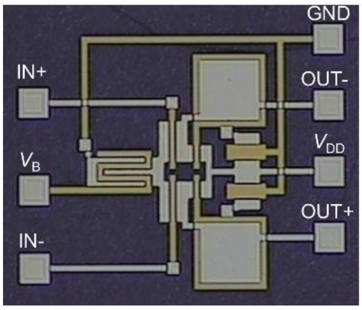

Fig. 1 Micrograph of differential amplifier composed of CNT TFTs.

We fabricated the differential amplifier (Fig. 1) using bootstrapped gain-enhancement (BGE) which can achieve both high gain and variation tolerance simultaneously with only p-type transistors. As shown in Fig.2, the fabricated circuit showed the gain of 25.5 dB and the bandwidth of 300 Hz at the power supply voltage of 5 V. We obtained good agreement between measured result and the circuit simulation based on Monte Carlo simulation, showing the reliability of our circuit design tools.

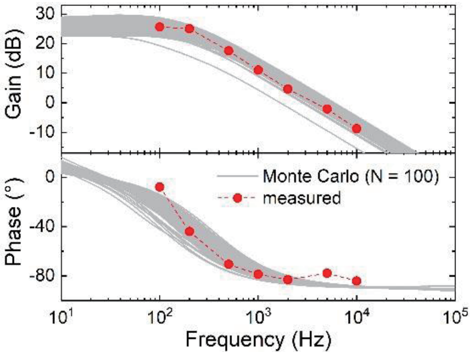

Fig. 2 Frequency characteristics of Monte Carlo simulated results and measured result of differential amplifier.

Acknowledgments: The semiconducting CNTs were provided by TASC. This work was partially supported by JST/CREST.

[1] D. -M. Sun *et al.*, *Nature Nanotechnol.* **6**, 156 (2011).
[2] B. Chen *et al.*, *Nature Lett.,* **16**, 5120 (2016).
[3] M. M. Shulaker *et al.*, *Nature,* **547**, 74 (2017).
[4] T. Kashima *et al.*, The 78th JSAP Autumn Meeting, 6a-C19-4.

Corresponding Author: Yutaka Ohno, Phone & Fax: +81-52-789-5387, E-mail: yohno@nagoya-u.jp

3P-5

Purity improvement of preferentially synthesized (6,4) single-walled carbon nanotubes by controlling plasma parameters

○Takuya Shima[1], Bin Xu[1], Toshiro Kaneko[1], Toshiaki Kato[1,2]

[1] *Department of Electronic Engineering, Tohoku University, Sendai 980-8579, Japan*
[2] *JST-PRESTO*

Single-walled carbon nanotubes (SWNTs) have many outstanding properties due to the unique 1-dimensional structure, which make them as a promising candidate of material for high performance optoelectrical devices. However, as the physical properties of SWNTs strongly depend on the chirality, obtaining specific single chirality SWNTs with high quality is regarded as a critical issue in this scientific community. Recently, we have succeeded in high purity (~57%) synthesis of (6,4) SWNTs by controlling the surface condition of the Co catalyst for the first time [1]. To further increase the purity of (6,4) SWNTs, we focused on correlation between (6,4) SWNT growth and plasma CVD conditions.

Synthesis of high purity (6,4) SWNTs was carried out by catalyst surface condition control. In this method, oxidation degree of catalyst surface can be well controlled by ultra-high vacuum annealing. The small amount of reactive gas species (H_2, N_2, etc) were added during the annealing process, which can precisely tune the surface state of catalyst. Synthesis of SWNTs was carried out using a home-made diffusion type plasma CVD apparatus [2]. The chirality distribution of SWNTs was measured by photoluminescence (PL)-excitation (PLE) mapping and ultraviolet-visible-near infrared (UV-Vis-NIR) absorption spectroscopy.

Systematic experiments were conducted to reveal the correlation between (6,4) SWNTs growth and plasma CVD conditions. Plasma CVD was performed by changing the radio frequency power (RF; 13.56 MHz) used for plasma generation. As a result, it is clarified that the purity of (6,4) SWNTs is influenced by the RF power (Fig. 1). The purity of (6,4) SWNTs can be increased up to 64% by adjusting plasma conditions. In addition, it is confirmed that the chirality distribution of (7,3), (6,5), (8,3) SWNTs is also changed by the RF power. This result suggests that certain reactive gas species in the plasma can contribute to increasing the purity of (6,4) SWNTs. In other words, gas phase information such as active species in plasma which has not attracted attention so far seems to influence chirality selectivity.

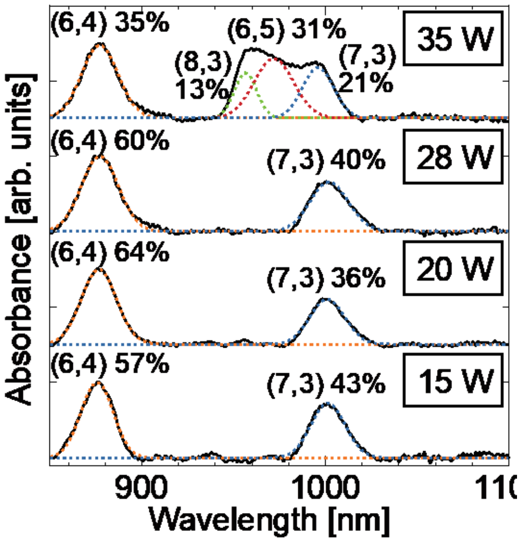

Fig.1: Typical UV-Vis-NIR spectra of SWNTs grown by various RF power used for plasma generation.

[1] B. Xu, T. Kaneko, Y. Shibuta and T. Kato: Sci. Rep. 7, 11149 (2017)
[2] T. Kato and R. Hatakeyama: Nat. Nanotechnol. 7, 651 (2012)

Corresponding Author: T. Shima
Tel: +81-22-795-7046, Fax: +81-22-263-9225, E-mail: takuya.shima.p6@dc.tohoku.ac.jp.

3P-6

Selective extraction of semiconducting single-walled carbon nanotubes with a thermoresponsive polymer

○Eriko Shimura, Toshiki Sugai, Shota Kuwahara

Department of Chemistry, Toho University, Chiba 274-8510, Japan

The separation techniques for obtaining single-walled carbon nanotubes (SWCNTs) with homogeneous electronic properties is crucial for the promising electronic devices in nanotechnology. The separation of SWCNTs in aqueous solution was employed by using the difference in hydrophobicity or surface charges of the SWCNT micelles with surfactants, which showed semiconducting and/or metallic SWCNTs in high yield [1]. Utilizing the difference in the hydrophobicity of the SWCNT micelles, we successfully demonstrated the selective extraction of semiconducting SWCNTs with poly-(*N*-isopropylacrylamide) (PNIPAM) [2], a well-known thermoresponsive polymer, which shows reversible phase transitions in aqueous solutions at the lower critical solution temperature (LCST). Above the LCST, PNIPAM forms aggregates, globules, where hydrophobic space is generated inside, and we separated the specific structure of SWCNTs with the solid (globule) and liquid phases.

A semi-oxidized solution of SWCNTs was prepared by mixing the dispersion of SWCNTs in sodium cholate (SC) and sodium hypochlorite (NaClO), which was followed by mixing an aqueous PNIPAM solutions. Then, the solution was heated to 45 °C above the LCST of PNIPAM, and incubated for 15 minutes. Finally, the liquid phase was collected. Optical absorption spectra of the obtained samples were collected on a UV-vis-NIR spectrophotometer.

In the case of small-diameter nanotubes, CoMoCAT, the semiconductor SWCNTs were successfully extracted into the liquid phase. The intensity corresponding to metallic SWCNTs reduced in the absorption spectrum of the liquid phase. The re-dispersed solution of SWCNTs captured in the globule phase of PNIPAM showed same absorption features as the original sample. The result indicated that a part of the semiconducting SWCNTs was selectively transferred to the aqueous phase rather than remaining in the hydrophobic space within the globules of PNIPAM. When the concentration of aqueous PNIPAM solutions was 5 wt%, (6,5) nanotubes were selectively extracted into the liquid phase (Fig. 1). The oxidized SWCNTs are understood to be easily covered by SC molecules, and to be captured in the globule of PNIPAM due to the interaction between SC and PNIPAM. (6,5) SWCNTs seem to be less oxidized by NaClO, and can be transferred to the liquid phase to escape from the space inside the globules.

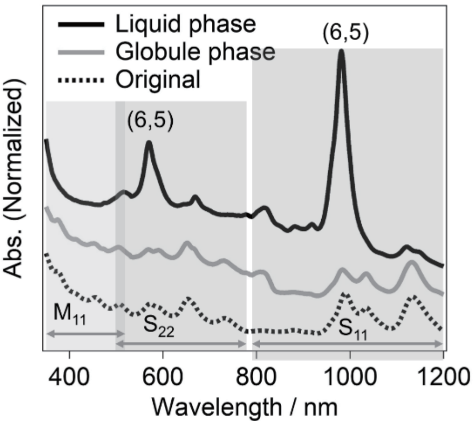

Fig. 1 Optical absorption spectra of the pristine SWCNT solution before extraction, the liquid phase and the globule phase after extraction.

[1] C. Y. Khripin, *et al.*, *J. Am. Chem. Soc.*, **135**, 6822 (2013).
[2] E. Shimura, *et al.*, *Chem. Commun.*, **54**, 3026 (2018).

Corresponding Author: S. Kuwahara
Tel: +81-47-472-4442
E-mail: syouta.kuwahara@sci.toho-u.ac.jp

3P-7

Optical properties of two-dimensional lateral heterostructure WS_2/MoS_2

○Masafumi Shimasaki[1], Tetsuki Saito[2], Yasumitsu Miyata[2],
Yuhei Miyauchi[1], and Kazunari Matsuda[1]
[1] *Institute of Advanced Energy, Kyoto University, Gokasho, Uji, Kyoto 611-0011, Japan*
[2] *Dept. of Physics, Tokyo Metropolitan University, Hachioji, Tokyo 192-0397, Japan*

Transition metal dichalcogenides (TMDCs, MX_2, M=Mo, W; and X=S, Se;) have attracted much attention due to stable excitons at room temperature with large binding energy of a few hundred meV.[1] This property offers potentially a great advantage for developing excitonic devices in which flow of excitons is used as an information carrier for data processing.[2] However, it is still unclear how to control the exciton flow in TMDCs.

Here, we report exciton transport phenomena in a lateral heterostructure of monolayer WS_2/MoS_2. The sample was prepared using salt-assisted chemical vapor deposition (CVD) method on a SiO_2/Si substrate. We carried out the excitation position dependent photoluminescence (PL) measurements on the lateral heterostructure WS_2/MoS_2 at room temperature under excitation energy of 2.41 eV. Figure 1 shows the position-dependent PL spectra near the border of WS_2 and MoS_2; the excitation spot center was located at the border. In this condition, the excitation laser was irradiated on both of WS_2 and MoS_2 equally, but almost no WS_2 PL signal was observed and PL spectral shape changed depending on the location. Even when the excitation spot was placed away from the border to excite only the WS_2 part, we observed MoS_2 signal at the border. These results suggest that the exciton transport is unidirectional from WS_2 to MoS_2; this implies the type Ⅰ band alignment is formed near the border of WS_2 and MoS_2.

[1] K. F. Mak *et al*, Phys. Rev. Lett. 105, 136805 (2010).

[2] Marc Baldo *et al*, Nature Photonics 3, 558 (2009)

Corresponding Author: Y. Miyauchi
Tel: 81-774-38-3463,
Fax: +81-774-38- 3467,
E-mail: miyauchi@iae.kyoto-u.ac.jp

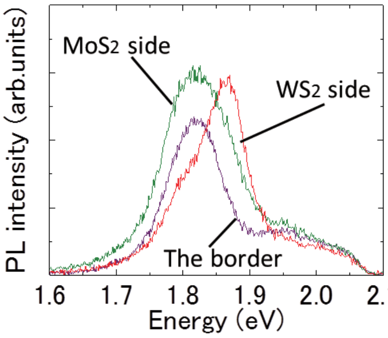

Fig 1. PL spectra near the border. Spectral shape changes depending on the location.

3P-8

Improved Crystallinity of CVD-Grown Atomic Layered WS_2 from H_2S and WF_6 Precursors with NaCl Assistance

○Mitsuhiro Okada[1], Naoya Okada[1], Wen Hsin Chang[1], Atsushi Ando[1], Toshifumi Irisawa[1]

[1] *Nanoelectronics Research Institute, AIST, Tsukuba 305-8568, Japan*

In recent years, alkali metal halide assisted chemical vapor deposition (CVD) growth of two-dimensional transition-metal dichalcogenide (TMD) semiconductors has been attracted a great deal of attention because the added alkali metal halide can greatly reduce the density of nuclei and promote 2D lateral growth of TMD [1]. With this assistance, TMD from various precursors such as solid metal oxides and gas phase organic precursors are successfully obtained [1]. Here, we report the effects of NaCl assistance on the crystallinity of monolayer WS_2 grown from inorganic gas phase precursors of H_2S and WF_6. These precursors have been reported to result in only small grains growth with the size of much smaller than 1 μm [2] without the help of alkali metal, which is probably due to their high reactivity. We found here that with NaCl assistance, grain size of WS_2 was remarkably increased and accordingly the optical and the electrical transport properties are significantly improved.

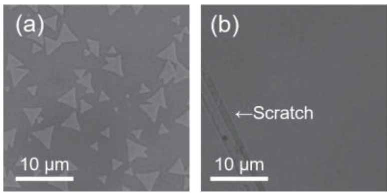

Figure 1. Optical microscope images of WS_2 (a): with and (b): without NaCl assistance.

Figure 1 shows typical optical microscope images of obtained WS_2. While NaCl-free growth leaded to continuous film with small nanocrystals, NaCl-assisted growth gave triangular contrasts, indicating formation of single crystal WS_2 with the size of several microns. This result clearly indicates that NaCl-assisted growth is very effective even in the case of highly reactive gas precursors such as H_2S and WF_6. The effect of NaCl assistance can also be seen in the difference of room-temperature photoluminescence (PL) spectrum (Figure 2). PL intensity of the NaCl-assisted grown WS_2 is much stronger (over 50x) than that of WS_2 grown without NaCl. And PL peaks around 1.9 eV which probably originate from defect states are only observed in the NaCl-free samples. These results strongly suggest that the crystal quality of NaCl-assisted grown WS_2 is much higher than that of NaCl-free one. And the full width half-maximum of the PL peak from WS_2 obtained by NaCl-assisted growth is ~48 meV, which is comparable to that of previous reports (~42-68 meV) [3] using solid precursors for CVD growth. Furthermore, we could obtain the field-effect transistor (FET) operations with on/off ratio of $\sim 10^4$ in WS_2 grown with NaCl assistance, while the NaCl-free grown WS_2 does not show any FET behaviors.

In summary, we succeeded to improve the crystal quality of WS_2 by introducing NaCl assistance in the synthesis with H_2S and WF_6.

Acknowledgement: This work is supported by JST-CREST Grant No. JPMJCR16F3, JST, Japan.

[1] H. Kim *et al*. Nano Lett., **17**, 5056 (2017).
[2] B. Groven *et al.* Chem. Mater. **29**, 2927 (2017).
[3] H. R. Gutiérrez *et al*. Nano Lett., **13**, 3447 (2012).

Corresponding Author: T. Irisawa
Tel: +81-29-861-3684, Fax: +81-29-861-5170,
Web: https://unit.aist.go.jp/neri/ja/teams/02_amdi/ja/index.html
E-mail: toshifumi1.irisawa@aist.go.jp

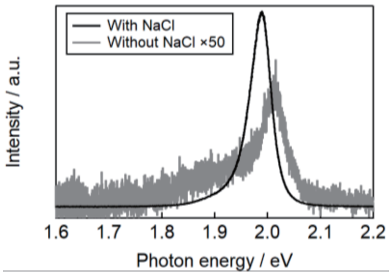

Figure 2. PL spectra of obtained WS_2.

3P-9

Sulfur- and phosphorous-doped graphene and its battery application

○Tsukasa Inoue[1], Haruka Omachi[1, 2], Zois Syrgiannis[3], Shuya Hatao[4], Hirofumi Yoshikawa[4],
Maurizio Prato[3] and Hisanori Shinohara[1, 5]

[1]Department of Chemistry, Graduate School of Science, Nagoya University, Nagoya, 464-8602, Japan
[2]Research Center for Materials Science, Nagoya University, Nagoya, 464-8601, Japan
[3]Cntre of Excellence for Nanostructured Materials (CENMAT), INSTM, Dipatrimento di Scienze Chimiche e Farmanceutiche, Università di Trieste, Piazzale Europa, 1, 34127 Trieste, Italy
[4]Department of Nanotechnology for Sustainable Energy, School of Science and Technology, Kwansei Gakuin University, Sanda, 669-8501, Japan
[5]Institute for Advanced Research, Nagoya University, Nagoya, 464-8601, Japan

Sulfur-doped graphene is expected various applications to oxygen reduction catalysis, t dye-sensitized solar cells and electrode material for lithium ion battery. Although a lot of synthetic studies have been reported, many problems still remain, such as low doping efficiency, unsalable and harsh synthetic conditions [1, 2].

Here we developed sulfur-doped graphene (dGO) synthesis by the reaction graphene oxide (GO) with Lawesson's reagent, which has a potential for mass production. X-ray photoelectron spectroscopy (XPS) measurement revealed resultant dGO contained sulfur and phosphorus atoms (Fig.1a). Adding to hetero-atoms doping, the reduction of GO was also confirmed by XPS and other spectroscopic measurements. We then fabricated a nanohybrid materials with dGO and polyoxometalate (POM) as a battery cathode material. The lithium battery using POM/dGO complex exhibited more stable cycle performance for charge-discharge process than the battery of the nanohybrid materials between POM and simple reduced graphene oxide (rGO) (Fig.1b) [3].

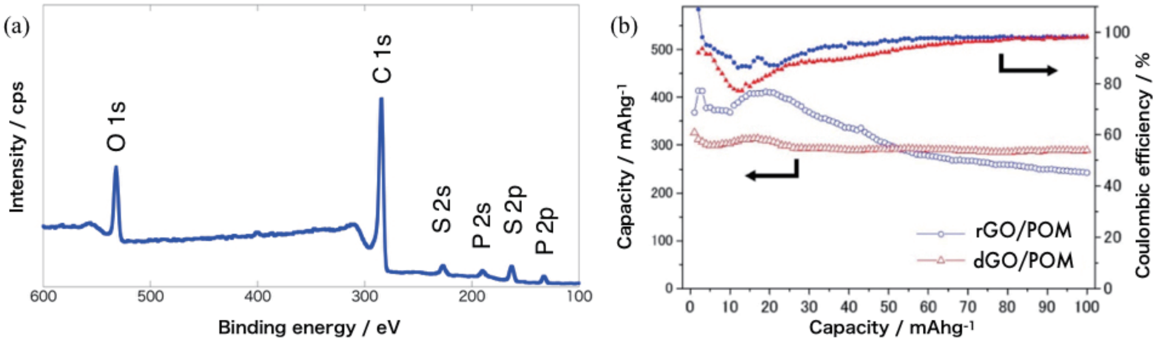

Fig. 1. (a) XPS spectrum of dGO. (b) Charge-discharge cycle performance of dGO and rGO complex

[1] F. Hassani, H. Tavakol, F. Keshavarzipour, and A. Javaheri, RSC Adv. **6**, 27158 (2016).

[2] L. Chen, X. Cui, Y. Wang, M. Wang, R. Qiu, Z. Shu, L. Zhang, Z. Hua, F. Cui, C. Wei, and J. Shi, Dalton Trans. **43**, 3420 (2014).

[3] K. Kume, N. Kawasaki, H. Wang, T. Yamada, H. Yoshikawa, K. Awaga, J. Mater. Chem. A. **2**, 3801 (2014).

Corresponding Author: Haruka Omachi
Tel: +81-52-789-2482, Fax: +81-52-747-6442,
Web: http://nano.chem.nagoya-u.ac.jp/japanese/
E-mail: omachi@chem.nagoya-u.ac.jp, noris@nagoya-u.jp

3P-10

Properties of graphene films synthesized by lamp heating CVD

○Masaki Komori[1], Takatsugu Onishi[1], Adam Pander[1,2], Akimitsu Hatta[1,2], Hiroshi Furuta[1,2]

[1] *Department of Systems Engineering, Kochi Univ. Technol., Kochi 782-0003, Japan*
[2] *Center for Nanotechnol., Research Inst., Kochi Univ. Technol. Kochi 782-0003, Japan*

Graphene requires high synthesis temperature about 1000 ℃ for thermal CVD method. Recently, Lamp heating CVD growth of high quality graphene films at relatively low synthesis temperature was reported[1]. In this paper, graphene formation process at relatively low temperature under lamp irradiation were investigated by Raman and XPS analysis.

A lamp heating CVD system was built using a cold wall chamber with a halogen lamp via a quartz window on the chamber[2]. A nickel catalyst film of 200 nm thickness was deposited on thermal CVD SiO (Ni/th-SiO) substrate by magnetron sputtering method. The Ni/th-SiO substrate was evacuated below 5.0×10^{-4}Pa and irradiated by the halogen lamp for 10 min in the lamp heating CVD, and substrate temperature was raised up to about 400℃. Subsequently, C2H2 gas was introduced into the chamber at the gas pressure of 0.25Pa to 45Pa for 10 min synthesis. Films qualities were evaluated by Raman spectroscopy (Horiba HR800) and XPS (Shimadzu AXIS-HS).

Figure 1 shows Raman spectra of deposited films by the lamp heating CVD[2]. Raman spectra showed multi-layered graphene films (MLG) films were synthesized on the Ni/th-SiO substrates., G/D ratio increased to 1.9 by decreasing deposition pressure from 44 Pa to 0.44 Pa, which indicates reduction of the defects concentration of MLG. It is also found that increase of 2D peaks by reducing deposition pressure, indicating decreasing of layer number of MLG.

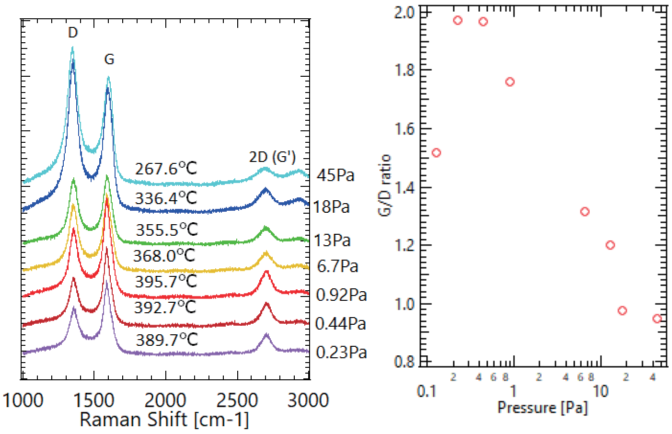

Fig.1 Raman spectra of graphitic films synthesized by Lamp heating CVD at 0.23Pa to 45Pa[2].

Figure 2 shows XPS C1s spectra of the MLG films deposited by the lamp heating CVD. With decreasing the deposition pressure from 45Pa, the C1s peak positions increased, which would correspond to the decrease of the vacancy and improve of film quality reaching to sp2 peaks at 284.4eV. The improve of film quality of the reduction of defect density in the MLG films was correspond to the increase of G/D ratio found in Fig.1. In the presentations, graphene synthesis on Cu substrates will be also discussed.

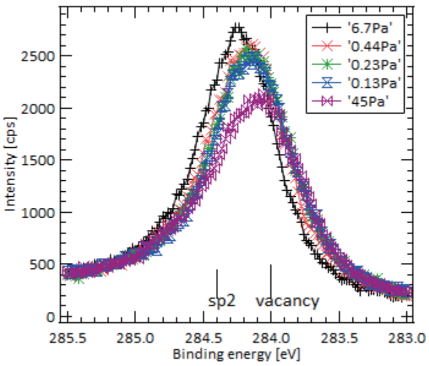

Fig.2 XPS spectra of MLG films synthesized by Lamp heating CVD at 0.13 to 45Pa (XPS Charge balance +2.5V)

[1] Y. Y. Tan *et al.*, Carbon 50(2) 668-673 (2012).
[2] 小森雅樹 *et al.*, 応物中四国支部講演会(2018)

Corresponding Author: H. Furuta
Tel: +81-887-57-2211,
Web: http://gecko.eng.kochi-tech.ac.jp
E-mail: furuta.hiroshi@kochi-tech.ac.jp

3P-11

Near-field optical transition in graphene

F.R. Pratama[1], M. Shoufie Ukhtary[1], R. Saito[1]
[1]Department of Physics, Graduate School of Science, Tohoku University

In the typical experimental set-up of tip-enhanced Raman spectroscopy (TERS), a metallic tip of scanning probe device whose radius around 10 nm is placed sufficiently near the sample of the characterized material. The presence of tip enhances the intensity of Raman signal [1] due to the localization of electric field in the vicinity the tip that is called near-field [1, 2]. The properties of optical transition of electron in graphene affected by near-field from the tip is not yet investigated even though the theoretical analysis is essential for explaining the observed near-field Raman spectra of graphene. Firstly, we calculate electric near-field enhancement around Au tip at optical wavelength λ=500-700 nm. The calculation is performed by solving the Laplace equation numerically with finite-difference method. Fig. 1 (a) depicts the calculated near-field distribution around parabolic Au tip at λ=534 nm.

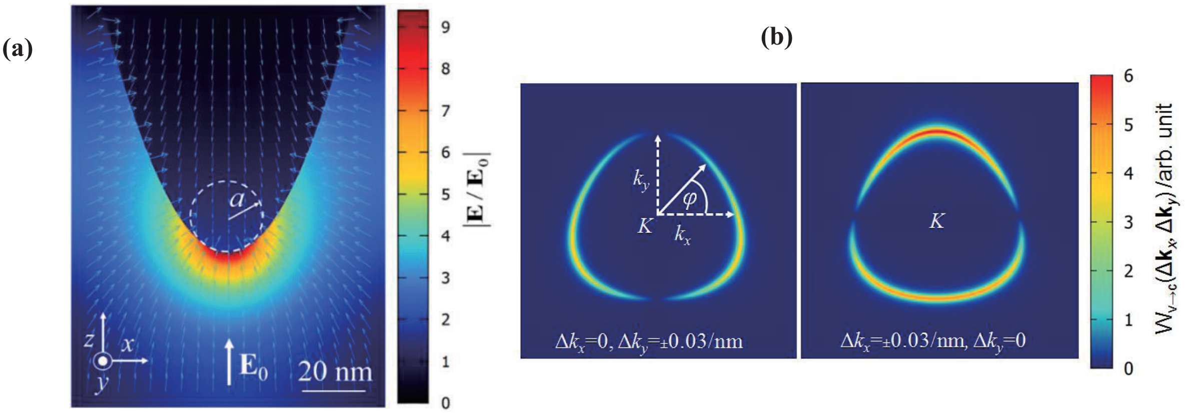

Figure 1. (a) Calculated near-field enhancement distribution in the vicinity of parabolic tip (a=10 nm) at excitation wavelength $\lambda \approx$ 534 nm. Arrows represent the directions of total electric field. (b) Calculated optical transition probability around K point for different directions of the change of electron wave vector $\Delta\boldsymbol{k}$.

Secondly, a monolayer graphene is placed few nm below the tip. We calculate the optical matrix element which describes the interaction of electrons with the planar components of induced near-field. We vary the distance of the Au tip relative to the graphene plane to capture the near-field effect on the properties of optical transition of electron in graphene. We found that while in the case of far-field spectroscopy the optical transition of electron from valence to conduction bands occurs vertically (with no change of electron wave vectors) [3], the presence of the planar components of the near-field on the graphene plane produce a new transition rule which imposes the change of electron wave vectors in the optical transition, and becomes larger as the tip is approached to the graphene plane. Finally, by utilizing the Fermi golden rule, we calculate the near-field optical transition probability around K point in Brillouin zone of graphene for and found that the properties of optical transition is determined by the change of electron wave vector $\Delta\boldsymbol{k}=(\Delta k_x,\Delta k_y)$ (see Fig. 1 (b)), instead of the polarization of incoming light as in the case of far-field spectroscopy. These phenomena are also predicted by very recent progress on theory of interaction between graphene and near-field from lattices of plasmonic nanoparticles [4].

References:

[1] E.C. Le Ru & P.G. Etchegoin, *Principles of Surface-Enhanced Raman Spectroscopy*, Oxford: Elsevier (2009).
[2] J. Cui et al., *Laser Phys*. **23**, 076003 (2013).
[3] A. Grüneis et al., *Phys. Rev. B* **67**, 165402 (2003).
[4] N.S. Mueller & S. Reich, *Phys. Rev. B* **97**, 235417 (2018).

Corresponding author: F.R. Pratama
Email: pratama@flex.phys.tohoku.ac.jp

3P-12

Graphene quantum dots as sensitizer in solid-state dye sensitized solar cells

○Suzuka Tachi, Hiroki Morita, Toshiki Sugai, Shota Kuwahara

Department of Chemistry, Toho University, Chiba 274-8510, Japan

Dye sensitized solar cells (DSSCs) composed of porous nanocrystalline titanium oxide, dyes and electrolyte are considered to be promising alternatives to the conventional silicon solar cells. The dyes on TiO_2 efficiently absorb the incident solar light in the visible region, and convert it to electricity; dyes with enhanced light absorption are expected for the improvement of photoelectric conversion efficiency (PCE). Graphene quantum dots (GQDs), nanometer-sized graphene fragments, have potential for the efficient photon conversion material due to their tunable optical and electronic properties, and upconversion optical characteristics [1, 2]. Here, we utilized GQDs as the sensitizer of DSSCs, and solid-state GQD-sensitized solar cells (GQDSSCs) were successfully fabricated with hole transport layers (HTLs).

GQDs were prepared by using single-walled carbon nanotubes (CoMoCAT; Aldrich) via oxidation process in the mixture of concentrated H_2SO_4 and HNO_3. Then, the synthesized GQDs in water were refluxed with 1-hexanol, resulting in the esterification at carboxy groups on the [3] GQDs. Finally, we obtained GQDs miscible with organic solvent, and GQD ink in ethanol for the following spin-coating procedure. Fig. 1 shows the structure of GQDSSC in this work. Briefly, titanium diisopropoxide bis(acetylacetonate) was spin-coated on the cleaned fluorine doped tin oxide (FTO) glass and sintered to form blocking layer (BL). Then, TiO_2 paste was spin-coated on the substrate and sintered again. After $TiCl_4$ treatment, the prepared GQD ink and HTL were spin-coated sequentially, following the fabrication of electrodes by vapor deposition of 30 nm thick gold films in vacuum.

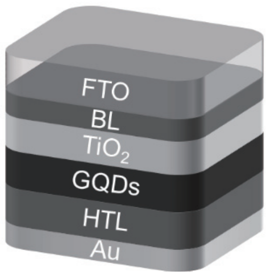

Fig. 1 Structure of GQDSSC.

Fig. 2 shows the current density-voltage (*J-V*) curves of GQDSSCs fabricated by using different HTLs: P3HT, spiro-OMeTAD, PTAA. Based on the obtained *J-V* curves, PCEs were calculated as 0.17 %, 0.075 % and 0.069 %, respectively, which is understood to be due to the difference in the energy gap between the HOMO energy level of the GQDs and the used HTLs. The photoexcited GQDs requires hole transfer to the HTL for the efficient charge separation at the TiO_2/GQD/HTL, and the sufficient potential difference between GQDs and HTLs is needed to obtain the driving force for the hole transfer. The increase in the current density of GQDSSC with P3HT is indicated that the sufficient potential difference was obtained with P3HT due to its appropriate energy level with the GQDs.

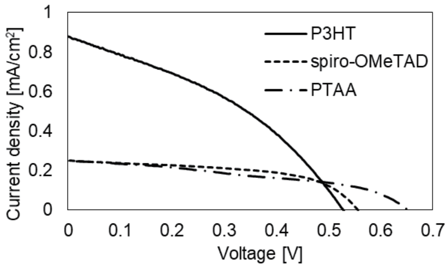

Fig. 2 *J-V* curves of GQDSSC with different HTLs.

[1] S. Chen, *et al.*, *J. Mater. Chem. C*, **6**, 6875 (2018).

[2] S. Zhuo, *et al.*, *ACS Nano*, **6**, 1059 (2012).

[3] H. Morita, *et al.*, *The 54th FNTG general symposium*, 3P36 (2018).

Corresponding Author: S. Kuwahara, Tel: +81-47-472-4442, E-mail: syouta.kuwahara@sci.toho-u.ac.jp

3P-13

Investigation of catalytic activity for reduction of 4-nitroaniline with [C_{60}]fullerene nanowhisker-platinum nanoparticle composites

○Jeong Won Ko [1], Weon Bae Ko [1,2]

[1] Nanomaterials Research Institute, [2] Department of Chemistry, Sahmyook University,
815 Hwarang-ro, Nowon-gu, Seoul 01795, Republic of Korea

Potassium tetrachloroplatinate(Ⅱ) (K_2PtCl_4) and PVP dissolved into distilled water, and then stirring for 10 min. The resulting solution was refluxed at 200 ℃ for 6 h. [C_{60}]Fullerene nanowhisker-platinum nanoparticle composites were synthesized using platinum nanoparticles solution, C_{60}-saturated toluene, and isopropyl alcohol by liquid-liquid interfacial precipitation(LLIP) method. The mixture of [C_{60}]fullerene nanowhisker-platinum nanoparticle composites was characterized by X-ray diffraction, scanning electron microscopy, Raman spectroscopy, and transmission electron microscopy. The catalytic activity of [C_{60}]fullerene nanowhisker-platinum nanoparticle composites was confirmed in the reduction of 4-nitroaniline by UV-vis spectroscopy.

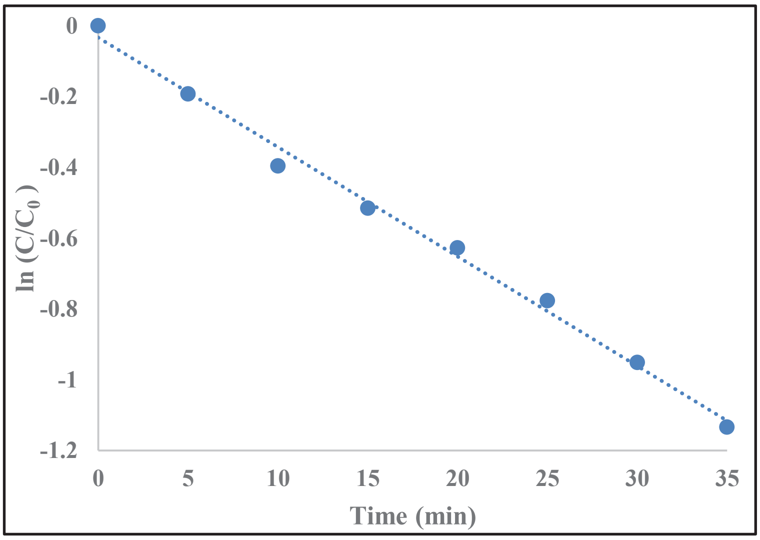

Fig.1 Kinetic study for reduction of 4-nitroaniline with [C_{60}]fullerene nanowhisker-platinum nanoparticle composites

[1] K. Miyazawa *et al*. Surf. Eng. doi.org/10.1080/02670844.2017.1396779 (2017).
[2] J. Wenhai *et al*. Nanomaterials **5,** 2203 (2015).

Corresponding Author: W. B. Ko
Tel: +82-2-3399-1700, Fax:, +82-2-979-5318,
E-mail: kowb@syu.ac.kr

3P-14

Isolation and Characterization of Sc-dimetallofullerenes: Sc_2C_n(n=76, 78, 80)

○Shun Yoshida, Koichi Kikuchi, Yohji Achiba, Takeshi Kodama

Department of Chemistry, Tokyo Metropolitan University, Tokyo 192-0397, Japan

In the previous symposium [1], we reported the partial separation of $(Sc_2C_{76})^-$ and $(Sc_2C_{78})^-$ and the isolation of $(Sc_2C_{80})^-$. For $(Sc_2C_{80})^-$, the ESR spectrum was measured, and the obtained ESR spectrum exhibited a large number of peaks over 100 although the nuclear spin of Sc is 7/2. Therefore, it was suggested that $(Sc_2C_{80})^-$ would be composed by at least two isomers such as cage structural or metal positional ones. In this study, we accomplished the isolation of $(Sc_2C_{76})^-$ and $(Sc_2C_{78})^-$ by using additional another column not used before: a C_{18}-AR-II column. Moreover, for $(Sc_2C_{80})^-$, two isomers were isolated and the ESR was reinvestigated.

Starting materials were obtained by the same method reported previously [1]. Next, we executed isolation of $(Sc_2C_{76})^-$ and $(Sc_2C_{78})^-$ by using a C_{18}-AR-II column. The HPLC chromatogram was shown in Fig. 1. The fraction A is $(Sc_2C_{76})^-$, and both the fraction B and C are $(Sc_2C_{78})^-$. Then, two isomers of $(Sc_2C_{78})^-$ were obtained. The UV-vis-NIR absorption spectra were measured for isolated $(Sc_2C_{78})^-$. As shown in Fig. 2, two isomers of $(Sc_2C_{78})^-$ show the different UV-vis-NIR absorption spectra each other. Furthermore, since the spectra of them are different from that of $(Y_2@C_{78}(D_{3h}))^-$, the cage structures of two $(Sc_2C_{78})^-$ could not be determined.

For $(Sc_2C_{80})^-$, two isomers were obtained by using a C_{18}-AR-II column. Therefore, the possibility of two cage structural isomers becomes much higher for two components indicated by ESR. The UV-vis-NIR absorption spectra of two $(Sc_2C_{80})^-$ isomers show different absorption spectra each other and the spectra also are different from that of $(M_2@C_{80}(I_h))^-$ (M=Y, Ce, etc.) respectively. The assignments of the peaks of ESR spectrum of two $(Sc_2C_{80})^-$ isomers are now in progress.

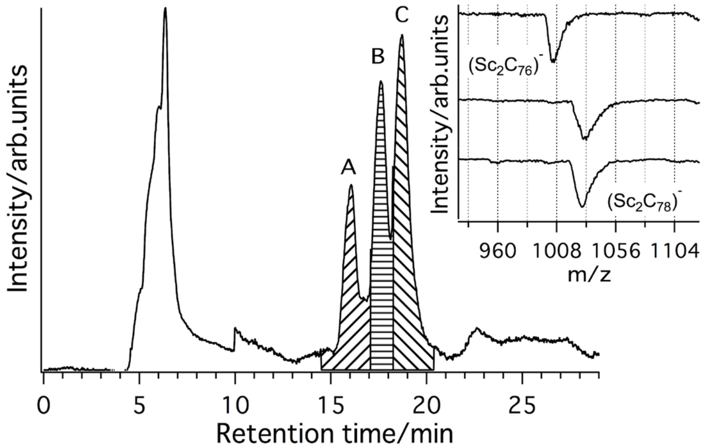

Fig. 1 HPLC chromatogram for the isolation of $(Sc_2C_{76})^-$ and $(Sc_2C_{78})^-$. (Inset: LD-TOF-MS spectra of them.)

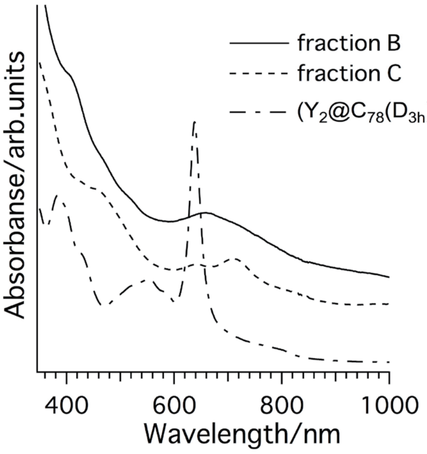

Fig. 2 UV-vis-NIR absorption spectra of fraction B, C, and $(Y_2@C_{78}(D_{3h}))^-$ [2].

[1] S. Yoshida, *et al. The 54th Fullerenes-Nanotubes-Graphene General Symposium* 123 (2018).
[2] N. Nakatori, *et al. The 50th Fullerenes-Nanotubes-Graphene General Symposium* 44 (2016).

Corresponding Author: Takeshi Kodama
Tel: +81-42-677-2530, Fax: +81-42-677-2525
E-mail: kodama-takeshi@tmu.ac.jp

3P-15

Isolation and Characterization of $Dy_2@C_n$ (n=78, 80) Anion

○Ryoya Takai, Koichi Kikuchi, Yohji Achiba, Takeshi Kodama

Department of Chemistry, Tokyo Metropolitan University, Tokyo 192-0397, Japan

The Dy(III) ion has long been interested as a magnetic center for single molecular magnets (SMM) because it has the large magnetic moment and anisotropy. To date, even in the research field on metallofullerenes, Dy-metallofullerenes were studied as a candidate for SMM. For example, Liu et al. reported the SMM behavior for the derivative of $Dy_2@C_{80}(I_h)$: $Dy_2@C_{80}(I_h)CH_2Ph$[1]. This compound has an endohedral unit [Dy^{3+}- e^--Dy^{3+}] and it leads to the SMM behavior with the high blocking temperature. In this study, we tried to isolate $Dy_2@C_n$ (n=78, 80) as an anion form with no functional group and characterize them by spectroscopic methods.

A soot containing Dy-metallofullerenes was produced and extracted by an almost identical method previously reported[2]. Dy-metallofullerenes were extracted as an anion form and separated by the multistage ion-pair chromatography (IPC). The IPC chromatogram at the first stage is shown in Fig.1. Fraction A and B contain $[Dy_2C_{80}]^-$ and $[Dy_2C_{78}]^-$, respectively. By the successive IPC, $[Dy_2C_{78}]^-$ and $[Dy_2C_{80}]^-$ were isolated and the isolation was confirmed by LD-TOF-MS. As shown in Fig. 2, the UV-vis-NIR absorption spectra of them are almost similar to those of $[Gd_2@C_{78}(D_{3h})]^-$ and $[Gd_2@C_{80}(I_h)]^-$[3], respectively. So, the structures of $[Dy_2C_{78}]^-$ and $[Dy_2C_{80}]^-$ are suggested to be $[Dy_2@C_{78}(D_{3h})]^-$ and $[Dy_2@C_{80}(I_h)]^-$, respectively. Furthermore, the ESR spectra of them were measured at 120 K, but no signal was obtained. More investigations for their magnetic properties are now in progress.

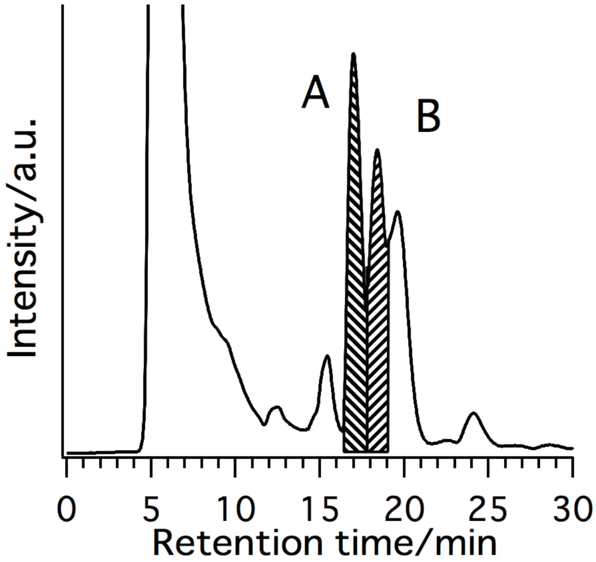

Fig. 1 IPC chromatogram at the first stage.

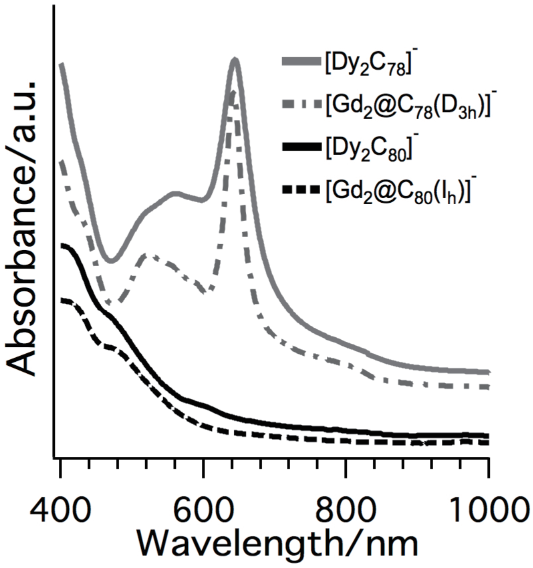

Fig. 2 UV-vis-NIR absorption spectra of $[M_2@C_n]^-$(M=Dy, Gd; n=78, 80).

[1] F. Liu *et al., Nat. Comm.*, **8**, 16098(2017).
[2] N. Nakatori *et al. The 49th Fullerenes-Nanotubes-Graphene General Symposium* 46(2015).
[3] T. Mitani *et al. The 50th Fullerenes-Nanotubes-Graphene General Symposium* 95(2016).

Corresponding Author: Takeshi Kodama.
Tell: +81-42-677-2530, Fax: +81-42-677-2525
E-mail: kodama-takeshi@tmu.ac.jp

3P-16

Influence of Purity on Thermoelectric Properties of Semiconducting SWCNTs Thin Films

○Yota Ichinose, Akari Yoshida, Kengo Fukuhara, Kanna Ikoma, Eda Junko, Hitomi Okubo,
Yohei Yomogida and Kazuhiro Yanagi

Department of Physics, Tokyo Metropolitan University, Tokyo 192- 0397, Japan

One-dimensional materials have potential to exhibit extremely efficient thermoelectric performance [1]. One of suggested approaches to achieve the highest thermoelectric performance is to tune the Fermi level of the 1D materials with sharp van Hove singularity (vHS). Single-walled carbon nanotubes (SWCNTs) are a model for 1D system with sharp vHS, and thus we can investigate how the location of Fermi level influences their thermoelectric properties. Previously, we have investigated the thermoelectric properties of SWCNTs as a function of Fermi-level using an electrolyte gating technique [2][3]. And then we demonstrated the large Seebeck coefficient using high-purity (6,5) SWCNTs, which was obtained by our separating technique [4]. However, influences of Metallic SWNCTs to thermoelectric properties have not been revealed experimentally. Therefore, in this study, we prepared high-purity (6,5) and (6,5) mixed with Metallic SWCNTs to investigate how the presence of metallic SWCNTs influences the thermoelectric properties.

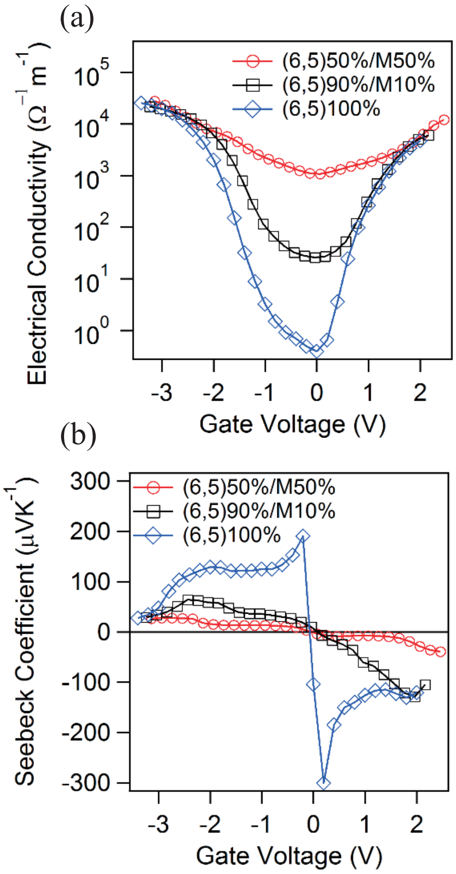

Fig. 1 Purity dependence and Fermi level dependence of thermoelectric properties. M in legends means Metallic SWNCTs. (a) Electrical conductivity. (b) Seebeck coefficient.

The high-purity (6,5) solution and Metallic SWCNTs solution, which was prepared by density-gradient sorting, were systematically mixed with the ratio of 100:0 (high-purity), 90:10 and 50:50 (alloyed), respectively. Fig. 1(a) shows the electrical conductivity of three types of purity films. The most high-purity (6,5) had the ON/OFF ratio of $\sim 10^5$, however, in the other films, the ratio was significantly decreased because of the presence of metallic SWCNTs. Fig. 1(b) shows the Seebeck coefficient of Fermi level dependence. The Fermi level dependence of high-purity and alloyed (6,5) films were remarkably different, especially around charge-neutral point. We experimentally demonstrate that preparation of high-purity of SWCNTs is crucial for understanding of the intrinsic properties and maximization of their thermoelectric properties.

[1] Hicks & Dresselhaus, PRB **47**, 16631 (1993) [2] K. Yanagi et al. Nano letters, **14** (11), 6437 (2014).
[3] Y. Oshima et al. Appl. Phys. Lett. **107**, 043106 (2015)
[4] Y. Ichinose et al. J. Phys. Chem. C, **121** (24), 13391 (2017)

Corresponding Author: K. Yanagi
Tel: +81-42-677-2494, Fax: +81-42-677-2483, Web: http://www.comp.tmu.ac.jp/nano2/index.html
E-mail: Yanagi-kazuhiro@tmu.ac.jp

3P-17

Passivation with Parylene-C in Carbon Nanotube Thin-film Transistors

○Yuto Shimasaki[1], Jun Hirotani[1], Shigeru Kishimoto[1], and Yutaka Ohno[1,2]

[1]*Department of Electronics, Nagoya University, Nagoya 464-8603, Japan*
[2]*Institute of Material and Systems for Sustainability, Nagoya University, Nagoya 464-8603, Japan*

Carbon nanotube thin-film transistors (CNT TFTs) are promising active device for flexible electronics because of their excellent electrical performance and mechanical flexibility. [1, 2] One of the key issues to be addressed is the reliability of the device, in particular, CNT TFTs still have electrical instability such as hysteresis [3, 4], drain current drift, and so on. In this work, we have investigated the surface passivation of CNT TFTs with Parylene-C.

Parylene-C is a hydrophobic polymer with rather low permeabilities for H_2O and O_2, and able to be deposited at low temperature on a plastic film. The back-gate CNT TFTs were fabricated on a Si substrate with a thermally-grown SiO_2 (100 nm) layer. Parylene-C passivation layer of a thickness of 1 μm was deposited by chemical vapor deposition at room temperature. Then, the device was baked at 180 to 300°C in the air to remove adsorbing oxygen and water. We evaluated the width of hysteresis, measuring the transfer (I_D-V_{GS}) characteristics by sweeping V_{GS} in forward and reverse directions for various sweep width (ΔV_{GS}). Figure 1 shows the width of hysteresis as a function of ΔV_{GS} before and after passivation, and after baking. The hysteresis width was reduced by the passivation and baking, especially, the hysteresis was effectively suppressed at $\Delta V_{GS} < 8$ V by baking at 250°C. Interestingly, the hysteresis width increased drastically at ΔV_{GS} above 10 V in the device baked at 250°C, suggesting there is a cause of hysteresis other than adsorbing oxygen and water.

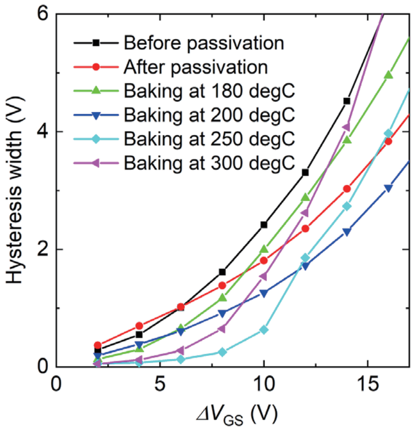

Fig. 1 Hysteresis width as a function of ΔV_{GS}.

Acknowledgments: The semiconducting CNTs were provided by TASC. This work was partially supported by Grant-in-Aid by MEXT, JST/SICORP, and JST/CREST.

[1] Q. Cao, et al., *Nature* **454**, 495 (2008).

[2] D. M. Sun, et al., *Nature Nanotechnology* **6**, 156 (2011).

[3] W. Kim, et al., *Nano Lett.* **3**, 193 (2003).

[4] C. M. Aguirre, et al., *Adv. Mater.* **21**, 3087 (2009).

Corresponding Author: Y. Ohno, Phone & Fax: +81-52-789-5387, E-mail: yohno@nagoya-u.jp

3P-18

Numerical Simulation on Thermoelectric Power of Carbon Nanotubes Modified by Diazonium Salts

○Nayu Araki[1], Takahiro Yamamoto[1,2]

[1] Department of Electrical Engineering, Tokyo University of Science, Tokyo 125-8585, Japan
[2]Division of Nano carbon Research, RIST, Tokyo University of Science, Tokyo 125-8585, Japan

Carbon nanotubes (CNTs) are expected to be potential candidates for flexible thermoelectric materials with high power factor [1]. In contrast to high power factor, the thermoelectric efficiency of a CNT is not so high because of its high thermal conductivity. Recently, several techniques to reduce the thermal conductivity of CNTs have been proposed [2,3]. The diazonium salt modification of CNTs is known as one of such techniques because chemical modification of diazonium salts introduces the sp^3 hybridizations, which play a role of phonon scatterers, to the sp^2-hybridized hexagonal network in a CNT. However, the details of influence the diazonium salt modification on thermoelectric properties of CNTs have not clarified yet.

In this work, we theoretically investigate thermoelectric properties of CNTs modified by diazonium salts using the NEGF+DFT method [5]. We clarify the dependence of the coverage of diazonium salts on the electrical conductivity, the Seebeck coefficient and the power factor.

As the modification density increases, the sp^3 hybridizations acts as scatterers of electrons, so the electrical conductivity decreases greatly. On the oter hand the Seebeck coefficient increases due to a charge transfer from the diazonium salts to the CNT. The power factor decreases due to the rapid reduction of electrical conductivity, but ZT is known to be increased by the diazonium-salt modification because of the rapid reduction of thermal conductivity [4]. In addition, we clarify the optimal carrier density of CNTs for a fixed coverage of diazonium salts.

[1] Y. Nakai, et al, Appl. Phys. Express **7**, 025103 (2014).
[2] T. Yamamoto, K. Sasaoka and S. Watanabe, Phys. Rev. Lett. **106**, 215503 (2011).
[3] M. Ohnishi, T. Shiga and J. Shiomi, Phys. Rev. B **95**, 155405 (2017).
[4] T. Fujigaya, *et al.*, The 78th JSAP Autumn Meeting 2017 (7a-C22-9).
[5] http://www.quantumwise.co.jp/products/atk/

Corresponding Author: T. Yamamoto
Tel: +81-3-5876-1492
Web: http://www.rs.tus.ac.jp/takahiro/
E-mail: takahiro@rs.tus.ac.jp

3P-19

Coarse-grained modeling of free thermal vibrations of singled-walled carbon nanotubes

○Heeyuen Koh[1], Yuta Yoshimoto[2], Junichiro Shiomi[2], Chiashi Shohei[2], Shigeo Maruyama[2,3]

[1] Center for Computational Science, KIST, Seoul 136-791, Republic of Korea
[2]Department of Mechanical Engineering, The University of Tokyo, 7-3-1 Hongo, Bunkyo-ku, Tokyo 113-8656, Japan
[3]Energy NanoEngineering Laboratory, National Institute of Advanced Industrial Science and Technology (AIST), 1-2-1 Namiki, Tsukuba, 305-8564, Japan

The motion of molecules is highly stochastic but yet there are possible analytical models and simulation methods that we can explore with different schemes. Single walled carbon nanotubes (SWNTs), which are researched in various fields of science, have well been described using continuum mechanics frame-works thanks to its simple and intuitively the similar shape to a cylinder. However, we need extra understanding for the modeling of the dynamics of SWNT into the coarse-grained molecular dynamics (CGMD) including its thermal motion characteristics.

The most recent progress on the macroscopic motion of SWNT [1] has established the dynamic features for the successful coarse-grained modeling proving that the free thermal vibration of SWNT is not a mere random motion but there is some specific behavior comparable to the analytical solution of the nonlinear bending equation derived from Green Lagrangian strain definition. In this presentation, we report how this thermally induced nonlinear motion which has turned out to be one of the most basic dynamic features of quasi one dimensional molecule, is modeled into a simple beads model in CGMD simulation. The difference of nonlinear continuum modeling and a conventional simple beads system in CGMD will be explained including how such understanding could be embedded in the coarse grained modeling.

More specifically, heat diffusion effect is incorporated into the equation of motion as new damping algorithm, and this consideration allows promising results such as a well synchronized nonlinear motion of CGMD to that of MD simulation in thermal equilibrium without external thermostat. The effect of this finding to enhance the morphological simulation will be briefly discussed.

[1] Koh et al., PRB, 92, 024306. (2015)

Corresponding Author: S. Maruyama
Tel: +81-3-5841-6421, Fax: +81-3-5800-6983,
Web: http://www.photon.t.u-tokyo.ac.jp/~maruyama/
E-mail: maruyama@photon.t.u-tokyo.ac.jp

3P-20

Growth Mechanism of (6,5) Carbon Nanotube on the Basis of Vibronic Coupling Density Analysis

○ Tomohiro Nishikawa[1,2], Tohru Sato[1,2,3], Naoki Haruta[2], Takeshi Kodama[4], Yohji Achiba[4]

[1] *Fukui Institute for Fundamental Chemistry, Kyoto University,*
[2] *Department of Molecular Engineering, Graduate School of Engineering,Kyoto University,*
[3] *Unit of Elements Strategy Initiative for Catalysts & Batteries, Kyoto University,*
[4] *Department of Chemistry, Graduate School of Science, Tokyo Metropolitan University,*

For the growth mechanism of single-walled carbon nanotubes by the laser ablation method, C_2 addition to the precursor cap structure on the transition metal catalyst has been proposed[1]. However, the reactivity of the capped nanotubes has not been theoretically discussed in detail. Sato *et al.* have reported that Vibronic Coupling Density (VCD) analysis is effective as a reactivity index for reactions, for examples, cycloaddition to fullerenes or nanographenes, which are difficult to be predicted based on the conventional frontier orbital theory[2,3,4]. In this work, we take all the possible edge structures of (6,5) tube into consideration, and investigate their regioselectivities of cycloaddition of C_2 to the edges based on the VCD analysis as well as frontier orbital theory in order to discuss the growth mechanism of (6,5) tube.

The extended Hückel and DFT calculations were performed for the $C_{109}H_{11}$ isomers which are the capped (6,5) tube with all the possible edge structures. The transition metal catalyst should give rise to charge transfer to the nanotubes. Thus, we consider anionic states of the $C_{109}H_{11}$ isomers. We regarded the length of the $C_{109}H_{11}$ isomers enough to discuss the frontier orbital patterns of the edges without influence of the cap. A C_2 adduct to a $C_{109}H_{11}$ isomer has a certain edge structure which we can find among the $C_{109}H_{11}$ isomers. Therefore, we can discuss the regioselectivities of the edges by using the $C_{109}H_{11}$ isomers. We found that there exist recurrent reaction paths in the case that the capped tube is an acceptor. However, if we assume the capped tube is a donor, it cannot grow up.

Following the obtained reaction paths, we sequentially added a C_2 unit starting from $C_{109}H_{11}$ to $C_{129}H_{11}$, and performed VCD analyses. All the analyses indicate reactive regions for C_2 cycloadditions. This means that we succeeded in finding one-layer growth paths of the capped (6,5) carbon nanotube.

[1] Y.Achiba , *Mol. Sci.* **6**, A0055 (2012). [2] T. Sato *et al.*, *J. Phys. Chem. A* **112**, 758 (2008). [3] T. Sato *et al.*, *Chem. Phys. Lett.* **531**, 257 (2012). [4] N. Haruta *et al.*, *Tetrahedron Lett.* **56**, 590 (2015).

Corresponding Author: Tohru Sato
Fukui Institute for Fundamental Chemistry, Kyoto University,
Nishihiraki-cho 34-4, Sakyo-ku, Kyoto 606-8103, Japan
Tel: +81-75-711-7849
E-mail: tsato@scl.kyoto-u.ac.jp

3P-21

Synthesis and characterization of one-dimensional heterostructures

○Yongjia Zheng[1], Yang Qian[1], Ming Liu[1], Akihito Kumamoto[1], Yuichi Ikuhara[1], Anton Anisimov[2],
Esko I. Kauppinen[3], Shohei Chiashi[1], Taiki Inoue[1], Rong Xiang[1], Shigeo Maruyama[1,4]

[1] *Departure of Mechanical Engineering, The University of Tokyo, Tokyo 113-8656, Japan*
[2] *Canatu Ltd., Konalankuja 5, FI-00390 Helsinki, Finland*
[3] *Department of Applied Physics, Aalto University, Otakaari 1, 02150 Espoo, FI-20742, Finland*
[4] *Energy NanoEngineering Lab., National Institute of Advanced Industrial Science and Technology (AIST), Tsukuba. 305-8564, Japan*

In recent years researchers have focused on two-dimensional van der Waals (vdW) heterostructures, which have generated great interests recently due to the possibility of combining diverse atomic layers to create novel materials and devices [1-2]. In this work, we demonstrate a new one-dimensional structure with similar heterostructure interfaces that combines the single-walled carbon nanotubes (SWCNTs), boron nitride nanotubes (BNNTs) and Molybdenum Disulfide nanotubes (MSNTs) in the radial direction [3]. BNNTs and then MoS_2 nanotubes were successfully grown on the surface of SWCNTs by a facile chemical vapor deposition (CVD) technique. Absorption spectra, Raman spectra and optical images confirmed the existence of boron nitride (BN) and MoS_2 (Fig. 1a, b and c). Fig. d and e clearly show a ternary nanotube that consists of SWCNT/BNNTs/MSNT in a coaxial structure. This structure may be used for field effect transistor, photovoltaics and light-emitting devices.

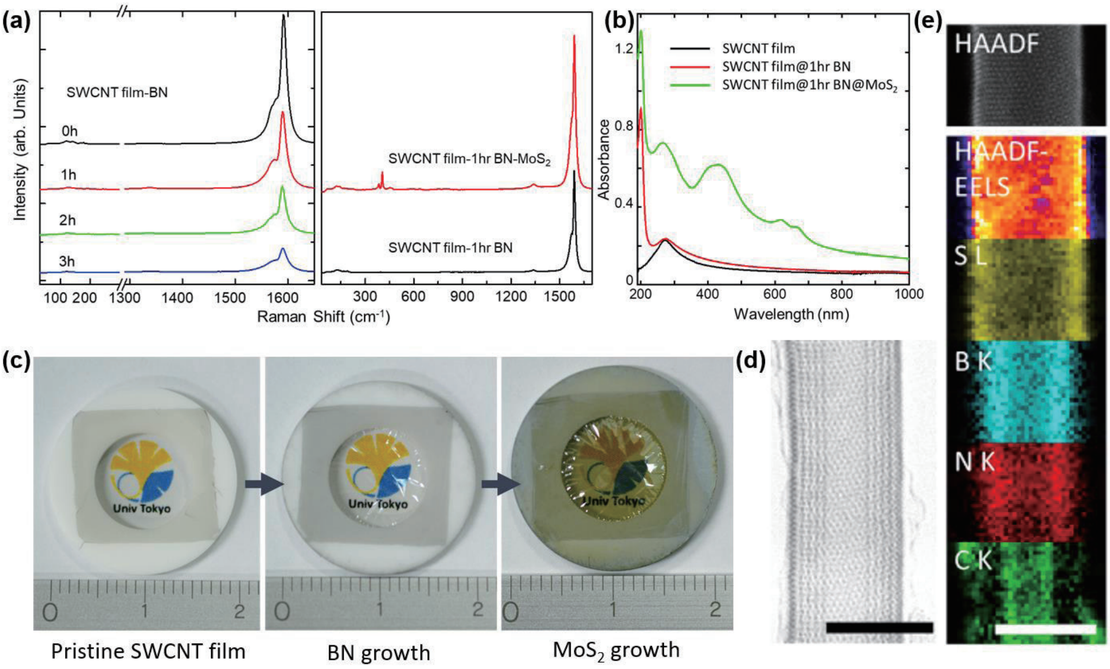

Pristine SWCNT film BN growth MoS_2 growth

Fig. 1: (a) Left plot is Raman spectra of SWCNTs/BNNTs with different BN growing time; Right plot is Raman spectra of SWCNTs/BNNTs before and after MoS_2 growth. (b) Absorbance of SWCNTs before and after BN and MoS_2 growth. (c) Optical images show how a SWCNTs film changes after BN and MoS_2 growth. (d) TEM image and (e) EELS mapping of a 5 nm diameter ternary nanotubes consisting one layer of carbon, three layers of BN and one layer MSNT. Scale bar, 5 nm.

[1] D. Jariwala *et al., Nature materials,* **16,** 170 (2017).
[2] Z. Liu *et al., Nature Nanotechnology,* **8,** 119 (2013).
[3] R. Xiang *et al.,* arXiv:1807.06154

Corresponding Author: S. Maruyama
Tel: +81-3-5841-6421,
Fax: +81-3-5841-6983,
E-mail: maruyama@photon.t.u-tokyo.ac.jp

3P-22

Growth of vertically-aligned single-walled carbon nanotubes having small diameters using Ir catalysts in alcohol gas source method

○Takuya Okada[1], Kamal P Sharma[1,2], Tomoko Suzuki[2], Takahiro Saida[1,2], Shigeya Naritsuka[3]
Takahiro Maruyama[1,2]

[1]*Department of Applied Chemistry, Meijo University, Japan*

[2] *Nanomaterials Research Center, Meijo University, Japan*

[3]*Department of Materials Science and Engineering, Meijo University, Japan*

1. Introduction

Single-walled carbon nanotubes (SWCNTs) have been anticipated for application in a lot of future nanodevices. To fabricate SWCNT devices in conventional LSI process, it is important to grow high-density semiconducting SWCNTs under high vacuum. So far, we succeeded in growth of small-diameter SWCNTs with narrow diameter distribution using Pt catalysts [1]. However, the SWCNT yield was not so high. In this study, we carried out SWCNT growth using Ir catalysts by alcohol catalytic chemical vapor deposition (ACCVD) method to increase the yield of small-diameter SWCNTs.

2. Experimental procedure

Using Ir catalysts, SWCNTs were grown on SiO_2/Si substrates by ACCVD in an ultra-high vacuum (UHV) chamber, a type of cold-wall CVD equipment. The growth temperature was 800°C and growth time was set between 10 and 180 min. The grown SWCNTs were characterized by FE-SEM and Raman spectroscopy.

3. Results and Discussion

Irrespective of the growth time, both G band and radial breathing mode (RBM) peaks were observed, indicating that SWCNTs were grown from Ir catalysts. Fig. 1 shows Raman spectra of SWCNTs grown under ethanol pressure of 1×10^{-1} Pa, when the growth time was 180 min. Taking into account "Kataura plot", the SWCNT diameters were considered to be distributed between 0.83 and 1.1 nm. Fig. 2 shows an SEM image of the sample in Fig. 1. High-density vertically-aligned SWCNTs were observed, whose lengths were about 2 μm. We will also discuss the electronic type of grown SWCNTs.

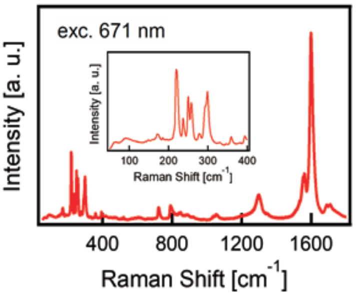

Fig.1 Raman spectra

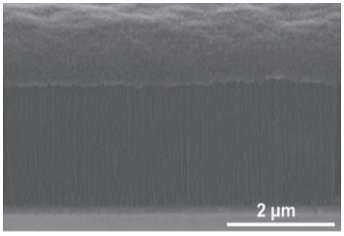

Fig.2 SEM image

This work was supported in part by Private University Research Branding Project from the Ministry of Education, Culture, Sports, Science and Technology (MEXT), Japan. Part of this work was conducted at the Institute for Molecular Science (IMS), supported by the "Nanotechnology Platform" of the Ministry of Education, Culture, Sports, Science and Technology (MEXT), Japan.

[1] T. Maruyama et al. Mater. Express 1 (2011) 267.

Corresponding Author: T. Maruyama
Phone: +81-52-838-2386, Fax: +81-52-832-1172
E-mail: takamaru@meijo-u.ac.jp

3P-23

Relationship between Catalysts and Diameter of Single-Walled Carbon Nanotubes

○Akio Nakano[1]

[1] *Yokohama Science Frontier High School (YSFH), Tsurumi-ku, Yokohama 230-0046, Japan*

Single-walled carbon nanotubes (SWCNTs) are expected to be applied to various industrial fields. The SWCNTs can be produced by arc discharge using carbon electrodes containing Ni or Y_2O_3 as a catalyst under low-pressure helium circumstance. In this study, the effect of molar ratio of Ni : Y_2O_3 (Table 1) contained in a carbon cathode on a diameter of SWCNTs was considered. The diameters (nm) of SWCNTs were calculated with the wavenumbers of Radial Breathing Mode (RBM, peaks at 160-240cm^{-1}) on Raman spectra, by formula [1] as below,

$Dt = 248 / \omega$ (Dt: diameter of tubes, ω :wavenumbers of RBM)

Table 1. The ratio of catalysts.

	ratio I	ratio II	ratio III
Molar ratio (Ni : Y_2O_3)	2:1	1:1	1:2
Ni (g / 2.00g Carbon)	0.0587	0.0294	0.0294
Y_2O_3 (g / 2.00g Carbon)	0.1129	0.1129	0.2258

Peaks of RBM at around 165cm^{-1} were mainly observed with small peaks on the larger side of wavenumbers. These peaks appeared at five positions on the Raman spectra, which were calculated in approximately 1.50, 1.45, 1.36, 1.32 and 1.09nm, as given on Table 2. With ratio I, only a single RBM peak was appeared, and Dt was in the largest region, 1.50nm. The double peaks were obtained with ratio II or III. The triple peaks were observed only with ratio III.

Table 2. Diameter (nm) of SWCNTs produced under ratio I-III of catalysts

Dt 1.50nm		Dt 1.45nm		Dt 1.36nm		Dt 1.32nm		Dt 1.09nm	
I(s)	1.486								
II(s)	1.519								
II(d)	1.502			II(d)	1.362				
III(s)	1.501	III(s)	1.445						
		III(d)	1.467			III(d)	1.323		
		III(t)	1.448			III(t)	1.317	III(t)	1.090

(s):RBM with single peak (d):with double peaks (t):with triple peaks

Double or triple peaks of RBM indicate the formations of SWCNTs with small diameters. The decrease in the diameter of the SWCNTs is related to the increase in the ratio of Y_2O_3. As a result, it is obvious that the diameter of the SWCNTs is related to the ratio of the catalysts of Ni : Y_2O_3.

[1] R.Saito, *et al.*, Phys.Rev.B, **61**, 2981 (2000).

Corresponding Author: A. Nakano
Tel: +81-45-511-3654, Fax: +81-45-511-3644 (YSFH)

3P-24

In situ synchrotron X-ray diffraction study of precipitation of multilayer graphene from Ni catalyst

○Jumpei Yamada[1], Yuki Ueda[1], Shun Takenaka[1], Takahiro Maruyama[2], and Shigeya Naritsuka[1]

[1]*Department of Materials Science and Engineering, Meijo University,*
Nagoya 468-8502, Japan
[2]*Department of Applied Chemistry, Meijo University, Nagoya 468-8502, Japan*

Because of the superior characteristics of graphene, it is highly supposed to apply in various fields, such as electrical wiring in integrated circuits, transparent electrodes of light emitting diodes. The precipitation method is able to grow multilayer graphene simply by annealing the sample. In the method, a carbon sauce and catalytic metal are deposited on a requested substrate. In order to obtain high-quality multilayer graphene, it is necessary to fully understand the behavior of carbon atoms during the process. In situ X-ray diffraction (XRD) measurement is one of excellent methods to detect the state of crystals. Therefore, in this study, BL11XU of SPring-8 was used to in situ monitor the precipitation of graphene using XRD measurement.

Amorphous carbon (a-C) (5 nm) and Ni (300 nm) layers were deposited on a sapphire (0001) substrate using electron-beam deposition. The sample was loaded in an ultra-vacuum chamber and annealed in BL11XU of Spring-8. The sample was firstly pre-annealed at 300 ºC, and the temperature was increased to 890 ºC at a rate of 100 ºC/min. After the annealing period of 30min, the temperature was cooled to 300 ºC at a rate of 100 ºC/min. During the thermal process, the sample was in situ monitored using XRD.

Figure 1 (a) shows an optical microscope image and Raman spectrum of a precipitated graphene sample. The observation of G and G' peaks with G'/G ratio of 0.32 indicates that multilayer graphene was successfully precipitated on the sample. Fig.1 (b) shows the intensity change of graphene (10) diffraction peak through the annealing. In the heating period, the intensity increased, and it continuously decreased during the annealing period. This possibly corresponds to the diffusion of carbon atoms from the a-C layer to the Ni catalyst. On the other hand, the peak intensity increased again during the cooling period. This can be ascribed to the precipitation of graphene. The in situ XRD is quite useful to directly observe the growth of graphene, and its behavior is clearly characterized by the analysis of the experimental data.

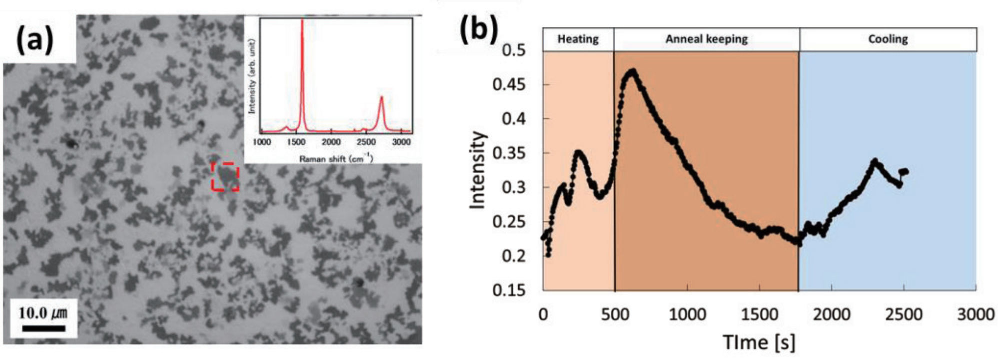

Fig. 1 (a) Optical microscope image and Raman spectrum of sample, and (b) intensity change of graphene (10) diffraction peak during annealing.

Acknowledgement: This work was supported in part by JSPS KAKENHI Grant Numbers 2660089, 15H03558, 26105002, 25000011. The author was indebted to several members of National Institutes for Quantum and Radiological Science and Technology (QST): Drs. M. Takahashi, T. Sasaki and S. Fujikawa for in situ XRD measurement.

Corresponding Author: J.Yamada, E-mail: jjjjjyyyyyy119@gmail.com

3P-25

Mechanism of on/off improvement of graphene nanoribbon transistors synthesized by advanced plasma CVD

○Noritada Ogura[1], Hiroo Suzuki[1], Toshiro Kaneko[1], and Toshiaki Kato[1,2]

[1] Department of Electronic Engineering, Tohoku University, Sendai 980-8579, Japan
[2] JST-PRESTO

In recent years, graphene nanoribbon (GNR), strips of two-dimensional (2D) graphene into one-dimensional (1D) structure gathers intense attentions because of their superior electrical features. Although GNR can be made in a variety of ways, the reliable site and alignment control of GNR with high on/off current ratios remains a challenge.

Our research group synthesized suspended GNRs by an advanced plasma CVD process combining with unique nanobar structures as a catalyst [1-3]. In our method, GNRs could be nucleated on the surface of the liquid phase Ni nanobar. The droplets of Ni move to electrode direction due to the capillary force, resulting in the formation of suspended GNR structures (Fig. 1(a)).

In our original method, the on/off current ratio of GNR transistor synthesized from Ni nanobar was low (~5). Recently, it is found that the on/off can be drastically improved by changing the materials of nanobars from Ni to Ge. However, the critical reason for this on/off improvement is not clear.

In this study, we carefully analyzed the structure of GNR grown from Ge nanobar by atomic force microscopy (AFM) and try to identify the origin of on/off improvement. Based on the systematic comparison between AFM data and electrical transport properties, it is found that the very narrow (< 10 nm) and thin (< 5 nm) GNR structures are locally formed in the GNR with higher on/off (Fig. 1(b)), denoting such local structures can effectively conduct the current switching through GNR. Since our unique plasma process possesses significant advantage for the integrated synthesis of GNR, this high on/off GNR grown from Ge nanobar can contribute to realizing high-performance logic circuit with integrated GNRs.

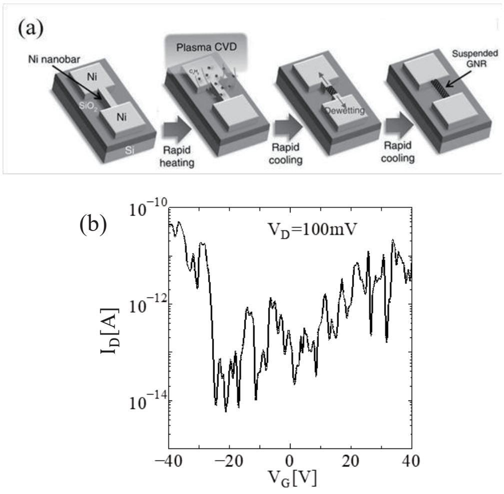

Fig. 1 (a) Schematic illustration of GNR growth with plasma CVD from nanobar catalyst. (b) Typical drain-source current (I_D) - gate bias voltage (V_G) curves of GNR devices fabricated with Ge nanobars under the adjusted plasma conditions.

[1] T. Kato and R. Hatakeyama: Nature Nanotechnology **7** (2012) 651.
[2] H. Suzuki, T. Kaneko, Y. Shibuta, M. Ohno, Y. Maekawa and T. Kato: Nature Communications **7** (2016) 11797.
[3] H. Suzuki, N. Ogura, T. Kaneko, T. Kato: Scientific Reports (2018) *in press*.

Corresponding Author: N. Ogura
Tel: +81-22-795-7046, E-mail: noritada.ogura.p6@dc.tohoku.ac.jp

3P-26

Hydrogen adsorption on atomic vacancies in Epitaxial graphene toward Hydrogen storage

○Y. Obata[1], K. Kusakabe[2], G. Sunnardianto[2] T. Enoki[3], I. Maruyama[4], T. Nishimura[5], K. Takai[1, 5]

[1] Dept. Applied Chemistry, Hosei University, Tokyo 184-8584, Japan, [2]Dept. Materials Engineering Science, Osaka University, Osaka 560-8531, Japan, [3]Tokyo Institute of Technology, Tokyo 152-8550, Japan,[4]Dept. of Information and Systems Engineering, Fukuoka Institute of Technology, Fukuoka 811-0295, Japan, [5]Research Center of Ion Beam Technology, Hosei University, Tokyo 184-0002, Japan

Defects introduction is one of the important strategy to tune graphene properties. Especially, it is known that an ion beam irradiation can introduce atomic vacancies in graphene [1]. In the previous study, we demonstrated that the chemical structure of defects in graphite surface and epitaxial graphene can be tuned by the subsequent adsorption of hydrogen and oxygen molecules after defect formation [2]. For hydrogenated atomic vacancies, the theoretical calculation shows a low energy barrier and little adsorption heat for the additional adsorption of hydrogen molecules [3], suggesting an efficient hydrogen storage and release in this system [4]. In this study, hydrogenated atomic vacancies are introduced into epitaxial graphene and the amount of hydrogen and carrier scattering related to vacancies are evaluated.

Atomic vacancies were introduced into the surface of epitaxial graphene grown on SiC by Ar ion beam sputtering at 100 eV after pre-annealing, followed by exposing to hydrogen molecules. Raman spectroscopy and Elastic recoil detection analysis (ERDA) were measured by LabRAM HR Evolution (532 nm) and Van der Graaff accelerator AN2500, respectively.

ERDA profile reveals epitaxial graphene consists of three layers; contamination layer composed of hydrocarbons, defects layer terminated with hydrogen, and bulk SiC. After the ion beam irradiation and hydrogen adsorption, the increment of hydrogen is comparable to the upper limit for the number of vacancies. The smaller Raman D-band for hydrogenated vacancies than that for oxygen terminated vacancies suggests the inter valley scattering depends on the chemical structure of defects in graphene.

[1] Hahn and Kang, *Phys. Rev. B*. **60**, 6007 (1996). [2] Obata, et al., *FNTG 54* (2018). [3] G. Sunnardianto,et al, *Int. J. Hydrogen Energy,* **43** (2017). [4]K. Kusakabe, G. Sunnardianto, T. Enoki, I. Maruyama, K. Takai, Patent No. PCT/JP2017/31325

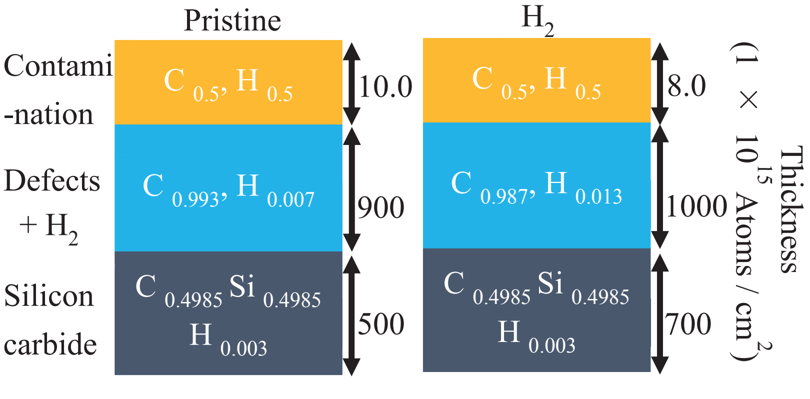

Fig.1 ERDA analysis

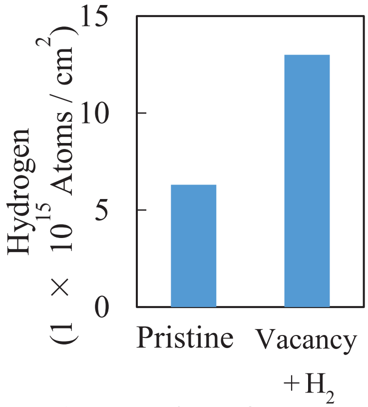

Fig.2 Hydrogen Amount in defects layer

3P-27

Plasmon Resonance-Induced Electronic Transition in Graphene

ZHANG Jinjiang[1]; ZHOU Ruifeng[1, 2], MINAMIMOTO Hiro[2]; ○MURAKOSHI Kei[2]

[1]*Department of Chemistry, Faculty of Science, Hokkaido University, Hokkaido 060-0810, Japan*
[2]*Institute for International Collaboration, Hokkaido University, Japan*

The fascinating electrical and optical properties of graphene render it wide application in photoelectronic devices. Its optical response and electronic interaction with substrate has been well investigated with Raman spectroscopy [1]. In the surface-enhanced Raman spectroscopy (SERS), band intensities are enhanced and new features may emerge due to the localized surface plasmon resonance (LSPR) of metal nanoparticles. In this work, the SERS spectra of monolayer graphene were investigated under electrochemical potential control. The influences of LSPR on the electronic excitation process in graphene were discussed.

Graphene was synthesized on Cu foil via chemical vapor deposition method and was transferred onto ITO glass (Gr/ITO glass) with poly(methyl methacrylate). The as-transferred graphene number of layer was confirmed to be single-layer and defect-free via the Raman spectroscopy. Au nano-dimers were fabricated onto Gr/ITO glass (Au/Gr/ITO glass) via angle-resolved nano-sphere lithography method [2]. The electrochemical Raman spectroscopy was carried out with a three-electrode system and 785 nm laser was used to excite the LSPR (Figure).

Around 1600 cm^{-1}, three sub-bands were observed in SERS of the single-layer defect-free graphene, in contrast to the single G band in the normal Raman spectrum. Electrochemical SERS showed that energy of one of the sub-bands shifts with potentials in a manner very similar to the G band, while the other two sub-bands were not sensitive to potential change. Thus, the three sub-bands can be assigned to the G band and two non-zero wavevector phonon modes, D7 and D'. The visualization of the non-zero wavevector phonon modes in a defect-free graphene is ascribed to the plasmon-induced non-vertical electronic excitation. Furthermore, the SERS spectra differ from the normal Raman spectra of graphene at both low and high doping levels. At low doping level, the G phonon renormalization was suppressed; at high doping level, the quantum interference was smeared out. These findings demonstrate the modification of photoexcitation by LSPR. The new photoexcitation pathways not only change the optical response of graphene, but also alter the electrochemical potentials of hot electrons and holes.

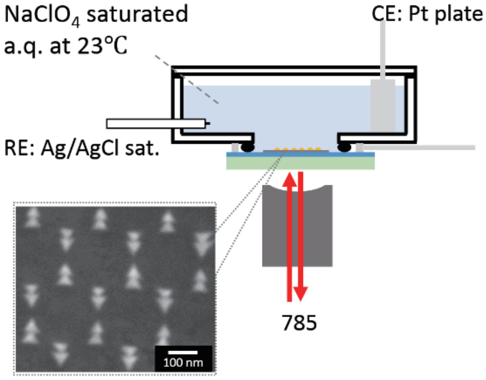

Figure. Electrochemical Raman spectroscopy and SEM image of Au-covered graphene.

[1] R. Zhou *et al.* ACS Omega, **3**, 2322 (2018).
[2] S. Yasuda *et al.* ACS Appl. Mater. Interfaces, **9**, 38992 (2017).

Corresponding Author: MURAKOSHI Kei
Tel: +81-(0)11-706-2704, Fax: +81-(0)11-706-4810,
Web: http://wwwchem.sci.hokudai.ac.jp/pc/
E-mail: kei@sci.hokudai.ac.jp

3P-28

Band gap modulation by chiral phonon oscillations in transition metal dichalcogenides

○ Ahmad R.T. Nugraha, Nguyen T. Hung, Riichiro Saito
Department of Physics, Tohoku University, Sendai 980-8578, Japan

A recent experiment has demonstrated that clockwise and anticlockwise rotations of atoms in transition metal dichalcogenides (TMDs) for a particular phonon mode can be understood as completely different modes with opposite angular momenta [1], known as chiral phonons [2]. The chiral phonons can be observed by applying pump-probe technique with combination of left- and right-handed circularly polarized light between the pump and probe light. By measuring the absorption in the TMDs and taking Fourier transform (FT) of the absorption difference due to left- and right-handed circularly polarized light, several peaks at certain frequencies of a phonon mode emerge in the FT spectra. For example, there is a series of peaks with integer multiple of longitudinal acoustic (LA) mode frequency in the FT spectra of TMDs. However, beyond the interpretation that chiral phonons exist, the reason why there could be higher-order overtone modes for a given chiral phonon remains unclear.

In this work, by using first-principles calculation, we propose that the chiral phonons in the TMDs modify the band gaps of the TMDs within a cycle of rotation in a particular direction. We take an example of LA phonon at K point in $MoSe_2$, in which it is possible to have each atom in the unit cell at three distinct phases (0, $2\pi/3$, and $4\pi/3$) before returning to the initial position of oscillation. We find that the bandgap of $MoSe_2$ is modified by the three phases of LA phonon because the atomic structure of $MoSe_2$ is also altered by the phonon oscillation. Since the absorption is affected by the band gap of the material, we argue that the band gap modulation by chiral phonons is a possible origin of the overtone of chiral phonons.

[1] H. Zhu *et al.*, Science 359, 579–582 (2018).

[2] L. Zhang and Q. Niu, Phys. Rev. Lett. 115, 115502 (2015).

Corresponding Author: A.R.T. Nugraha
Tel: +81-22-795-6442, Fax: +81-22-795-6447
E-mail: nugraha@flex.phys.tohoku.ac.jp

3P-29

Improved interlayer coupling in suspended MoS_2/WS_2 van der Waals heterostructures

○Kana Kojima, Hong En Lim, Takahiko Endo, Yu Kobayashi,
Yutaka Maniwa, Yasumitsu Miyata

Department of Physics, Tokyo Metropolitan University, Hachioji, 192-0397, Japan

The van der Waals (vdW) heterostructures of two-dimensional materials have attracted much attention for their superior electrical and optical properties. The superconductivity illustrated in bilayer graphene and the formation of interlayer excitons in the TMDC-based vdW heterostructures for instance, are promising for optoelectronic applications [1-3]. Recently, large-area vdW heterostructures with clean interface have been successfully prepared on Si substrates using chemical vapor deposition (CVD) method. However, for such CVD-grown heterostructures on SiO_2 surface, the lattice strain caused by the substrate has resulted in a weakened interlayer coupling and PL broadening. Herein, by removing the underlying SiO_2/Si substrate used, we demonstrate an improved interlayer coupling in CVD-grown MoS_2/WS_2 heterostructures.

MoS_2/WS_2 heterostructures grown on SiO_2 surface by CVD were transferred onto a TEM grid to form the suspended structure. This process can suppress tensile strain induced by the supporting substrate, as confirmed by the blue shift in the PL peak of monolayer TMDCs. For the suspended MoS_2/WS_2 heterostructures fabricated, an interlayer exciton peak appears at 1.63 eV, which is not observed on the substrate supported one. This implies an enhanced interlayer coupling in the free-standing sample, highlighting the importance of studying these atomically thin vdW heterostructures without the substrate influence. Our results provide a simple method for understanding the intrinsic physical properties of TMDCs and the development of sophisticated optoelectronic devices.

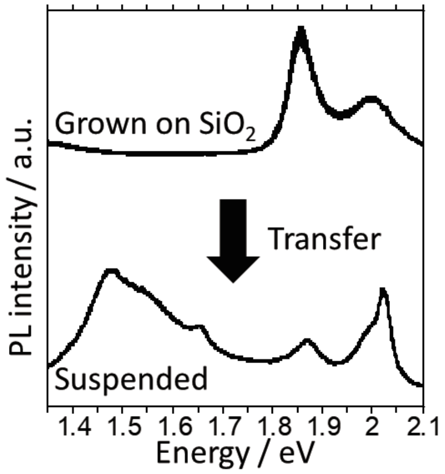

Fig. 1 PL spectra of MoS_2/WS_2 vertical heterostructures grown on SiO_2 and after the transfer on a TEM grid.

[1] Y. Cao *et al.* Nature **556**, 43-50 (2018).
[2] P. Rivera *et al.* Nat. Commun. **6**, 6242 (2015)
[3] L. Britnell *et al.* Science **340**, 6138 (2013)

Corresponding Author: Y. Miyata, Tel: 042-677-2508, E-mail: ymiyata@tmu.ac.jp

3P-30

Electric Double Layer Transistors of CVD-grown monolayer InS and InSe

○Jiang Pu [1], Han-Ching Chang [2], Chien-Liang Tu [2], Kuang-I Lin [3], Chien-Nan Hsiao [4]
Chang-Hsiao Chen [2], and Taishi Takenobu [1]

[1] *Department of Applied Physics, Nagoya Univ., Nagoya 464-8603, Japan*
[2] *Department of Automatic Control Engineering, Feng Chia Univ., Taichung 40724, Taiwan*
[3] *Center for Micro/Nano Sci. and Tech., National Cheng Kung Univ., Tainan 70101, Taiwan*
[4] *Instrument Tech. Research Center, National Applied Research Lab., Hsinchu 30076, Taiwan*

Current progress of group-VI transition metal dichalcogenides has provided attractive platform to explore new functional electronic and optoelectronic device applications [1]. More recently, group-III monochalcogenides, especially for InS and InSe, gain further attentions due to their potential high mobility of 10^3 cm^2/Vs and high on/off ratio of 10^8 at room temperature arising from lighter electron effective mass than that of group-VI [2]. Therefore, group-III monochalcogenides are promising for high-performance transistor applications, however, most of the InS and InSe transistors have been fabricated on exfoliated flakes, which results in uncontrollable sample size/thickness and poor reproducibility of device fabrication/performance. Hence, the chemical vapor deposition (CVD) of high-quality monolayers is necessary, and the evaluation of transistor properties using such CVD-grown samples should be addressed. Here, we establish scalable CVD synthesis of highly crystalline InS and InSe monolayers. Using these samples, we fabricate transistors with both SiO_2-back-gated and electrolyte-gated structures to compare their transport properties, resulting in significant mobility enhancement in the high carrier density of > 10^{13} /cm^2 [3,4].

The InS and InSe monolayers were synthesized on mica substrate through a vapor phase reaction by putting In_2O_3 and S (Se) powders together inside a tube furnace system. Then, the monolayer flakes were transferred onto SiO_2/Si substrate to deposit Au electrodes. Finally, ion gels, a mixture of ionic liquids and polymers, were drop-casted, followed by putting Pt foil on the top of ion gels as a top gate (Fig. 1). Figure 2 shows the transfer curve of ion-gel-gated InSe transistors. We obtained n-type behavior with on/off ratio of 10^5. Interestingly, as shown in the inset of Fig. 2, the comparison between SiO_2 gating and ion-gel gating indicates several orders enhancement of electrical conductivity in ion-gel transistors. This result suggests the trap density which might be originated from defects and/or disorders during CVD process affected transport properties; thus, high carrier density accumulations effectively screened them to improve performance. Based on capacitance measurements, the electron mobility was calculated up to 30 cm^2/Vs in CVD-grown InSe monolayers. We'll also present the transistor characteristics of InS monolayers and discuss their transports on hBN substrates.

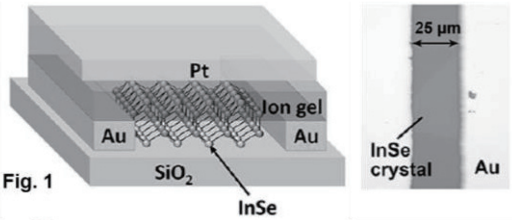

Fig. 1

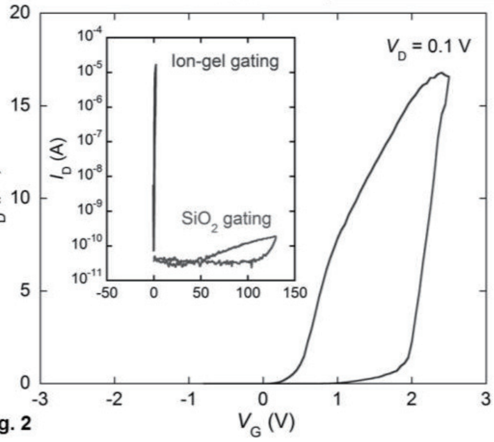

Fig. 2

[1] Q. H. Wang *et al.*, *Nat. Nanotechnol.* **7**, 699 (2012).
[2] D. A. Bandurin *et al., Nat. Nanotechnol.* **12**, 223 (2017).
[3] J. Pu *et al.*, *Adv. Mater.* **28**, 4111 (2016).
[4] H.-C. Chang *et al., Small* under review (2018).

Corresponding Author: J. Pu, T. Takenobu
Tel/Fax: +81-52-789-5165,
E-mail: jiang.pu@ngoya-u.jp, takenobu@nagoya-u.jp

3P-31

Chalcogen substitution in monolayer transition metal dichalcogenides

○Hiroshi Shimizu, Hong En Lim, Takahiko Endo, Yu Kobayashi,
Yutaka Maniwa, Yasumitsu Miyata*

Department of Physics, Tokyo Metropolitan University, Hachioji 192-0397, Japan

In recent years, heterostructures of transition metal dichalcogenide (TMDC) atomic layers have been actively studied for their unique physical properties and potential applications in electronics and opto-electronics. Even though TMDC-based heterostructures are mainly fabricated by transfer and direct growth techniques, a chalcogen substitution approach may also provide a simple way to produce a vast array of heterostructures and superlattices [1]. However, there are only a few works reported so far, and it remains unclear whether the reactivity in chalcogen substitution will be affected by the defect density and the chemical composition of sample used. To clarify this issue, we have investigated the chalcogen substitution in various monolayer semiconducting TMDCs, including MoS_2, $MoSe_2$, WS_2, and WSe_2.

Monolayer TMDCs were grown at 820 ℃ on silicon substrates using salt-assisted CVD method [2]. For the chalcogen substitution, monolayers of $MoSe_2$ (MoS_2) and WSe_2 (WS_2) were annealed under sulfur (selenium) atmosphere. Figure 1 shows the Raman spectra of the $MoSe_2$ and WSe_2 before and after the annealing process. A notable change is observed for the $MoSe_2$ after annealing, where the A'_1 mode at 240 cm^{-1} has diminished, along with the emergence of peaks derived from MoSSe [3] and MoS_2 at the edge and center regions of the grain. Interestingly, the Raman peaks of MoS_2 is recorded mainly at the center region. In contrast, there is no noticeable difference registered for the monolayer WSe_2 under the same annealing condition. These results suggest that the reactivity of TMDCs depends strongly on their composition and defect density, offering a facile way to fabricate the desired heterostructures based on TMDCs.

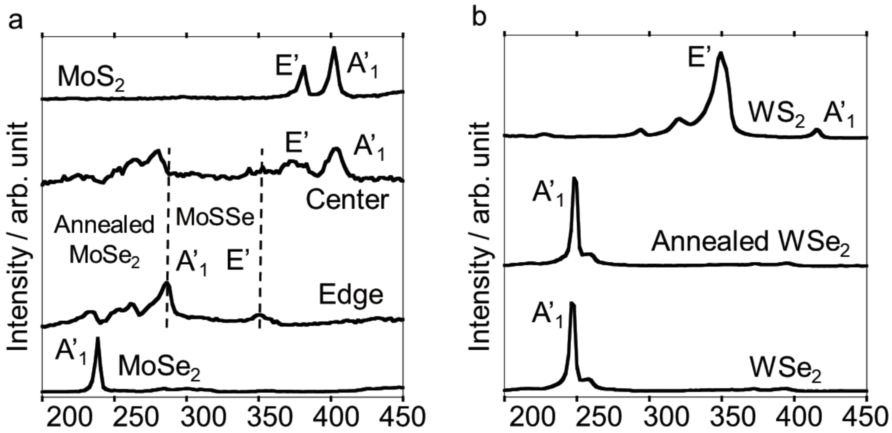

Fig. 1 Raman spectra of (a) monolayer $MoSe_2$ and (b) monolayer WSe_2 before and after the annealing, together with those of monolayer MoS_2 and monolayer WS_2 for comparison.

[1] M. Mahjouri-Samani *et al*., Nat. Commun, **6**, 7749 (2015).
[2] S. Li *et al*., Appl. Mater. Today, **1**, 60 (2015).
[3] J. Zhang *et al*., ACS Nano, **11**, 8 (2017).

Corresponding Author: Yasumitsu Miyata, Tel: 042-677-2508, E-mail: ymiyata@tmu.ac.jp

3P-32

Energetics and electronic structures of MoS_2 nanoribbons

○Hisaki Sawahata[1], Mina Maruyama[1], Susumu Okada[1]

[1] Graduate School of Pure and Applied Sciences, University of Tsukuba, Tsukuba 305-8571, Japan

Atomic layer materials are attracting much attention as emerging materials for the nanoscale low-dimensional devices, such as sensing, optical, optoelectronic, and electronic devices, because of their unique geometric and electronic structures. Following the synthesis of graphene, various atomic layer materials have been synthesized using exfoliation and CVD techniques. Transition metal dichalcogenides (TMDCs) are representative two-dimensional materials with the semiconducting electronic properties which are sensitive to constituent elements. Because of tunable electronic structures by the constituent elements, TMDCs are now considered to be promising materials for functional devices in the next generation. Besides the choice of the constituent elements, by analogy with graphene, TMDCs may exhibit further variation in their electronic properties by controlling their local and global network topologies. Thus, in this work, we aim to investigate the energetics and electronic structures of MoS_2 nanoribbons with respect to their edge shape for proving the theoretical insight into the fundamentals of material and device designs using TMDCs.

All calculations are conducted using the density functional theory combined with the effective screening medium method to exclude the unintentional dipole effect arising from its polar edges. Figure 1 shows optimized structures of MoS_2 nanoribbons with armchair, chiral, and zigzag edges. The substantial structural reconstruction occurs at the armchair edges or around the armchair portion of the chiral edges. In contrast, the reconstruction is absent in the nanoribbon with zigzag edges. Our calculations demonstrate that the MoS_2 nanoribbon with zigzag edges has the lowest total energy among the nanoribbons studied here, even though the ribbon has polar edges.

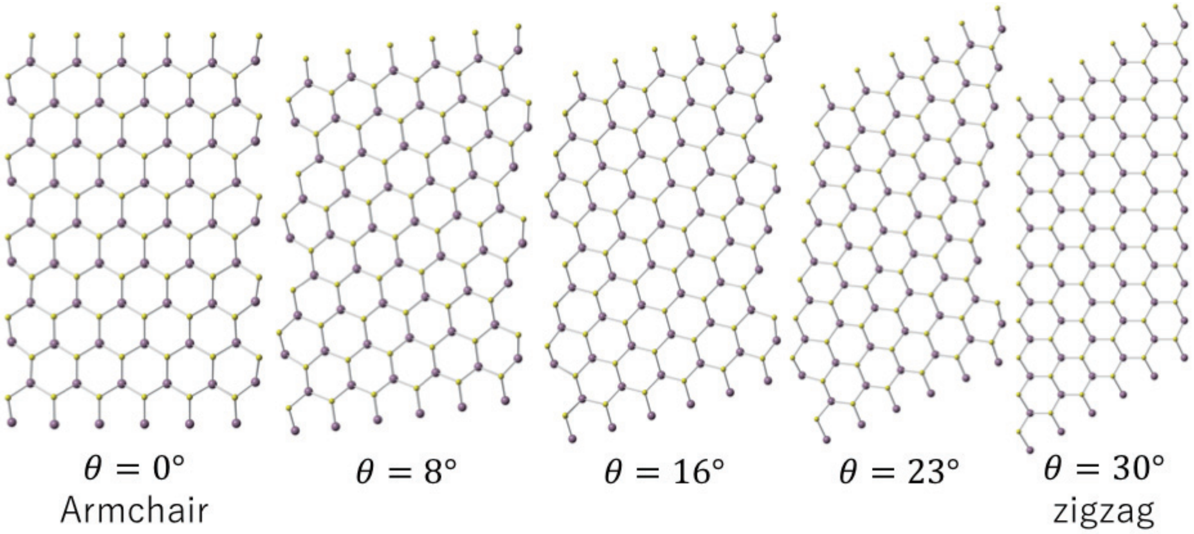

Fig.1 The optimized structures of the MoS_2 nanoribbons.

Corresponding Author: H. Sawahata
Tel: +81-29-8535921
E-mail: hsawahata@comas.tsukuba.ac.j

3P-33

Fabrication and transport properties of PN diodes based on monolayer MoS_2/WSe_2 vertical heterostructures

○Shintaro Yoshimura, Yu Kobayashi, Takahiko Endo, Hong En Lim,
Yutaka Maniwa, Yasumitsu Miyata

Department of Physics, Tokyo Metropolitan University, Hachioji, 192-0397, Japan

Two-dimensional transition metal dichalcogenides (TMDCs) have attracted much attention because of their unique structural and highly-tunable electronic properties. In particular, TMDC-based PN junctions are promising for the application in light emitting devices and tunneling field effect transistors. In previous studies, the PN diodes were generally prepared using exfoliated atomic layers of TMDCs such as p-type WeS_2 and n-type MoS_2 [1, 2]. Meanwhile, as chemical vapor deposition (CVD) provides a useful way to prepare large-area and uniform monolayers of TMDCs, it is therefore important to develop a device fabrication process and to understand the device performance of the PN diodes formed using the CVD-grown monolayers. In this work, we have fabricated the PN diodes based on the CVD-grown monolayer MoS_2/WSe_2 vertical heterostructures and investigated their transport properties.

The MoS_2 and WSe_2 monolayers were grown separately on silicon substrates by salt-assisted CVD method [3]. They were then transferred onto a Si substrate by means of a polymer-assisted process to form the heterostructures. As shown in the optical microscope image (Fig.1a), large-area (~100 μm) grains of MoS_2 and WSe_2 can be successfully stacked, as confirmed by the PL spectra (Fig. 1b). The PN diode was fabricated by depositing Ni/Au and Cr/Pd/Au electrodes onto the MoS_2 and WSe_2, respectively. The I_d-V_{ds} curves of the device operated at different gate voltage are illustrated in Figure 1c, where it shows clear rectification property, characteristic of a PN junction. Detailed fabrication process and the transport properties of the devices will be further discussed in this presentation.

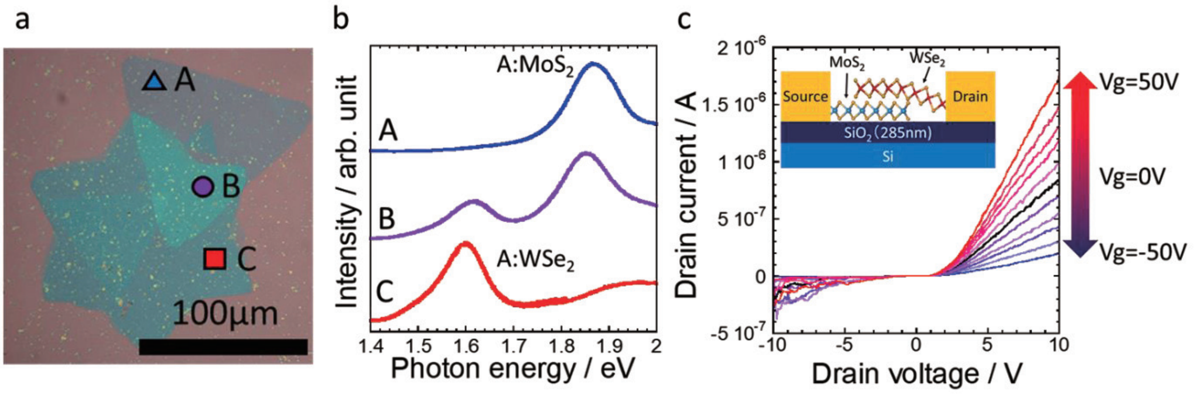

Fig.1 (a) The optical microscope image and (b) PL spectra of a vertically stacked MoS_2/WSe_2 heterostructure. (c) The I_d-V_{ds} curves of the MoS_2/WSe_2 device operated at various gate voltages. Inset: Model of the present device.

[1] T. Roy *et al., ACS Nano,* 9, 2071-2079 (2015).
[2] C. Lee *et al., Nature Nanotech.,* 9, 676-681 (2014).
[3] S. Li *et al., Appl. Mater. Today,* 1, 60-66 (2015).

Corresponding Author: Yasumitsu Miyata, Tel: 042-677-2508, E-mail: ymiyata@tmu.ac.jp

3P-34

Resonance characteristics of the cantilevered BN by electrostatic actuation

○Daiki Yoshikawa[1], Kuniharu Takei[1], Takayuki Arie[1], and Seiji Akita[1]
[1]*Department of Physics and Electronics, Osaka Prefecture University, Sakai 599-8531, Japan*

Two-dimensional atomic layer materials are attracting much attention as many useful device materials due to their excellently electrical, optical and mechanical properties. Among others, optically transparent materials such as BN is expected to be high performance nano-electro-mechanical resonators (NEMR). For sensor application of NEMR, photothermal effect affects its resonance property, so elimination of the photothermal effect is very crucial for accurate sensing. Here, we demonstrate the effect of the electric field on the resonance characteristics of an electrostatically actuated BN-NEMR, which is an electric insulator, based on the dielectric effect.

BN flakes were prepared by a mechanical exfoliated method. To fabricate the BN-NEMR, a multilayered BN was transferred onto insulator (SU-8) ridge with a height of 1.5 μm by the gel transferring method as shown in Fig. 1. Note that a pair of Au electrodes for the actuation of BN-NEMR is placed underneath the SU-8 support. The resonance of the cantilevered BN-NEMR was measured using optical detection method[1].

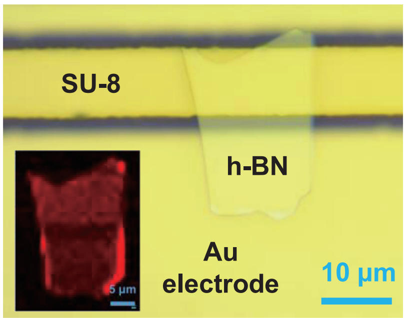

Fig. 1 Optical microscope image of BN NEMR. An inset shows the mapping of h-BN peak of Raman spectroscopy around 1365 cm^{-1}.

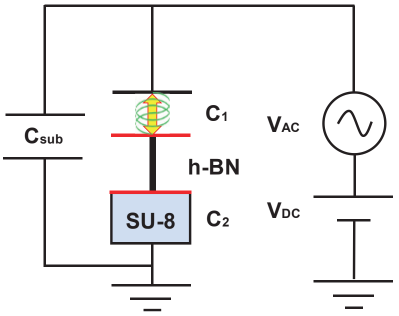

Fig. 2 An equivalent circuit model.

Figure 2 represents the simplified equivalent circuit of the proposed BN-NEMR. AC bias (V_{AC}) + DC bias (V_{DC}) was applied between the electrodes for the electrostatic actuation, where the cantilevered BN acts as the movable dielectric layer between the electrodes as shown in Fig. 2. Based on this model, the electrostatic force F acting on the BN-NEMR is approximately described as

$$F \approx \alpha V_{DC} V_{AC} \tag{1}$$

in linear response regime with small vibration amplitude, where α is constant determined from the device configuration.

Figure 3 shows V_{AC} dependence of the resonance characteristics of the cantilevered BN-NEMR. At V_{AC}=1 V and V_{DC}=0 V, the amplitude increases with larger V_{AC} with the resonance frequency around 1347.5 kHz. Thus, we have successfully actuated the cantilevered BN, which is an insulator. Figure 4 shows V_{AC} dependence of the oscillation amplitude with various V_{DC}. The oscillation amplitude of BN-NEMR was linearly changed with respect to V_{AC} according to Eq. 1.

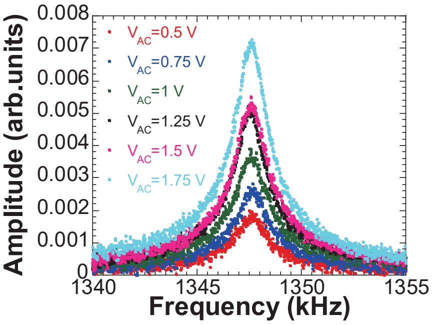

Fig. 3 V_{AC} dependence of resonance characteristics applied V_{DC}=1.5 V.

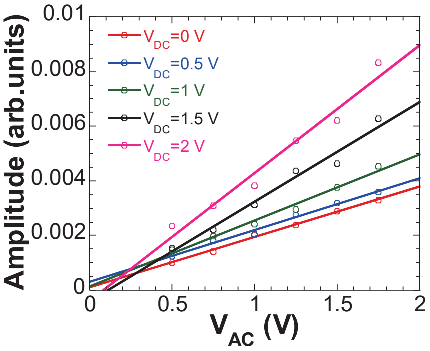

Fig. 4 V_{AC} dependence of the vibration amplitude with a parameter of V_{DC}.

[1] A. Yoshinaka et al, Appl. Phys. Lett. **98**, 133103 (2011).

Acknowledgement This study was partially supported by JSPS KAKENHI Grant Numbers JP15H05869, JP16K14259, JP16H00920, JP17H01040.

Corresponding Author: D.Yoshikawa, Tel: +81-72-254-9261, E-mail: yoshikawa-4@pe.osakafu-u.ac.jp

3P-35

Vibrational spectra of methylated forms of the cytosine in the region specific to hydrogen bonding relative to graphene pore interaction

○Tatiana Zolotoukhina[1], Toshihito Nitta[1]

[1] *Department of Mechanical Engineering, University of Toyama, Toyama 930-8555, Japan*

DNA methylation is an epigenetic mechanism involving the transfer of a methyl group onto the cytosine to form 5-methylcytosine (5MC) and 5-hydroxymethylcytosine (HMC) that regulate, as a signaling tool in the human genome, gene expression and silencing and can lead to oncology. Gradual development of single-molecule resolution in the tip-enhanced and surface-enhanced Raman spectroscopy, (TERS & SERS) promotes experimental work on DNA sequencing by SERS method and approaches single oligomer resolution [1-2]. As the next clinically important step, the optical identification of methylated forms of cytosine and adenine in the confirmed DNA sequence will be required with single-base precision. Numerical simulations to characterize vibrational spectra of different polymorphisms in the DNA strands become an instrument of prediction of spectral maps of the methylated nucleotides that were predicted by molecular dynamics (MD) simulation. Fourier transfer of the density of states (DOS) let us to obtain the spectra of various bonds in reaction coordinates for DNA nucleotides during transport through the 1.5nm graphene nanopore [4]. The vibrational frequencies were acquired for the methylated forms of cytosine vs. unmethylated ones at the range 400-2000 cm^{-1} at a numerical resolution 20 to 40 cm^{-1}. The frequencies that can serve as markers of the corresponding base methylation status have been evaluated. To confirm obtained MD results, calculation of DFT based Raman frequencies of the cytosine nucleobase methylation have been carried out.

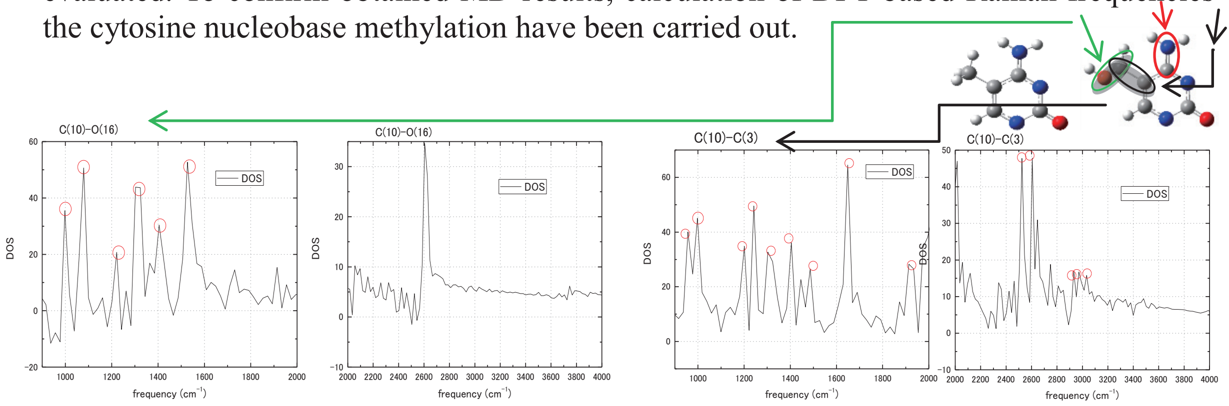

Fig.1 Spectral frequencies of hydroxymethylcytosine calculated by MD outside of graphene pore (vz=0) and as compared to the DFT calculations of Raman frequencies for the C(10)-C(3) & C(10)-O(16) bonds.

The vibrational frequencies were acquired for the C5'methylated and hydroxymethylated cytosine at the range 400-2000 cm^{-1} in MD simulation using reaction coordinates. Translocation through the graphene nanopore was shown to suppress a number of frequencies, especially H bond stretching. The frequencies of the methylated forms defined by H bond stretching at the region 2000-4000 cm^{-1} were resolved for the H-X (X=C, N, O) bonds. Comparison of MD and DFT calculation outside the graphene pore gave close frequency values in that region in the absence of interaction with graphene.

[1] L.-J. Xu, Zh.-Ch. Lei, J. Li, et al., JACS 137, 5149-5154 (2015).
[2] D.M. Sagar, L. E. Korhoj, K. B. Hanson, et al., Small 14, 1703165 (2018)

Corresponding Author: T. Zolotoukhina
Tel: +81-76-445-6739, Fax: +81-76-445-6739, E-mail: zolotu@eng.u-toyama.ac.jp

3P-36

First-principles study of magnetism in vanadium selenide thin films

○Mohammad Saeed Bahramy[1,2], Masaki Nakano[1], Satoshi Yoshida[1], Yue Wang[1], Hideki Matsuoka[1], Yuki Majima[1], Yuta Ohigashi[1], Yuta Kashiwabara[1], Masato Sakano[1], Kyoko Ishizaka[1,2], Yoshihiro Iwasa[1,2]

[1] *Department of Applied Physics, The University of Tokyo, Tokyo 113-8656, Japan*
[2] *RIKEN Center for Emergent Matter Science (CEMS), Wako 351-0198 Japan*

Transition-metal dichalcogenides have attracted a great deal of attention in the recent years due to their rich and varied properties. The single layer variants of these systems are considered as one of the most prominent examples of two-dimensional materials beyond graphene. Remarkably it's been recently proposed that the monolayer of the transition metal dichalcogenide VSe_2 can exhibit room temperature ferromagnetism, making it one of a few examples of two-dimensional ferromagnetic materials discovered so far [1]. However, this finding has been challenged by the recent angle-resolved photoemission spectroscopy measurements, showing no sign of time reversal breaking in the electronic structure of the pristine VSe_2 [2]. To address this issue, we have performed systemic first-principles calculations for both bulk and thin films of VSe_2 and its $V_{1+x}Se_2$ derivatives. Our calculations indicate that while the pristine VSe_2 can in principle form a weakly ordered ferromagnetic phase, introducing intercalated V sites substantially affects such an ordering. In this presentation, we compare the electronic structure properties of these systems in two and three dimensions and further discuss the effect of V interaction on the magnetic properties of $V_{1+x}Se_2$.

[1] M. Bonilla *et al., Nat. Nanotechnol.* **13**, 289 (2018).

[2] J. Feng *et al., Nano Lett.*, **18**, 4493 (2018).

Corresponding Author: M. S. Bahramy
Tel: +81-03-5841-6840,
E-mail: bahramy@ap.t.u-tokyo.ac.jp

発表索引
Author Index

Author Index

複写をご希望の方へ

フラーレン・ナノチューブ・グラフェン学会は、本誌掲載著作物の複写に関する権利を一般社団法人学術著作権協会に委託しております。

本誌に掲載された著作物の複写をご希望の方は、（社）学術著作権協会より許諾を受けて下さい。但し、企業等法人による社内利用目的の複写については、当該企業等法人が社団法人日本複写権センター((社)学術著作権協会が社内利用目的複写に関する権利を再委託している団体)と包括複写許諾契約を締結している場合にあっては、その必要はございません(社外頒布目的の複写については、許諾が必要です)。

権利委託先：一般社団法人学術著作権協会
〒107-0052　東京都港区赤坂 9-6-41　乃木坂ビル 3 階
URL：http://www.jaacc.jp/　E-Mail：info@jaacc.jp
電話：03-3475-5618　FAX：03-3475-5619

注意：複写以外の許諾（著作物の引用、転載・翻訳等）に関しては、（社）学術著作権協会に委託致しておりません。直接、フラーレン・ナノチューブ・グラフェン学会へお問い合わせください。

Reprographic　Reproduction outside Japan

- Making a copy of this publication
  Please obtain permission from the following Reproduction Rights Organizations (RROs) to which the copyright holder has consigned the management of the copyright regarding reprographic reproduction.

- Obtaining permission to quote, reproduce; translate, etc.
  Please contact the copyright holder directly.

Users in countries and regions where there is a local RRO under bilateral contract with Japan Academic Association for Copyright Clearance(JAC) are requested to contact the respective PROs directly to obtain permission.

Users in countries or regions in which JAC has no bilateral agreement are requested to apply for the license to JAC.

Japan Academic Association for Copyright Clearance (JAC)
Address：9-6-41 Akasaka, Minato-ku, Tokyo 107-0052 Japan
URL：http://www.jaacc.jp/　E-mail：info@jaacc.jp
Phone：+81-3-3475-5618　FAX：+81-3-3475-5619

2018 年 9 月 11 日発行

第 55 回フラーレン・ナノチューブ・グラフェン総合シンポジウム
講演要旨集

≪フラーレン・ナノチューブ・グラフェン学会≫
〒113-8656 東京都文京区本郷 7-3-1
東京大学大学院工学系研究科　機械工学専攻
丸山研究室内
Phone/Fax：03-3830-4848
E-mail：fntg@photon.t.u-tokyo.ac.jp
URL：http://fullerene-jp.org
印刷　/　製本　（株）創志企画

HORIBA
Scientific

ナノ材料イメージング装置

HORIBA NanoRaman

AFM-Raman ＋ TERS・SNOM

NanoRaman 特長

- ✔ ラマン光に干渉しない IR AFM ダイオード
- ✔ チップ交換時にヘッドの移動が不要
- ✔ カンチレバーのオートアライメント
- ✔ TERS 用 高 NA 対物レンズ（0.7 NA）

NanoRaman 用途

- ✔ AFM/ ラマン同一領域測定

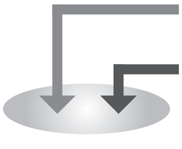

ラマン
有機物、無機化合物、結晶性などの化学情報

AFM
形状、電気・磁気的性質、機械特性、熱特性
などの可視化

- ✔ TERS（Tip Enhancement Raman Spectroscopy）分析
  - ▶ 回折限界を超える測定空間分解能（数十 nm～）によるラマン測定

アプリケーション例

- ✔ TERS hyperspectral imaging

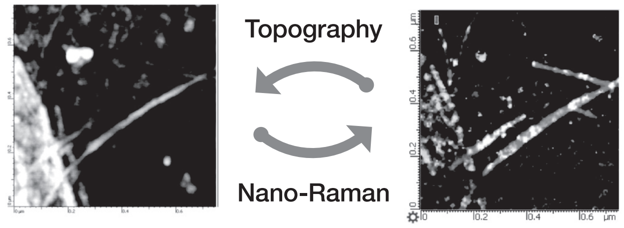

- ✔ Gap mode TERS response of 1-D patterns

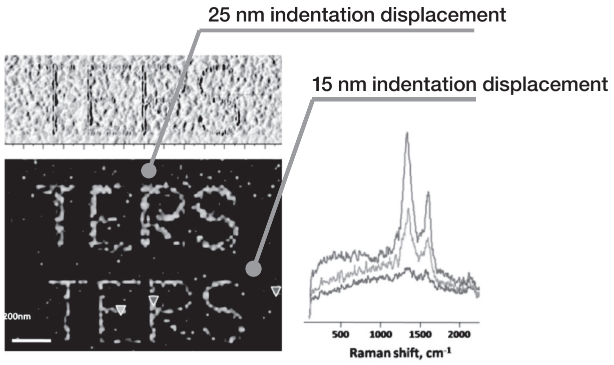

測定例）金基板上カーボンナノチューブ・グラフェンの TERS

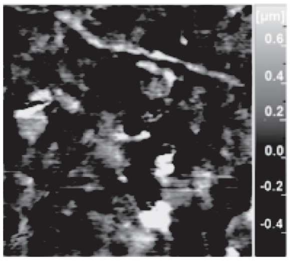

（a）AFMイメージ

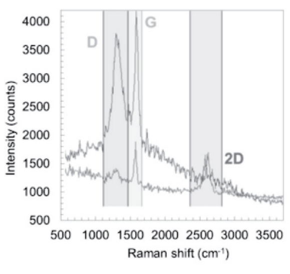

（b）TERSスペクトル

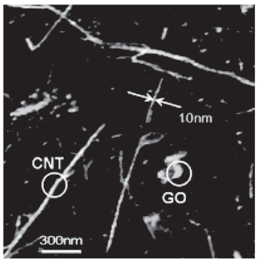

（c）TERSスペクトルイメージ

HORIBA Raman は
今年で販売 50 周年！

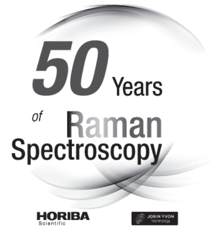

株式会社 堀場製作所

本社 〒601-8510京都市南区吉祥院宮の東町2番地　TEL（075)313-8121 http://www.horiba.com/jp/scientific/
●東京(03)6206-4717 ●名古屋(052)936-5781 ●大阪(06) 6390-8011 ●福岡(092)292-3593

Explore the future　Automotive Test Systems | Process & Environmental | Medical | Semiconductor | Scientific　**HORIBA**

モデルチェンジ　～スマートなデザインに簡単操作～

BRANSON超音波ホモジナイザー

長くご愛顧いただいておりますBRANSON超音波ホモジナイザーで新たなモデルが誕生しました。

主な特長

1.電気エネルギーから超音波振動への変換効率が95%以上
→ 無駄なエネルギーロスが小さく、安定した振幅が得られる。

2.通常では、液体の種類によって振幅が安定し難い。
→ 条件を変えても一定の振幅を保つ機能がついている。

3.ジュール（watt×sec）による発振制御が可能
→ Total何ジュールでこの処理が完了するという情報が論文に掲載できる。

20kHz超音波ホモジナイザー
BRANSON SONIFIER SFX250,550

40kHz超音波ホモジナイザー
BRANSON SONIFIER SFX150HH

主なアプリケーション

分散

カーボンナノチューブ　有機顔料　無機顔料　セラミック　セメント　感光体　記録材料
磁性粉　粉末冶金　酸化鉄　金属酸化物　シリカ　アルミナ　カーボンブラック
ポリマー　ラテックス　製紙　ファンデーション
研磨剤　電池　フィラー　光触媒　触媒　ワクチン　体外診断薬　歯磨き粉　シャンプー
半導体　電子基盤　液晶　貴金属　金属　宝石　タイヤ　発酵菌類　その他

乳化

エマルジョン製剤　農薬　トナー　ラテックス　界面活性剤　クリーム　乳液　その他

日本国内販売総代理店
株式会社セントラル科学貿易

東京本社:　〒136-0071 東京都江東区亀戸1-28-6　タニビル3F　TEL 03-5627-8150 FAX 03-5627-8151
技術物流センター:〒272-0146 千葉県市川市広尾2-1-9　TEL 047-701-6100 FAX 047-701-6116
大阪支店:　〒533-0031 大阪府大阪市東淀川区西淡路1-1-36 新大阪ビル　TEL 06-6325-3171 FAX 03-6325-5180
福岡営業所:　〒812-0016 福岡県福岡市博多区博多駅南1-2-15 事務機ビル　TEL 092-482-4000 FAX 092-482-3797
札幌出張所:　〒001-0911 北海道札幌市北区新琴似11条13-7-13-2　TEL 011-764-3611 FAX 011-764-3612
http://www.cscjp.co.jp


PicoQuant
SYNC
CH 1
CH 2
CH 3
CH 4
CH 5
CH 6
CH 7
CH 8
MultiHarp 150
Multichannel Event Timer
WR
USB
STATUS
CTRL


Taiko
PDL M1
LASER
STBY
ON/OFF
LASER APERTURE
PicoQuant

himac

カーボンナノチューブの
分離・精製に

himac 超遠心機シリーズ!

バイオ研究 & ナノ粒子研究 の強い味方　世界トップクラスの高性能、床置き・卓上、当社なら選べます!

小形超遠心機

エコでスリムな
床置きタイプ

himac CS-FNX Series

世界最高速150,000rpm ＊(CS150FNX)
世界最大遠心加速度1,050,000×g ＊(CS150FNX)
クラス最静音45dB(A) ＊
省スペース床置きタイプの小形超遠心機は当社だけ!

特長
- 世界標準の安全規格CE マーキング適合製品
- サンプルのバランスは目分量でOK!
- ロータは全て載せるだけ!（ロータクイックセッティング方式）
- エコ対応省エネモデル
- 7mLスイングロータ（S50ST）が回せます。

CE
CEマーキング適合

■仕様

形　名	CS150FNX	CS120FNX	CS100FNX
最高回転速度（rpm）	150,000	120,000	100,000
最大遠心加速度（xg）	1,050,000	771,000	571,000
サイズ（W×D×H mm）	440×520×910		
質　量（kg）	105		
標準価格（税別）	￥5,700,000	￥5,000,000	￥4,500,000

卓上超遠心機

コンパクトなボディに
世界トップクラスの性能

himac CS150NX

世界最高速150,000rpm ＊
世界最大遠心加速度1,050,000×g ＊
世界最小コンパクトサイズ＊
クラス最静音45dB(A) ＊

特長
- 短い真空待ち時間
- サンプルのバランスは目分量でOK!
- ロータは全て載せるだけ!
- 7mL スイングロータが回せます。

CE
CEマーキング適合

■仕様

形　名	CS150NX
最高回転速度（rpm）	150,000
最大遠心加速度（xg）	1,050,000
サイズ（W×D×H mm）	590×582×408
質　量（kg）	97
標準価格（税別）	￥6,200,000

＊（2018年7月現在当社調べによる小形超遠心機比）


S110AT

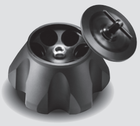
S50A


S50ST


S140AT


S58A


S55A2

■ロータ仕様

形　名	S110AT	S50A	S50ST
最高回転速度（rpm）	110,000	50,000	50,000
最大チューブ容量（mL×本）	5.0×8	30.0×6	7.0×4
標準価格（税別）	￥1,100,000	￥950,000	￥1,500,000
形　名	S140AT	S58A	S55A2
最高回転速度（rpm）	140,000	58,000	55,000
最大チューブ容量（mL×本）	2.0×10	13.5×8	1.5×12
標準価格（税別）	￥1,290,000	￥1,000,000	￥750,000

バイオ研究 & ナノ粒子研究 のスタンダード

超遠心機

遠心分離が楽しくなる
機能満載!

himac CP-NX Series

クラス最高速100,000rpm ＊(CP100NX)
クラス最大遠心加速度803,000×g ＊(CP100NX)
＊（2018年7月現在当社調べによる超遠心機比）

特長
- 離れていても運転状況がわかるLEDインジケーター搭載!
- ロータ寿命自動管理と寿命延長機能搭載（RLMアダプタ付ロータ）
- カラー液晶タッチパネルを操作しやすい前面に配置


P100AT2


P70AT


P45AT


P21A2


P40ST

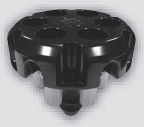
P32ST

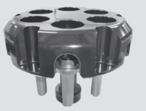
P32ST2

CE
CEマーキング適合

■仕様

形　名	CP100NX	CP90NX	CP80NX
最高回転速度（rpm）	100,000	90,000	80,000
最大遠心加速度（xg）	803,000	700,000	615,000
サイズ（W×D×H mm）	790×690×880（テーブルまでの高さ863）		
質　量（kg）	390		
標準価格（税別）	￥11,000,000	￥9,500,000	￥8,500,000

■ロータ仕様

形　名	P100AT2	P70AT	P45AT	P21A2	P40ST	P32ST	P32ST2
最高回転速度（rpm）	100,000	70,000	45,000	21,000	40,000	32,000	32,000
呼称容量（mL×本）	6.5×8	40×8	94×6	230×6	13×6	40×6	16×6
標準価格（税別）	￥2,250,000	￥2,200,000	￥2,350,000	￥1,800,000	￥2,490,000	￥2,480,000	￥2,480,000

※本広告に掲載した以外にもロータを取り揃えております。最寄りの営業所へお気軽にお問い合せください。

【製造・販売・保守】
工機ホールディングス株式会社 ライフサイエンス機器事業部
東日本地区　03-6738-0860　西日本地区　0798-23-4125

URL http://www.himac-science.jp ▶
himac お客様相談センター
☎ 0120-024125
受付時間 9:00～12:00 / 13:00～17:00（土・日・祝日・弊社休業日除く）

※日立工機株式会社は、2018年6月「工機ホールディングス株式会社」に社名変更致しました。ライフサイエンス機器事業ブランド「himac（ハイマック）」は継続致します。これからもよろしくお願い致します。

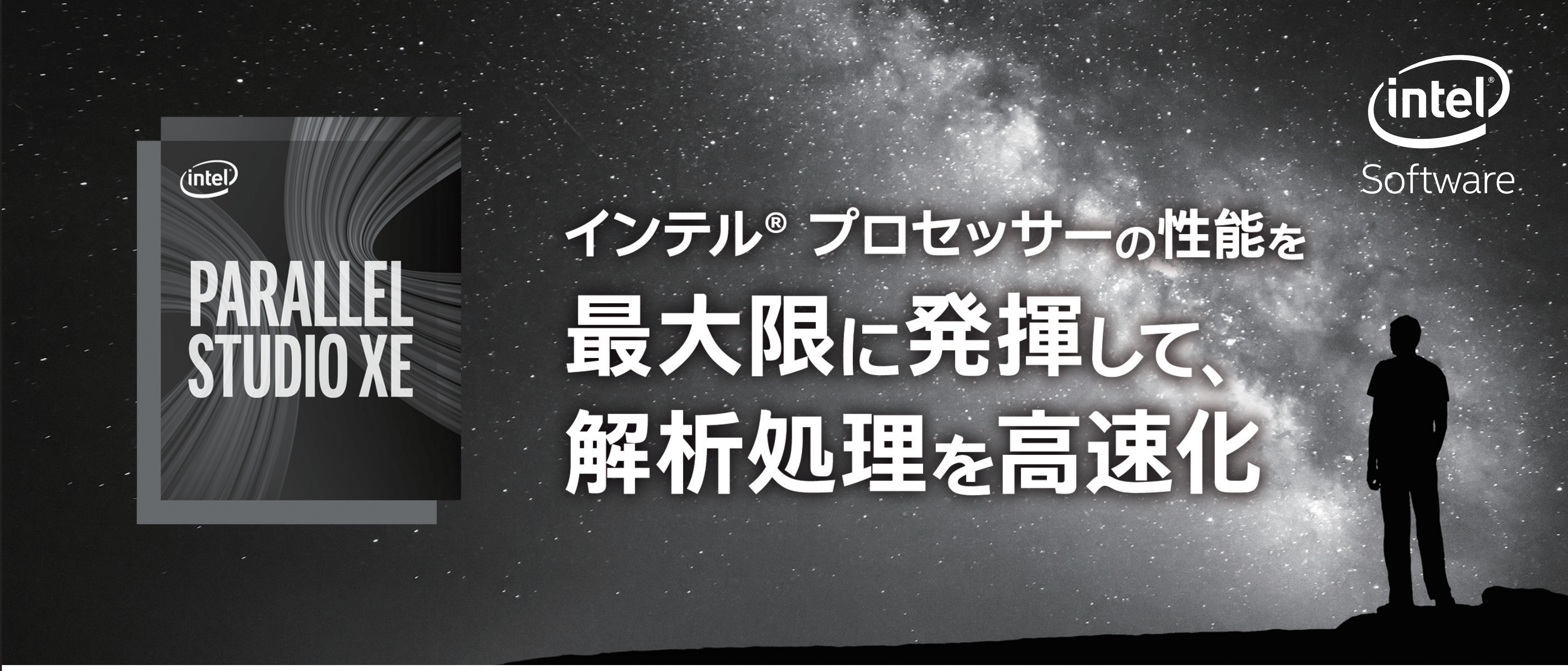
intel
PARALLEL
STUDIO XE
intel
Software